Imperial College London

A New Microscopic Model for the Simulation of Shared Space Schemes

by Bani Anvari

A thesis submitted to Imperial College London
for the degree of Doctor of Philosophy and the Diploma of Imperial College

to

Imperial College London
Department of Civil and Environmental Engineering
Centre for Transport Studies

May 2014

Abstract

Shared space is an innovative streetscape design which seeks minimum separation between vehicle traffic and pedestrians. Urban design is moving towards space sharing as a means of increasing the community texture of street surroundings. Its unique features aim to balance priorities and allow cars and pedestrians to co-exist harmoniously without the need to dictate behaviour. There is, however, a need for a simulation tool to model future shared space schemes and to help judge if they might represent suitable alternatives to traditional street layouts.

This thesis presents a microscopic mathematical model to simulate pedestrians and 4-wheeled motorised vehicles in shared space schemes. The complete development of the model is addressed: mathematical formulation of three interrelated layers based on the Social Force Model (SFM), software implementation, calibration and validation using the case studies from New Road (Brighton) and Exhibition Road (London).

Microscopic pedestrian, vehicle and mixed traffic models are reviewed and evaluated with respect to their ability to reproduce behavioural phenomena, resulting in the SFM being adopted as the most suitable basis for this thesis. The

behavioural patterns of shared space users are analysed to identify specific manoeuvres that need consideration. These patterns are realised in a three-layer model: The first layer introduces the flood fill algorithm to define intermediate destinations for agent's path around obstacles to the final destination. The second layer explains how the SFM is modified for pedestrians and vehicles. The third layer describes conflict avoidance with minimal change of speed and direction. The new mathematical model is calibrated and validated according to defined performance indicators using real data from the two case study sites. The results show that this model is suitable to simulate shared space users but that the physical parameters depend on how a shared space scheme is realised compared to the original philosophy. The achievements of this thesis can be beneficial to urban planners and councils considering the implementation of a new shared space scheme.

Declaration

I herewith declare that I have produced this thesis without the prohibited assistance of third parties and without making use of aids other than those specified; notions taken over directly or indirectly from other sources have been identified as such. This thesis has not previously been presented in an identical or a similar form to any other British or foreign examination board.

London, May 2014

Contents

List of Figures

List of Tables

Nomenclature

Abbreviations

AFVDM	Asymmetric Full Velocity Difference Model
APM	Action Point Model
BHCC	Brighton and Hove City Council
CAM	Cellular Automata Model
CNU	Congress for the New Urbanism
CPA	Closest Point of Approach
CSV	Comma Separated Value
CW	City of Westminster
DfT	Department for Transport
EU	European Union
FLM	Fuzzy Logic Model
FVADM	Full Velocity and Acceleration Difference Model
FVDM	Full Velocity Difference Model
GAs	Gehl Architects
GAM	Gap Acceptance Model
GDB	Guide Dogs for the Blind association
GFM	Generalised Force Model
GMM	General Motor Model

GUI	Graphical User Interface
ICL	Imperial College London
IDM	Intelligent Driver Model
ITS	Intelligent Transport System
LHT	Left-hand Traffic
OD	Ordinary Differential
ODEs	Ordinary Differential Equation
OVM	Optimal Velocity Model
MAVDM	Multiple Ahead and Velocity Difference Model
MHVDM	Multiple Headway and Velocity Difference Model
MSAs	Martin Stockley Associates
MVA	Martin and Voorhees Associates
PCBVRS	Pedestrian Crossing Behaviour Virtual Reality System
RBKC	Royal Borough of Kensington and Chelsea
SITRAS	Simulation of TRAnsport Systems
SDM	Safety Distance Model
SFM	Social Force Model
SUE	Stochastic User Equilibrium
TfL	Transport for London
UK	United Kingdom
VLC	Verlet Link Cell

Notation

A	Interaction strength
$\boldsymbol{a}$	Acceleration
$a^{Centrifugal}$	Centrifugal acceleration
B	Interaction range

$B^{'}$	Acceleration interaction range
$B^{''}$	Braking interaction range
C	Constant attracting force
c	Cost function
d	Distance between the centre of two shared space users
d_c	Safe distance
d_γ	Minimal distance of a car
$d(v_{\gamma\delta})$	Speed-dependent safe distance between two cars
d^{CPA}	Minimum distance between the agents at their Closest Point of Approach (CPA)
$\boldsymbol{d}$	Desired destination vector
$d(v)$	Speed-dependent safe distance
D^{C}	Chessboard distance between two points
$D^{\mathrm{Euclidean}}$	Euclidean distance between two points
D^{M}	Manhattan distance between two points
D^{V2}	Variant 2 distance between two points
δx_i	Horizental distance between two points
δy_i	Vertical distance between two points
Δx	Horizental distance between two agents
Δy	Vertical distance between two agents
$\Delta \boldsymbol{v}_{\gamma\delta}$	Velocity difference of two cars
E	Relative distance error as a function of the empirical and simulated time series
$\boldsymbol{v}^{min}$	Minimum velocity change
$\xi_{relative}$	Relative error
$\boldsymbol{\xi}$	Fluctuation force
$\boldsymbol{e}^0$	Desired direction
F	Form factor

$\boldsymbol{f}^{repulsive}_{\gamma(\gamma-1)}$	Repulsive force between car γ and the car ahead $(\gamma - 1)$
$\boldsymbol{f}_{\alpha\beta}$	Interaction/Repulsive force between pedestrian α and pedestrian β
$\boldsymbol{f}_{\alpha \mathrm{b}}$	Interaction/Repulsive force between pedestrian α and boundary/obstacle b
$\boldsymbol{f}_{\alpha\delta}$	Interaction/Repulsive force between pedestrian α and car δ
$\boldsymbol{f}_{\delta\gamma}$	Interaction/Repulsive force between two cars
$\boldsymbol{f}^{att}$	Joining force
$\boldsymbol{f}^{conflict}$	Conflict avoidance force
$\boldsymbol{f}^{following}$	Car-following force
$\boldsymbol{f}^{ph,friction}$	Friction physical force
$\boldsymbol{f}^{norm}$	Perpendicular/normal force
$\boldsymbol{f}^{ph,pushing}$	Pushing physical force
$\boldsymbol{f}^{ph}$	Physical force
$\boldsymbol{f}^{soc}$	Social force
$\boldsymbol{f}^{tan}$	Tangential force
$\boldsymbol{f}^{0}$	Driving force
$\boldsymbol{f}_{\alpha \mathrm{i}}$	Attractive interaction between a pedestrian and an attraction
J	Flow
k, κ	Obstruction effect constants
$k_s, \lambda_s, \lambda_{s1}, \lambda_{s2}$	Sensitivity coefficients
l_e	Constant parameter
$2l$	Length of a car
L	Distance between the front and the rear axle
λ	Form factor constant
m	Mass
max	Maximum
max	Minimum
m_e	Constant parameter

n	Number of vehicles ahead
$\boldsymbol{n}$	Normalised vector
ω	Coefficient
p	Predictor
$\boldsymbol{p}$	Boundary vertex
φ	Angle between the desired direction and centre of another agent
ψ	Steering angle
q	Effective factor
$\boldsymbol{q}$	Boundary vertex
r	Radius
r_α	Radius of a pedestrian
$r_{\alpha U}$	Sum of the radii of a pedestrian and another agent
r_γ	Radius of a car
$r_{\gamma U}$	Sum of the radii of a car and another agent
r_{Verlet}	Maximum interaction distance
ρ	Radius of the arc dependent on the steering angle
ρ_1, ρ_2	Constant parameters
$\boldsymbol{s}$	Clearance
t	time
$\boldsymbol{t}$	Tangential vector
τ	Relaxation time or reaction time
$\tau_\gamma^{'}$	Braking time of a car
Θ	Function depending on its argument
θ_0	Constant parameter
T_γ	Safe time headway
U	Shared space user (pedestrian or car)
ϑ_l	Constant parameter
ϑ	Effective view angle

v^0	Desired speed
v^{opt}	Optimal speed
$\boldsymbol{v}$	Actual velocity
$\boldsymbol{v}$	Optimal velocity
$\boldsymbol{r}_\alpha^k$	Intermediate destination
$\Delta\boldsymbol{v}$	Relative velocity
$\boldsymbol{v}^e$	Traffic-dependant velocity
$V(\Delta x)$	Optimal speed function
$2w$	Width of a car
X	Random number from a normal distribution
Δx	Space headway
x_{video}	Video image horizontal location
x_{real}	Real world horizontal location
$\boldsymbol{x}$	Actual location
$\boldsymbol{\xi}$	Random fluctuation term
y_{video}	Video image vertical location
y_{real}	Real world vertical location
γ_t	Expected time for a driver to reach the leading car
$\dot{\eta}$	Yaw angle velocity
ν	Slip angle
$\dot{\nu}$	Slip angle velocity

Chapter 1

Introduction

This chapter provides a comprehensive outline of the motivation for this thesis. Shared space is an innovative streetscape design which seeks minimum separation between vehicle traffic and pedestrians. Space sharing is becoming an increasingly important aspect of urban design as a means of increasing the community texture of street surroundings. In a shared space environment, traffic control infrastructures (such as kerbs, traffic signs) are removed to introduce a degree of uncertainty as to the right-of-way. This integration concept of shared space encourages a considerate style of driving and aims to balance priority for all road users. There is, however, a need for a micro-simulation tool capable of representing future shared space schemes so as to help judge whether shared space may represent a suitable alternative to traditional street layouts in any given particular context. This need underpins the aim of this thesis which is to understand mathematically the main behaviours of pedestrians and vehicles in shared space layouts, to model their complex interactions and to develop a micro-simulation tool to replicate mixed traffic movements. This chapter presents the background to the research and the objectives, contributions and structure of the thesis.

1.1 Background

Motor vehicles are an important part of the world's cities and many traffic networks, traffic signals and regulations have been created to serve and support motorised transport. Motor vehicles have a significant influence on the quality of the streetscapes of cities, and contribute positively to the quality of human life. In order to avoid conflicts between different street users, and in the belief that this would improve safety and efficiency of mobility, city planners in the UK after the post-war European reconstruction have aimed to segregate pedestrians from streets and from vehicle movements.

During the last century, governments regulated streets through a variety of standardised mechanisms, control systems and markings which aimed to balance the accessibility of public spaces. Buchanan [1] was the first to outline the concept of separating vehicular traffic from pedestrian movement and social activities. He established a key policy framework for streets with the aim of improving traffic flow, safety and accessibility. Buchanan believed that pedestrian movements and vehicle traffic cannot coexist and argued that modern design should be based on traffic segregation. As a result of this type of planning, main roads are no longer part of city activities and towns have become full of underpasses, bridges and traffic signs, each with the aim of promoting automobility [2].

More recently, Hamilton-Baillie [2] has argued that individuals tend to spend less time in public areas if they perceive streets to be less attractive for their social interaction activities or transport movements. As a result, human activities transfer from public to private spaces. An attractive environment and a well-connected road stimulate people to walk and cycle to their destinations and reduces vehicular traffic and pollution [3]. Traffic segregation separates daily life from the streets [4] and fails to provide a high-quality social environment [5]. There is a

need for new city designs incorporating areas where pedestrians can share space with automobiles. The intention of this new approach to urban design is to strike a balance between the competing societal functions of roads and public spaces in order to encourage the informal human activities that are related to physical health and well-being.

Urban design is moving towards streets with a single surface pavement, and minimal traffic signals and road markings, as an alternative to traditional controlled traffic designs [6–8]. Space sharing makes pedestrians road users as opposed to obstacles in the way of traffic, which balances the social and civic function of streets [9]. This new design aims to keep the important function of the road as a transport link for the surrounding area, while creating an integrated street environment for pedestrians and vehicles [9].

1.1.1 The Origin and Philosophy of Shared Space

Space sharing (see Table 1.1) can be traced back to Lynch's [10] and Jacobs' [11] ideas on re-designing urban environments, which were developed further by the woonerf (living playground) concept in the Netherlands in the late 1960s [12]. A

	Woonerf	**Traffic Calming**	**Shared Space**
Alternative Names	Home Zone Residential Yard	Traffic Control	Naked Intersection Liveable Streets Shared Streets/Zones
Land Use	Residential	Any Land Use	Any Land Use
Is Social Interaction an Aim?	Yes	No	Yes
Design Approach	Flexible	Standardised	Flexible
Objective	Slow Traffic to Allow Social Interaction	Slow Traffic	Multi-faceted
Who has the Priority?	Pedestrian	Traffic	Equal
Initiated in	the 1960s	the 1980s	1991 (first applied in 2004)

Table 1.1: The characteristics of new design approaches [13]

woonerf is a residential street, designed to provide safe and pleasurable areas for pedestrians (specifically children), and where pedestrians are given priority over motor vehicles. In particular, a woonerf street is designed without a clear segregation between pedestrians and cars, so that all road users should travel with caution [14]. In the UK, from the late 1990s, a woonerf was known as a home zone. Collarte [15] described a woonerf as comprising of an entrance threshold (Figure 1.1 (a)), a curve-linear arrangement (Figure 1.1 (b)), a single surface environment with interspersed trees and seating areas (Figure 1.1 (c)) and irregular parking (Figure 1.1 (d)). A clear and distinct entrance for a woonerf makes road users aware that they are entering another area with different traffic rules. A traffic sign placed at this entrance will provide the corresponding area information. A curve-linear arrangement of the road/pavement surfacing design breaks the sight lines of drivers, makes them cautious, and encourages them to slow

(a) An entrance threshold

(b) A curve-linear arrangement

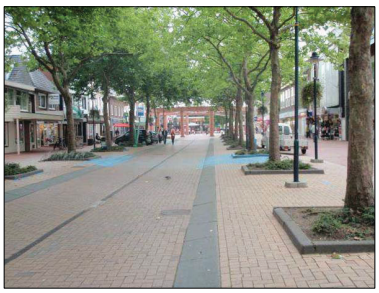

(c) Single surface environments

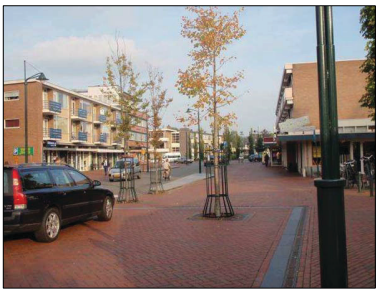

(d) Irregular parking

Figure 1.1: Typical features of woonerf designs [13]

down. A single shared surface encourages road users to travel more carefully and slowly as there is no clearly defined travel lane for pedestrians and cars. It also stimulates pedestrians to move freely across the entire space. Tree planting and seating areas make the environment attractive and encourage people to spend more time in the area. Irregular parking arrangements are used as a traffic calming strategy. By 1980, about 3500 areas had been redesigned around Europe based on the woonerf principles [16]. Bendixson [17] believed that this was a promising link to a shared context with automobiles, as drivers had to consider the behaviour of pedestrians and children.

Some of the ideas and characteristics of the woonerf approach were introduced to traffic calming design [18]. Compared to woonerfs, traffic calming schemes are focused only on slowing down traffic and lack elements to improve social interactions. Hence, traffic calming schemes use physical design elements such as speed bumps, maximum speed signs of $30\,\frac{\mathrm{km}}{\mathrm{h}}$ $(8.3\,\frac{\mathrm{m}}{\mathrm{s}})$, chicanes, narrowing of the carriageway, and reduced corner radii to reduce vehicle speeds [15]. Vehicular traffic, however, is still given priority over pedestrians.

Appleyard noted that less traffic flow would result in more social interactions and argued that a reduction of traffic flow is a requirement for creating "liveable streets" [19]. His ideas were a major influence on the Congress for the New Urbanism (CNU[1]) in 1996, which recommended changes to the design of urban areas that would incorporate both pedestrians and motor vehicles. In this spirit, urban designers have tried to connect buildings and neighbourhood areas so as to increase the community texture and improve social interaction.

Adams [20] noted that space sharing permits humans to change the balance of

[1] The CNU is the leading organisation promoting walkable, mixed-use neighbourhood development, sustainable communities and healthier living conditions.

risk according to their situation, in contrast to segregation policies which aim to minimise the interaction risk. Human beings adapt to various environmental changes and there is a need for streets with social interactions [21]. The purpose, is for pedestrians to pay more attention to their surroundings and for drivers to drive more consciously since there is uncertainty in terms of who has the right of way. Space sharing is a rejection of the concept of distinguishing street users and introduces equal rights for both pedestrians and vehicles, though drivers are deemed responsible in the case of any accidents.

In 2005, Monderman [22] removed road markings, traffic signals, signs, kerbs, bollards and barriers in a village in northern Holland in order to create a strong relationship between the street and its surroundings. He believed that cultural signals and informal social rules have a stronger influence on the interaction of pedestrians and vehicles than formal regulations. Monderman explained that integration makes drivers a part of the social context. As a result, they rely on eye-contact and drive more carefully in order to be able to understand and predict situations. Thus, human presence and activity on streets brings about a qualitative change in behaviour as drivers and pedestrians each become more vigilant.

The most recent version of the space sharing idea is called "shared space". This is a concept that promotes a sense of vigilance and responsibility by reducing demarcations and any physical distinction between the streets and pedestrian areas. Attractive features are added to shared space environments to provide a pleasurable area that stimulate pedestrians to walk and cycle to their destinations. While woonerf and home zones are small scale examples of disregarding the traditional separation between the footpath and carriageway, the shared space approach is a more flexible approach which is defined as "*an approach to improving streets and places where both pedestrians and vehicles are present, with layouts related*

more to the pedestrian scale and with features encouraging drivers to assume priority having been reduced or removed".[2]. Hamilton-Baillie and Jones [23] indicated that the removal of traffic restrictions reduces traffic speed and improves vehicles' journey times in many shared space observations. Lutz [24] argues that shared space designs reduce the stop-and-go behaviour of drivers by assigning the speed limit of $32\,\frac{\mathrm{km}}{\mathrm{h}}$ $(8.9\,\frac{\mathrm{m}}{\mathrm{s}})$ and reducing average waiting times at intersections. Hence, shared space can reduce carbon emissions of vehicles travelling through such spaces [13]. It should be noted that high quality street design like shared space increases property values in an area [25, 26]. Table 1.2 lists a number of shared space schemes that have already been implemented around the world. In the UK, one of the first steps towards sharing street spaces with

Country	**Towns/Councils**
Australia	Bendigo
Austria	Feldkirchen bei Graz, Gleinstätten, Graz, Vöcklabruck, Gnas, Velden am Wörther See
Belgium	Ostende
Denmark	Ejby
Germany	Blomberg, Bohmte, Calau, Duisburg, Endingen am Kaiserstuhl, Ettenheim, Frankfurt am Main, Hamburg, Haslach im Kinzigtal, Luckenwalde, Potsdam, Rudersberg, Wolfach, Hatten OT Kirchhatten
Netherlands	Emmen, Donkerbroek, Drachten, Makkinga, Nijega, Oldeberkoop, Opeinde, Oosterwolde, Olderberkoop, Oudehaske, Wolvega, Haren
New Zealand	Auckland, Christchurch, Dunedin, Hamilton, Napier, Nelson, Orewa, Papakura, Waitakera, Wellington
Sweden	Norrköping
United Kingdom	Ashford, Bath, Brighton, Hove, Caernarfon, Leeds, London, Newbury, Newcastle, Oxford, Shrewsbury, Southampton, Taunton, Woking
United States	West Palm Beach

Table 1.2: A number of shared space schemes worldwide [9, 13, 25, 27–30]

pedestrians was introduced by the term 'home zone' which was applied to residential areas [31]. A home zone is the English expression for what was known as woonerf in the Netherlands. Biddulph [32] outlined the concept of shared

[2]I. Kaparias, M.G.H. Bell, A. Miri, C. Chan, and B. Mount."Analysing the Perceptions of Pedestrians and Drivers to Shared Space". p. 297-310, 2012.

street environments to some local authorities in the 1970s. They were discouraged, however, by concern about potential legal responsibilities in the case of accidents with pedestrians. By the end of the 1990s, however, shared space design was established in an increasing number of residential areas due to a high demand for safer street surroundings for children, but the home zone experience did not provide practicable policies on the regulation of shared space principles.

An awareness and implementation of shared space principles started in Seven Dials (London) and New Road (Brighton) in 2007. Following the improved safety records of the implemented schemes, more UK local councils applied shared space approaches, for example in Elwick Square (Ashford), Caernarfon (Wales), Milsom Street (Bath), High Street (Shrewsbury), London Road (Southampton), St James Street (Taunton), New Inn Hall Street (Oxford), George Street (Hove), Blackett Street (Newcastle), St Johns Road (London) and Exhibition Road (London). According to their design characteristics, Andrews [33] classified thirteen shared space schemes into three typologies (such as junctions, links and squares). She highlighted that each typology influences the operation allowing to grade shared space designs with regards to the degree of implementation. In 2011, the Department for Transport (DfT) issued national guidance on the design of shared space schemes based on research carried out by Martin and Voorhees Associates (MVA) consultancy. The factors influencing the willingness of pedestrians to share space with drivers were studied by Kaparias et al. [34]. Seven elements were considered: vehicular traffic and pedestrian flow rate, existence of safe zones, street surface conditions, street lightening, greenery provision and attraction facilities. A survey was carried out before changing Exhibition Road (London) to a shared surface and binary logistic regression models have been applied to the empirical data [34]. The results showed that the existence of safe zones and the lighting level are the determining factors for pedestrians. Furthermore,

Kaparias et al. [34] investigated the pedestrian-vehicle conflicts before and after implementing shared space on Exhibition Road. In this study, 17 characteristics of pedestrians and drivers were considered, with the occurrence of a conflict and its severity defined according to different elements such as time and distance to collision, and severity and complexity of a sudden action. Sutcliffe [35] also showed that a significant increase in pedestrian movements and a general drop in traffic conflicts were reported after the redesign of Exhibition Road [35]. Mixed traffic in shared space schemes transfer interaction responsibilities strongly onto road users themselves rather than managing these by traffic signs. The concept accomplishes this through giving equal rights to all users on the road. The only rule of the shared space concept is that drivers should give way to the right, and must drive at an appropriate speed (speed limit of maximum $32\ \frac{\mathrm{km}}{\mathrm{h}}$ $(8.9\ \frac{\mathrm{m}}{\mathrm{s}})$, based on the application) [36].

1.1.2 The Shared Space Discussions

Debate on the development of shared space environments is largely polarised between those of the view that it is essential in order to improve safety, social-lifestyle and economic stability, and those concerned about its adoption due to a lack of research on perceptions and on the safety of road users.

Gaventa [37] identified shared spaces as slow and safe environments that develop social negotiation between pedestrians and drivers with the aim of providing civilised urban places. Hamilton-Baillie [2] argued that the success of space sharing depends on changing the road users' understanding of safety and risk within a mixed environment. New designs should be structured in a way that encourages behavioural changes among users. In 2007, Monderman [22] stated that the absence of demarcations and traffic facilities in shared spaces can cause uncertainties for both drivers and pedestrians and that this results in slower driv-

ing speeds and an increased awareness of safety. Road users will become more conscious of the movement patterns around them due to interactions based on eye contact and by predicting behaviours. Ben-Joseph [38] and Hamilton-Baillie [2] argued that shared space can increase the safety of street spaces and consequently decrease the amount of fatal accidents and injuries. Southworth and Ben-Joseph, meanwhile, [16] sought to prove this idea based on observations and research reports in different countries that had applied shared spaces. They concluded that shared space contributes to fewer vehicle movements than traditional traffic separation.

Quimby and Castle, however, [9] criticised the results reported by Southworth and Ben-Joseph [16]. They argued that these results were based on small, isolated locations with low traffic flows. They added that the cultural and social context of the studied areas were critical elements that could significantly impact the results in different countries and that this should therefore be taken into account. Steve Melia [39] believes that separation is required when the aim is to encourage a specific traffic mode, protect non-motorised modes and give a feeling of comfort to non-motorised users in cities and towns. He added that shared space schemes can contribute to these aims, particularly when the traffic volumes are low. Jenks [40] and Clayden et al. [41] argued against shared space by noting that some road users would neither accept or understand the allocation of rights, with the result that space sharing is unsafe for walking. Moreover, the Guide Dogs for the Blind Association (GDB) [42] in London voiced concerns about vision impaired people, who are usually dependent on kerb lines and spatial settings. It recommended that this feature should be considered when implementing shared space. Given the concerns above, Quimby and Castle [9] argued that the shared space idea needs to be implemented in a different way from its original concept (in residential streets) when it comes to big cities and town centres. Luca

et al. [43] supported this idea, emphasizing the importance of studying the social, environmental, economical and behavioural factors of a given city before implementing a shared space environment in city centres.

Having explained the shared space philosophy and discussed its pros and cons, it is clear that shared space can be considered as a design alternative to traditional traffic separation considering traffic volumes, land uses, vulnerable users and size of the potential area [44]. As with all design plans, shared space struggles to achieve all of its theoretical objectives dependant on different contexts [44]. However, it is successful if the primary objectives are improving the social context of streets and encouraging a considerate style of driving [13, 44].

1.1.3 Research Problem

The visualisation, judgment and environmental response of pedestrians, cyclists and drivers are important criteria in achieving a successful, socially connected shared space [35]. These criteria depend partly on how new designs influence the perception of road users [2], and partly on social culture in terms of the understanding and acceptance of shared space as a safe scheme [9]. The concept that the street context is no longer purely the domain of cars requires time to become embedded in the community but, over time, both driver behaviour and the status of pedestrians or other users will change to accommodate the social connection of the street [35].

There is a need to identify the conditions under which shared space might be a feasible alternative to traditionally controlled traffic designs. Hence, this thesis focuses on incorporating pedestrian movements and vehicular traffic despite the fact that cyclists and motorists are present in shared space environments. In order to reduce the influence of cyclists and motorised behaviours on the ob-

served behaviour of pedestrian and car drivers in shared space schemes, a link typology with a low number of cyclists and motorists is considered for the case study sites. The complex interactions of pedestrians and drivers in shared space environments cannot be handled fully by available well-known software such as VISSIM or Aimsum [45]. To the best knowledge of the author, there is no appropriate mathematical model for simulating shared space utilising a full consideration of the original philosophy of equal priority and single surface modelling [45]. Predicting the responses of pedestrians to the behaviour of vehicles, neighbouring pedestrians and obstacles in a shared space environment is also important from the standpoint of traffic management. A computer model of shared space environments should make it possible to evaluate the performance of new designs with different traffic volumes. The motivation of this thesis is to simulate a shared space system with suitable and essential characteristics of pedestrians and car drivers in order to gain a better understanding of their behaviours. Since the advanced nature of simulation allows the visualisation of future shared space schemes, it should allow designers to predict pedestrian and vehicle behaviours and, in turn, help to validate and improve designs so as to achieve solutions for requirements such as optimal traffic capacities or delays.

1.2 Aim and Objectives

The aim of this thesis is to develop a new microscopic model for pedestrian and car behaviours in a shared space environment. The research challenge is to formulate mathematically the behaviour of and interaction between the two travel modes/agents: non-motorised transport (pedestrians) and motorised transport (4-wheeled vehicles) in order to simulate a shared space scheme. Two operational schemes, New Road (Brighton) and Exhibition Road (London), will be used to test and validate the model.

Four objectives have been formulated to achieve the aim of this thesis:

1. Establish a suitable and sufficient basis of a new mathematical model for shared space users according to the state-of-the-art of pedestrian, vehicle and mixed traffic modelling.

2. Identify pedestrian and vehicle behaviour patterns and classify the essential factors that comprise these patterns. This leads to a characterisation of their behaviour as the basis for the development of the model.

3. Develop a microscopic model in a traffic simulation tool describing the identified characteristics and behaviour of pedestrians and vehicles in a shared space environment.

4. Calibrate and validate the new mathematical model for shared space users with operational case studies.

1.3 Research Contributions

The contribution of this thesis is in the field of engineering modelling. The major contributions made to mixed traffic modelling are summarised below:

1. A consolidated literature review on vehicle, pedestrian and mixed traffic modelling in order to determine the research gap and address the potential ground base for shared space modelling.

2. A new three-layer microscopic mathematical model to simulate interactions between road users capturing the key behaviours of pedestrians and vehicles in shared space layouts.

3. Implementation of the new mathematical model, calibration and validation process in a software tool with user interface which is simple, adoptable to other shared space environments and automated.

1.4 Thesis Structure

This thesis contains nine chapters which explain the steps taken to achieve the aim in Section 1.2. In line with the objectives, a detailed structure of the thesis is shown in Figure 1.2.

Chapter 1 presents the research motivation of this thesis, the research aim and objectives, the main contributions and thesis structure.

Chapter 2 classifies vehicular traffic and crowd models into phenomenological and generic models. The literature on generic models for vehicular traffic, crowds and mixed traffic on the microscopic scale is reviewed. These models are compared according to well-known vehicular traffic and crowd phenomena. This review reveals that the generic approach of force directed models is the most appropriate to reproduce crowd self-organising phenomena.

Chapter 3 presents the objectives of shared space on the part of urban planners and their intentions in respect to pedestrian and vehicular behaviours. Recent shared space studies on behaviour patterns are reviewed. Behaviour characteristics such as moving along the shortest path via intermediate destinations to the final destination using prior knowledge of the infrastructure while interacting with other users and obstacles, are highlighted. Shared space is designed without any lane discipline although car-following features are observed for some vehicle patterns. These unique design and behaviour characteristics are translated in this thesis into a force directed model. The analysis of elementary behaviour patterns results in a structure for the conceptual framework which consists of three interrelated layers. The core model is defined by the Social Force Model (SFM). Additionally, a geometrical model is defined in this chapter.

Chapter 4 describes the first layer of the new mathematical model. Since the SFM considers and reacts to static obstacles only within a close interaction range of each agent, a global path planning algorithm is generated to find the shortest path to a destination according to the infrastructure of the environment. A comprehensive review of path planning methods is presented and the flood-fill algorithm is chosen. Distance maps are calculated using the flood-fill algorithm, based on the Variant 2 metric, to define intermediate destinations between an agent's origin and final destination along the shortest path.

Chapter 5 defines shared space users' behaviour patterns based on their socio-psychological considerations. Hence, the SFM is applied to simulate the two modes (pedestrians and vehicles) considering equal priority and negotiating the right of way. Using this force directed model also allows all agents to move within a two dimensional space which is one of the key objectives of shared space schemes. In some scenarios, however, observations show a car-following behaviour which is included in the force directed model.

Chapter 6 presents the third layer of the new mathematical model. The flexibility of car motion is constrained by a relation between the steering angle and speed. Furthermore, potential conflicts between cars and pedestrians might occur if the SFM is followed exclusively since cars are not assigned with a physical interaction force. Any physical contact which is equivalent to an accident should be prevented. Hence, possible conflicts are predicted based on their states and resolved by a combination of change of speed and change in heading direction. A potential conflict is detected as soon as agents intersect each other's shadow. By minimising a defined cost function, the detected potential conflicts are solved for car-pedestrian interactions. Considering left-hand traffic in the UK, this concept was also adopted for confronting car-car conflicts.

Chapter 7 describes the implementation of the mathematical model in software (using the C#-Programming language). Flowcharts explain how the algorithms of the three layers are interrelated: the flood-fill algorithm and the Variant 2 distance metric derive the shortest path to the destination via intermediate destinations before running the simulation. The SFM is calculated considering a combination of the Verlet and the link cell algorithm. The Ordinary Differential (OD) Equations are solved based on the Gear's predictor-corrector algorithm. Potential conflicts are resolved by running an optimisation for minimum velocity change. Pedestrian phenomena are reproduced and prove the correct implementation of the SFM. Furthermore, the Graphical User Interface (GUI) of the simulation tool for modelling the shared space traffic flow is introduced.

Chapter 8 is focused on data collection, model calibration and validation. Data such as trajectories, speeds and accelerations is extracted from video recordings using the Trajectory Extractor software for two shared space schemes in the UK: New Road (Brighton) and Exhibition Road (London). A hybrid method is utilised to calibrate the microscopic model based on the relative distance errors between the simulation results and empirical data. Quantitative validation is performed by comparing the performance indicators such as trajectories, speed and acceleration distributions between real data and simulation results. The validation results are discussed, demonstrating that the new mathematical model is suitable for simulating shared space environments.

Chapter 9 is the final chapter of this thesis and summarises the research findings. The contribution of the thesis to science and practice is summarised. Finally, future work resulting from the limitations of this new mathematical model is suggested and discussed.

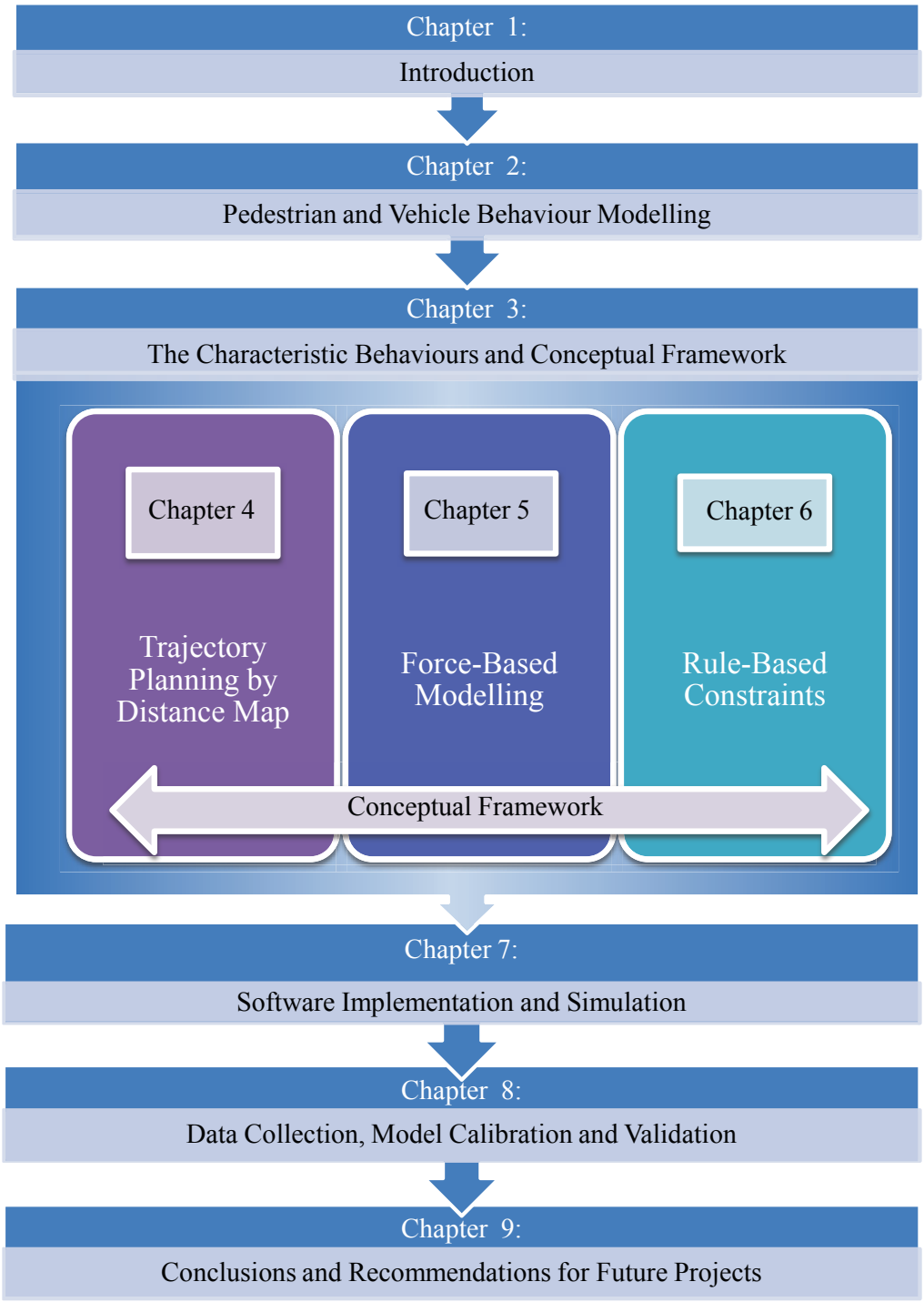

Figure 1.2: Outline of this thesis

Chapter 2

Pedestrian and Vehicle Behaviour Modelling

This chapter describes the state-of-the-art in vehicular traffic, crowd dynamic and mixed traffic modelling. In order to define a theoretical foundation of a unified approach for reproducing a shared space behaviours, vehicular traffic and pedestrian modelling methodologies are classified into phenomenological and generic models. The former develop relevant behavioural features to explain a specific case. Generic models cover different behavioural features to show classes of observed phenomena. The existing generic models on vehicular traffic, crowds and mixed traffic are reviewed and compared based on the relevant observed phenomena that they can reproduce. There are three modelling scales: microscopic, mesoscopic and macroscopic. This thesis focuses on the microscopic scale which defines the behaviour of an agent based on traffic characteristics such as individual location, velocity and interaction over time. Taking into account known traffic and crowd phenomena, it is determined that force directed models are capable of capturing essential crowd phenomena. These models can be applied to vehicular traffic and adapted to describe the lateral movement of vehicles in shared spaces. The Social Force Model (SFM) is chosen as a basis for modelling the behaviour of shared space users.

2.1 Modelling Methodologies

Representing vehicular traffic and pedestrian motion requires a model capable of simulating the interactive behaviours and phenomena that might emerge during traffic flow and crowd movements. The two main types of methodology for modelling are:

- Phenomenological Models: These models are developed to reproduce one specific phenomenon realistically. Phenomenological models attempt to show that developing certain relevant features is sufficient to explain that phenomenon. These models are also referred to as "one shot" approaches [46].

- Generic Models: This category models relevant rules of local interaction that lead to classes of observed phenomena. For instance, in the case of crowd behaviour, speed and direction changes for short distance avoidance can be modelled to result in lane formation, freezing by heating, oscillation, and the faster-is-slower effect.

Section 2.2 presents self-organising phenomena observed in crowds and vehicular traffic flow. Different generic modelling scales are explained in Section 2.3. Existing vehicle, pedestrian and mixed traffic models at the microscopic scale are reviewed in Section 2.4. In Section 2.5, the reviewed microscopic models are then compared according to well-known vehicular traffic and crowd phenomena to identify the best one for modelling the motion of pedestrians and cars in shared space areas.

2.2 Modelling Phenomena

This section includes different dynamical patterns in crowds and vehicular traffic flow. The literature identifies six crowd self-organisation phenomena and three

types of vehicular traffic flow phenomena. Self-organisation is when collective behaviours occurs spontaneously as a result of the interaction of many agents without the interference of external influences [47]. The well-known crowd phenomena are classified as below:

Lane Formation: Lane formation occurs when two crowds of pedestrians walk towards each other from opposite directions. In order to avoid collisions, pedestrians change their walking direction toward one side (see Section 7.4.1). The effect is caused by pedestrians, walking in the same direction, lining up behind each other to form a number of lanes. Lane formation reduces the frequency and strength of avoidance behaviour. The street width, pedestrian density and fluctuation level lead to a number of lanes. This effect can be reproduced by defining a collision avoidance behaviour in which pedestrians are moving in opposite directions [48, 49].

Stripe Formation: Stripe formation can be described as lane formation with a different angle from 180 degrees. It occurs when crowds intersect at an arbitrary angle [50]. As a result of this effect, pedestrians walk through the intersecting pedestrian stream and do not necessarily stop.

Freezing by Heating: This effect occurs in computer simulation when the lane formation effect breaks down due to a high density of pedestrians (agents). The flow of pedestrians slows and clogging occurs, resulting in a complete halt [49] (see Section 7.4.2). This immobility of pedestrians (freezing) is caused because many pedestrians are attempting (heating) to move towards the same destination. In this case, a pedestrian (agent) has no control over the movement and local force based interactions between pedestrian bodies [51]. However, an entire halt is usually not permanent in a real scenario as body turns (shoulders) often allows

pedestrians getting out of a deadlock [52].

Oscillation: Oscillatory flows at bottlenecks arise when pedestrians move in opposite directions and pass through a bottleneck, i.e. a narrowing of a passageway. When it is not possible for groups of pedestrians to pass each other at the bottleneck, crowds line up on both sides of the bottleneck, trying to push through. This results in an oscillatory flow when small groups of pedestrians will pass through in one direction, making room for a small group to pass through in the other (see Section 7.4.3). This flow continues until the pressure of the other side stops the flow. A short period of balance occurs until another few pedestrians reach the other side. This can be seen as oscillations in the measured flow rate in each direction and has been seen in both simulations and real life observations [49].

Faster-is-Slower: This effect appears when a crowd of pedestrians tries to exit through a narrow passageway. When pedestrians become impatient and attempt to move faster (e.g. in panic situations), a longer time is required for all pedestrians to leave the room. This is because pedestrians block each other on the way out and the physical interaction slows down the evacuation of the crowd [53], [47] (see Section 7.4.4). Waiting, therefore, often helps to speed up the average evacuation time.

Herding: When there is an unclear situation, individuals follow each other instead of going along their most optimal path. This behaviour has been observed in stressful evacuation situations in [49].

Some observed vehicle traffic flow phases are as follows [54, 55]:

Free Flow: This traffic phase occurs in regions with low to medium density and

low interactions between vehicles. The average velocity is constant in the free flow phase [56].

Synchronised Flow: A medium and high density of traffic can result in free or jammed flow which is defined by interactions between vehicles.

Wide-moving Jam: This traffic phase happens when an increase in the density of traffic results in a decrease in flow. The flow is then mainly controlled by density fluctuations.

In the transition between different traffic phases, some self-organised phenomena emerge, as explained below:

Traffic Hysteresis: This phenomenon emerges in the transition between free flow and synchronised flow phases. It also occurs during the transition between synchronised flow and wide-moving jam phases, which shows the instability of traffic [57]. Traffic hysteresis occurs because drivers behave differently in various traffic phases when accelerating or decelerating.

Capacity Drop: Congested regions are usually followed by a capacity drop [58, 59]. Drivers seem to prefer larger time headways when their local traffic is unstable [60].

Stop-and-go Wave: This feature can be observed when the density of vehicular traffic is high and traffic movement breaks down. In stop-and-go flow, drivers stop and wait for free space in front of them to continue moving. No frequency is characterised for a stop-and-go traffic wave [61].
The application of a mathematical model can be improved by calibration and

validation. However, the application of a mathematical model is influenced to a great extent influenced by the key characteristics of the mathematical model and its simulation scheme. The modelling scales in traffic flow and crowd dynamics are explained in the following section.

2.3 Generic Modelling Scales

The simulation of vehicular traffic and crowds models has increased over the last decades to investigate their applicabality. There are a large number of different modelling approaches and model applications for vehicular traffic flow [55, 61–70] and crowds [71–98]. These models can be classified into three scales with respect to the level of detail in the modelling of the behaviour of road users: microscopic, mesoscopic, and macroscopic [99, 100]. The microscopic scale identifies the state of the system according to the behaviour of each road user and is defined by traffic characteristics such as individual position, velocity and interaction over time. Macroscopic studies do not differentiate road users and aggregate road user movements into flow, average speed and density. These models are capable of dealng with large networks, whereas microscopic models provide more detailed analysis of road users' interactions. Mesoscopic traffic models, meanwhile, are aimed at balancing the computational task and realism of macroscopic simulation properties (intermediate between the microscopic and the macroscopic). The state of the system is described by the location and velocity of the microscopic individuals, but they are demonstrated for instance, by a probability distribution. In this thesis, modelling approaches at the microscopic scale are reviewed since the aim is to create a new microscopic shared space model.

The mathematical descriptions applied for rendering vehicular traffic, crowd dynamics and mixed traffic at the microscopic scale are explained in Section 2.4.

Section 2.2 explained the ability of models to reproduce observed common motions and emerging behaviours in traffic flows and crowds. In Section 2.5, all the modelling approaches are outlined and their advantages and disadvantages described with respect to the requirements for modelling mixed traffic in shared space environments.

2.4 Microscopic Models

In microscopic models (see Figure 2.1), the state of the system is described by the location, velocity and acceleration of each road user. Hence, the behaviour of pedestrians or vehicles is modelled independently and their complex interactions are captured by physical and/or physiological terms. Section 2.4.1 explains the available traffic flow models at the microscopic level. This is followed in Section 2.4.2 by a review of the existing crowd models. Section 2.4.3 reviews available mixed traffic models for pedestrian-vehicular interactions, which is particularly important for modelling shared spaces.

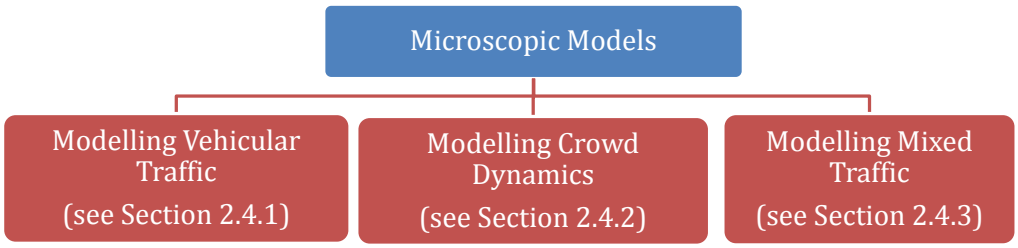

Figure 2.1: Microscopic models categorisation

2.4.1 Modelling Vehicular Traffic

Drivers' basic tasks can be classified in to the longitudinal and lateral control of vehicle's movement along and across the road or lane. The longitudinal control is achieved by adjusting vehicle speeds and the lateral control is accomplished by

an optimal choice of steering angles. These tasks are both interdependent. Different microscopic models alter in their assumptions on the interaction of vehicles. Mathematical models for traffic flow have a structure similar to Newtonian dynamics. They describe the acceleration of vehicles based on the behaviour of the nearby vehicles. For instance, various traffic models relate acceleration of vehicles to the behaviour of the leader, namely the vehicle ahead, and the complexity of the description of acceleration over time varies in different mathematical models. Drivers adjust their position and speed of their vehicles based on the behaviour of road users in their visibility zones.

Microscopic models (see Figure 2.2) are commonly used to estimate macroscopic quantities such as average velocity or density. Hence, macroscopic quantities are recovered from the local averages of the microscopic state of agents. The macroscopic quantities are averaged over a certain time period over an area or at specific position over a given time period.

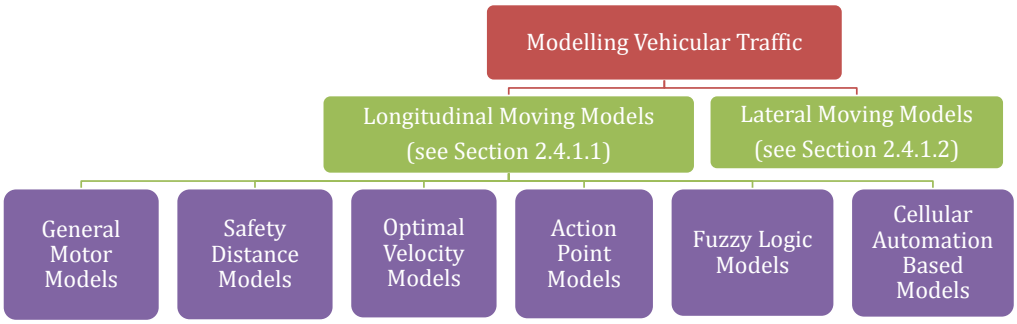

Figure 2.2: Microscopic models for describing traffic flow

In this section, the microscopic models describing traffic flow behaviours are divided into two categories: longitudinal and lateral moving models, as shown in Figure 2.2. These models are discussed in detail in Section 2.4.1.1 and Section 2.4.1.2.

2.4.1.1 Longitudinal Moving Models

Microscopic traffic models assume that the acceleration of a vehicle γ is dependent on nearby vehicles and that the dominant influence on driving behaviours is caused by the vehicle ahead $(\gamma - 1)$ [99]. The model of vehicle behaviour is generally modelled as follows [61]:

$$\frac{d\boldsymbol{v}_\gamma(t)}{dt} = \boldsymbol{f}_\gamma^0 + \boldsymbol{f}_{\gamma(\gamma-1)}^{repulsive}(\boldsymbol{v}_\gamma(t), \Delta\boldsymbol{v}_\gamma(t), s_\gamma(t)) \tag{2.1}$$

where $\boldsymbol{f}_\gamma^0$ is the driving force towards the destination. Repulsive force $\boldsymbol{f}_{\gamma(\gamma-1)}^{repulsive}$ describes the effect of the vehicle ahead $(\gamma - 1)$ on vehicle γ as a function of the velocity $\boldsymbol{v}_\gamma(t)$, the relative velocity $\Delta\boldsymbol{v}_\gamma(t) = \boldsymbol{v}_{\gamma-1}(t) - \boldsymbol{v}_\gamma(t)$ and the space headway $\Delta x_\gamma(t) = x_{\gamma-1}(t) - x_\gamma(t)$ or clearance $s_{\gamma-1}(t) = \Delta x_\gamma(t) - length_{\gamma-1}$.

The traffic-dependent velocity that a driver γ tries to adapt is defined in Equation 2.2 [61].

$$\boldsymbol{v}^e(\boldsymbol{v}_\gamma(t), \Delta\boldsymbol{v}_\gamma(t), s_\gamma(t)) = \boldsymbol{v}_\gamma^0 + \tau\boldsymbol{f}_{\gamma(\gamma-1)}^{repulsive} \tag{2.2}$$

Equation 2.1 can be simplified to [101]:

$$\frac{dv_\gamma}{dt} = \frac{\boldsymbol{v}^e(\boldsymbol{v}_\gamma(t), \Delta\boldsymbol{v}_\gamma(t), s_\gamma(t)) - \boldsymbol{v}_\gamma}{\tau} \tag{2.3}$$

Models of the type of Equation 2.3 are called car-following models [61, 102, 103]. The different types of car-following models are described below.

General Motor Models

The General Motor Model (GMM) was first proposed by Chandler et al. [102] based on vehicle's relative velocity: each driver keeps up with the speed of the front vehicle. In Equation 2.4, the acceleration of the vehicle at time $(t + \tau)$ (τ is the driver's reaction time) is dependent on the velocity difference of the two

successive vehicle ($\boldsymbol{v}_{\gamma-1}(t) - \boldsymbol{v}_{\gamma}(t)$).

$$\frac{d\boldsymbol{v}_{\gamma}(t+\tau)}{dt} = k_s \cdot [\boldsymbol{v}_{\gamma-1}(t) - \boldsymbol{v}_{\gamma}(t)] \tag{2.4}$$

Thus, a car-following relationship is defined so that the velocity of each vehicle adapts to its nearby stimuli. A major limitation of this model is the use of a constant sensitivity coefficient k_s for all situations [104]. This model is not able to describe stop-and-go waves since in these situations the behaviour of drivers does not depend on the relative distance between vehicles. Gazis et al. [103] proposed a more realistic model by incorporating the space headway $\Delta x_{\gamma}(t)$ between the leading and following vehicles in Equation 2.5. This model reproduces stop-and-go waves but also causes accidents.

$$\frac{d\boldsymbol{v}_{\gamma}(t+\tau)}{dt} = k_s \cdot \frac{\boldsymbol{v}_{\gamma-1}(t) - \boldsymbol{v}_{\gamma}(t)}{\Delta x_{\gamma}(t)} \tag{2.5}$$

Edie [105] modified this model by considering the vehicle velocity $(v_{\gamma}(t))^{m_e}$ as an influencing factor on driver behaviours in Equation 2.6 in order to avoid accidents.

$$\frac{d\boldsymbol{v}_{\gamma}(t+\tau)}{dt} = k_s(\boldsymbol{v}_{\gamma}(t+\tau))^{m_e} \frac{\boldsymbol{v}_{\gamma-1}(t) - \boldsymbol{v}_{\gamma}(t)}{(\Delta x_{\gamma}(t))^{l_e}} \tag{2.6}$$

Here, $m_e > 0$ and $l_e > 0$ are constant parameters. In this model, only some parameters are linked directly to the identifiable characteristics of drivers. Many researchers have attempted to find the best combination of m_e and l_e with contradictory results [63, 106, 107]. This uncertainty regarding the parameter values makes the validation of this model challenging. The manoeuvres of vehicles are highly sensitive to the local stimulus while the parameters vary between traffic conditions. The follower reacts to actions of its leader even within a large distance. Moreover, the follower response disappears as soon as the relative speed reaches zero. Therefore, some models are not attractive for realistic description of the dynamic state of vehicles [108]. Furthermore, the model does not distin-

guish drivers with different preferred velocities. In addition, they do not consider the interaction between the longitudinal headway and lateral position, which is required for simulation of vehicles in shared space areas.

Safety Distance Models

Safety Distance Models (SDMs) (or collision avoidance models) aim to maintain a safe headway to the front vehicle. The vehicle adjusts its speed to the safety distance in order to avoid a rear-end collision as shown in Equation 2.7 [63].

$$\Delta x(t-\tau) = \vartheta_l v_{\gamma-1}^2(t-\tau) + \rho_1 v_\gamma^2(t) + \rho_2 v_\gamma(t)\theta_0 \tag{2.7}$$

where $\vartheta_l, \rho_1, \rho_2, \theta_0$ are constant coefficients. A major limitation of the SDM is its inability to handle unexpected movements of preceding vehicles. Collisions are unavoidable if the distance is smaller than the safety distance as a result of a sudden deceleration of a vehicle ahead. To overcome this issue, Gipps [109] developed a model including safety features e.g. considering reaction times. The parameters of this model (such as speed and acceleration) can be determined from real data since they correspond to realistic driver behaviour. Some latent and unobservable parameters (such as reaction time, safety reaction time and safety headway margin) need to be calibrated, however. The advantage of Gipps' model is that it represents the propagation of disturbances well and is easy to modify. In reality, however, a driver might react to the behaviour of several preceding vehicles and this is not captured in the Gipps model [63]. In addition, Gunay [110] integrated the lateral offset of the following vehicle into Gipps' model and presented a two-dimensional movement of car-following behaviour.

Optimal Velocity Models

Bando et al. [111] proposed the Optimal Velocity Model (OVM) assuming that drivers aim for a safety velocity determined by a safety distance to the leading

vehicle. In Equation 2.8, the acceleration of each vehicle is defined as a function of the space headway $\Delta x_\gamma(t)$ and vehicle speed $v_\gamma(t)$.

$$\frac{dv_\gamma(t)}{dt} = k_s[V(\Delta x_\gamma(t)) - v_\gamma(t)] \tag{2.8}$$

Here, $k_s > 0$ is a constant sensitivity coefficient. $V(\Delta x_\gamma(t))$ is the optimal speed function, a monotonically increasing function of the space headway as presented in Equation 2.9.

$$V(\Delta x_\gamma(t)) = 0.5 v_{max}[tanh(\Delta x_\gamma(t) - d_c) + tanh(d_c)] \tag{2.9}$$

v_{max} is the maximum speed of a vehicle and d_c the safe distance. In 1998, Bando et al. [112] modified the OVM by taking the reaction time τ into account (Equation 2.10).

$$\frac{dv_\gamma(t+\tau)}{dt} = k_s[V(\Delta x_\gamma(t)) - v_\gamma(t)] \tag{2.10}$$

Helbing and Tilch [101] calibrated the OVM using empirical follow-the-leader data. They discovered that the OVM results in high acceleration and unrealistic deceleration, with the unrealistic values of the latter not avoiding accidents. A Generalized Force Model (GFM) [101] was proposed in the form of Equation 2.11 to show the impact of negative speed difference of successive vehicles when the leading vehicle is faster than the following one.

$$\begin{gathered} \tfrac{dv_\gamma(t+\tau)}{dt} = k_s[V(\Delta x_\gamma(t)) - v_\gamma(t)] + \lambda_s \Delta v_\gamma \Theta(\Delta v_\gamma), \\ \text{where} \begin{cases} \Theta(\Delta v_\gamma) = 1, & \text{if } (\Delta v_\gamma) > 0) \\ \Theta(\Delta v_\gamma) = 0, & \text{otherwise} \end{cases} \end{gathered} \tag{2.11}$$

Here, $\lambda_s > 0$ is a sensitivity coefficient.

In [101], the results retrieved by simulation were equivalent to empirical data. The GFM only considers the effects of a negative speed difference between leading and following vehicles. When the preceding vehicle is faster, however, the following vehicle may not decelerate, even if the relative gap is smaller than the safety distance. The Intelligent Driver Model (IDM) is an adaptation of the GFM and defines acceleration as a continuous function of speed, speed difference and headway [113]. This model is able to generate accident-free traffic with realistic acceleration and deceleration behaviour. It can also reproduce the capacity drop.

Since drivers do not only pay attention to the headway of one but also of a number of vehicles, using Intelligent Transport Systems (ITSs), Ge et al. [114] proposed a differential equation of motion (Equation 2.12) to include the headway of an arbitrary number of vehicles ahead.

$$\frac{dx_\gamma(t+\tau)}{dt} = V[\Delta x_\gamma(t), \Delta x_{\gamma-1}(t), \cdots, \Delta x_{\gamma-n+1}(t)] \tag{2.12}$$

in which n denotes the number of vehicles ahead. On the other hand, recognising that vehicle deceleration capability is higher than acceleration, Gong et al. [115] defined an Asymmetric Full Velocity Difference Model (AFVDM) for car-following processes in the form of the GFM in Equation 2.13.

$$a_\gamma(t+\tau) = k_s[V(\Delta x_\gamma(t)) - v_\gamma(t)] + \lambda_{s1}\Delta v_\gamma \Theta(\Delta v_\gamma) + \lambda_{s2}\Delta v_\gamma \Theta(-\Delta v_\gamma) \tag{2.13}$$

$\lambda_{s1} > 0$ and $\lambda_{s2} > 0$ are sensitivity coefficients to support sufficient acceleration and deceleration. Ge [116] also improved the unrealistic high deceleration caused in the FVDM by considering the velocity difference of two vehicles ahead.

In both the GFM and FVDM, a large velocity difference of successive vehicles

has a significant effect on traffic behaviour (e.g. the reaction of a moving vehicle to standing vehicles in front). However, if the successive vehicles have the same speed and the velocity difference is small, the follower may not react correctly to a sudden deceleration of the leader in order to avoid collision. Hence, Zhao et al. [117, 118] claimed that acceleration differences should be considered for modelling traffic dynamics. They proposed the Full Velocity and Acceleration Difference Model (FVADM) by taking the acceleration difference into account. Their numerical investigations show that no accident occurs and the decelerations are realistic.

Most car-following models consider the headway or velocity difference of two successive vehicles. As mentioned earlier, in reality, the following driver may react to multiple preceding vehicles. Hence, Xie et al. [119] (cited in [107]) developed the Multiple Headway and Velocity Difference Model (MHVDM) which considers both the headway and the velocity difference of multiple vehicles ahead. Their numerical investigations reveal a smaller value for the best sensitivity coefficient in the MHVDM and the stable region cover a wider range in comparison to the FVDM [119] (cited in [107]).

Another version, the Multiple Ahead and Velocity Difference Model (MAVDM), is proposed by Sun et al. [120] by considering key factors of other vehicle models and distinguishing the extent of multiple vehicles.

Action Point Models

Action Point Models (APMs) are also called physiology-psychology models as thresholds are defined for behaviour changes. These models assume that drivers control their acceleration according to changes in relative speed in order to retain their safety distance (Figure 2.3). When a car driver is approaching a slower

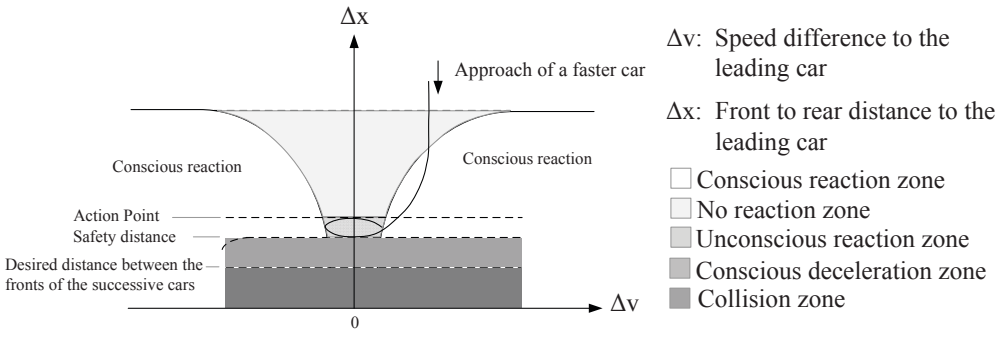

Figure 2.3: A psycho-physical car-following model [121]

leading car some reactions are made unconsciously and some consciously. The action point of conscious reactions depends on the speed difference to the leading car, relative distance to the leading car and driver's behaviour. Hence, car following behaviour is defined in four stages with its oscillating process in this type of models (see Figure 2.3).

Michaels [122] first proposed a physiology-psychology car-following model. The basic approach is to attempt to describe the features of daily driving behaviour but since most of the perceptual thresholds in these studies are derived arbitrarily from the human factors literature it is not possible to prove or disprove the validity of these models [63]. APMs are, however, able to represent the phenomenon of oscillation observed in many studies [123], and have been employed in a number of traffic simulation packages such as PARAMICS and VISSIM. Some models, such as Simulation of TRAnsport Systems (SITRAS) [124] use the concept of APMs to address traffic flow with lane changing.

Fuzzy Logic Models

In Fuzzy Logic Models (FLMs), vehicle manoeuvres are dependent on the perception of a driver to a situation ahead. The concept of fuzzy logic covers the observation, thinking, understanding, and decision-making process of drivers [63,

106]. It is assumed that drivers do not know the exact speed of and distance to other vehicles. For instance, the speed of a front vehicle is categorised as low, moderate or high and a decision is made according to assigned rules. The first fuzzy-logic model was proposed by Kikuchi and Chakroborty [125]. In this model a driver is assigned as a fuzzy controller whose input is the status of the preceding vehicles ($\Delta x, \Delta v$ and a_{n+1}) divided into multiple 'fuzzy sets'. The output is a decision made through a membership function, e.g.:

$$\begin{aligned} &\text{IF } \Delta x =' Adequate', \\ &\text{THEN } a_{n,i} = \frac{(\Delta v_i + a_{n+1,i} x \tau)}{\gamma_t}, \end{aligned} \tag{2.14}$$

where τ is the reaction time and γ_t is the expected time of a driver to reach the leading car. In order to represent real traffic situations, many rules need to be defined for the fuzzy logic model which limits the application of this model to complex situations.

Cellular Automation Models

Nagel and Schreckenberg [126] simulate freeway traffic with a stochastic discrete automation model, which they called the N-S model, although it is also commonly known as the Cellular Automata Model (CAM). In [126], the model is defined as a one-dimensional array of L cells with boundary conditions. A vehicle occupies a cell and its speed is between zero and v_{max}. Four consecutive steps (acceleration, deceleration and randomisation and movement updates) are defined for each update of a system for all vehicles according to the boundary conditions. Further research was undertaken on cellular automation of traffic flow [127–129] based on the N-S model. Jia and Ma [130] claimed that the N-S model represents a discrete type of the OVM. The CAMs are capable of representing lane-based homogeneous vehicular traffic where the speeds are higher than $80\ \frac{\text{km}}{\text{h}}$ [131]. Although changing the time intervals allows a reduction in the

speeds, it makes measurement of microscopic aspects of the flow difficult. In the case of heterogeneous traffic, there is no strict lane discipline, and smaller vehicles move side by side along the road.

In summary, car-following theories relate the acceleration of a vehicle to perceived stimuli by considering the desired velocity, velocity difference, and distance to the leader. Each of the models could fit one particular traffic application well. The requirements for a car following model differ according to the application of that model. For instance, the requirements to generate macroscopic outputs, such as average flow and speed, are less stringent than those for generating microscopic outputs such as individual speed and trajectory. In order to simulate driver behaviour in a shared space environment, a highly detailed database of vehicle trajectories would be required so as to develop a model that fully captures the related characteristics.

2.4.1.2 Lateral Moving Models

Lateral movement of vehicles consists of a process of lane selection and movement execution without interfering with vehicles in the destination lane. Lane changing behaviour can be either mandatory or discretionary [132]. A mandatory lane change occurs when it is essential, whereas a discretionary lane change happens to improve the perceived driving conditions. Lane-changing models describe lateral movements of vehicles by lane selection and Gap Acceptance Models (GAMs). These two types of models are introduced below.

Lane Selection Models

Lane selection behaviour is modelled according to the motivation of drivers. For instance, lane changing behaviour takes place because of an unsatisfactory driving condition in the current lane and a good driving condition in another lane.

Different types of motivations may lead to different specifications of the lane selection models. The models can be divided into two categories according to the decision behaviour: the deterministic rule-based and random utility. The former assigns a set of rules to describe choice behaviour. For instance, Sparmann (cited in [132]) linked the lane-changing behaviour to locations of obstructions with psychophysical thresholds. Fritzsche [133] defined lane-changing behaviour based on thresholds for speeds and headways. Gipps [134] developed a lane-changing model by using a set of decision rules. Drivers select a lane according to their prioritisation of these rules. Oketch [135] and Hidas [124] used fuzzy logic rules to describe lane-changing decisions. Wei et al. [136], meanwhile, conducted an empirical study and developed a set of decision rules to model lane-changing behaviour in two-lane urban arterials. Lane-changing behaviour is linked to the distance to intended turns and headways. Thresholds of headways are estimated by using vehicular trajectory data. The parameters of these rule-based models are rarely calibrated due to the model structure, while the decision rules are developed according to observations. Being easily adjustable, these models are capable of application to complex environments. There is no solid framework for calibrating model parameters, however, and interactions between different rules are not considered in these models [132].

In random utility models, the lane-changing behaviour is defined as a sequence of decision-making processes in which three steps are involved [137]: making a decision for changing the lane, choosing the target lane and considering the gap acceptance in the target lane. The calibration processes of these models are conducted by the maximum likelihood approach, for instance according to vehicular trajectory data [137]. The random utility model is suitable for describing the lane selection process because it executes discrete choices based on the competition between utilities of driving on different lanes. The model specification and calibration process for a random utility model is resource intensive, however. Also,

it is still not clear whether its model parameters are transferable. Random utility models are therefore currently not appropriate for large scale urban networks with complicated contexts.

Gap Acceptance Models

After selecting a lane to continue driving, drivers should evaluate whether the gap between the lead and lag vehicles in the selected lane is acceptable. When applying gap acceptance behaviour to the lane-changing manoeuvre, both the lead gap (the gap to the oblique front vehicle in the target lane) and the lag gap (the gap to the oblique rear vehicle in the target lane) are important factors. Basic gap acceptance models were formulated as a binary choice problem and determined gap acceptance behaviour by comparing the available and critical gap. Herman and Weiss [138] assumed that the critical gap was exponentially distributed. The influence of different factors upon the gap acceptance behaviour of drivers has been discussed in many studies. For instance, Daganzo [139] used a multinomial probit model to estimate parameters. His model considers variations of both the critical gaps and drivers. Mahmassani and Sheffi [140] found that the rejected gaps and critical gaps are depends since drivers get impatience. Madanat et al. [141] used queuing time to investigate the effects of impatience. Cassidy [142] indicated that the fit of the model could be improved by differentiating between the first gap from the subsequent ones, and the gaps in the inner lane from those in the outer lane. Other parameters affecting the gap acceptance behaviour are the type of manoeuvres, vehicles' speed, geometric characteristics and sight distances, intersections' control, the presence of pedestrians or police, and daylight [132]. Gipps [134] used the deceleration rate of the lag vehicle (the oblique rear vehicle in the target lane) as a threshold for gap acceptance behaviour. This threshold was calculated by the deceleration that the lag vehicle had to apply in order to react to the presence of the new preceding vehicle.

Ahmed [143] developed a discrete choice model, that allows different sets of parameters for both the mandatory and discretionary lane change situations. The former situation had lower critical gaps due to the fact that drivers under mandatory lane-changing conditions usually behave more aggressively. In congested traffic, the headways between vehicles are small. Thus, acceptable gaps may not be available. Under such circumstances, a successful lane-changing manoeuvre relies on cooperative driving. The factors that influence lane-changing behaviour are the lead relative speed, distance for lane-changing, the length of the gap and aggressiveness of a driver and its lag drivers [124, 143, 144].

In conclusion, the models discussed are developed considering lane-based environments for cars. Shared space users, however, travel according to virtual, rather than absolutely defined, lanes in their surroundings, and this difference should be taken into account.

2.4.2 Modelling Crowd Dynamics

In microscopic modelling of crowds, uni-directional and multi-directional flows are distinct (see Figure 2.4): uni-directional flows cause straight flows (flows rounding corners, flows entering a bottleneck or flows exiting a bottleneck); multi-directional flows, meanwhile, are either parallel or intersecting flows.

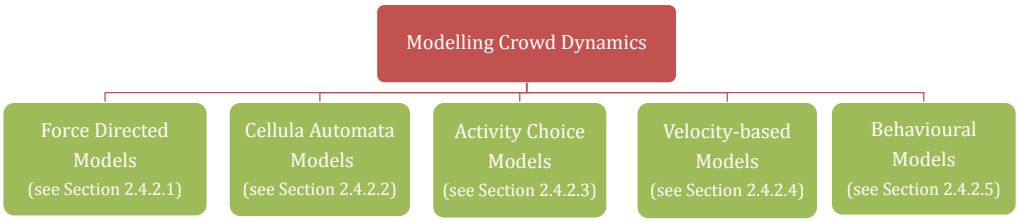

Figure 2.4: Microscopic models for describing traffic flow

A number of simulation models have been developed that include several areas in pedestrian motion, such as evacuation planning [145–156], pedestrian move-

ments in transit areas [88, 157, 158] and crowd interactions [72–74, 86, 87, 159, 160] have been studied. This section explains key features of various methodologies for modelling pedestrian movements. In the following subsections force directed, cellular automata, activity choice, velocity-based and behavioural models are discussed. Cellular automata are grid-based microscopic models with discrete dynamical systems. The force directed models are microscopic models with a continuous representation of space. In velocity-based models, pedestrians search for a free path through the crowd and avoid dynamic agents in their field of view. The behavioural models consider more strategic/social/psychological influences. The conceptual framework and the unique features of each type of models are reviewed.

2.4.2.1 Force Directed Models

In force directed models, pedestrians are modelled as particles subject to forces. The concept is that pedestrian movements are influenced by social forces exerted by other individuals and obstacles within their interaction range. The sum of all forces is numerically solved at discrete time intervals and it persuades the movement and direction, although the exact forces might differ between pedestrian models. The Social Force Model (SFM) was first implemented by Helbing [161] with Molnar [72] and Farkas and Visek [53] improving the fluid crowd modelling method of Henderson [75]. Later adaptations of the original SFM include a vision field [86, 162], collision offset [86] and group formation [163]. The model assumes that pedestrians face common situations. Pedestrians motions are more influenced by the macroscopic behaviour of crowds (e.g. free flow velocities) than the identical characteristics of individuals. In comparison to other models, the SFM is a realistic method for explaining various phenomena (such as self-organisation phenomena) that take place during pedestrian movements. The variables have physical meanings that can be calibrated and adjusted with respect

to a particular application [164]. However, the model focuses on the physical behaviour of individuals more than the traffic flow. Collision issues should be analysed separately for this model.

2.4.2.2 Cellular Automata Models

Cellular Automata Models (CAMs) divide space into a uniform grid of cells and consider pedestrians as entities (automata) in a cell moving according to localised occupancy rules and the status of neighbouring cells. Blue and Adler [77] proposed to model pedestrian movements using CAMs. The pedestrian decisions depend on the infrastructure, the status of the nearby pedestrians and static objects in the environment. Their direction of movement is assigned after solving all conflicts in each time interval.

Schadschneider [165] improved CAMs changing long range interactions into local interactions by introducing floor fields and integrated pedestrians' dynamic movement probabilities. The implementation of floor fields varies between different applications. In CAMs, all cells are updated at each time step which can be improved by sequential updating incorporating behavioural factors. The calculation of pedestrian velocities has also been adapted by extending stepping possibilities during each iteration [166]. Song et al. [167] adapted the stepping probability for friction between individuals. Changing properties of the grid itself is another means of modification. Alghadi et al. [168] changed the original CAM to a diffusion model allowing each cell to be occupied by more than one pedestrian. The CAM can be easily developed and implemented, although the results are sometimes contradictory to observed behaviours [164]. Its rules are simple and sufficient to capture essential behavioural changes in pedestrian dynamics [164] and this means that CAM simulation is computationally inexpensive [164]. The validity of simulations using Cellular Automata depends,

however, on the defined grid size [149].

2.4.2.3 Activity Choice Models

Activity choice models are combinations of a generalised SFM with a route choice and activity scheduling model [169]. These models are based on behavioural assumptions, activity sets and route choices in continuous time and space. Pedestrians observe the activity areas in their environment, consider their distance to their destinations and the travel times, and schedule their activities based on the dynamic traffic conditions under uncertainties. An activity choice model is implemented in the Nomad software [170]. In this microscopic simulation tool, pedestrians interact with each other and change their desired direction and velocity in order to perform their activities efficiently.

2.4.2.4 Velocity-based Models

Velocity-based models have been proposed in many studies [171–173]. This type of model predominantly simulates collision avoidance manoeuvres among static and dynamic agents which is similar to the Velocity Obstacle model of Fiorini and Shiller [174]. Velocity-based models are founded on the following behavioural heuristics:

1. A pedestrian moves along the most direct path to the destination considering any obstacles and infrastructure of the environment.

2. A pedestrian keeps a certain distance from obstacles or pedestrians along their path to the destination.

Individuals look for a path through a crowd in three steps: search for reachable space, investigatation of potential collisions with other neighbouring individuals, and judgment of the optimal path. The computational complexity can be decreased by reducing the set of movement options as in [173].

2.4.2.5 Behavioural Models

Behavioural models have been widely used to reproduce flocking behaviour of animals and virtual humans. Reynolds' local rules "boids" model is the most well known behavioural model [175]. In this model, each agent is implemented as an independent entity (boid) that moves according to the local rules of the dynamic environment. The flocking behaviour is defined according to the following basic rules (Figure 2.5):

- Separation: steering to avoid getting too close to neighbouring flock members.
- Cohesion: steering towards the average position of neighbouring flock members.
- Alignment: steering towards the average velocity of neighbouring flock members.

Local flock mates of a boid are defined based on its distance and direction of movement. Each boid not only avoids collisions with each other but also with obstacles. In addition to the explained rules, Reynolds [71] enhanced steering behaviours in the original boids model by building a three level hierarchy of action selection, steering and locomotion for a complex autonomous system.

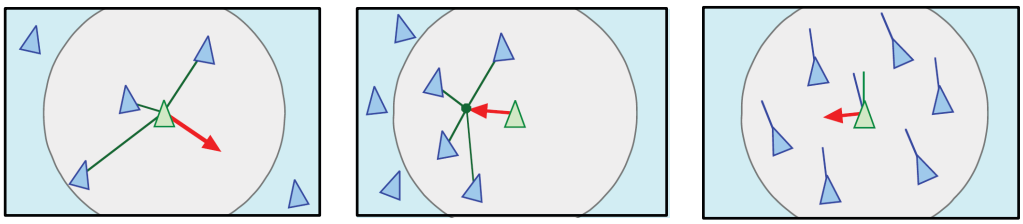

Figure 2.5: Reynolds' boids rules: (a) Separation, (b) Cohesion and (c) Alignment [71]

The particle swarm optimisation by Kennedy and Eberhard [176] is inspired by the Reynolds behavioural model. A "roost" is included in a simple Reynolds-like simulation with the following rules: all agents should be attracted to the location of a randomly placed roost, they should save the close proximity of the roost and share this information with their nearby agents. The agents do not know the exact location of the roost but they are aware of the coordinates of the swarm member with the closest position. Each agent compares its position both to its closest previous position during its movement (personal experience) and the closest position achieved by nearby agents over the past time steps (other's experience). At each time step, agents adjust their velocity in order to get closer to the actual location of the roost. Hence, the coordinates of the closest position to the roost will be achieved by the cooperation of all individual agents.

Robin et al. [92] proposed a model for pedestrians' short range behaviour. In this model, the acceleration and deceleration of pedestrians are minimised along the shortest path with a desired direction by evading close-by pedestrians and obstacles. In this model, the route choice model is calculated externally. It also includes spontaneous behaviour of pedestrians to lighting, social safety and shadows.

Wijermans [177] introduced a multi-level behavioural model for the strategic movement decisions of pedestrians. He simulated behavioural patterns of pedestrian according to an activity list by taking the social context into consideration. However, this dynamic relationship between pedestrians and their social context requires an operational movement model for simulation.

2.4.3 Modelling Mixed Traffic

Research on mixed pedestrian and driver traffic has largely focused on empirical studies instead of simulation models [178–181] and there are only a limited number of studies modelling the integration of vehicular traffic and pedestrians.

Among these studies, researchers have investigated interactions of pedestrians and drivers at the crossing points of streets: Li [182] proposed a statistical model for analysing field data on the street-crossing behaviour of pedestrians. He extracted different waiting time distributions for pedestrians before crossing the street. Among pedestrian and vehicle interaction models, Helbing et al. [49] analysed and formulated the interaction of pedestrians with vehicles at crossing sections with a force directed model. Pedestrian arrival rates and safety factors of pedestrian gap acceptance are the main factors in this proposed car-following model. Pretto et al. [183] used a combination of force directed and rule-based approaches for modelling interactions of pedestrians and vehicles at crossing points. Sun et al. [184] defined a gap acceptance model for pedestrian-vehicle interactions on a crosswalk. They proposed a deterministic gap acceptance model for pedestrians and a probabilistic gap acceptance model for drivers. A decision making process is modelled using a binary logit model. Sun et al. [185] developed a Pedestrian Crossing Behaviour Virtual Reality System (PCBVRS), based on the traffic microscopic simulation software, VISSIM, to study issues of pedestrian crossing behaviours. Wang et al. [186], meanwhile, used jaywalk data of pedestrians outside crossing facilities and developed a pedestrian gap acceptance model based on a discrete choice approach. Zhang and Chang [187] investigated the use of the CA model for simulating vehicle-pedestrian interactions. A conflict (competition) is detected when a cell is assigned as the target for multiple agents. In this case, the waiting time of an individual is considered as a factor on winning the competition. Ottomanelli et al. [188] proposed a gap acceptance model for interaction of pedestrians and vehicles at crossings. They used the CA model at crossing areas and derived interaction parameters from a probabilistic distribution. CA models make simulation of mixed traffic computationally efficient, since a rule set is applied over many time steps rather than finding solutions for differential equations. They are discrete in nature, however, and it

may be difficult to explain the cause of an unexpected macroscopic behaviour when it emerges from locally defined interaction. Pedestrian traffic is analysed in [189, 190] using VISSIM, where vehicle and pedestrian modes operate independently and are controlled by the traffic signals at potential conflicting areas with vehicle priority.

For shared space scenarios, the interaction of pedestrians and vehicles was modelled on the microscopic level by using the SFM for pedestrian behaviour, the single track model for car dynamics and a game theoretic force for solving conflicts in [8]. This is the only available shared space model which is very accurate and, as a result, computationally expensive. Therefore, there is a need to develop a mathematical model for the simulation of shared space schemes that provides practically feasible simulation results.

2.5 Summary

One fundamental difference between vehicle and pedestrian modelling is due to the dimensional space within which these agents move. In traditional traffic systems, vehicle flow is along lanes (roads) and lateral movements are described as lane changes. In reality, however, pedestrians interact in a two dimensional space either in a bounded domain or in the whole space. A common feature of pedestrian and vehicle modelling is their strategy to communicate. The mathematical model in this thesis for mixed traffic in shared areas should capture both these similarities and differences.

This chapter has reviewed key types of vehicle, pedestrian and mixed traffic models at the microscopic level. It presents a critical summary of the current state of the art of traffic and crowd motion models.

In Table 2.1, an assessment of General Motor, Safety Distance, Optimal Velocity, Action Point, Fuzzy Logic and Cellular Automata Models is made based on their parameters, calibration method, longitudinal and lateral movement representation, and capability to capture vehicular traffic flow phenomena. In terms of capturing vehicular traffic flow phenomena, the Optimal Velocity and Cellular Automata Models reproduce most of these kinds of phenomena. The conventional car-following and lane-changing models are developed based on the assumption of lane-based flow. In shared space schemes, however, there is neither a concept of lane discipline nor one of lane changing for vehicular traffic, since vehicles are allowed to move anywhere along the cross section of the road. The lateral position of the vehicles is, therefore, more likely to be a continuous variable rather than a discrete variable. Consequently, it is inappropriate to apply these conventional models to non-lane based mixed traffic flow in shared spaces. However, a combination of these approaches is a promising candidate for modelling non-lane based traffic in shared spaces.

Approach	Key Authors and Year	Parameters/Calibration	Movements		Phenomena		
			Longitudinal	Lateral	Traffic Hysteresis	Capacity Drop	Stop-and-go Wave
General Motor Models	Gazie et al. (1961) [103]	Arbitrary/Real Time Data Comparison	Yes	No	No	No	Yes
Safety Distance Models	Guay (2007) [110]	Physical Determination/Real Time Data Comparison	Yes	Yes	Yes	No	Yes
Optimal Velocity Models	Bando et al. (1995) [111]	Physical Determination/Real Time Data Comparison	Yes	No	Yes	No	Yes
	Helbing and Tilch (1999) [101]	Physical Determination/Real Time Data Comparison	Yes	No	Yes	No	Yes
	Treiber and Helbing (1999) [113]	Physical Determination/Real Time Data Comparison	Yes	No	Yes	Yes	Yes
Action Point Models	Michaels (1963) [122]	Arbitrary/Human Factor Literature	Yes	Yes	-	-	-
Fuzzy Logic Models	Brackstone and McDonald (1999) [63]	Physical Determination/Real Time Data Comparison	Yes	Yes	-	-	-
Cellular Automation Based Models	Nagel and Schreckenberg (1992) [126]	Physical Determination/Real Time Data Comparison	Yes	No	Yes	Yes	Yes

Table 2.1: Summary of microscopic vehicular traffic models

A comparison of Force Directed, Cellular Automata, Activity Choice, Velocity-based and Behavioural Models is made in Table 2.2 based on their parameters, calibration method, space and time representation, and capability to reproduce crowd phenomena. Building a crowd motion requires a model capable of represnting the behaviour of individuals and their interactions over time. This can be obtained on the microscopic scale [191]. Microscopic physics models are also capable of providing a realistic model for pedestrian interactions with their strong mathematical practice [192] and can explain behavioural changes in high densities [192]. The model used for crowd simulation should be capable of capturing essential crowd phenomena. As dicussed in this chapter, crowd models have a large computational burden, some have route choice problems between an origin and destination or cannot be used for scenarios that they are not calibrated for. An overview of the review in Table 2.2 shows that force directed models, and specifically the SFM of Helbing and Molnar [72], can describe the largest set of crowd dynamics. This model can be selected as the most suitable mathematical model for simulation of crowd motion.

In shared space, road users are perceived as individuals with their own characteristics and decision-making techniques. Modelling vehicular and crowd dynamics at the microscopic scale requires solving a number of equations that are computationally expensive. In addition, the microscopic information needs to have physical interpretations in order to be observed and measured. At present, vehicle following and gap acceptance rules govern microscopic traffic simulation within a lane-based system, while pedestrian modelling explains motions in a free two dimensional space. This review reveals that the literature does not provide a unified theory that can explain both vehicle and pedestrian movement, both separately and in interaction with each other.

			Representation		Phenomena					
Approach	**Key Authors and Year**	**Parameters/Calibration**	**Space**	**Time**	**Lane Formation**	**Stripe Formation**	**Freezing by Heating**	**Oscillation**	**Faster-is-Slower**	**Herding**
Force Directed Models	Helbing and Molnar (1997) [72]	Physical Determination/Real Time Data Comparison	Continuous	Discrete	Yes	Yes	Yes	Yes	Yes	Yes
	Xi et al. (2011) [163]	Physical Determination/Real Time Data Comparison	Continuous	Discrete	Yes	Yes	Yes	Yes	Yes	-
Cellular Automata Models	Song et al. (2005) [167]	Physical Determination/Real Time Data Comparison	Discrete	Discrete	Yes	Yes	Yes	No	No	Yes
	Sarmady (2010) [166]	Physical Determination/Real Time Data Comparison	Discrete	Discrete	Yes	Yes	Yes	No	Yes	Yes
Activity Choice Models	Hoogendoorn and Bovy (2004) [169]	Physical Determination/Real Time Data Comparison	Continuous	Discrete	Yes	Yes	Yes	-	Yes	-
Velocity-based Models	Moussaid et al. (2009) [171]	Physical Determination/Real Time Data Comparison	Continuous	Discrete	Yes	Yes	Yes	Yes	Yes	No
Behavioural Models	Wijermans (2011) [177]	Physical Determination/Real Time Data Comparison	Continuous	Discrete	-	-	-	No	-	No

Table 2.2: Summary of microscopic crowd dynamic models

Force-based models explain the acceleration of an object (a pedestrian) in two dimensions (bi-directional movements) as the resolution of forces exerted by neighbouring objects (other pedestrians, fixed obstacles) and the goal (destination). It is challenging to capture the complete range of crowd behaviours in one model but force directed models are able to reproduce all of the crowd phenomena. While there is considerable experience with simulating pedestrians using in particular the SFM, there has not yet been an attempt to model mixed traffic. The SFM, however, offers the possibility to model mathematically, not only pedestrians, but also vehicular traffic and their interactions with each other. The result of the literature review shows that the SFM is promising for realistic simulations of shared space dynamics. Constraining the dimensional movements in the SFM could potentially result in the opportunity to describe gap acceptance and a car-following model. One of the main advantages of this model is that its variables have physical interpretations that can be calibrated due to particular interactions [73, 164, 193–195]. In addition, "the Social Force Model gives the possibility to easily implement different behaviours or actions for the occupants by changing the desired direction and desired velocity."[1], thereby ensuring that even multi-directional flows can be captured.

[1] S. HeliÄovaara. "Computational Models for Human Behaviour in Fire Evacuations". In *Helsinki University of Technology, Department of Engineering Physics and Mathematics*, p. 10, 2007.

Chapter 3

The Characteristic Behaviours and Conceptual Framework

This chapter analyses pedestrian and driver behaviours in shared space environments. Pedestrians and drivers show specific manoeuvres when sharing space: obstacles have a guiding effect, pedestrians and drivers follow the shortest path to the destination according to the infrastructure of the environment, and equal priority can be observed. Agents move and interact with each other keeping a certain distance from other users and obstacles along the way to their final destination. Road users seem to be more conscious about their surroundings and avoid collisions. These extracted behaviour patterns lead to the conceptual framework for the model that will be proposed in this thesis, with three interrelated layers for modelling pedestrian and car motions in shared spaces: a global trajectory planning layer, an operational force-based model layer and a diplomatic rule-based layer. Furthermore, the geometrical model for pedestrians and cars in the shared space environments is introduced.

3.1 Introduction

Microscopic traffic simulation tools are often used to evaluate proposed traffic engineering approaches and Intelligent Transport Systems (ITSs) before implementation. The reliability of these tools depends on how realistically road user behaviour is modelled. A need to model heterogeneous traffic behaviour mathematically emerges due to its presence and growth in developed countries. Human behaviours partially result from the new environmental design concepts of shared space (see Section 1.1.1). In these schemes, there is a lack of lane discipline, as shown in Figure 3.1, and the traffic stream therefore consists of different pedestrian and vehicle performances: road users tend to adopt an active travel plan, make use of free space and exhibit characteristic movements which are distinct from the typical movements of homogenous traffic.

This chapter investigates mixed traffic behaviours in a single surface of shared space environments and addresses the possibility of describing the movement of pedestrians and drivers mathematically. The expected impact of shared space designs and observed behaviour of shared space users are reviewed in Section 3.2 and Section 3.3, respectively. An identification of characteristic behaviour patterns of pedestrians and cars in shared areas is provided in Section 3.4, leading to the conceptual framework for modelling shared space users. As concluded in Chapter 2, the Social Force Model (SFM) is sufficient for modelling the travel path and behavioural interactions of pedestrians and cars within shared space environments and forms the basis upon which a new mathematical model is built in this thesis. In this chapter, elementary behaviour patterns are considered mathematically.

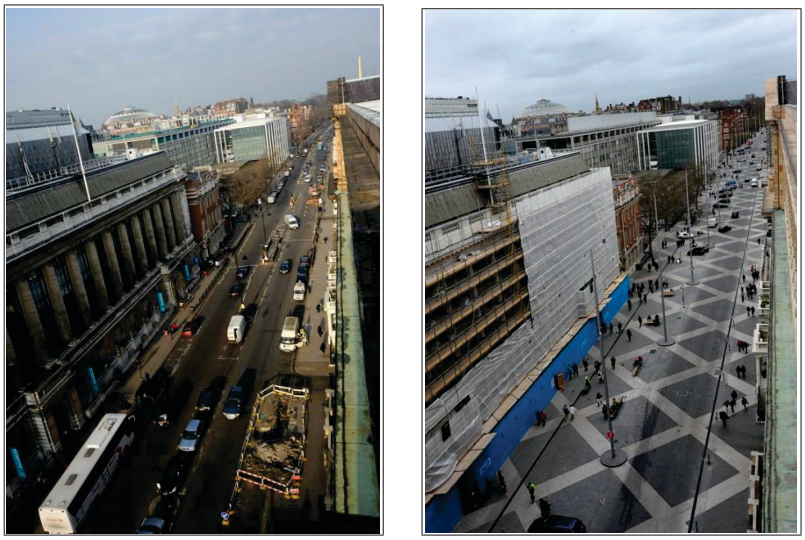

(a) (b)

Figure 3.1: Exhibition Road (London, UK) top view: (a) Previous design and (b) Shared space conversion [196]

3.2 Expected Impacts on Shared Space Users

The performance of a shared space can be defined on the basis of the effect it has on functionality, accessibility and flexibility of a public area. The UK Department for Transport (DfT) defines the following essential goals for a shared space scheme that needs to be attained by following the relevant performance indicators [25, 197]:

1. **Place Making:** Streets should invite road users to spend their time in the given public space with an attractive environment. This principle can be achieved by providing various street activities. The performance indicators include total time spent in the public space or person's 'dwell time', which is a measurement indicating that the public area is an origin/destination rather than a transit space. In addition, the usage of available amenities, kind of performed activities such as having lunches or socialising and the impression left on users are also included in the list of indicators.

2. **Pedestrian Focus:** This goal refers an area with higher priority of free movement for pedestrians that enables them to stroll across streets without restrictions. The performance indicators comprise of the pedestrian flow, the number of pedestrians and their density, their safety as well as perceptions.

3. **Driver's Behaviour Change:** Current superiority of vehicles within the traditional traffic space should be diminished. The amendment in this field should invite drivers to experience the feeling of being welcome in the public space. The performance indicators comprise of traffic volume and speed regulations, rise in commuting time within the zone and pragmatic space sharing behaviour.

4. **Safety for all Users:** Shared space should create an environment equally enjoyable for all users such as cyclists, elderly and young people. The aim of shared space is that road users co-exist harmoniously and reach a pleasant equilibrium in terms of priority. The performance indicators comprise of accident history, severity of sustained injuries and financial loss attributed to them, the population study of users and their perception.

3.3 Review of Behaviour Patterns in Shared Spaces

The influence of shared space on both drivers and pedestrians' behaviour is studied and assessed in [8, 13, 198, 199]. The operational assessment of selected shared space schemes provides a basis for making assumptions for reliable traffic simulation as summarised below:

Design Consideration: Different design elements can alter traffic performance in a number of different ways [8]. Street users evade trees, hedges, seats or poles. Landmarks such as kerbs, areas covered with grass and trees have a separating

and guiding effect on traffic behaviour. Points of interest like shops and seats attract road users. Stations of public transport are origins and destinations for vehicles and passengers. Entrances are primary origins and destinations of residents. Shops and restaurants are origin and destination points for pedestrians. Some elements such as shop windows attract people and invite people to stay for a while.

Desire Line[1] Analysis: The assessment of desire line shows that pedestrians movements are more distributed over shared space areas than traditional roads [198]. It has been conveyed by the UK DfT that the percentage of pedestrians walking through carriageway according to their desire line is between 80-100% in shared space areas [198] in contrast to areas which are considered to be more traditional such as London Road, Southampton or St. John's Road in London (UK) this percentage does not exceed 60% [198]. In other words, removal of separation barriers invites pedestrians and cars to share space. It has been also noted by the UK DfT that traffic flow has an influence on the pedestrian density on the carriageway [198]. In particular during low traffic, the usage of available space changes. Both pedestrians and cars make use of shortcuts that will shorten their commuting time [8].

Encounter Analysis: Bliek [199] examined the likelihood of cars stopping at intersections of conventional roads to that at redesigned shared spaces in Montreal. A study was conducted comparing two traditional crossings with two shared space areas, both with comparable size and amount of traffic. It was observed that drivers acknowledge the presents of pedestrians in the shared space areas more than the traditional crossings. This behaviour can be evoked by a number of aspects such as, for instance, the design of the area, speed restrictions, traf-

[1] A desire line is road users preferred path between two points which is often the shortest or the most convenient path between an origin and destination.

fic and crowd flow and density in encounters [198]. Shore et al. [198] reports that the design of the area is not considerably influencing the rate of encounters[2]. The objective of the study was to determine to which degree drivers are willing to give way and, perhaps, what kind of features influences drivers' desire to give way, based on the assumption that the sharing space ought to provide the 50-50 share of use. After analysing observational data from shared space schemes in the UK, it was reported that the number of encounters was mainly caused by the traffic and pedestrian flows. In 69% of the observed encounters between pedestrians and vehicles, pedestrians gave way. However, a 50% of giving way during encounters was observed on New Road (Brighton), Elwick Square (Ashford, Kent), Seven Dials (London) and High Street (Shrewsbury) [198]. In areas with speed limit, cars tended to give way to pedestrians more. Where the speed limit exceeded 25 $\frac{\mathrm{km}}{\mathrm{h}}$, the number of drivers giving way to pedestrians decreased dramatically. Interestingly, when pedestrians flocked, drivers felt more obligated to give way to a group, rather than to an individual.

Vehicle Speed Analysis: Traffic behaviour and safety in shared space is facilitated by speed limits [8, 198]. Reducing demarcations of the environment in an attempt to lower the division between footpath and carriageway spaces has some impact on encouraging drivers to reduce their speed. The analysis suggests that the speed of traffic has been mostly influenced by designing the space in totality: the higher the rate of space sharing between all users, the lower the traffic haste. In addition, less stop-and-go behaviour and more continuous movement of all modes are observed in shared spaces [8, 13, 198]. The mean and maximum speeds has declined following enforcement of designed in the shared space [8, 198].

[2]Encounters are defined as two road users trying to occupy the same space at the same time [198].

3.4 Elementary Considerations for a Shared Space Model

Shared space is a rarely implemented design concept which makes it challenging to determine particular behaviours. Shared space schemes also vary due to different cultures, design elements and traffic mixes. The behaviour analysis of Section 3.3 supports the argument that the intended objectives (see Section 3.1) of mixing traffic in shared space is established. In order to develop models of shared space and implement behaviours that are specific for shared space environments, the patterns that should be considered for mathematical modelling are:

1. Obstacles should be defined as a guiding effect on traffic behaviour of shared space users. Shared space users should follow the shortest path to their destination according to the static obstacles and infrastructure of the environment.

2. Encouraging all road users to share the available road space and balancing priority is a major objective of the shared space concept. The way pedestrians use space in shared space areas should be modelled by considering design characteristic (e.g. single surface) to reduce priority for car drivers and to increase priority for pedestrians.

3. Traffic calming and reducing stop-and-go behaviour is another objective of the shared space concept. Shared space should therefore, be modelled in totality (no lane discipline). In order to reduce traffic speed, road users should be modelled dynamically adaptive to the behavioural changes of others. The desired speed as well as the maximum speed should be defined according to shared space traffic rules and observations.

4. Shared spaces are designed to encourage motorised and non-motorised users to move freely in a two dimensional space. It is assumed that road users are more conscious about their surrounding and avoid conflicts. This

behaviour should be modelled by considering the traffic factors involved in encounters: road users speed, direction of movement, minimum distance from each other and density of vehicular traffic and crowd.

Given the design elements and specific behavioural patterns for shared space users, the following section explains the conceptual framework.

3.5 Methodology

The conceptual framework for modelling pedestrians and car motions in shared space environments is represented by three interrelated layers as shown in Figure 3.2. The first layer, the global trajectory planning layer, minimises the unnecessary detours of pedestrians and cars by calculating the shortest path to the final destination via intermediate destinations with respect to the infrastructure of the shared area (see Section 3.5.1). The second layer, the operational force based layer, uses the SFM and modifies it to generate individual trajectories of pedestrians and cars from their starting point following the shortest path. The road users are assigned with social/physical forces in this layer to reproduce their interac-

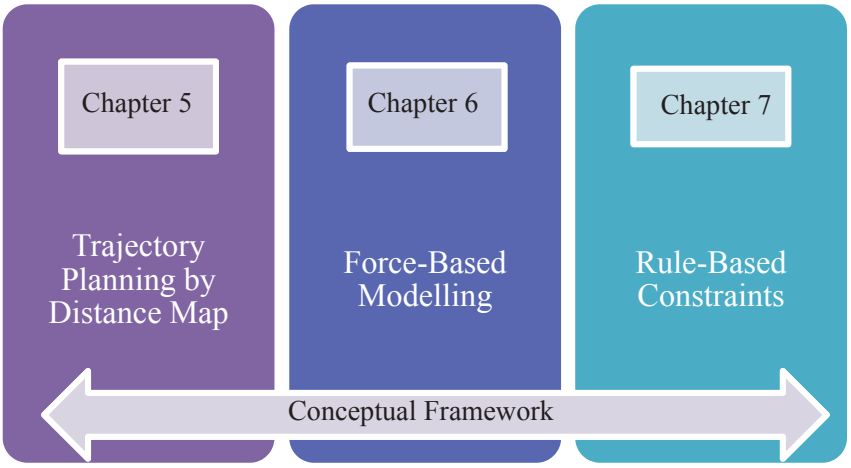

Figure 3.2: Conceptual framework

tion, their negotiation on the right of way and their obstacle avoidance behaviour (Section 3.5.2). In the third layer, the diplomatic rule-based layer, the motion limitation of car drivers is taken into account with a relationship between the steering angle and velocity. In case of potential encounters, rules are assigned to avoid collision (see Section 3.5.3). The geometrical model for simulating pedestrians and cars in all of the layers is described in Section 3.6.

3.5.1 Global Trajectory Planning Layer

Shared space users change their travel path based on the surrounding information (e.g. other agents or obstacles or the traffic condition). Road users plan their travel route according to static obstacles, not only within their interaction range, but also within their sight distance (see Figure 3.3). The task of making a shared space user to move from their present location to their destination location involves:

1. Finding an obstacle-free path from the current location to the goal according to the infrastructure of the activity area.

2. Making the shared space users move along the generated path.

The dynamic model of the second layer applies forces on the shared space users to drive the motion. Regarding the first task, the function of this layer is to calculate the shortest path to the destination for each agent with respect to the infrastructure of the shared area. Therefore, even though the operational model is primarily proposed to generate road user trajectories, the global trajectory planning layer minimises the deviation of agent paths towards their destination by assigning intermediate destinations [200]. Chapter 4 describes this layer, which is based on the flood field algorithm, in more detail.

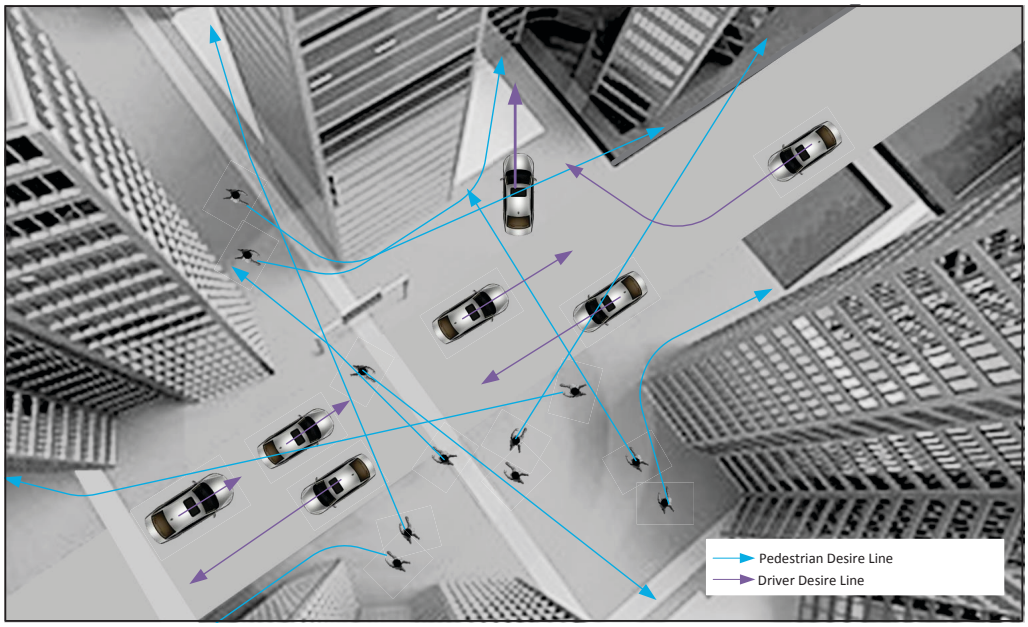

Figure 3.3: Trajectory planning of shared space users based on empirical data

3.5.2 Operational Force-Based Layer

Shared space user routes towards their final destination along the intermediate destinations may change depending on non-static obstacles and other (moving) agents. The function of the operational force-based layer is to generate the walking and driving manoeuvres that users are likely to perform under shared space conditions. As concluded in Chapter 2, the SFM is chosen for modelling road user behaviours because of its capability to produce the decision process, local route choice and collision avoidance activities with force fields. The SFM assigns equal priority to all road users, which supports the argument of negotiation on the right of way, and it provides constant agent movements. Since the original SFM by Helbing [161] only considers social/physical forces exerted by pedestrians or obstacles, the existence of cars in a shared space environment is expressed by socio-repulsive forces exerted by vehicles onto pedestrians and other cars. This force explains the most important interaction behaviour of a pedestrian which results in keeping a certain distance to cars as no physical inter-

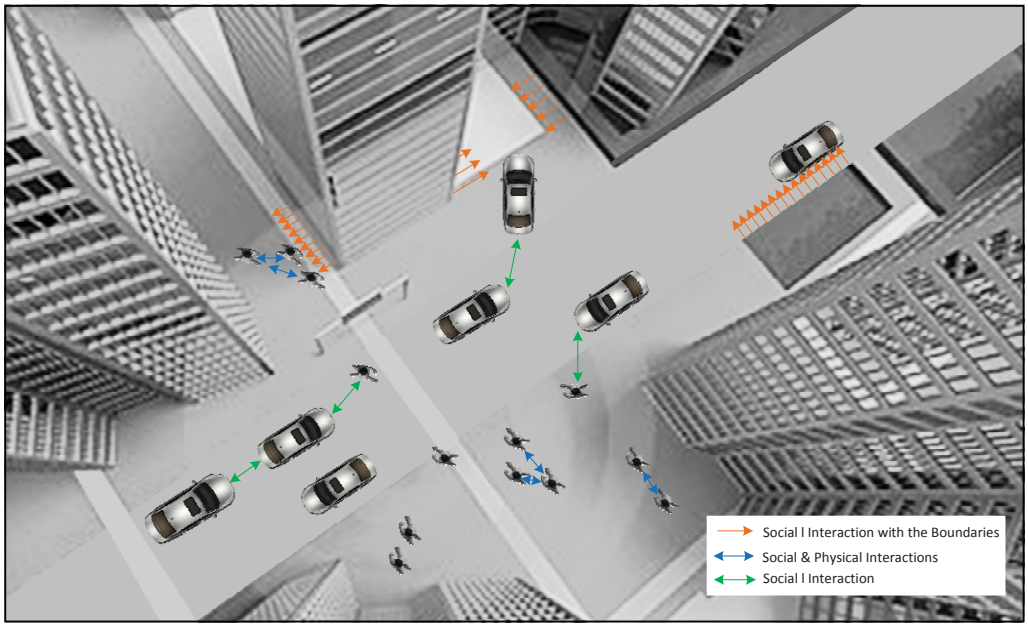

Figure 3.4: Social force model for shared space users

action should occur. In addition, socio-repulsive forces are added and exerted by obstacles, pedestrians and other vehicles onto vehicles [201] (see Figure 3.4). The momentary behavioural change of vehicles is described by a sum of different force terms considering both individual personal characteristics and the social situation. Vehicles are not expected to have any physical contact with obstacles or other cars. When social forces are not able to capture reality, the third layer modifies the manoeuvres to avoid the potential encounter. The second layer is the core of the new mathematical model presented in this thesis and is the focus of Chapter 5.

3.5.3 Diplomatic Rule-Based Layer

After defining the characteristics of the overall shared space system, the third layer is implemented to describe constraints of car motions by a relationship between the steering angle and speed. The second part of this layer handles road conflicts that cannot be resolved by the SFM exclusively. Potential conflicts be-

tween agents are predicted based on their states and resolved by a speed change and a correction of the heading direction (considering left-hand traffic for car-car interactions) [202]. The aim is to find the minimum speed change and direction change for each agent to avoid possible conflicts while deviating as little as possible from the desired direction of movement. The mathematical description of this layer is presented in detail in Chapter 6.

3.6 Geometrical Agent Modelling for Pedestrians and Cars

In the SFM by Helbing, Farkas and Vicsek [53], each simulated pedestrian has a certain body size which can be expressed by circles (symmetrical configuration) of a radius r_α. This is translated to the average area occupied by a pedestrian throughout this thesis (see Figure 3.5). Since the definition of shared space is the integration of pedestrians and vehicles, a car is now introduced by an ellipse with the radius $r_\gamma(\varphi_{\gamma U})$. As shown in Figure 3.6, the radius $r_\gamma(\varphi_{\gamma U})$ depends on the angle between the desired direction of a car γ and the centre of a close-by pedestrian $U = \alpha$ or car $U = \delta$. The radius of the ellipse $r_\gamma(\varphi_{\gamma U})$ in polar coordinates is described by Equation 3.1.

$$r_\gamma(\varphi_{\gamma U}) = \frac{w}{\sqrt{1 - \epsilon^2 cos^2(\varphi_{\gamma U})}}, \text{ where } \epsilon = \frac{\sqrt{l^2 - w^2}}{l} \tag{3.1}$$

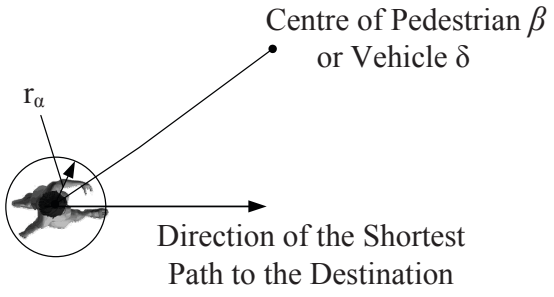

Figure 3.5: Pedestrian modelling using a geometrical approximation of a circle

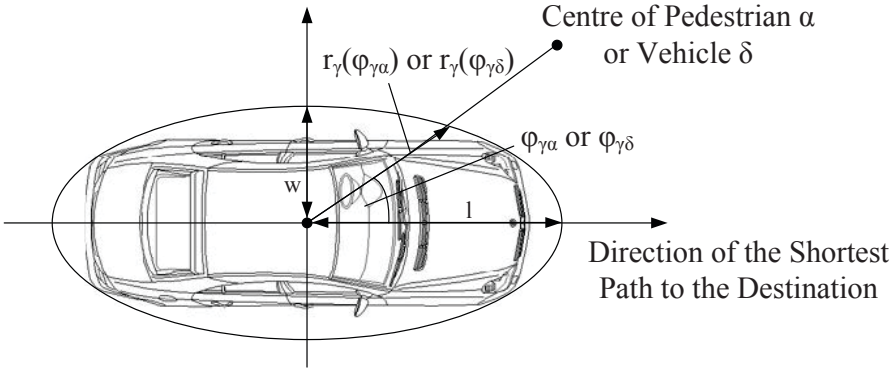

Figure 3.6: Vehicle modelling using a geometrical approximation of an ellipse

where, $2l$ and $2w$ are the average length and width of a modelled car. Considering the pedestrian as a circle and the car as an ellipse, the following chapters will present the mathematical model to describe the behaviour of pedestrians and cars in a shared environment.

3.7 Summary

This chapter introduced urban planners' objectives and expectations regarding pedestrian and vehicle behaviour after implementing a shared space environment. This led to a review of the specific behavioural patterns of shared space users from the literature and field observations. The key characteristics were then realised in a framework of three interrelated layers (similar to theories of pedestrian dynamics [155, 203]) for modelling pedestrian and car motions: the global trajectory planning layer, operational force-based model layer and diplomatic rule-based layer. The geometrical models for pedestrians and cars in the shared space environments were also introduced. The mathematical methods used in each layer are explained in detail in Chapters 4, 5 and 6.

Chapter 4

Trajectory Planning by Distance Map

In this chapter, a global path planning strategy is presented. Since the Social Force Model (SFM) only considers and reacts on static obstacles within a defined interaction range of the agents, this global trajectory planning algorithm is essential. As the literature reveals that the flood-fill algorithm is computationally fast compared to other path finding methods, this algorithm is implemented as the first layer of the mathematical model developed in this thesis. The aim is to model the path of each shared space user from its current location to a destination according to the infrastructure in the environment. The first layer introduces a distance map based on the flood-fill algorithm to define intermediate destinations between agent's origin and destination in order to find the shortest path.

4.1 Introduction

Two groups of path planning algorithms are distinguished: global and local path planning. The former model the path of agents from their current location to a destination according to a priori information about the infrastructure in the environment. Local path planning algorithms cover dynamic interactions between agents and static obstacles within a defined distance referred to as the interaction range in the SFM. The focus of this chapter is on developing a global path planning algorithm while the local path planning is addressed in Chapter 5 with the SFM. The SFM is adapted to shared space user movements representing an agent with a certain velocity (which includes its desired direction and speed) at each time interval. A driving force is assigned to define the motivation of agents to move towards the destination with a desired speed. Social forces of the SFM make agents avoid each other and obstacles that are within their interaction range along their path to the destination. It is considered that each obstacle has a repulsive potential field around it. As discussed in Chapter 3, static obstacles (e.g. buildings) might intersect the direct line between the start location and destination. The sole performance of the SFM using local forces would result in a path which is similar to a trajectory by the Bug 0 algorithm [204]. However, shared space users follow the shortest path via intermediate destinations towards the final destination. So, it is insufficient to guide a pedestrian or a car only by the local interaction range. There is also a need for global path planning according to the infrastructure of their activity area. Shared space users follow the shortest path towards their destination on the global scale.

There are several definitions for a desired global path (trajectory) to the destination for pedestrians/cars:

- the most comfortable path where the road user needs to provide the least effort with the fewest changes of direction;

- the shortest path;
- the fastest path to move from one place to another [205].

It is possible to combine two strategies in a simulation or change the preferred strategy during simulation (adaptive path planning algorithms).

This chapter presents a two dimensional path planning algorithm that determines the shortest path strategy. Intermediate destinations are positioned to obtain the shortest paths for each road user by moving around obstacles. This chapter first reviews path planning approaches (Section 4.2). This is followed in Section 4.3 by details of different flood-fill algorithms based on two metrics (the Mahattan and Chessboard metric) for shared space users. Section 4.4 presents an example of the developed path planning algorithm for shared space users. Conclusions are drawn in Section 4.5.

4.2 Shortest Path Algorithms

An overview of existing methods to calculate the shortest path to the destination using global knowledge of road users, is given in this section.

4.2.1 Dijkstra's Algorithm on a Visibility Graph

In order to model global-scale path planning, "graph-based approaches are used in most multi-scale models"[1]. Here, possible polyline routes connecting many point locations around a polygon obstruction are identified by a visibility graph in a given geometry (Figure 4.1). Agents reach their final destination via intermediate destinations that are defined by the vertices of the visibility graph. The

[1] A. Kneidl, D. Hartmann and A. Borrmann. "A Hybrid Multi-scale Approach for Simulation of Pedestrian Dynamics." *Transportation Research Part C: Emerging Technologies*, vol. 37, pp. 224, 2013.

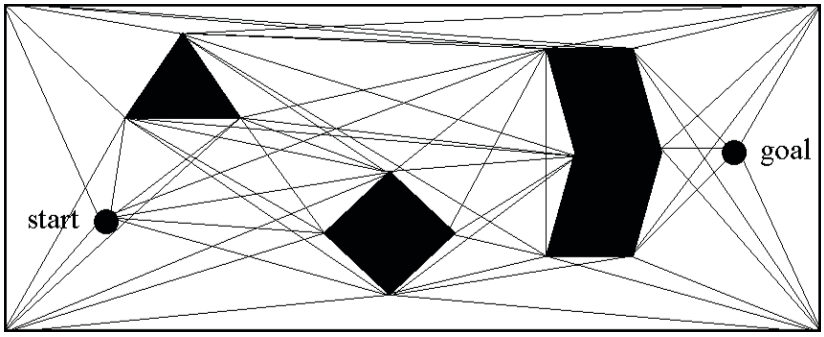

Figure 4.1: A visibility graph determined from possible polyline routes connecting point locations around a polygon obstruction

shortest path can be found by applying the Dijkstra's algorithm [206] to the network between the starting point and the goal to find the closest corner points to the destination polygon. If agents are moving within low density geometries, navigation points can be very close to corners of obstacles [207]. However, a minimum distance has to be considered for coming close to these points before proceeding towards the next navigation point. In addition, local path planning is handled by repulsive forces in the operational force-based layer. The computational time of calculating the shortest path based on the visibility graph increases based on the complexity of the obstacle filled environment as reported in [208].

4.2.2 Ray Casting Algorithm on a Distance Map

This method measures the distance to the nearest obstacle by emitting rays. Rays are lines from an agent's start location to many end points. Agents move along a ray towards the destination until this ray intersects with an obstacle (e.g. a wall). For a given start point, a sufficient number of rays are casted so that every cell that could potentially be part of the field of view is passed by at least one ray. There is a need to define a maximum range for rays in order to avoid casting an unlimited number. In order to use this method effectively, it is necessary to quickly cast rays (draw lines) using for instance the Bresenham's line algorithm [209]. All

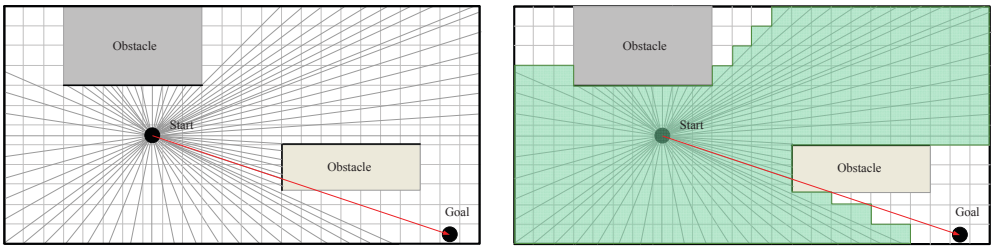

(a) Ray Casting (b) Field of View

Figure 4.2: Calculate field of view with ray casting on a grid-based map

cells covered by ray lines are part of the field of view as shown in Figure 4.2. Each cell in the field of view is assigned to a distance value with respect to the destination. The agent then follows the closest cell to the destination. The computational time of using ray casting algorithm is discussed in [208].

4.2.3 Flood-fill Algorithms

Another method for calculating the shortest path is by generating a flood field. The activity area is divided in to grids of cells. Each cell is assigned to a distance value to its nearest cell. Various algorithms are proposed for the calculation of distances in an obstacle filled space based on their relative error from the Euclidean distance or their calculation time [208]. The direction of the shortest path can be retrieved by following the direction of the negative gradient [207]. Gradients can be calculated using the Moore metric without calculating the flood-fill [210].

Flood-fill methods and related path modification methods are commonly used due to their effectiveness at coordinating motions. The calculation of the flood-fill algorithm is computationally less expensive than other algorithms such as the Dijkstra's algorithm (on a visibility graph) or ray casting as reported in [208].

The flood-fill algorithm was chosen in this thesis to be used for navigating shared space users. A combination of standard metrics is used for the flood-fill al-

gorithm in order to reduce relative errors from the Euclidean distance [208]. Standard metrics (the Manhattan and Chessboard metric) and their combination called Variant 2 are explained in Section 4.3.

4.3 Flood-fill Methods

In the flood-fill algorithm, space is divided into separate cells where each cell is assigned a distance value to its nearest cell. The exact distance between two coordinates can be calculated by the Euclidean distance formula. Calculating a distance map requires finding the nearest neighbourhood cells and calculating the distance according to Equation 4.1. In this process, the calculation of the shortest path in the presence of obstacles is challenging because of local minima resulting of unknown obstacle shapes. As a result, other distance metrics such as the Manhattan, Chessboard or Variant 2 metric have been suggested to calculate the distance with an approximate Euclidean distance map by considering less complex algorithms.

$$D^{\text{Euclidean}} = \sqrt{(|\delta x_i|^2 + |\delta y_i|^2)} \tag{4.1}$$

Among the proposed distance transform algorithms, the Manhattan distance map is the most sufficient in terms of complexity and computational time. It measures the distance between two coordinates based on a 4-connected neighbourhood (North, East, West and South) in Equation 4.2. However, the results overestimate diagonal distances largely in comparison to the Euclidean distance.

$$D^{\text{M}} = \sum_i |\delta x_i| + \sum_i |\delta y_i| \tag{4.2}$$

To calculate the Manhattan distance map, the distance values for all obstacle cells are initially assigned to a large number and the empty cells are set to zero.

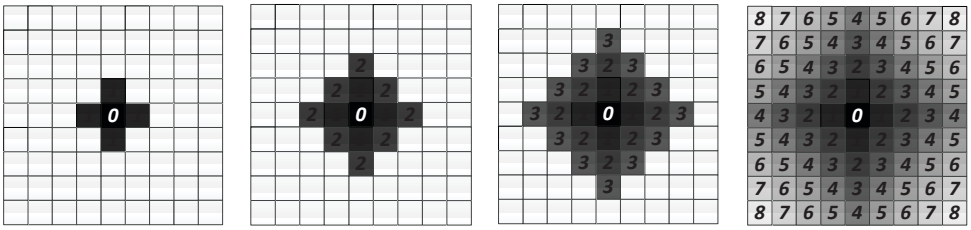

(a) First Iteration (b) Second Iteration (c) Third Iteration (d) Final Iteration

Figure 4.3: Transmission of local distance in a manhattan distance map

The distance map is generated through iterations. In each iteration, the distance values of direct neighbourhood cells are added. The process is repeated until the distances for all pixels are calculated. Figure 4.3 illustrates the transmission of local distance in a Manhattan map starting from the cell in the centre with assigned distance values. A more efficient metric is the Chessboard distance as in Equation 4.3 which leads to an underestimated distance.

$$D^{\mathrm{C}} = \sum_{i} max(|\delta x_i|, |\delta y_i|) \tag{4.3}$$

Another metric is called Variant 2 (D^{V2}), based on a combination of the Manhattan metric D^{M} and the Chessboard metric D^{C} [208] (Equation 4.4). In comparison to the Manhattan and Chessboard metrics, the Variant 2 distance is a more accurate estimation. This can be clearly seen in Figure 4.4 where the distortion

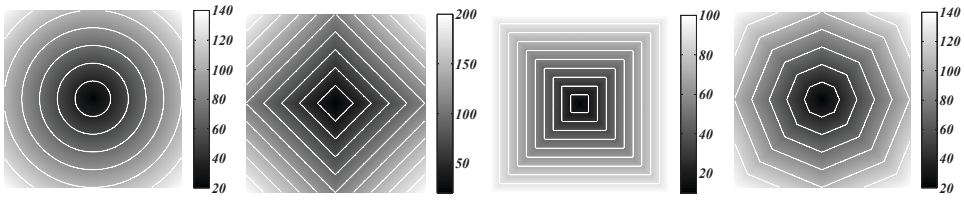

(a) Euclidean (b) Manhattan (c) Chessboard (d) Variant 2

Figure 4.4: Distance transformation for a cell using different metrics

from the isotropic distance map is shown.

$$D^{V2} = (\sqrt{2} - 1)D^{\mathrm{m}} + D^{C}, \text{ where, } D^{\mathrm{m}} = D^{\mathrm{M}} - D^{\mathrm{C}} \tag{4.4}$$

Relative approximation errors of the Euclidean distance based on Equation 4.5 show that the Manhattan and Chessboard metrics result in maximum relative errors of 0.47 and 0.38. The use of the Variant 2 metric leads to a maximum relative error of 0.16 which is why this method is used here for shared space environments. However, the Variant 2 metric requires two operations for calculating distances.

$$\xi_{relative} = \left| \frac{D - D^{\mathrm{Euclidean}}}{D^{\mathrm{Euclidean}}} \right| \tag{4.5}$$

The application of the Variant 2 metric for the model of shared space users is explained in Section 4.4.

4.4 Distance Map for Shared Space Users

In the initialisation phase of the shared space simulation, a global-scale layer is set up by defining the geometry of the environment, starting points and destinations for all agents. This layer generates a distance map by the flood-fill algorithm between agent origins and destinations in order to find the shortest path via intermediate destinations. This layer is implemented to assure adequate realism for the force directed model in the second layer.

Agent movements are modelled for shared areas based on the SFM framework proposed by Helbing et al. [72]. In this model, an agent moves towards its destination using a driving force. The driving force $\boldsymbol{f}_{\alpha}^{0}$ motivates agent α to walk towards its destination while avoiding other agents (U) and obstacles b due to the influence of the repulsive forces $\boldsymbol{f}_{\alpha U}$ and $\boldsymbol{f}_{\alpha b}$ within its interaction range. A random fluctuation force $\boldsymbol{\xi}$ is added to the sum of the exerted forces to represent the velocity fluctuation due to diverse behaviours. The sum of all the forces causes

the movement towards the direction as defined in Equation 4.6 by assuming a mass of $m = 1\,\mathrm{kg}$, the unit mass.

$$\frac{d\boldsymbol{v}_\alpha(t)}{dt} = \boldsymbol{f}_\alpha^0 + \sum_{\delta(\delta\neq\alpha)} \boldsymbol{f}_{\alpha U} + \sum_b \boldsymbol{f}_{\alpha b} + \boldsymbol{\xi} \tag{4.6}$$

The first term of Equation 4.6, $\boldsymbol{f}_\alpha^0$, encourages agent α to move in a desired direction $\boldsymbol{e}_\alpha^0$ with the desired speed $\boldsymbol{v}_\alpha^0$ that is adapted to the actual velocity $\boldsymbol{v}_\alpha$ within a certain relaxation time τ_α (Equation 4.7).

$$\boldsymbol{f}_\alpha^0 = \frac{v_\alpha^0 \cdot \boldsymbol{e}_\alpha(t)}{\tau_\alpha} - \frac{\boldsymbol{v}_\alpha(t)}{\tau_\alpha}, \text{ where } \boldsymbol{e}_\alpha(t) = \frac{\boldsymbol{r}_\alpha^n - \boldsymbol{r}_\alpha}{|\boldsymbol{r}_\alpha^n - \boldsymbol{r}_\alpha|} \tag{4.7}$$

Here, $\boldsymbol{r}_\alpha^n$ is the final destination or goal of an agent. When an agent tries to avoid a static obstacle located between the position of the agent and its goal, the SFM plans the path similar to the Bug 0 algorithm resulting in a non-human behaviour as shown in Figure 4.5 - Trajectory (a). Two static obstacles are positioned intersecting the straight line between the starting point and goal. Without the distance

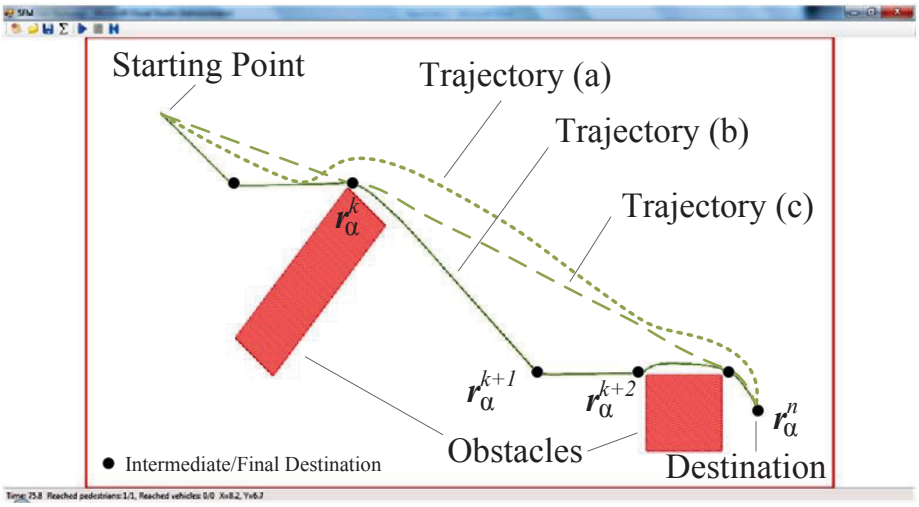

Figure 4.5: Obstacle avoidance and way-finding manoeuvres: Trajectory (a) is simulated without distance map, Trajectory (b) is simulated with route map and Trajectory (c) is the optimal path simulation

map, the desired destination component of the driving force is dominant until the first boundary enters the interaction range of the agent. After navigating around the first obstacle due to the repulsive forces exerted from the obstacles to the agent, the driving force again dominates until the second obstacle comes within defined proximity. Thus, the calculation of the shortest route to the destination using a distance map and predefining intermediate destinations overcomes this limitation.

In order to define intermediate destinations, a global shortest path strategy is presented based on a priori knowledge of the environment. In this process, the floor area is divided into square cells. The distance values for all obstacle cells are assigned to a large number and the empty cells are set to -1. The global shortest path strategy is adapted to cars as well as pedestrians. Then, a distance map is generated through iterations of calculating the Manhattan and Chessboard map. The distance values of direct neighbourhood cells are added starting from the destination point to the starting point. This is achieved by calculating the Variant 2 flood-fill (D^{V2}) based on a combination of the Manhattan metric D^{M} and the Chessboard metric D^{C} [208] as in Equation 4.4. This effect is illustrated in Figure 4.5 - Trajectory (b).

Some of the calculated intermediate destinations are unnecessary. Let $\boldsymbol{r}_{\alpha}^{k}$ be any intermediate destination while $\boldsymbol{r}_{\alpha}^{n}$ is the final destination (see Figure 4.5). In order to reduce the unnecessary intermediate destinations, line connections between intermediate destinations $\boldsymbol{r}_{\alpha}^{k}$ and $\boldsymbol{r}_{\alpha}^{k+2}$, where $(k+2) \leq n$, are checked for intersections with obstacles. This is referred to as an obstacle check. If the line does not intersect with any obstacle, the intermediate destination $\boldsymbol{r}_{\alpha}^{k+1}$ will be removed. The driving force considering the explained intermediate destinations is redefined for pedestrians' movement in Section 5.2.1 (Equation 5.1) and for car drivers' motion in Section 5.3.1 (Equation 5.14).

The geometrical information of the environment and the shortest path to the destination is given before running the simulation. Intermediate destinations are automatically generated for all agents according to the distance map calculations and collision checks with obstacles as illustrated in Figure 4.5 - Trajectory (c). The agent navigates via the intermediate destinations assigned to the vertices of the generated shortest path.

Therefore, the direction of the driving force is largely determined by the position of the agent and the intermediate destination. In this case agents continue until the final destination is reached with a more human-like behaviour.

4.5 Summary

In this chapter, a global path planning algorithm was described to navigate pedestrians and cars within the shared area. This layer is essential to ensure adequate realism for the force directed model in the second layer. Hence, a two dimensional path planning algorithm based on a combination of the Manhattan and Chessboard metric determines the shortest path for each agent. Intermediate destinations are positioned to obtain the shortest path by moving around surrounding obstacles. The local path planning is then handled by repulsive forces in the operational force-based layer (Chapter 5).

Chapter 5

Force-Based Modelling

This chapter presents the second layer which is the core of the mathematical model for shared space users. It describes the movement of each pedestrian and vehicle in a shared space environment considering their interactions with other pedestrians, cars and obstacles according to the intermediate destinations derived by the global trajectory layer. The Social Force Model (SFM) is a concept to describe pedestrian motions and is able to reproduce a wide range of self-organising phenomena. The SFM is now extended for shared space users. As observations show that vehicles organise themselves without an explicit lane system, the car-following feature is added for cars according to traffic conditions. The framework of the SFM is used to model driver behaviour within a shared layout and to make the necessary manoeuvres.

5.1 Introduction

The most essential phenomena when modelling mixed traffic areas are social behaviours and interactions between pedestrians and other pedestrians, pedestrians and drivers, and drivers and other drivers. Modelling interactions between cars and pedestrians is one of the main challenges when developing a shared space simulation. All agents are modelled individually using the microscopic model of social forces. Hence, the second layer, the operational force-based layer, is based on a combination of factors considered in the SFM by Helbing [72, 161], Farkas and Vicsek [53] as the framework to simulate and describe shared space user dynamics.

The idea of force directed models is to reproduce behaviour patterns of pedestrians [72]. The social interaction forces which do not obey Newton's third law of motion affects each pedestrian in the system. There is no action-reaction effect and social forces can be asymmetric. The social forces are a measure of pedestrian motivations for acting in specific ways. The force directed model makes use of established methods from physics: several exerted forces are summed up to generate a resulting force for a pedestrian. The resulting force can be used to describe acceleration and thus affect the movement of pedestrians. The desire of pedestrians to avoid physical interaction with each other is modelled by repulsive forces. Social forces are a way to estimate pedestrian behaviours and tendencies to move in a certain direction which differs from physical forces. They can affect pedestrians over a distance whereas physical interaction forces (pushing and sliding friction forces) between two pedestrians only occur when in physical touch. Furthermore, social force models can be found in several versions in the literature. Though the basic idea is similar, some details vary. For instance, the SFM by Helbing [161] and Molnar [72] is modified by considering interaction forces that are perpendicular to the direction of the repulsive force [53] or by imple-

menting an effective angle factor in the interaction forces [162] or by including the density effects in the social repulsive force [86] or by defining velocity-dependent repulsive forces [73] or by adding a self-stopping mechanism in the social forces [195]. The interaction forces are used as both, a means of simulating a tendency of pedestrians to avoid each other and a frictional force when pedestrians are in physical contact. Other models add an additional layer to the SFM to simulate higher-level decisions such as path finding and communication between pedestrians as well as incorporating pedestrians that fall down and turn into obstacles in dense crowds [149].

In this chapter, the SFM is extended for pedestrians by considering cars in the environment. Also, the force directed concept is applied for cars in a non-lane based shared environment and their interactions with pedestrians.

5.2 Social Force Model for Pedestrians by Helbing, Molnar, Farkas and Vicsek

The SFM is based on Lewin's [211] idea in social science that behavioural changes are driven and self-possessed by social forces or social fields. Helbing [161], Molnar [72], Farkas and Vicsek [53] explained this idea mathematically and applied the concept to pedestrian dynamics. In this model, pedestrian movements are influenced by forces exerted by other pedestrians and obstacles. The sum of the all forces determines the movement and direction as shown in Figure 5.1. The social forces evoke a pedestrian to accelerate or decelerate as a reaction to perceived information that is obtained from the environment. At each time interval, the acceleration or deceleration is calculated for all pedestrians within the system based on the sum of forces. Hence, the velocity and consequently the position at the following time interval is returned. In the following subsections, the forces acting on a pedestrian are explained in detail by assuming a mass of $m = 1\,\mathrm{kg}$, the unit mass.

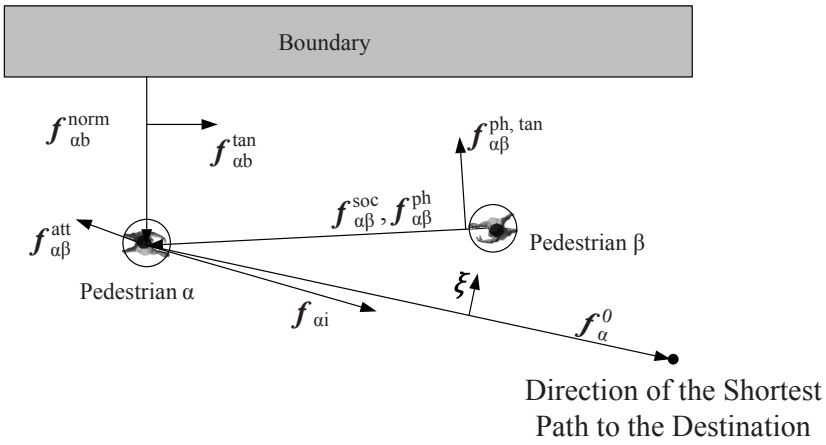

Figure 5.1: Social Force Model for pedestrians

5.2.1 Driving Force for Pedestrians

As initially explained in Chapter 4, pedestrians follow the direct and shortest path without detours. The shortest path to the final destination for pedestrian α is defined as a sequence of intermediate destinations $\boldsymbol{r}^1_\alpha, \ldots, \boldsymbol{r}^n_\alpha := \boldsymbol{r}^k_\alpha$ as explained in Chapter 4. The first term of the SFM, the 'driving force', encourages a pedestrian α to move towards the next intermediate destination $\boldsymbol{e}_\alpha$ with a desired speed v^0_α that is adapted to the current velocity $\boldsymbol{v}_\alpha$ within a constant relaxation time τ_α as in Equation 5.1. The relaxation time determines how quickly an agent changes its velocity to the desired velocity.

$$\boldsymbol{f}^0_\alpha = \frac{v^0_\alpha \cdot \boldsymbol{e}_\alpha(t)}{\tau_\alpha} - \frac{\boldsymbol{v}_\alpha(t)}{\tau_\alpha}, \text{ where } \boldsymbol{e}_\alpha(t) = \frac{\boldsymbol{r}^{\boldsymbol{k}}_{\boldsymbol{\alpha}} - \boldsymbol{r}_\alpha}{|\boldsymbol{r}^{\boldsymbol{k}}_{\boldsymbol{\alpha}} - \boldsymbol{r}_\alpha|} \tag{5.1}$$

where $\boldsymbol{e}_\alpha$ points to the next intermediate destination r^k_α at time t. $\boldsymbol{r}_\alpha(t)$ denotes the actual position of pedestrian α at time t. If a pedestrian is not affected by surrounding forces, movement is towards the desired direction $\boldsymbol{e}_\alpha$ with the assumed desired velocity v^0_α. Small values of τ_α make pedestrians walk more aggressively when the forces of all agents or obstacles are exerted on them.

5.2.2 Interaction Forces between Pedestrians

The motion of a pedestrian is influenced by other pedestrians. Each agent tries to keep a certain distance (private sphere) from other pedestrians depending on density and desired speed. In fact, the closer a pedestrian gets to a neighbouring pedestrian, the more uncomfortable they become. Repulsive effects from pedestrian β to pedestrian α and vice versa play an important role in their interaction. The interaction between pedestrians $\boldsymbol{f}_{\alpha\beta}$ is introduced by two repulsive forces in [53] (Equation 5.2). The social force $\boldsymbol{f}_{\alpha\beta}^{\mathrm{soc}}$ reflects the socio-psychological behaviour of a pedestrian to keep a certain distance from nearby pedestrians. The physical force $\boldsymbol{f}_{\alpha\beta}^{\mathrm{ph}}$ represents physical interactions (pushing and sliding friction forces) when pedestrians touch each other.

$$\boldsymbol{f}_{\alpha\beta}(t) = \boldsymbol{f}_{\alpha\beta}^{\mathrm{soc}}(t) + \boldsymbol{f}_{\alpha\beta}^{\mathrm{ph}}(t) \tag{5.2}$$

The socio-psychological force $\boldsymbol{f}_{\alpha\beta}^{\mathrm{soc}}$ is an exponential function to consider distance dependency as in [53] (Equation 5.3). The repulsive force increases when pedestrians get closer and almost vanishes when they move far away from each other. This describes the avoidance manoeuvres of pedestrians.

$$\boldsymbol{f}_{\alpha\beta}^{\mathrm{soc}} = A_{\alpha\beta} e^{\frac{r_{\alpha\beta} - d_{\alpha\beta}}{B_{\alpha\beta}}} \boldsymbol{n}_{\alpha\beta} F_{\alpha\beta} \tag{5.3}$$

where $d_{\alpha\beta} = \|\boldsymbol{r}_\alpha - \boldsymbol{r}_\beta\|$ is the distance between the mass centre of pedestrian α and β, $r_{\alpha\beta} = (r_\alpha + r_\beta)$ is the sum of their radii, $\boldsymbol{n}_{\alpha\beta} = \frac{(\boldsymbol{r}_\alpha - \boldsymbol{r}_\beta)}{d_{\alpha\beta}}$ is the normalised vector pointing from β to α and $F_{\alpha\beta}$ is the form factor that varies the amount of exerted forces with respect to the direction of movement. $A_{\alpha\beta}$ is the constant interaction strength that indicates the effect of repulsive forces on pedestrian α. $B_{\alpha\beta}$ is the constant interaction range which determines the influence of distance $(r_{\alpha\beta} - d_{\alpha\beta})$ on the repulsive force $\boldsymbol{f}_{\alpha\beta}$. A and B need to be calibrated using real data.

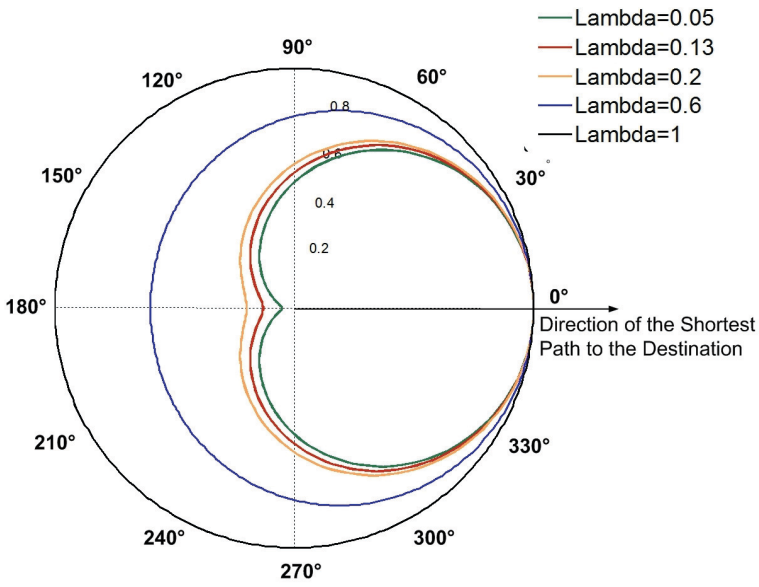

Figure 5.2: Form factor (Equation 5.4) for anisotropic pedestrian behaviour regarding pedestrians

Human beings have an anisotropic behaviour managing that movements in their field of view can persuade them to react more than movements behind them. The form factor $F_{\alpha\beta}$ has the form of a limacon in polar coordinates and it includes the anisotropic behaviour of pedestrians [162]. This can be described by a polar curve term of the form:

$$F_{\alpha\beta} = \lambda_\alpha + (1 - \lambda_\alpha)\frac{1 + cos(\varphi_{\alpha\beta})}{2} \tag{5.4}$$

$\varphi_{\alpha\beta}$ is the angle between the desired movement direction of pedestrian α and the repulsive force exerted from pedestrian β. Figure 5.2 illustrates the form factor value with respect to different λ_α values. As is shown in Figure 5.2, $F_{\alpha\beta}$ is larger for forces occurred in front of a pedestrian ($-90^o < \varphi_{\alpha\beta} < 90^o$) than those behind. The physical interaction force or "body force" [53] (Equation 5.2) acts

on pedestrian α only in case of physical contact such as panic situations or high density conditions. In general, people try to avoid physical injuries by pushing other pedestrians.

$$\boldsymbol{f}_{\alpha\beta}^{\mathrm{ph,pushing}} = k\Theta\left(r_{\alpha\beta} - d_{\alpha\beta}\right)\boldsymbol{n}_{\alpha\beta} \tag{5.5}$$

The function $\Theta\left(r_{\alpha\beta} - d_{\alpha\beta}\right)$ in Equation 5.5 is equal to its argument in Equation 5.6 if the pedestrians touch each other, otherwise it is zero.

$$\text{where} \begin{cases} \Theta\left(r_{\alpha\beta} - d_{\alpha\beta}\right) = r_{\alpha\beta} - d_{\alpha\beta}, & \text{if } r_{\alpha\beta} > d_{\alpha\beta} \\ \Theta\left(r_{\alpha\beta} - d_{\alpha\beta}\right) = 0, & \text{otherwise} \end{cases} \tag{5.6}$$

A "sliding friction force" [53] is also calculated in case of physical contact to include the aspect that pedestrians cannot pass each other quickly when touching because of friction. This force is perpendicular to the pushing force and is defined in Equation 5.7.

$$\boldsymbol{f}_{\alpha\beta}^{\mathrm{ph,friction}} = \kappa\Theta\left(r_{\alpha\beta} - d_{\alpha\beta}\right)\Delta v_{\beta\alpha}^{t}\boldsymbol{t}_{\alpha\beta}, \text{ where } \Delta v_{\beta\alpha}^{t} = \left(\boldsymbol{v}_{\beta} - \boldsymbol{v}_{\alpha}\right)\cdot\boldsymbol{t}_{\alpha\beta} \tag{5.7}$$

where $\boldsymbol{t}_{\alpha\beta}$ is a normal vector tangential to the pushing force exerted from pedestrian β to pedestrian α. k and κ are constant parameters to present obstruction effects. Thus, the physical force $\boldsymbol{f}_{\alpha\beta}^{\mathrm{ph}}$ is calculated as follows:

$$\boldsymbol{f}_{\alpha\beta}^{\mathrm{ph}} = k\Theta\left(r_{\alpha\beta} - d_{\alpha\beta}\right)\boldsymbol{n}_{\alpha\beta} + \kappa\Theta\left(r_{\alpha\beta} - d_{\alpha\beta}\right)\Delta v_{\beta\alpha}^{t}\boldsymbol{t}_{\alpha\beta} \tag{5.8}$$

5.2.3 Interaction Forces between Pedestrians and Boundaries/Obstacles

In the SFM [53], boundary/obstacle repulsive effects are considered similarly to that of pedestrians. Therefore, this force is defined based on Equation 5.3, 5.5 and 5.7.

$$\boldsymbol{f}_{\alpha\mathrm{b}} = A_{\alpha\mathrm{b}}e^{\frac{r_{\alpha}-d_{\alpha\mathrm{b}}}{B_{\alpha\mathrm{b}}}}\boldsymbol{n}_{\alpha\mathrm{b}} + k\Theta(r_{\alpha} - d_{\alpha\mathrm{b}})\boldsymbol{n}_{\alpha\mathrm{b}} - \kappa\Theta(r_{\alpha} - d_{\alpha\mathrm{b}})\left\langle\boldsymbol{v}_{\alpha}, \boldsymbol{t}_{\alpha\mathrm{b}}\right\rangle\boldsymbol{t}_{\alpha\mathrm{b}} \tag{5.9}$$

where $\boldsymbol{n}_{\alpha\mathrm{b}}$ is the normal vector perpendicular to the surface of a boundary and $\boldsymbol{t}_{\alpha\mathrm{b}}$ is parallel to $\boldsymbol{n}_{\alpha\mathrm{b}}$. In addition, the scalar product of the momentary pedestrian velocity $\boldsymbol{v}_\alpha$ and $\boldsymbol{t}_{\alpha\mathrm{b}}$ is introduced as $\langle \boldsymbol{v}_\alpha, \boldsymbol{t}_{\alpha\mathrm{b}} \rangle$.

Obstacles are defined as polygons as shown in Figure 5.3 with $\boldsymbol{p}$ and $\boldsymbol{q}$ as its vertices. The line between $\boldsymbol{p}$ and $\boldsymbol{q}$ establishes the boundary. If pedestrian α is within the area of a boundary, the shortest distance between the boundary and pedestrian is the Euclidean distance between the pedestrian position and the boundary line. If a pedestrian is outside the area of the boundary the closest distance is between the pedestrian position $\boldsymbol{x}_\alpha$ and the boundary vertex $\boldsymbol{p}$ and $\boldsymbol{q}$ respectively. The momentary distance is therefore, introduced by the algebra vector $\boldsymbol{d}_{\alpha\mathrm{b}}$ as:

$$\boldsymbol{d}_{\alpha b} = \begin{cases} \boldsymbol{p} - \boldsymbol{x}_\alpha & \text{for} \quad \langle \boldsymbol{x}_\alpha - \boldsymbol{p}, \boldsymbol{e}_{qp} \rangle \leq 0 \\ \boldsymbol{p} - \boldsymbol{x}_\alpha - \langle \boldsymbol{e}_{qp}, \boldsymbol{x}_\alpha - \boldsymbol{p} \rangle \, \boldsymbol{e}_{qp} & \text{for} \quad 0 < \langle \boldsymbol{x}_\alpha - \boldsymbol{p}, \boldsymbol{e}_{qp} \rangle < |\boldsymbol{q} - \boldsymbol{p}| \\ \boldsymbol{q} - \boldsymbol{x}_\alpha & \text{for} \quad |\boldsymbol{q} - \boldsymbol{p}| \leq \langle \boldsymbol{x}_\alpha - \boldsymbol{p}, \boldsymbol{e}_{qp} \rangle \end{cases} \tag{5.10}$$

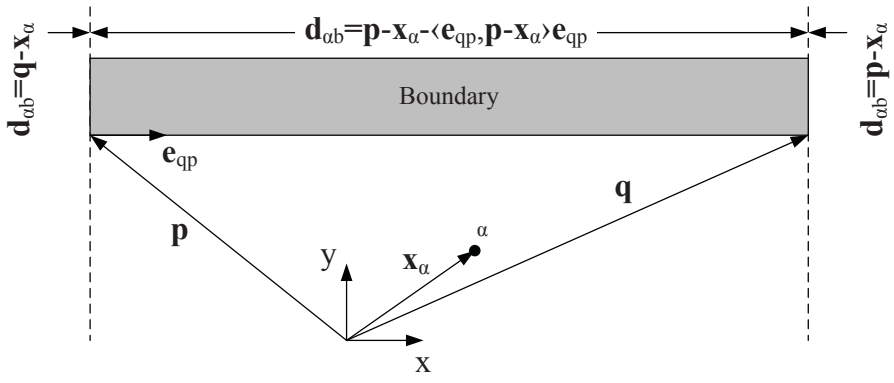

Figure 5.3: Determination of the distance between a boundary and pedestrian

5.2.4 Attractive Interactions

Pedestrians occasionally start walking towards attractions (shops, exhibitions). This behaviour change linearly decreases to zero over time as they continue to move towards the desired destination. This behaviour is introduced by a time-dependent attractive force $\boldsymbol{f}_{\alpha i}$ in the SFM that has the same form as Equation 5.3 with a smaller value for interaction range $B_{\alpha i}$ and a negative time-dependent value for interaction strength $A_{\alpha i}$.

5.2.5 Joining Behaviours for Pedestrians

The tendency of humans to walk in groups is included in a constant attracting force $\boldsymbol{f}_{\alpha\beta}^{\mathrm{att}}$ exerted from pedestrian β to pedestrian α:

$$\boldsymbol{f}_{\alpha\beta}^{\mathrm{att}} = -C_{\alpha\beta}\boldsymbol{n}_{\alpha\beta} \tag{5.11}$$

5.2.6 Fluctuation Term

Human behaviour varies from one to another. Therefore, a random fluctuation force $\boldsymbol{\xi}$ is added to the sum of the exerted forces to present velocity fluctuation due to diverse behaviours. $\boldsymbol{\xi}$ has a Gaussian form and is perpendicular to the desired direction of movement $\boldsymbol{e}_{\alpha}^{0}$:

$$\boldsymbol{\xi} = \left\langle \boldsymbol{e}_{\alpha}^{0}, \boldsymbol{f}_{\alpha} \right\rangle X \cdot \boldsymbol{e}_{\alpha}^{\mathrm{norm}} \tag{5.12}$$

Here, $\boldsymbol{f}_{\alpha}$ is the sum of the forces exerted to the individual α. X is a normal distributed random number with $\mu = 0$ and variance $\sigma^2 = 0.2$ within the interval $[-1, 1]$ [162]. In computer simulations, agents may not be able to pass each other due to entirely oppositional velocities. Hence, the fluctuation force resolves these deadlocks with minimal influence on the sum of the forces exerted to an agent.

5.2.7 Summary of the Social Force Model for Pedestrians

In conclusion, different forces are introduced by the SFM to reflect diverse phenomena taking place during pedestrian movements. The sum of all forces in Equation 5.13 represents the acceleration at time t.

$$\frac{d\boldsymbol{v}_\alpha(t)}{dt} = \boldsymbol{f}_\alpha + \sum_\beta \boldsymbol{f}_{\alpha\beta} + \sum_b \boldsymbol{f}_{\alpha b} + \sum_i \boldsymbol{f}_{\alpha i} + \sum_\beta \boldsymbol{f}^{\text{att}}_{\alpha\beta} + \boldsymbol{\xi} \tag{5.13}$$

The forces of attracting elements $\boldsymbol{f}_{\alpha i}$ and joining behaviour of pedestrians $\boldsymbol{f}^{\text{att}}_{\alpha\beta}$ are excluded in this study. Based on the sum of the forces and thus the acceleration $\frac{d\boldsymbol{v}_\alpha(t)}{dt}$ for pedestrian α at time t, the velocity and position at time $(t + \Delta t)$ is computed. Since the SFM is chosen as a unified theory for explaining both vehicle and pedestrian movements in shared space environments, the SFM for pedestrians is applied to a model for cars in Section 5.3. In Section 5.4, the SFM for pedestrians is extended to include the impact of cars to pedestrians in shared space areas.

5.3 Social Force Model for Cars

Since vehicles and pedestrians move within shared space environments, the SFM for pedestrians is now considered and applied to a model for cars. As discussed in Section 3.6, the geometrical model for cars is introduced by an ellipse with the radius of $r_\gamma(\varphi_{\gamma U})$. The new arrangement of a shared space environment integrating cars is shown in Figure 5.4.

The sum of the force terms exerted on a car γ from pedestrian α, boundary b and car δ can be seen in Equation 5.14. Each summand is explained in the following sections.

$$\frac{d\boldsymbol{v}_\gamma(t)}{dt} = \boldsymbol{f}^0_\gamma + \sum_{\delta(\delta\neq\gamma)} \boldsymbol{f}_{\gamma\delta} + \sum_\alpha \boldsymbol{f}_{\gamma\alpha} + \sum_b \boldsymbol{f}_{\gamma b} + \boldsymbol{\xi} \tag{5.14}$$

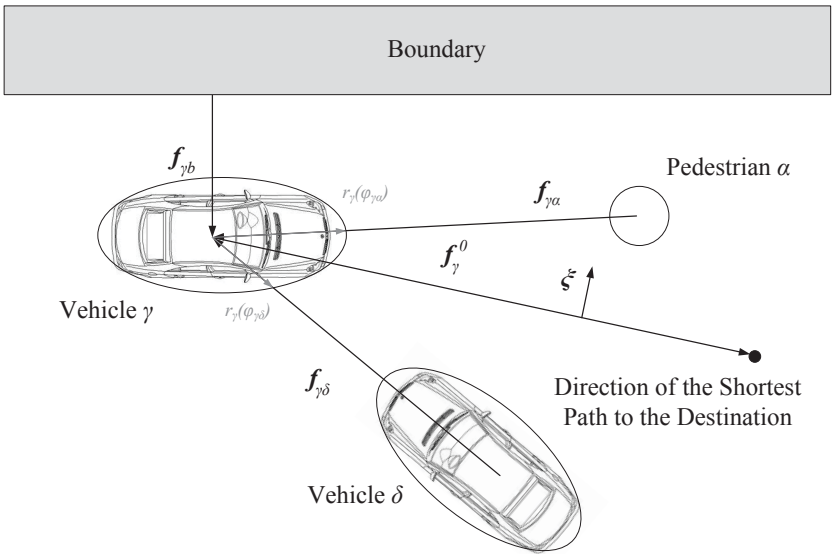

Figure 5.4: Force terms exerted to a car from a pedestrian/car/boundary

5.3.1 Driving Force for Cars

The driving force of a car is similar to the one applied for pedestrians in the original SFM. This force term describes the motivation of a driver to move towards a certain (intermediate) destination. The driver γ is assumed to move in a desired direction $\boldsymbol{e}_\gamma$ with a desired speed v_γ^0 that is adapted to the actual velocity $\boldsymbol{v}_\gamma(t)$ within a constant relaxation time τ_γ.

$$\boldsymbol{f}_\gamma^0 = \frac{v_\gamma^0 \cdot \boldsymbol{e}_\gamma(t) - \boldsymbol{v}_\gamma(t)}{\tau_\gamma}, \text{ where } \boldsymbol{e}_\gamma(t) = \frac{\boldsymbol{r}_\gamma^k - \boldsymbol{r}_\gamma}{|\boldsymbol{r}_\gamma^k - \boldsymbol{r}_\gamma|} \tag{5.15}$$

The shortest path to the final destination for car γ is defined as a sequence of intermediate destinations (see Chapter 4). Therefore, the desired direction $\boldsymbol{e}_\gamma$ points in the direction of the next intermediate destination $\boldsymbol{r}_\gamma^k$ on the shortest path to the final destination.

5.3.2 Interaction between Cars and Shared Space Users

Shared space layouts aim to achieve a constant traffic flow by reducing stop-and-go behaviours [13]. Drivers try to adapt to the behaviour of other shared space users. Any deviation from their path to their destination is mainly due to local social interactions. The interaction force $f_{\gamma U}$ between a car γ with either another car ($U = \delta$) or a pedestrian ($U = \alpha$) is presented by Equation 5.16. The socio-psychological force $\boldsymbol{f}_{\gamma U}^{\text{soc}}$ is to keep a certain distance from nearby agents. The car-following force $\boldsymbol{f}_{\gamma\delta}^{\text{following}}$ is to describe a follow-the-leader behaviour of drivers if a car is faster than a leading car in front. Some drivers may have the habit of tailgating (following too close) other cars to show they are impatience or to indicate that they want to pass. However, tailgating was not an observed behaviour of car drivers in shared spaces and is excluded here. More details about the car-following force are explained in Section 5.3.3. Assuming physical contact being equivalent to an accident, no physical force is included.

$$\boldsymbol{f}_{\gamma U}(t) = \boldsymbol{f}_{\gamma U}^{\text{soc}}(t) + \boldsymbol{f}_{\gamma\delta}^{\text{following}}(t) \tag{5.16}$$

To describe the socio-psychological force $\boldsymbol{f}_{\gamma U}^{\text{soc}}$, an exponential function is applied to reflect the role of distance. The repulsive force increases when agents get closer and almost vanishes when they move far away from each other.

$$\boldsymbol{f}_{\gamma U}^{\text{soc}} = A_{\gamma U} e^{\frac{r_{\gamma U} - d_{\gamma U}}{B_{\gamma U}}} \boldsymbol{n}_{\gamma U} F_{\gamma U} \tag{5.17}$$

$\boldsymbol{n}_{\gamma U}$ is the normalized vector pointing from another user (car or pedestrian) to car γ. $A_{\gamma U}$ and $B_{\gamma U}$ are constant parameters that represent the interaction strength and interaction range of the repulsive force $\boldsymbol{f}_{\gamma U}^{\text{soc}}$ which require calibration. $d_{\gamma U}$ is the distance between the centre of agents and $r_{\gamma U}$ is the sum of their radii. The sum of the radii is therefore, $r_{\gamma U} = r_\gamma + r_U$. The radius r_γ depends on the angle $\varphi_{\gamma U}$ between the desired direction of a car and the direction of a neighbouring

pedestrian or car.

Similar to [48], the anisotropic character of interactions is included to provide a more realistic form of forces. Considering that car movements are restricted to change of direction and lateral movement is not possible, an effective field of view is included in the form factor $F_{\gamma U}$ (see Equation 5.18). In addition, the cases for a pedestrian forecasting a car or a car following another car are distinguished because in contrast to pedestrians a car driver does not only react to cars in front but also to those behind it.

$$F_{\gamma U} = \left(\lambda_\gamma + (1 - \lambda_\gamma)\frac{1 + cos(\varphi_{\gamma U})}{2}\right) \cdot q \tag{5.18}$$

q is the effective factor that distinguishes between car-pedestrian or car-car interactions. The view angle of a driver is compared to the effective field of view in Figure 5.5. The effective field of view for car drivers is considered 60^o based on the area that is overlooked by drivers with easy head movements [212]. Regarding a car-pedestrian interaction, q is:

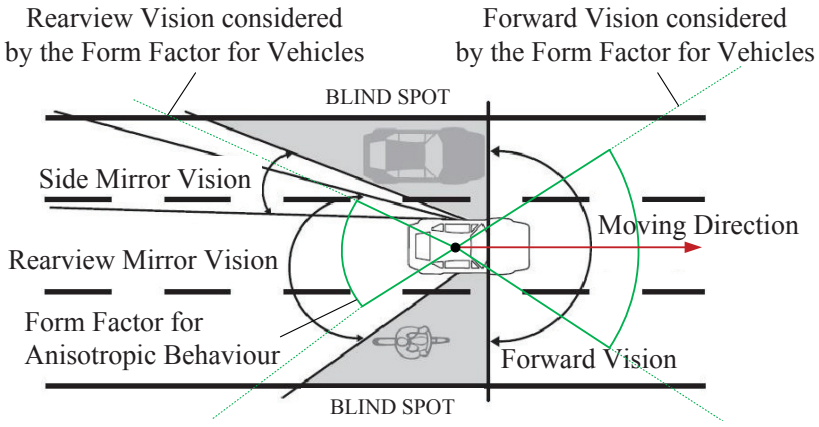

Figure 5.5: Effective field of view compared to driver's vision

$$\begin{aligned} q &= 1, \quad \text{if } -30^{\circ} \leq \varphi_{\gamma\alpha} \leq 30^{\circ} \\ q &= 0, \quad \text{otherwise} \end{aligned} \tag{5.19}$$

This is illustrated in Figure 5.6. Considering a car-car interaction, the following

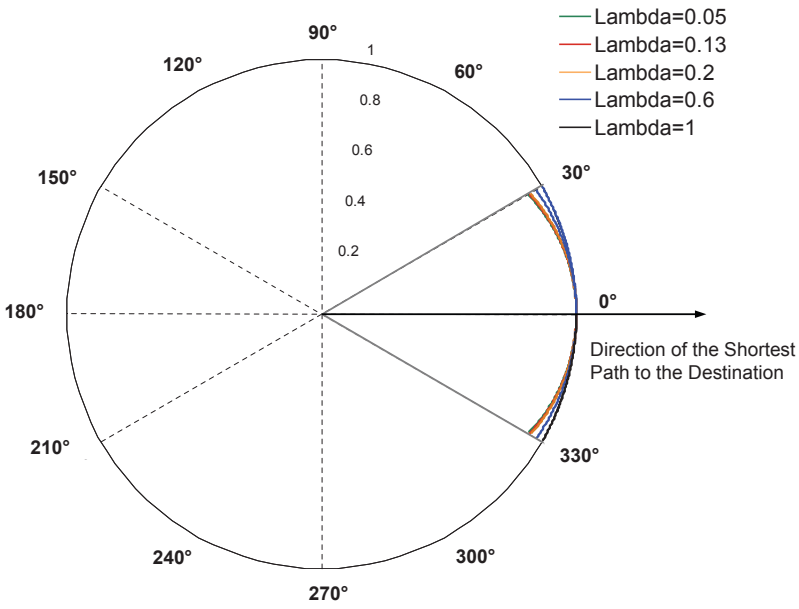

Figure 5.6: Effective field of view compared to driver's vision for a car-pedestrian interaction (Equation 5.18 and 5.19)

can be summarised for the effective factor q:

$$\begin{aligned} q &= 1, \quad \text{if} \begin{cases} -30^{\circ} \leq \varphi_{\gamma\alpha} \leq 30^{\circ} \,\& \\ (180^{\circ} - 30^{\circ}) \leq \varphi_{\gamma\alpha} \leq (180^{\circ} + 30^{\circ}) \end{cases} \\ q &= 0, \quad \text{otherwise} \end{aligned} \tag{5.20}$$

Figure 5.7 visualises the form factor $F_{\gamma\delta}$ for car-car interaction. By varying λ_{γ}, the influence of the exerted forces of the cars behind the leading car changes.

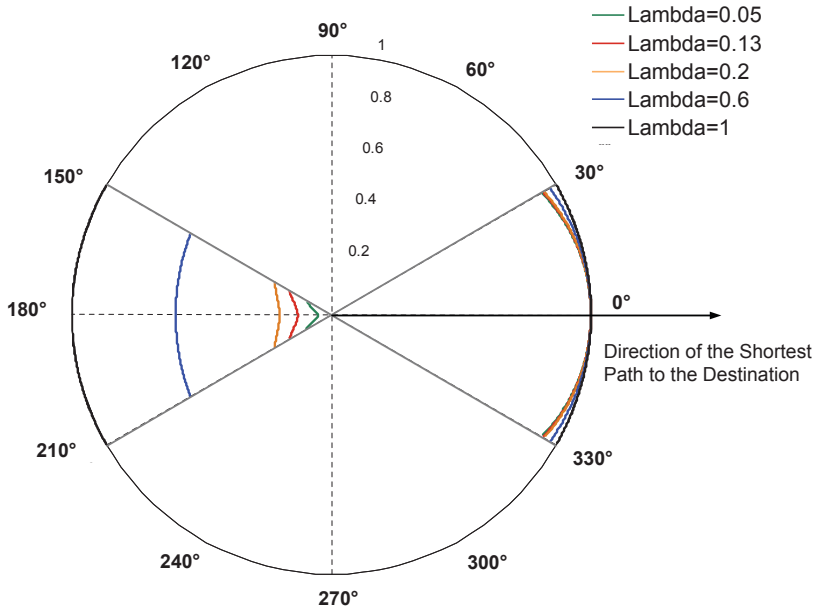

Figure 5.7: Effective field of view compared to driver's vision for a car-car interaction (Equation 5.18 and 5.20)

5.3.3 Car-following Feature

As discussed in Chapter 1, shared space schemes are realised as a single surface without any road markings for defined lanes. The philosophy of shared space gives freedom to all agents, pedestrians and vehicles, to move in a two dimensional space. However, empirical data from observation show that vehicles merge into assumed lanes by car drivers. This becomes noticeable when a number of cars move towards the same destination within a close distance of each other. Modelling driver behaviours with social forces exclusively, in cases where the leading car decelerates the following cars with a higher speed will try to avoid the leading car immediately (instead of queuing in the assumed lane system). The effect is illustrated in Figure 5.8 (a): Two cars travel from the starting points on the left to their destination points on the right of the environment. On the way, the leading car is obstructed by two randomly defined pedestrians. Pedestrian 1 crosses the trajectory of the leading car in order to reach the desti-

nation point. The desired direction of movement (left to right) of Pedestrian 2 intersects the desired direction of the leading car. The leading car decelerates and changes its desired direction to avoid conflict. The following car overtakes the slowed down car due to social interaction which does not generally match observations. The car-following force $\boldsymbol{f}_{\gamma\delta}^{\text{following}}$ in Equation 5.16 addresses this flexible car-following feature and is considered for drivers in the same direction of movement within a certain distance to adopt the behaviour of the leading car. The social force $\boldsymbol{f}_{\gamma\delta}^{\text{soc}}$ is assigned zero in this case.

The deceleration force $\boldsymbol{f}_{\gamma\delta}^{\text{following}}$ is defined in Equation 5.21 [101] and its magnitude depends on the distance between cars $d_{\gamma\delta}$ considering the speed-dependent

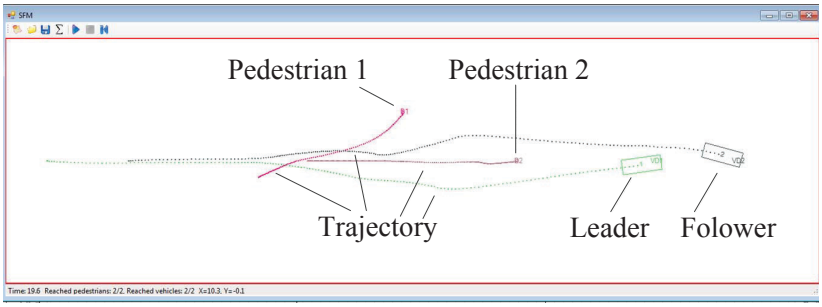

(a)

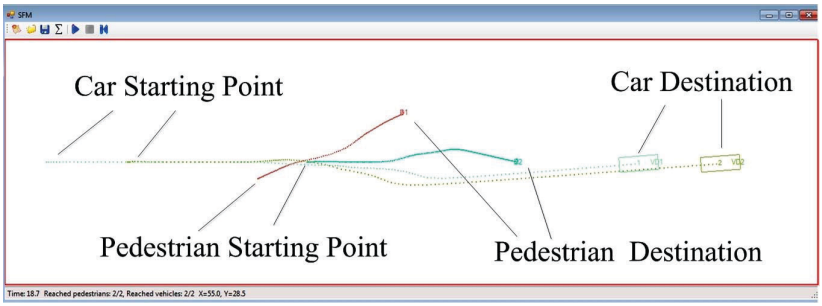

(b)

Figure 5.8: Trajectory simulation of an obstructed car and the following car according to (a) the social force and (b) the deceleration force

safe distance $d(v_{\gamma\delta})$, velocity differences $\Delta \boldsymbol{v}_{\gamma\delta}$ and braking time $\tau_{\gamma}^{'}$.

$$\boldsymbol{f}_{\gamma\delta}^{\text{following}} = -\frac{\boldsymbol{v}_{\gamma}^{0}}{\tau_{\gamma}} e^{\frac{d(v_\gamma)-d_{\gamma\delta}}{B_{\gamma\delta}^{\prime}}} - \frac{\Delta v_{\gamma\delta} e^{\frac{d(v_\gamma)-d_{\gamma\delta}}{B_{\gamma\delta}^{\prime\prime}}}}{\tau_{\gamma}^{'}} \Theta(\Delta v_{\gamma}), \tag{5.21}$$

$$\text{where} \begin{cases} \Theta(\Delta v_{\gamma}) = 1, & \text{if } (\Delta v_{\gamma}) > 0) \\ \Theta(\Delta v_{\gamma}) = 0, & \text{otherwise} \end{cases}$$

Here, the speed-dependent safe distance is $d(v_{\gamma\delta}) = d_{\gamma} + T_{\gamma} v_{\gamma}$ where d_{γ} is the minimal vehicle distance and T_{γ} is the safe time headway. $B_{\gamma\delta}^{\prime}$ and $B_{\gamma\delta}^{\prime\prime}$ are acceleration interaction range and braking interaction range. The angle between the desired direction of driver γ and the desired direction of the leading driver δ determines whether their movements are confluent or opposed. Therefore, the deceleration force is only included in the sum of forces when $|\varphi_{\gamma\delta}| > 10^{o}$ or $|\varphi_{\gamma\delta} + \varphi_{\delta\gamma} - 180| < 10^{o}$. Equation 5.21 is applied to the previous scenario in Figure 5.8 (b).

The interaction between cars and boundaries/obstacles is described by considering that cars are not expected to have any physical contact with boundaries or obstacles. An expression similar to Equation 5.17 is defined to model car-obstacle interactions.

5.4 Social Force Model Extension to Pedestrians

Since the original SFM [161] only considers forces exerted by pedestrians and obstacles onto other pedestrians, forces exerted by vehicles onto pedestrians need to be included (see Figure 5.9). The existence of cars in a shared space environment is expressed by a new socio-repulsive force $\boldsymbol{f}_{\alpha\gamma}$ from cars to pedestrians (Equation 5.22). This new force explains the most important interaction behaviour of a pedestrian keeping a certain distance to the nearby car since no physical interaction should occur.

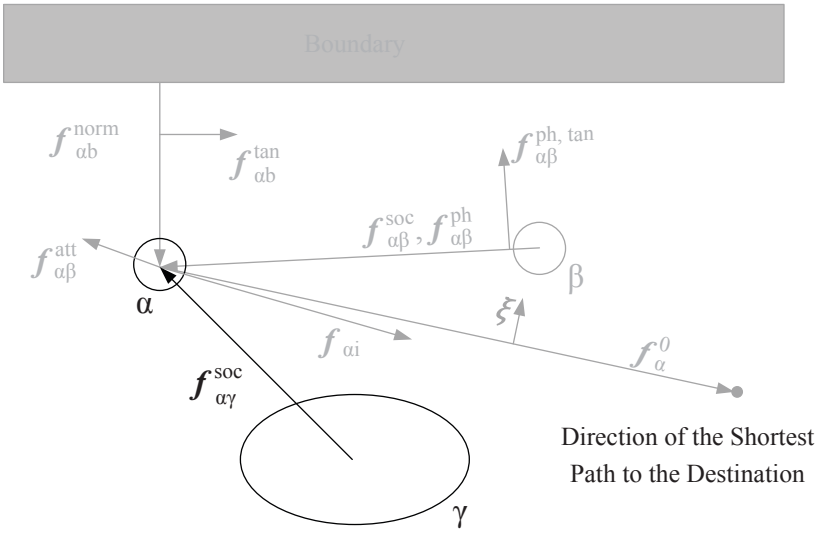

Figure 5.9: Force term exerted from a car to a pedestrian

$$\frac{d\boldsymbol{v}_\alpha(t)}{dt} = \boldsymbol{f}^0_\alpha + \sum_{\beta(\beta\neq\alpha)} \boldsymbol{f}_{\alpha\beta} + \sum_b \boldsymbol{f}_{\alpha b} + \sum_\gamma \boldsymbol{f}_{\alpha\gamma} + \boldsymbol{\xi} \tag{5.22}$$

Similar to the interaction force between pedestrians in the SFM, an exponential function is applied to pedestrian α to represent the influence of distance between pedestrians and the close-by car γ as

$$\boldsymbol{f}^{soc}_{\alpha\gamma} = A_{\alpha\gamma} e^{\frac{r_{\alpha\gamma}-d_{\alpha\gamma}}{B_{\alpha\gamma}}} \boldsymbol{n}_{\alpha\gamma} F_{\alpha\gamma}, \tag{5.23}$$

where $r_{\alpha\gamma} = r_\alpha + r_\gamma$; $d_{\alpha\gamma}$ is the distance between the centre of pedestrian α and car γ, $\boldsymbol{n}_{\alpha\gamma}$ is the normalized vector from car γ to pedestrian α. The form factor $F_{\alpha\gamma}$ is also set similar to Equation 5.18 to explain the anisotropic behaviour of pedestrian α when facing car γ.

5.5 Summary

This chapter presented the SFM for modelling socio-psychological behaviour patterns of pedestrians and vehicles. Applying this force directed model allows agents to move in a two dimensional space with no intrinsic lane system, to have equal priority and negotiate the right of way. The SFM is able to cover these main ideas of share space schemes. However, empirical data shows that vehicles tend to merge into assumed lanes when a number of cars move towards the same destination within a close distance between each other. Hence, a car-following feature has been added according to traffic conditions. However, some road conflicts cannot be resolved by following the SFM exclusively. As a result the third layer is added for providing a collision free motion planning. In addition, restrictions to car motion are explored in Chapter 6.

Chapter 6

Rule-Based Constraints for Shared Space Users

The third layer is added to constrain the flexibility of car motion by a relation between the steering angle and speed considering the centrifugal acceleration expressed by the driver. Having described the key characteristics of shared space by the Social Force Model (SFM) in the previous chapter, this chapter sets out how the potential road conflicts that might occur by following the SFM exclusively are handled. Possible conflicts between agents are predicted based on their states, resolving these with a combination of speed change and correction of heading direction. A potential conflict is detected as soon as agents intersect each other's shadow. The diplomatic rule-based layer is activated in order to avoid potential physical contact between cars and pedestrians. The agent that reaches the predicted conflict location first chooses a conflict avoidance strategy (a combination of speed change and correction of heading direction). By using this conflict avoidance strategy, left-hand traffic is introduced for car-car interactions when passing in opposite directions.

6.1 Introduction

In Section 6.2, the flexibility and type of car motion are constrained by a relation between the steering angle and speed. Furthermore, interactions involving cars require attention as cars do not have a physical force, when modelling mixed traffic using the SFM. Physical contact between pedestrians can be psychologically disturbing for some pedestrians but physical contact between a pedestrian and a car is an accident. As explained in the previous chapter, all agents in the simulation are modelled individually using social forces. Diverse forces are introduced to reflect behavioural changes taking place during pedestrian and driver interactions in the operational force-based layer in Chapter 5. However, some road conflicts cannot be resolved by following the social force theory exclusively within the interaction range of agents. As cars do not have a physical force, the diplomatic rule-based layer is added to assess if pedestrian and car routes cross and then optimise speed and direction change of road users in order to avoid potential conflicts in these scenarios (see Section 6.3). This conflict avoidance strategy is also chosen to model left-hand traffic.

6.2 Relation between Steering Angle and Moving Speed

The angle of movement for pedestrians can be within $[0, 2\pi]$, whereas the desired speed should be $v_\alpha(t) = 1.5\,\frac{\mathrm{m}}{\mathrm{s}}$. With respect to cars, the speed is restricted to $v_\gamma(t) = 8.9\,\frac{\mathrm{m}}{\mathrm{s}}$. The angle of steering is limited since a car cannot drive sideways. In general, vehicles have a maximum steering angle ψ_γ which is limited to $\psi_\gamma^{\max} = 30°$. However, the speed $|\boldsymbol{v}_\gamma|$ needs to be considered when driving along a curve since the lateral or centrifugal acceleration $a_\gamma^{\mathrm{Centrifugal}}$ of a car is speed-dependent. In this thesis, a car is modelled as an ellipse (see Section 3.6) which is acceptably close to the real shape. This simple car model moves in a two dimensional space. Figure 6.1 shows car γ and its parameters. $x_\gamma(t)$ and $y_\gamma(t)$

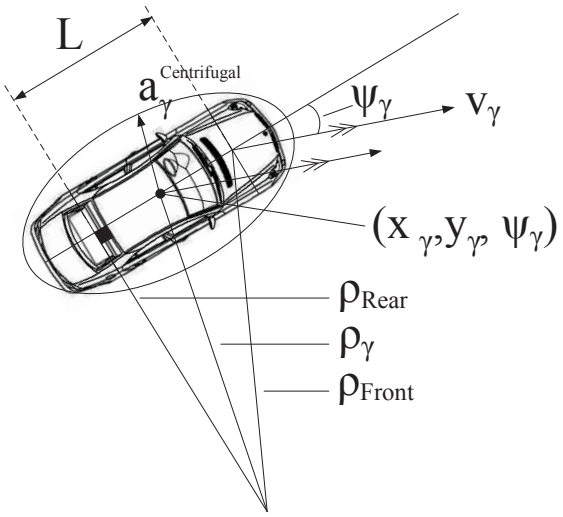

Figure 6.1: Parameters of a turning car model in two dimensional space

describe the centre position of the car and ψ_γ the rotation around this point. L is the distance between the front and the rear axle. If the steering angle ψ_γ is fixed, the car moves around a circle of the radius ρ_γ. Researchers have investigated what amount of lateral acceleration is common and acceptable for car drivers. In Figure 6.2 (a), the lateral acceleration is classified in three areas: traffic in

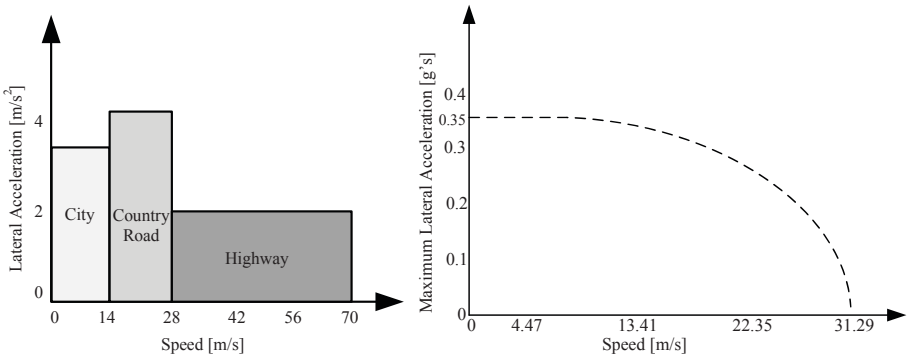

Figure 6.2: Relation between centrifugal acceleration and speed: (a) categorisation of lateral acceleration [213] and (b) comparison of lateral acceleration-speed relations [214]

cities ($0 < |\boldsymbol{v}_\gamma| \leq 50\,\frac{\mathrm{km}}{\mathrm{h}}$), on country roads ($50\,\frac{\mathrm{km}}{\mathrm{h}} < |\boldsymbol{v}_\gamma| \leq 100\,\frac{\mathrm{km}}{\mathrm{h}}$) and on highways ($|\boldsymbol{v}_\gamma| > 100\,\frac{\mathrm{km}}{\mathrm{h}}$). As shown in Figure 6.2 (a), drivers commonly accept a centrifugal acceleration of up to $4\,\frac{\mathrm{m}}{\mathrm{s}^2}$. In particular, vehicle drivers in cities where shared space schemes are realised have even less lateral acceleration. Herrin and Neuhardt [214] recorded lateral acceleration and speed for multiple subjects during normal road driving. They found that lateral acceleration is constant $a_\gamma^{\mathrm{Centrifugal}} = 0.35 \cdot \mathrm{g} = 3.4\,\frac{\mathrm{m}}{\mathrm{s}^2}$ at below $8.9\,\frac{\mathrm{m}}{\mathrm{s}}$ (see Figure 6.2 (b)). Schimdl [215] also reported that the acceptable lateral acceleration is constant below $8.9\,\frac{\mathrm{m}}{\mathrm{s}}$.

The lateral acceleration $a_\gamma^{\mathrm{Centrifugal}}$ for a linear single track vehicle can be determined as presented in Equation 6.1. This equation is derived based on vehicle dynamic control by Isermann [216].

$$a_\gamma^{\mathrm{Centrifugal}} = |\boldsymbol{v}_\gamma|\,(\dot{\eta} + \dot{\nu})\cos(\nu) \underset{|\nu|<<1}{\approx} |\boldsymbol{v}_\gamma|\,(\dot{\eta} + \dot{\nu}) = \frac{|\boldsymbol{v}_\gamma|^2}{\rho_\gamma} \tag{6.1}$$

$\dot{\eta}$ is the yaw angle velocity, ν the slip angle, and $\dot{\nu}$ the slip angle velocity respectively. For very small slip angles and by considering that the normal component of acceleration is dependent on the ρ_γ and the speed of the car v_γ, the centrifugal acceleration can be simplified as shown in Equation 6.1. This assumption can be made as any slip angle would consider over- or understeering behaviour which is not applicable to shared space areas. The radius ρ_γ of an arc depends on the steering angle ψ_γ. From geometry, Equation 6.2 can be derived.

$$\tan\psi_\gamma = \frac{L}{\rho_{\mathrm{Rear}}} \tag{6.2}$$

The assumptions that $\rho_{\mathrm{Rear}} = \rho_\gamma$ and $L = 2l$ ($2l$ is the length of a vehicle) can be estimated because $\rho_\gamma >> 2l$ for this application.
Inserting Equation 6.2 into Equation 6.1 results in Equation 6.3 after transposing

to ψ_γ:

$$\psi_\gamma = \arctan \frac{2l \cdot a_\gamma^{\text{Centrifugal}}}{|\boldsymbol{v}_\gamma|^2} \tag{6.3}$$

Figure 6.3 shows the relation between the steering angle and speed of a car γ. Two intervals are distinguished:

$$\begin{aligned} \text{for} \quad & 0 < |\boldsymbol{v}_\gamma| \leq 5.3\,\tfrac{\text{m}}{\text{s}}, \\ & \psi_\gamma \leq 30^\circ \\ \text{for} \quad & 5.3\,\tfrac{\text{m}}{\text{s}} < |\boldsymbol{v}_\gamma| \leq 8.9\,\tfrac{\text{m}}{\text{s}}, \\ & \psi_\gamma \leq \arctan \tfrac{2l \cdot a_\gamma^{\text{Centrifugal}}}{|\boldsymbol{v}_\gamma|^2} \end{aligned} \tag{6.4}$$

Following these two conditions, the steering is limited according to the speed if necessary. Figure 6.4 shows the trajectory of a single car for the example of a right turning with and without the steering angle constraint. As illustrated in Figure 6.4 (a) and Figure 6.4 (b), the turning angle of the car becomes smooth after applying the steering angle limitation for the speed limit of $8.9\,\frac{\text{m}}{\text{s}}$. Figure 6.5 shows the deceleration and acceleration process with different steering angular

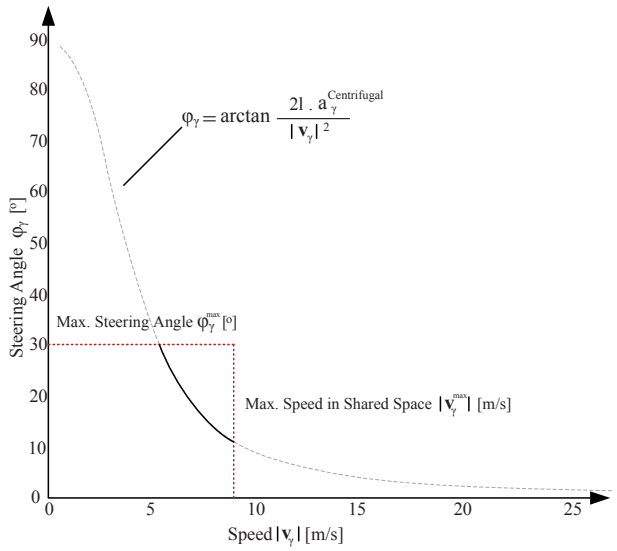

Figure 6.3: Intrinsic function between speed and steering angle of car γ

velocity constraints. From the graph, it is clear for instance that the steering impulse of $60°$ can result in a very unrealistic deceleration.

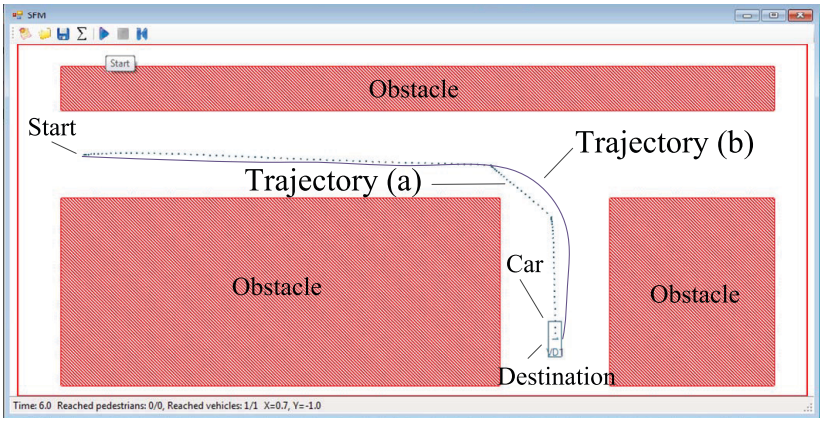

Figure 6.4: Driving trajectory simulation of a turning car (a) without steering angle constraints and (b) with steering angle constraints

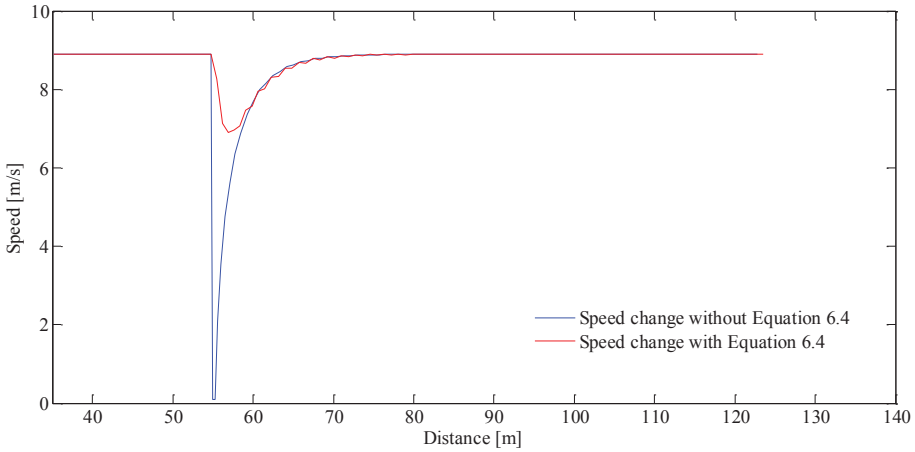

Figure 6.5: Speed change of a turning car as a result of steering angle constraints of Equation 6.4

6.3 Optimal Manoeuvre for Conflict Avoidance

The strategy for potential conflict avoidance is implemented for car-pedestrian interactions and - in a modified way - for car-car interactions in order to model

left-hand traffic in the UK. As explained in the previous chapters, each agent has an initial position and a desired destination which is reached based on the shortest path and exerted social forces along the way. A prediction of an interaction between two agents which results in a potential conflict is determined within a certain distance to each other. The conflict will occur if physical contact is estimated to be at a future time interval between these two agents. The term 'shadow' is introduced to detect potential conflicts. In general, reaction strategies can be classified into speed change, steering change or a combination of both. In this thesis, agents prevent potential conflicts using a combination of speed and direction change based on their relative position. The aim is then to find the minimum velocity change $\Delta \boldsymbol{v}^{\min}$ for each agent while deviating as little as possible from their desired direction of movement. In Section 6.3.1, a definition of the shadow is presented to predict potential conflicts. An optimisation is applied in order to calculate the minimum velocity change $\Delta \boldsymbol{v}^{\min}$ for car-pedestrian interactions (Section 6.3.2). The passing preference on the left hand side in the UK for two vehicles driving in opposite directions is described in Section 6.3.3.

6.3.1 Prediction of Potential Conflicts

If two agents are within a distance larger than their interaction range B_U, the possibility of a potential conflict is analysed. The conflict avoidance constraints are explained based on the geometrical considerations of two agents. Figure 6.6 illustrates the predicted intersecting trajectories of a pedestrian ($U_1 = \alpha$) and a car ($U_2 = \gamma$). The position, direction of movement and initial velocity of pedestrian α and car γ are shown in Figure 6.6 (a). $\varphi_{\alpha\gamma}$ is the angle between the direction of movement of pedestrian α and the force $\boldsymbol{f}_{\alpha\gamma}$ exerted from car γ to pedestrian α. Two lines are indicated parallel to the velocity difference that are tangential to pedestrian α in order to assign a section on the desired direction of car γ. This section is defined as the shadow of pedestrian α along the direction

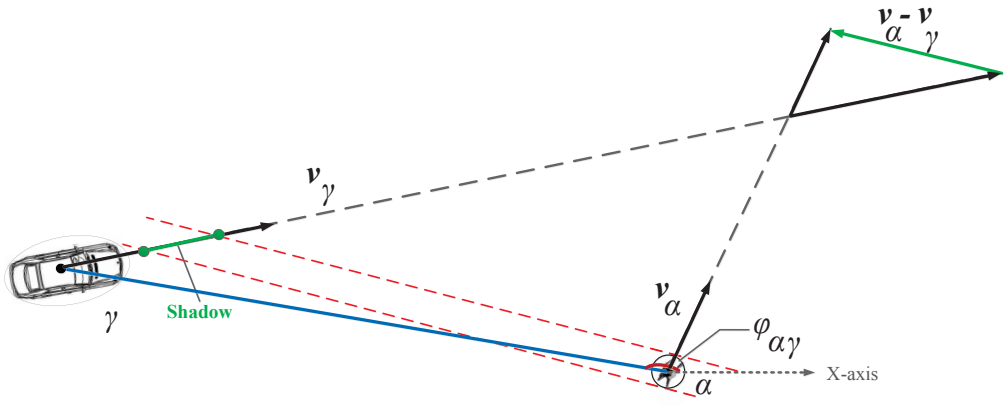

(a) Car γ does not intersect the shadow generated by pedestrian α

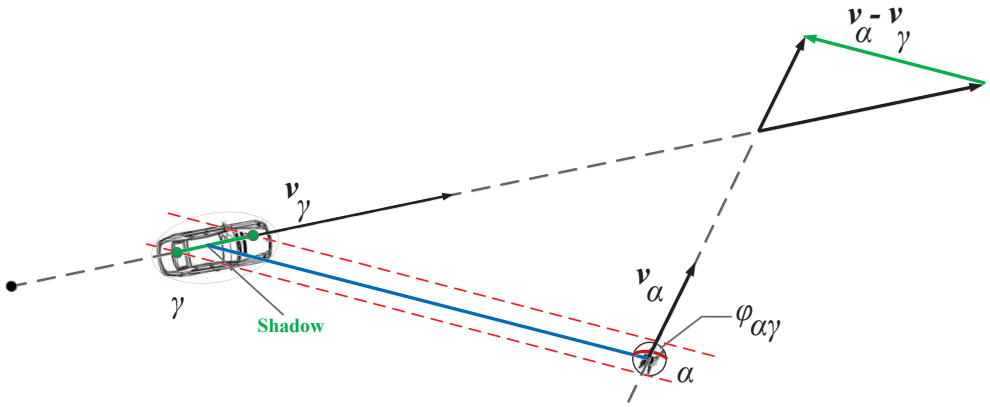

(b) Car γ intersects the shadow generated by pedestrian α

Figure 6.6: Geometric construction for conflict detection

of car γ similar to air traffic management systems [217]. A potential conflict is detected as soon as car γ intersects the shadow as shown in Figure 6.6 (b). This is explained mathematically in Equation 6.5.

$$\frac{(v_{y,\alpha} - v_{y,\gamma})}{(v_{x,\alpha} - v_{x,\gamma})} < tan(\varphi_{\alpha\gamma}) \tag{6.5}$$

The time t^{CPA} indicating the period to reach the location of minimum distance d^{CPA} between the agents at their Closest Point of Approach (CPA) needs to be determined. The minimum distance at the CPA is $d^{\mathrm{CPA}} = \left| r_\alpha(t^{\mathrm{CPA}}) - r_\gamma(t^{\mathrm{CPA}}) \right|$

and should not be less than the sum of their radii ($r_\alpha + r_\gamma(\varphi_{\gamma\alpha})$) as shown in Figure 6.7. The position of agent α and γ is given by $(x_\alpha(t), y_\alpha(t))$ and $(x_\gamma(t), y_\gamma(t))$. Their time-dependent velocity vectors are $(v_{x,\alpha}(t), v_{y,\alpha}(t))$ and $(v_{x,\gamma}(t), v_{y,\gamma}(t))$. At any time instance t, the distance between the two agents is given by $d(t) = \sqrt{\Delta x(t)^2 + \Delta y(t)^2}$. The time to the minimum distance is now calculated as $t^{\mathrm{CPA}} = -\frac{\Delta x \Delta v_x + \Delta y \Delta v_y}{\Delta v_x^2 + \Delta v_y^2}$. The time t^{CPA} to reach the CPA should be positive (in other words, in future) and less than a defined higher bound of $t^{\mathrm{CPA,max}}$ (in other words, in close future). If the time $0 < t_{\gamma\alpha}^{\mathrm{CPA}} < t_{\gamma\alpha}^{\mathrm{CPA,max}}$ and distance to reach the CPA is less than a certain value (in other words, in close future), the conflict avoidance strategy is activated. In the following section, an optimisation is applied in order to avoid conflict between agents.

6.3.2 Optimisation of Minimum Speed and Direction Change

The agent with a larger speed starts to accelerate and deviate whereas the other agent decelerates and deviates accordingly. An optimisation is applied to calculate a minimum velocity change $\Delta \boldsymbol{v}^{\min} = \boldsymbol{v}^{\mathrm{opt}}(t) - \boldsymbol{v}(t)$ in order to avoid

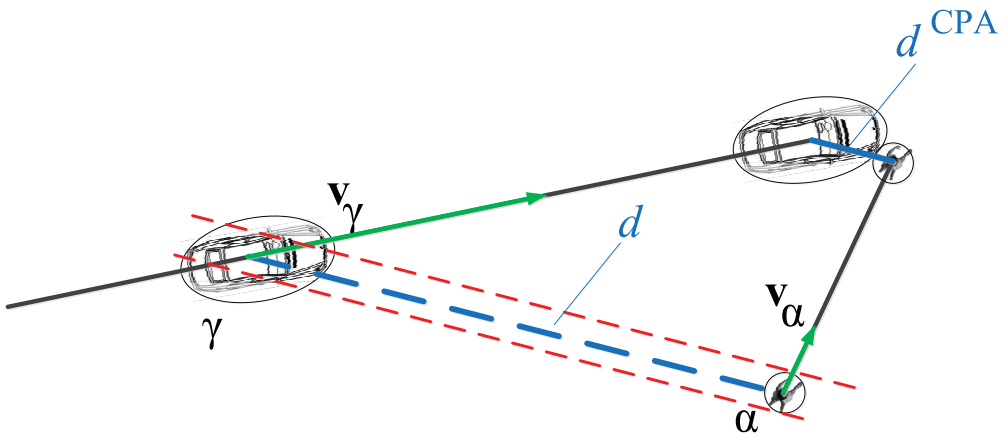

Figure 6.7: Closest Point Approach (CPA) illustration between car γ and pedestrian α.

conflicts. The cost function $c(v_x^{\text{opt}}(t), v_y^{\text{opt}}(t))$ in Equation 6.6 is optimised.

$$c\left(v_x^{\text{opt}}(t), v_y^{\text{opt}}(t)\right) = \left(v_x^{\text{opt}}(t) - v_x(t)\right)^2 + \left(v_y^{\text{opt}}(t) - v_y(t)\right)^2 \tag{6.6}$$

Equation 6.6 is to be minimised subject to constraints which are linear inequalities of variables used in the cost function. Firstly, the optimal speed should be within a defined speed interval $v_U^{\min} < v_U^{\text{opt}} < v_U^{\max}$. Secondly, the minimum distance between the agents at the CPA should be more than the sum of their radii. Thirdly, the distance to reach the CPA should be less than a certain value in order to be considered as a potential conflict. The optimisation problem incorporating all these constraints can be formulated as follows:

Minimize $c\left(v_x^{\text{opt}}(t), v_y^{\text{opt}}(t)\right)$

Subject to $v_U^{\min} < v_U^{\text{opt}} < v_U^{\max}$

$d_{\gamma\alpha}^{\text{CPA}} > r_\alpha + r_\gamma(\varphi_{\gamma\alpha})$

Distance to reach the CPA $>$ Minimum acceptable distance

A conflict avoidance force $\boldsymbol{f}_U^{\text{conflict}} = \frac{\Delta \boldsymbol{v}^{\min}}{\tau_U}$ is calculated and added to the sum of forces. A simulation of intersecting trajectories of a pedestrian and a car is presented before and after including the conflict avoidance force in Figure 6.8. According to social forces, pedestrian α starts decelerating and deviating from the desired direction of movement when within the interaction range B_α to a car (see Figure 6.8 (a)), without prior evaluation of the potential conflict. This is while pedestrian α and car γ start deviating from their desired direction of movement much earlier, as a result of conflict avoidance constraints in Figure 6.8 (b).

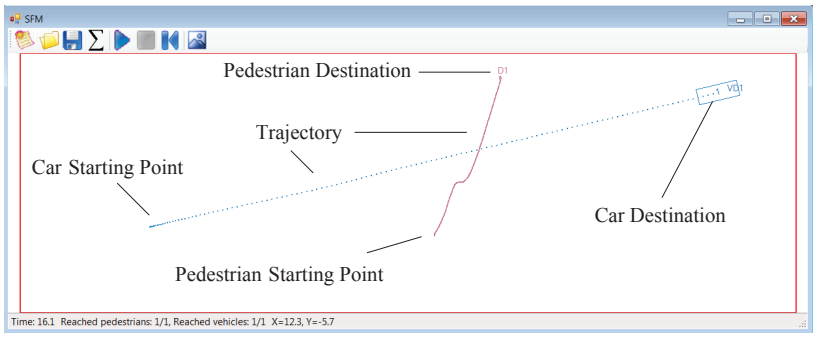

(a)

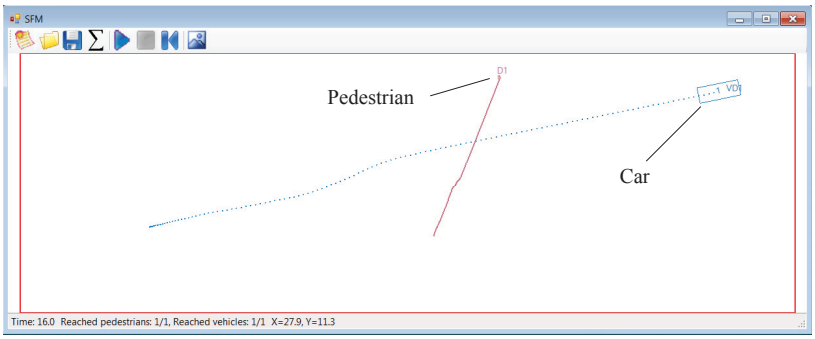

(b)

Figure 6.8: Simulation of the interaction between a car and pedestrian (a) without conflict avoidance force and (b) with conflict avoidance force

6.3.3 Left Hand Driving Preference in the UK

The UK is a left-hand traffic country which means that two cars facing each other in opposite directions keep to the left hand side. This general rule avoids confusion between car drivers and decreases the possibility of accidents. A conflict in this situation appears when

$$170^o \leq \arccos \frac{\boldsymbol{v}_\gamma(t) \cdot \boldsymbol{v}_\delta(t)}{|\boldsymbol{v}_\gamma(t)| \cdot |\boldsymbol{v}_\delta(t)|} \leq 190^o \tag{6.7}$$

and Equation 6.5 is met. Drivers' preference for the left hand side can be solved by minimising the cost function in Equation 6.6 with the following constraints:

$$\textbf{Minimize} \quad c\left(v_x^{\mathrm{opt}}(t), v_y^{\mathrm{opt}}(t)\right)$$

$$\textbf{Subject to} \quad v_U^{\min} < v_U^{\mathrm{opt}} < v_U^{\max}$$

$$d_{\gamma\delta}^{\mathrm{CPA}} > r_\alpha + r_\gamma(\varphi_{\gamma\delta})$$

$$\text{Distance to reach the CPA} > \text{Minimum acceptable distance}$$

$$0 \leq \arccos \frac{\boldsymbol{v}^{\mathrm{opt}}(t) \cdot \boldsymbol{v}(t)}{|\boldsymbol{v}^{\mathrm{opt}}(t)| \cdot |\boldsymbol{v}(t)|} \leq \psi_\gamma^{\max}$$

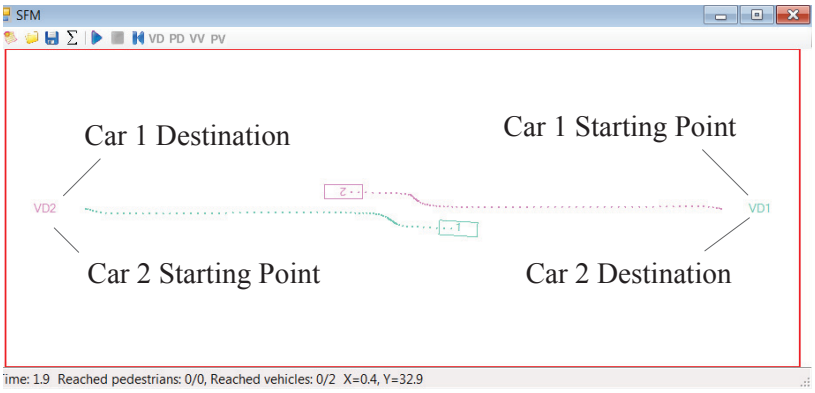

(a)

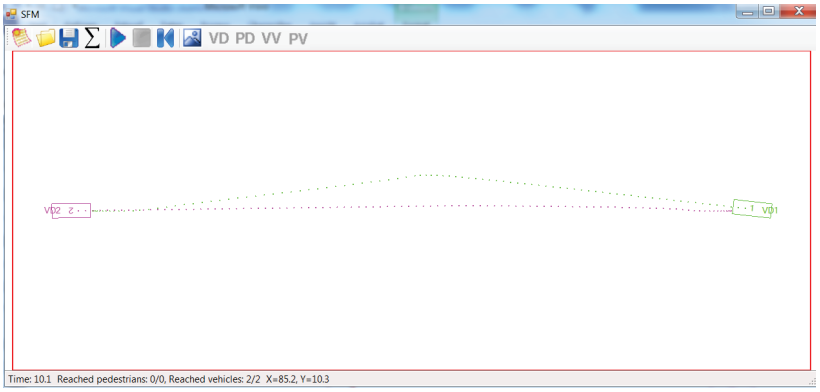

(b)

Figure 6.9: Simulation of car drivers behaviour when moving in opposite directions (a) without conflict avoidance force and (b) with conflict avoidance force (contained to the left-hand driving)

The latter condition results in an optimal change of direction by passing the other agent on the left hand side. Figure 6.9 demonstrates a situtation between two cars passing each other without (see Figure 6.9 (a)) and with (see Figure 6.9 (b)) applying this left-hand traffic constrain for car-car interactions.

6.4 Summary

This chapter investigated handling possible conflicts between pedestrians and cars based on their states. A potential conflict is detected as soon as agents enter each other's shadow, and resolved by a combination of speed and heading direction change. Conflict avoidance constraints were assigned for each agent to provide realistic conflict free interactions between pedestrians and cars while deviating as little as possible from the desired direction of movement. An optimisation was presented to calculate the minimum velocity change for both agents in order to avoid conflicts. Furthermore, a relationship was defined between car speed and steering angle considering the centrifugal acceleration to restriction of the lateral movement of cars. The three interrelated layers presented are implemented in software as explained in Chapter 7.

Chapter 7

Software Implementation and Qualitative Validation

This chapter describes the implementation in software of the three interrelated layers for shared space schemes. In the global path planning layer, the flood-fill algorithm and the Variant 2 distance metric are used to calculate the shortest path to the destination. Intermediate destinations are assigned for each agent before running the simulation. The second layer containing the force-based model is handled considering two operations. Firstly, a combination of the Verlet and the link cell algorithm is used to identify neighbouring agents within a certain radius. Then, the differential equations of the force-based layer are solved based on the Gear's predictor-corrector algorithm to perform the dynamic movement of pedestrians and cars. The third rule-based layer predicts potential conflicts and resolves them by running an optimisation algorithm and calculating the minimum velocity change. The optimised velocity is computed by satisfying a lower and higher bound of the speed and keeping a minimum distance of approach between agents. Pedestrian phenomena such as lane formation, freezing by heating, oscillations and faster-is-slower prove the correct implementation of the SFM. Furthermore, the Graphical User Interface (GUI) of the simulation tool for modelling the shared space traffic flow is introduced.

7.1 Implementation of the New Shared Space Model

The developed mathematical model is implemented using the C#-programming language with the Microsoft Visual C# 2008 compiler. The algorithms used for the implementation and simulation procedure of the shared space dynamics are explained in this chapter. The overall flowchart for the implementation of the shared space simulation is shown in Figure 7.1. At the beginning of the simulation, the environmental set up and the model parameters for pedestrians and cars are defined. After the path planning (see Section 7.2), the calculation of the force directed model is required for the agents in the environment. This is computationally demanding and in order to optimise the calculations, a maximum interaction distance (Verlet radius) is defined between road users to calculate exerted interaction forces of neighbouring agents. Then, the social, physical and following forces are calculated for all agents (see Section 7.3). The conflict avoidance force developed in this thesis is also added using a conflict detection and resolution approach based on the state of the agents (see Section 7.3). The positions, velocities and accelerations of each agent are stored. Forces for each agent are calculated until all the agents reach their destination (see Section 7.3). Several phenomena such as lane formation, freezing by heating, oscillations and faster-is-slower are reproduced for pedestrian flows by the simulation in Section 7.4. Furthermore, the simulator for modelling the shared space traffic flow is introduced in Section 7.5.

7.2 Trajectory Planning Layer

The path finding algorithm searches for the shortest trajectory from a start point to a destination point through a grid of cells. Kretz [208] investigated the calculation of distances for various geometries based on a visibility graph, the ray casting algorithm and the flood-fill algorithm (using Variant 2 metric). He re-

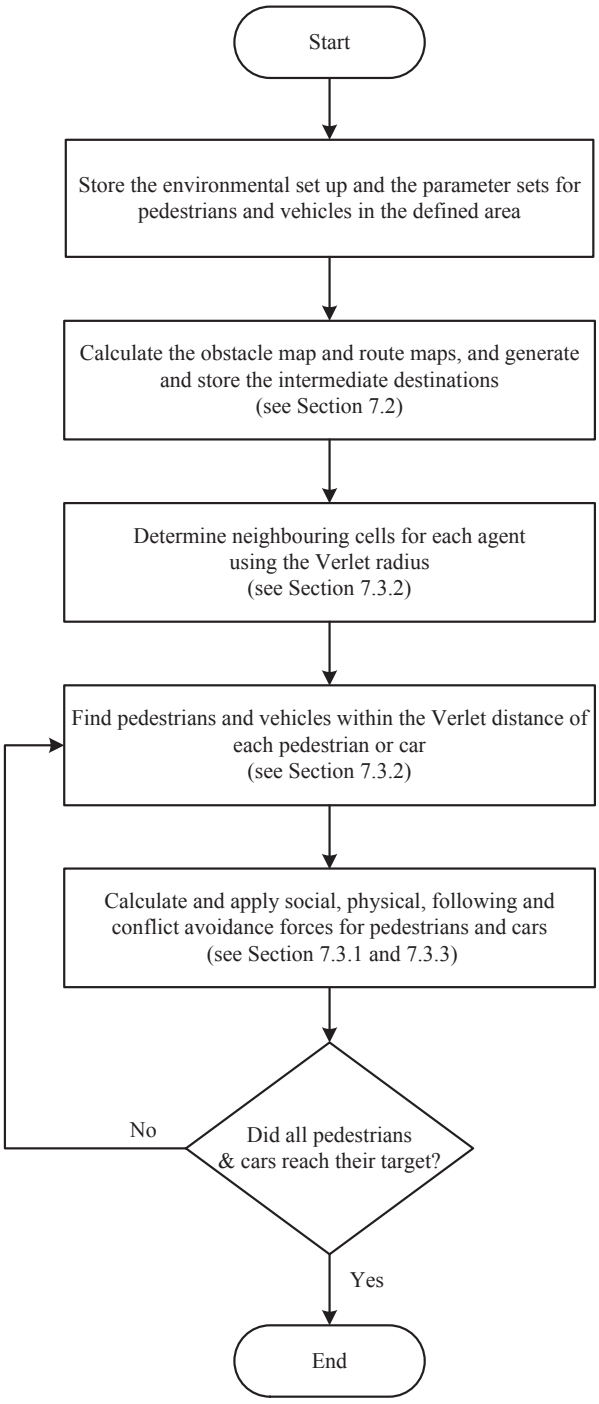

Figure 7.1: Overall flowchart of the shared space simulation

ported on the computation time and the deviation of the calculated distance from the Euclidean distance. It was concluded that the distance map calculation time can be reduced significantly while the error from the Euclidean distance remains balanced by using a combination of the Manhattan and Chessboard metrics.

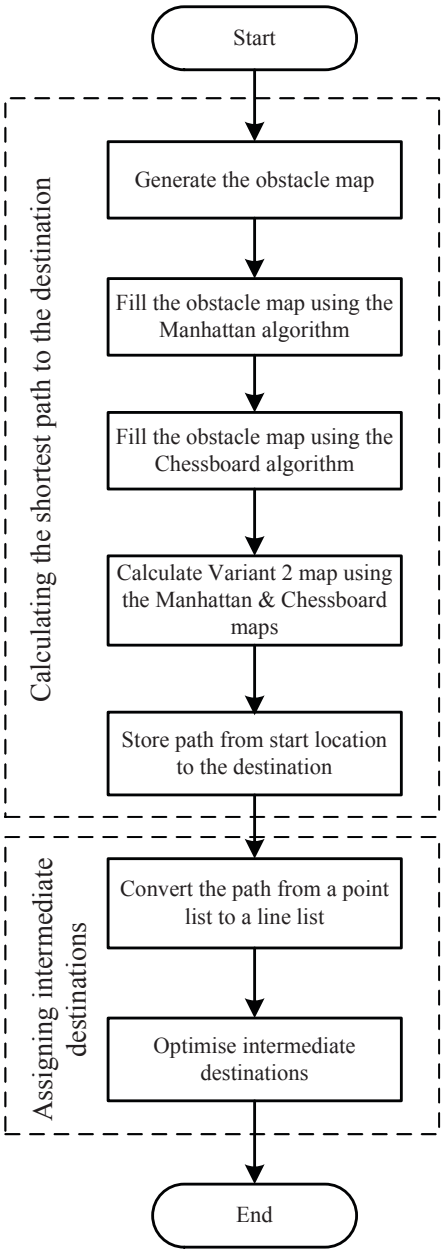

Figure 7.2: Flowchart of the global path finding algorithm

The flood-fill algorithm and Variant 2 metric are used for path planning of shared space users. As explained in Chapter 4, the algorithm has two main operation modes: calculating the shortest path to the destination for each agent according to the infrastructure of the environment and then assigning a number of intermediate destinations to the path of each agent. The flowchart is shown in Figure 7.2. The flood-fill algorithm is used to generate an obstacle map, a distance map based on the Manhattan metric and on the Chessboard metric, and a distance map based on a combination of the Manhattan and Chessboard map (Variant 2 distance map). The shortest path to the destination is then stored according to the Variant 2 distance map and intermediate destinations are assigned.

To find the shortest path, the flood-fill algorithm "floods" the area by assigning each cell with a distance value calculated to the nearest cell until reaching the start cell from the destination cell as discussed in Chapter 4. In order to represent the concept behind the flood-fill algorithm, the activity area is divided into a grid of cells. The obstacle map is generated by assigning a large number (max value) to all obstacle and boundary cells. Empty cells are set to -1 as shown

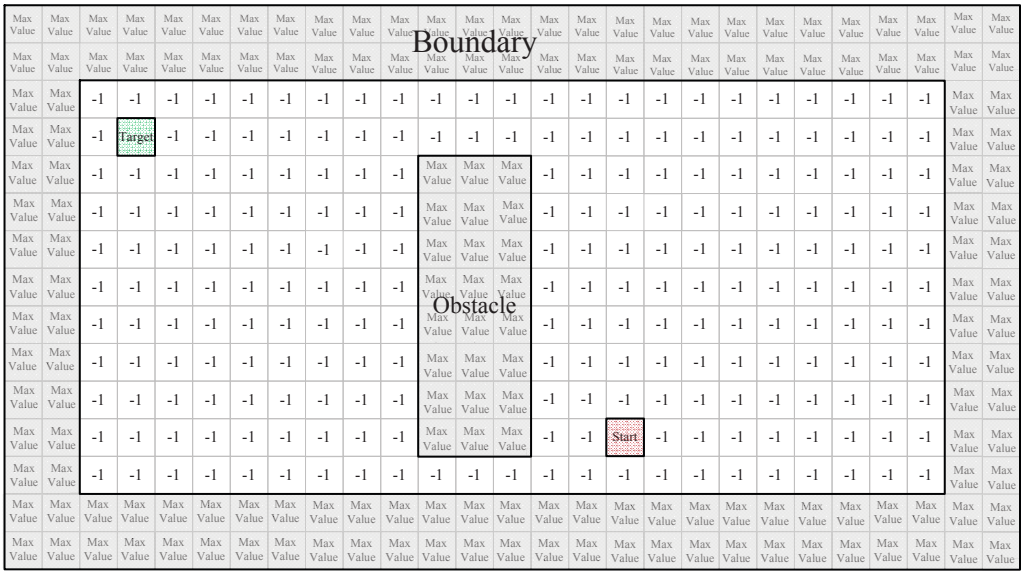

Figure 7.3: Conceptual example of an obtacle map

in Figure 7.3. The destination cell is set to 0. The flood-fill algorithm requires three parameters: the start cell, target cell, and replacement distance value. The algorithm considers all empty cells in the activity area which are connected to the start cell, queues them and changes their assigned value to the replacement distance value. These cells form the first level of expanded cells. In each iteration, a cell is de-queued and expanded into its neighbourhood. If the new cells are not enumerated in earlier iterations, they are added to the queue and their enumeration level increases by one. Obstacle and boundary cells are discarded and never enter the queue. In this simulation tool, shared space areas are divided into cells of size $15 \times 15\,\mathrm{cm}^2$ for pedestrians and cells of size $50 \times 50\,\mathrm{cm}^2$ for cars which are sufficient for the physical size of the agents. The replacement distance value is calculated based on the Variant 2 metric. This method measures the distance between two coordinates based on a combination of the Manhattan metric D^{M} and the Chessboard metric D^{C} as in Equation 4.4 [208]. As explained in Chapter 4, two distance maps are calculated in order to flood a route map based on the Variant 2 metric.

The Manhattan distance value between two coordinates is calculated based on Equation 4.2, a 4-connected neighbourhood (North, East, West and South). A Manhattan distance map is generated by using the flood-fill algorithm and searching towards the start cell as shown in Figure 7.4. A similar flowchart as shown in Figure 7.5 is followed to flood the 8-connected neighbourhood to produce the Chessboard map. The distance values are generated based on Equation 4.3.

A distance map is calculated for the direct neighbourhood (8-connected neighbourhood) by a combination of the Manhattan and Chessboard distance value by following Equation 4.4 as shown in Figure 7.6. The value assigned to each cell on the route map indicates the corresponding distance from the goal. As a result, the shortest path can be found by moving from the start point to the neighbouring cell following the lowest value as shown in Figure 7.6. The nodes at the end of

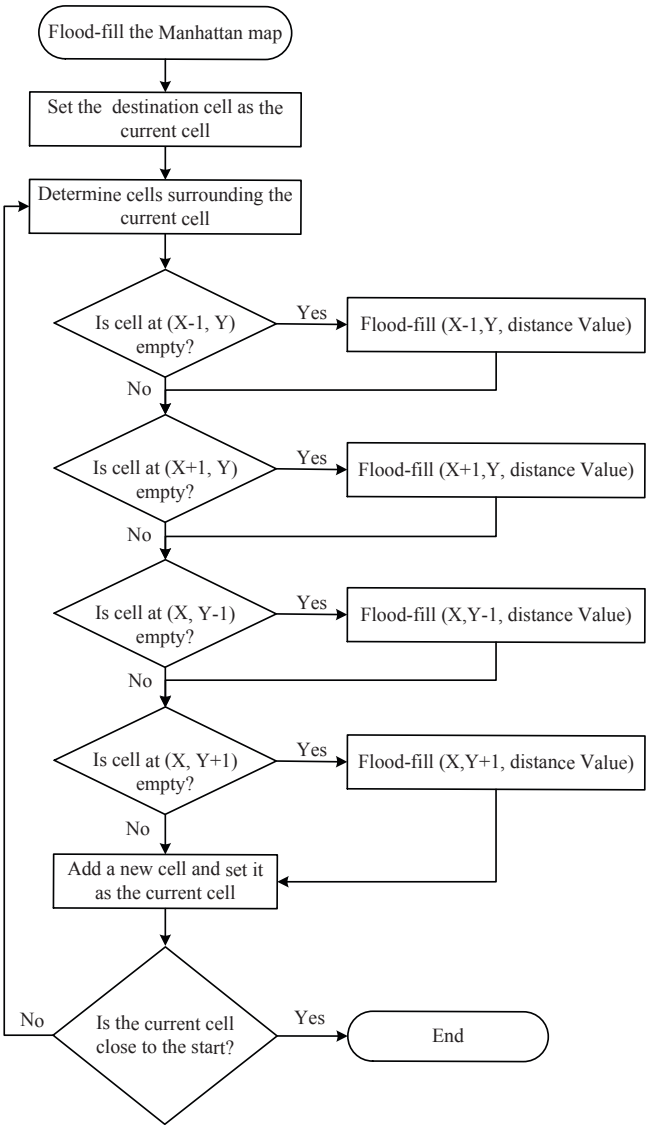

Figure 7.4: Flood-fill algorithm for 4-connected neighbouring cells

each line are assigned as the intermediate destination for the shared space users. However, if a line between three successive intermediate destinations does not overlap with any obstacle, the middle intermediate destination is omitted. The minimum numbers of intermediate destinations are saved after collision checks with obstacles. The flowchart is shown in Figure 7.7.

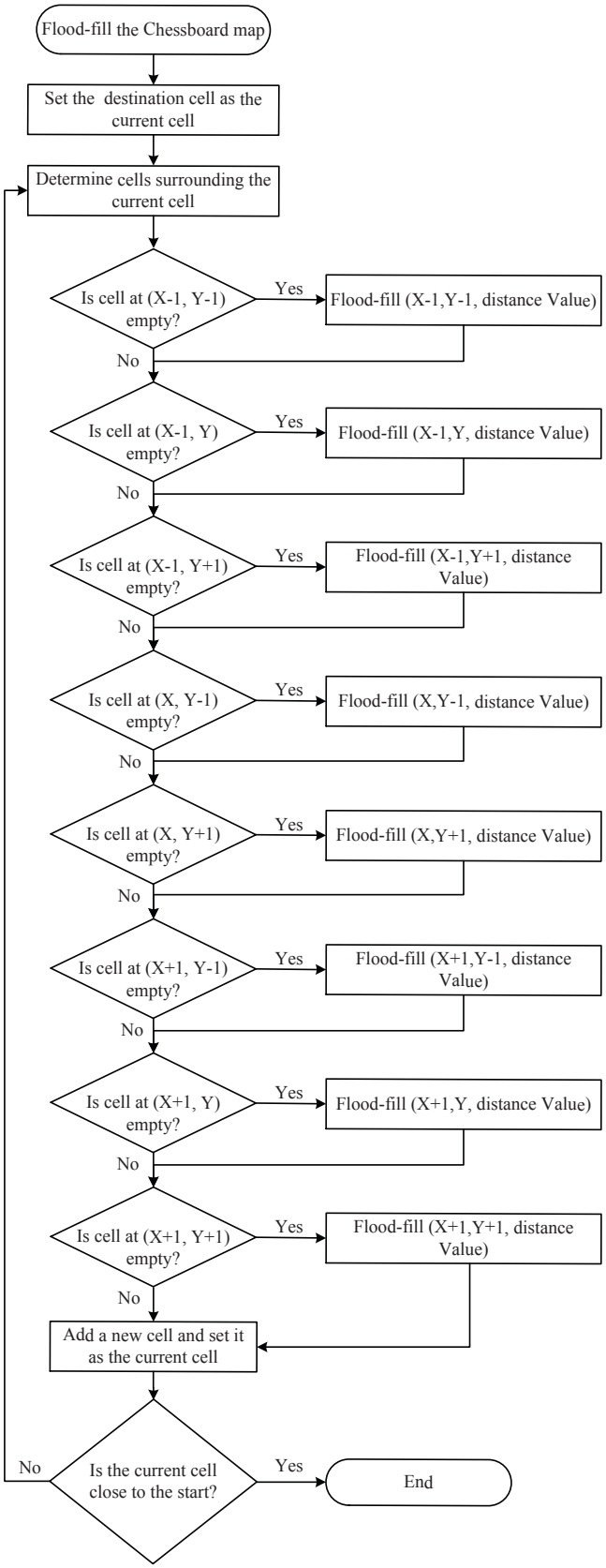

Figure 7.5: Flood-fill algorithm for 8-connected neighbouring cells

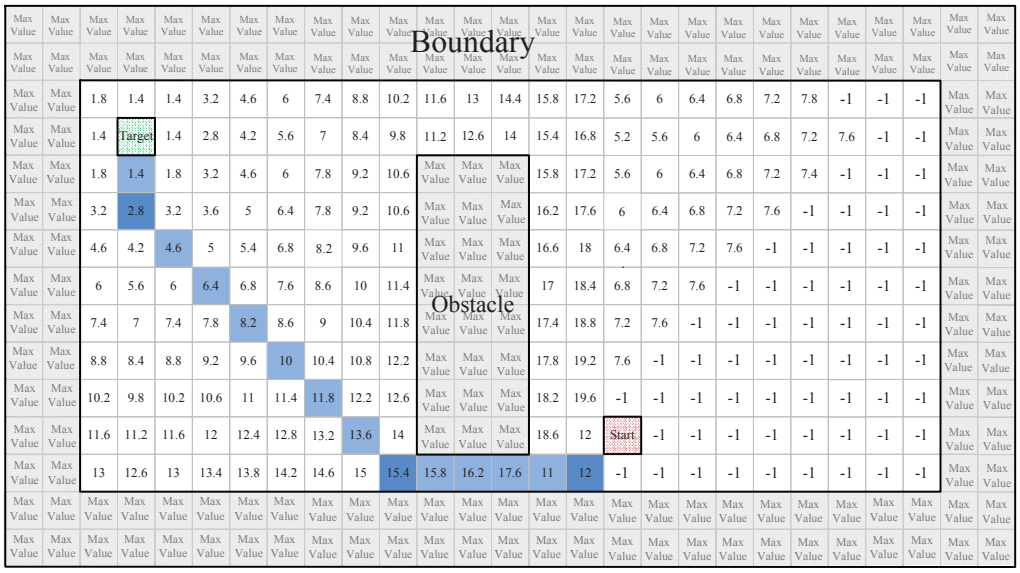

Figure 7.6: Distance map based on Variant 2 metric

7.3 Force and Rule-based Layer

The force-based layer is the core of the dynamic shared space traffic. The overall flowchart of the force directed model is explained in Section 7.3.1. In order to reduce the complexity of the calculations in this layer, the Verlet Link Cell algorithm is used to optimise the road users interactions (see Section 7.3.2). The Ordinary Differential Equations (ODEs) are solved by using a Gear's predictor-corrector algorithm as explained in Section 7.3.3. The conflict detection and handling with optimisation is explained in Section 7.3.4.

7.3.1 Force-based Model

The algorithm for deriving the forces for each agent is shown in Figure 7.8. The simulation of movement based on the proposed force directed model requires solving the Ordinary Differential (OD) Equation 5.14 and 5.22 numerically over time. The Gear's fourth order predictor-corrector algorithm is used to solve the ODEs leading to the calculation of the predictor and corrector values for solving

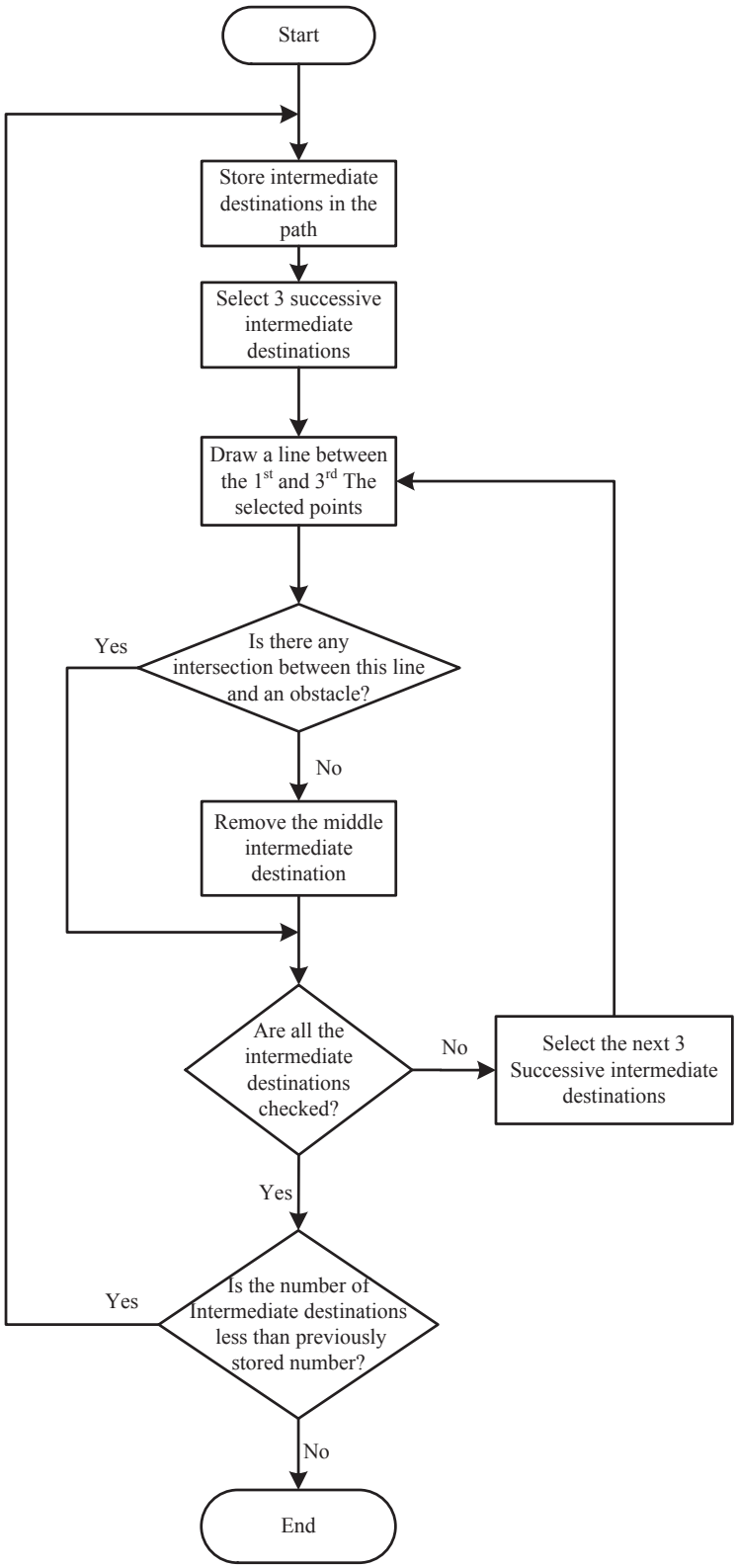

Figure 7.7: Flowchart of optimisation of the intermediate destinations after collision checks

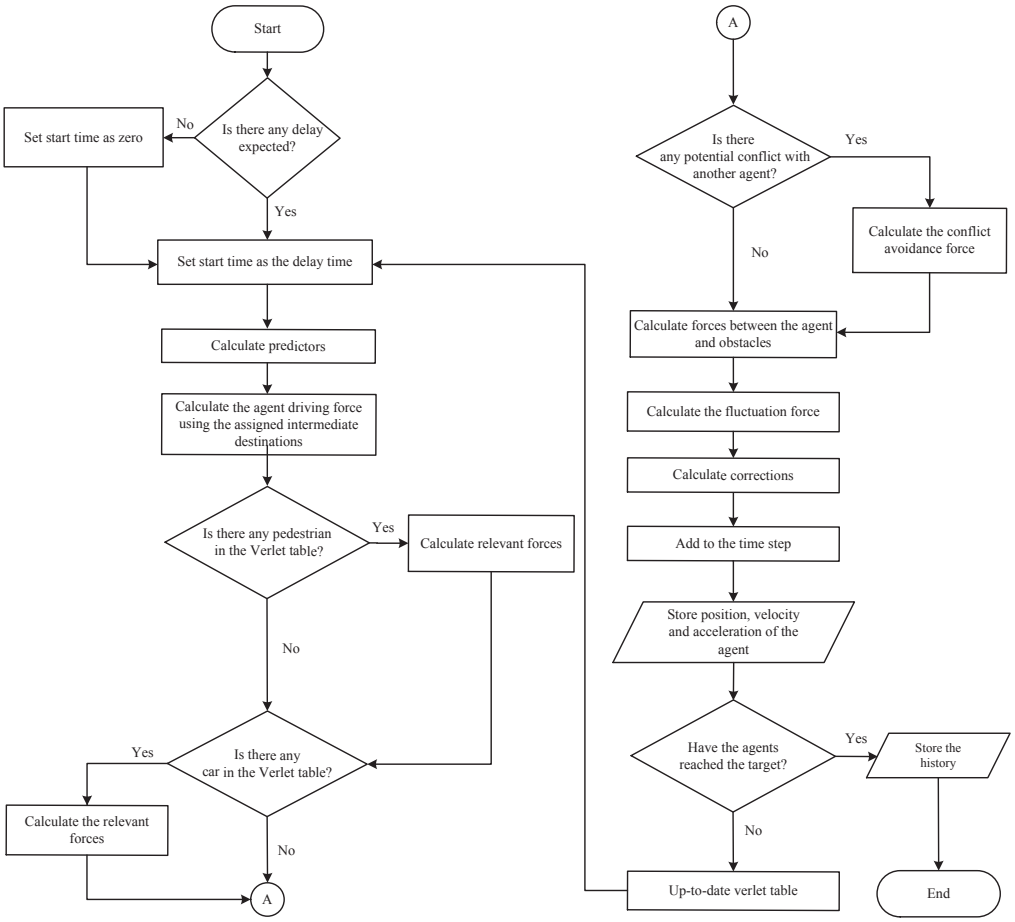

Figure 7.8: Flowchart of determining interaction forces

the ODEs in the shared space model (Section 7.3.3). The predicted values for each agent at each time step are calculated considering the speed limit in shared space environments. Subsequently, the driving force is derived by considering an acceleration limit. The exerted interaction force from one agent to the others is calculated. The conflict avoidance force is included after detecting a potential conflict according to the state of agents and assigned rules. For each agent, the interaction force with polygon elements of obstacles/boundaries is determined and added to the previously computed sum of forces. The last calculated force is the fluctuation force. Then, the calculation of the corrector values and determination of position, velocity and acceleration using the corrector values is conducted.

7.3.2 Verlet Link Cell Algorithm

The force impact of agents further than a certain distance can be neglected as it is small. These agents do not need to be considered for the force calculations. Hence, the Verlet link cell algorithm is added as in [162] which is a combination of the Verlet algorithm and the cell lists algorithm. In the latter algorithm, the simulation area is divided into cells with a width which is equal to the maximum interaction distance r_{Verlet} between agents. As shown in Figure 7.9, it is sufficient to take into account that a given agent (black circle) interacts only with other agents appearing in its own cell and those that are close neighbours (8 adjacent cells). The cell lists algorithm is an effective method to reduce computational complexity of the force directed model. The interactions between agents in neighbouring cells can be further optimised by using the Verlet algorithm. A circle is introduced for each agent (see Figure 7.10) with the radius r_{Verlet} for the maximum interaction distance within which the interaction forces are calculated. Agents outside the Verlet circle do not affect the agent. Since the agents motion is dynamic with changing position and neighbourhood, the update time for the neighbouring agents within the Verlet circle should be chosen carefully.

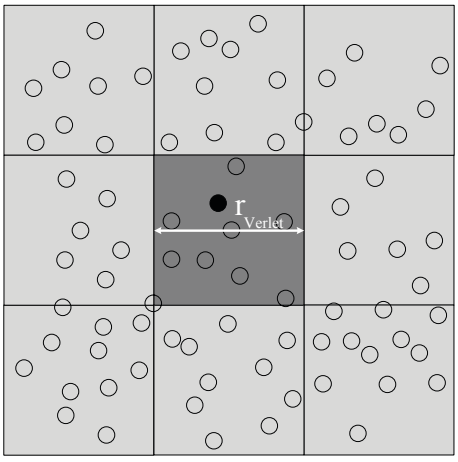

Figure 7.9: Cell list structure for maximum interaction distance

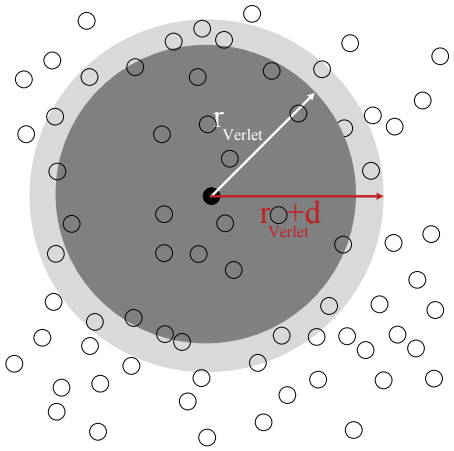

Figure 7.10: Verlet circle for maximum interaction distance

If Verlet lists are extended and include agents outside the maximum distance of interaction, $r_{\text{Verlet}} + d$, the lists should be updated only when the maximum displacement of an agent is larger than d. If the displacement is smaller, Verlet lists are still valid. The implementation of the Verlet algorithm involves checking which agents are within the Verlet circle. In case of small force changes and time steps, the interacting agents do not change during a specific period. Changes only occur at the edges of the Verlet circle when agents either leave or enter it having only a small impact from this distance. Hence, the Verlet algorithm is optimised by splitting the simulation field into cells with each agent assigned to a specific cell (called cell lists algorithm). The width of cells is set to $r_{\text{Verlet}} + d$ so that the possible interacting neighbouring agents are within this cell (see Figure 7.11). Therefore, only the agents within the 9 cells have to be evaluated for possible interaction with a neighbouring agent. The assignment of agents to cells is updated frequently. The radius of the Verlet circle is set at the beginning of the simulation. The simulation field is then divided into cells of width $r_{\text{Verlet}} + 0.05 \cdot r_{\text{Verlet}}$ and the number of agents in each cell is calculated. All cells are evaluated to find the interacting neighbouring agents. Firstly, the interactions within a cell are considered and, secondly, the interactions with the neighbouring cells are

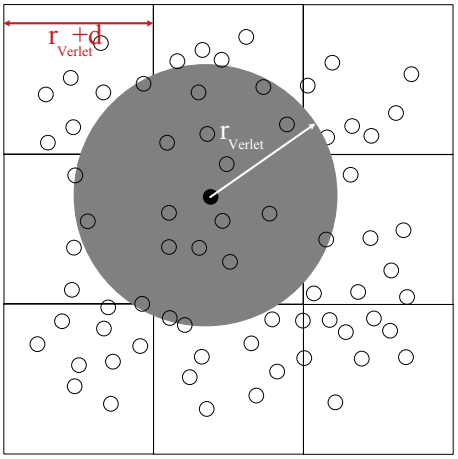

Figure 7.11: Verlet link cell for maximum interaction distance

evaluated. Finally, possible interactions within the Verlet circle of the agent are checked. The forces are calculated using the Gear's integrator as explained in Section 7.3.3.

7.3.3 Solving the Differential Equations

The simulation of movement based on the force directed model requires the solution of the OD Equations 5.14 and 5.22 numerically over time. The two relevant numerical integration methods are one-step and multi-step. The former use one previous value to evaluate the next value. These include the first order Euler and fourth order Runge-Kutta methods [218]. The first order ODE $\frac{dy}{dx} = \frac{x}{y}$ with the initial condition of $y(0) = 1$ is solved with the Euler and Runge-Kutta methods and the estimate errors are shown in Figure 7.12. The main limitation of the Euler method is its inaccuracy due to its simplicity (see Figure 7.12). The Runge-Kutta method is accurate and computationally demanding since it requires four calculations for every time step. Multi-step methods have the advantage of using multiple previous values to evaluate the next one. Runge-Kutta algorithm at large time steps of $0.1\,\mathrm{s}$ is still more accurate than the Euler's method with small time steps of $0.05\,\mathrm{s}$.

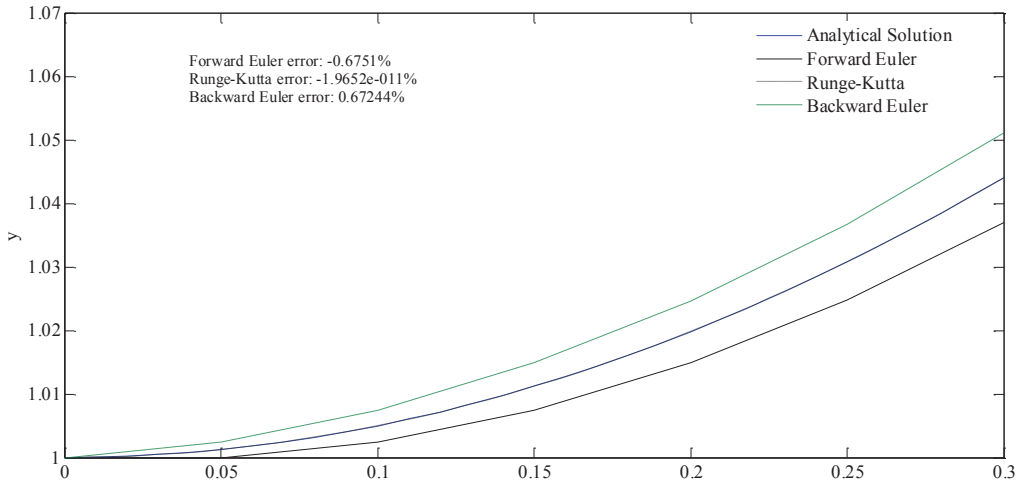

Figure 7.12: Comparison of analytical solution of $\frac{dy}{dx} = \frac{x}{y}$ ($y(0) = 1$ and $0 < x_0 < 0.3$) with one-step and multi-step methods

In this thesis, the gear predictor-corrector method is used due to the fact that it can deal efficiency with nonlinear differential equations (velocity and position-dependent forces) with one force call compared to four force calls in Runge-Kutta. This multi-step method is well-known as one of the economical numerical integration method [219]. The fourth order Gear's predictor algorithm keeps two higher derivatives to be able to get a sufficient estimation of the new position and velocity. The position and its higher derivations are approximated by the Taylor series expansion in the predictor step as in Equation 7.1.

$$\begin{aligned}
\boldsymbol{r}^p(t+\Delta t) &= \boldsymbol{r}(t) + \tfrac{\Delta t}{1!}\boldsymbol{v}(t) + \tfrac{\Delta t^2}{2!}\boldsymbol{a}(t) + \tfrac{\Delta t^3}{3!}\dot{\boldsymbol{a}}(t) + \tfrac{\Delta t^4}{4!}\ddot{\boldsymbol{a}}(t),\\
\boldsymbol{v}^p(t+\Delta t) &= \boldsymbol{v}(t) + \tfrac{\Delta t}{1!}\boldsymbol{a}(t) + \tfrac{\Delta t^2}{2!}\dot{\boldsymbol{a}}(t) + \tfrac{\Delta t^3}{3!}\ddot{\boldsymbol{a}}(t),\\
\boldsymbol{a}^p(t+\Delta t) &= \boldsymbol{a}(t) + \tfrac{\Delta t}{1!}\dot{\boldsymbol{a}}(t) + \tfrac{\Delta t^2}{2!}\ddot{\boldsymbol{a}}(t),\\
\dot{\boldsymbol{a}}^p(t+\Delta t) &= \dot{\boldsymbol{a}}(t) + \tfrac{\Delta t}{1!}\ddot{\boldsymbol{a}}(t),\\
\ddot{\boldsymbol{a}}^p(t+\Delta t) &= \ddot{\boldsymbol{a}}(t)
\end{aligned} \tag{7.1}$$

The integrator algorithms generate errors due to the truncation of the Taylor expansion. The difference between the predictor acceleration $\boldsymbol{a}^p(t+\Delta t)$ and that calculated from $\boldsymbol{r}^p(t+\Delta t)$ and $\boldsymbol{v}^p(t+\Delta t)$ is assumed as the error presented by parameter c:

$$c = \boldsymbol{a}^c(t+\Delta t) - \boldsymbol{a}^p(t+\Delta t) \tag{7.2}$$

In the correction step, the position, velocity and the higher derivative are calculated and the coefficients depend on the order of both the differential equation and the Taylor series as follows:

$$\begin{aligned}
\boldsymbol{r}^c(t+\Delta t) &= \boldsymbol{x}^p(t+\Delta t) + \alpha_0 \tfrac{\Delta t^2}{2} c,\\
\boldsymbol{v}^c(t+\Delta t)\tfrac{\Delta t}{1!} &= \boldsymbol{v}^p(t+\Delta t)\Delta t + \alpha_1 \tfrac{\Delta t^2}{2} c,\\
\dot{\boldsymbol{a}}^c(t+\Delta t)\tfrac{\Delta t^3}{3!} &= \dot{\boldsymbol{a}}(t)\tfrac{\Delta t^3}{3!} + \alpha_3 \tfrac{\Delta t^2}{2} c,\\
\ddot{\boldsymbol{a}}^c(t+\Delta t)\tfrac{\Delta t^4}{4!} &= \ddot{\boldsymbol{a}}(t)\tfrac{\Delta t^4}{4!} + \alpha_4 \tfrac{\Delta t^2}{2} c
\end{aligned} \tag{7.3}$$

The Gear corrector coefficients are parameterised for q^{th} order predictors and

Coefficient	3^{th} **order**	4^{th} **order**	5^{th} **order**
α_0	$\frac{1}{6}$	$\frac{19}{120}$	$\frac{3}{20}$
α_1	$\frac{5}{6}$	$\frac{3}{4}$	$\frac{251}{360}$
α_2	1	1	1
α_3	$\frac{1}{3}$	$\frac{1}{2}$	$\frac{11}{18}$
α_4	0	$\frac{1}{12}$	$\frac{1}{6}$
α_5	0	0	$\frac{1}{60}$

Table 7.1: Gear corrector coefficients for q^{th} order predictors based on [220]

summarised in Table 7.1 based on a linear stability analysis [220]. The correcting stage is summarised accordingly as follow:

$$\begin{aligned}
\boldsymbol{r}^c(t+\Delta t) &= \boldsymbol{x}^p(t+\Delta t) + \tfrac{19}{120} \cdot \tfrac{\Delta t^2}{2} c, \\
\boldsymbol{v}^c(t+\Delta t) &= \boldsymbol{v}^p(t+\Delta t) + \tfrac{3}{4} \cdot \tfrac{\Delta t}{2} c, \\
\dot{\boldsymbol{a}}^c(t+\Delta t) &= \boldsymbol{a}^p(t+\Delta t) + \tfrac{1}{2} \cdot \tfrac{3}{\Delta t} c, \\
\ddot{\boldsymbol{a}}^c(t+\Delta t) &= \dot{\boldsymbol{a}}(t) + \tfrac{1}{12} \cdot \tfrac{12}{\Delta t^2} c
\end{aligned} \tag{7.4}$$

This numerical solver leads to numerical simulations for pedestrian and car movements.

The accuracy of the Gear predictor-corrector method depends on the time step size. The time step size is set to 0.1 since any value higher than 0.2 leads to inacceptable results in the simulation (i.e. breakthroughs) while values less than 0.1 does not contribute to a significant improvement for the simulation [162].

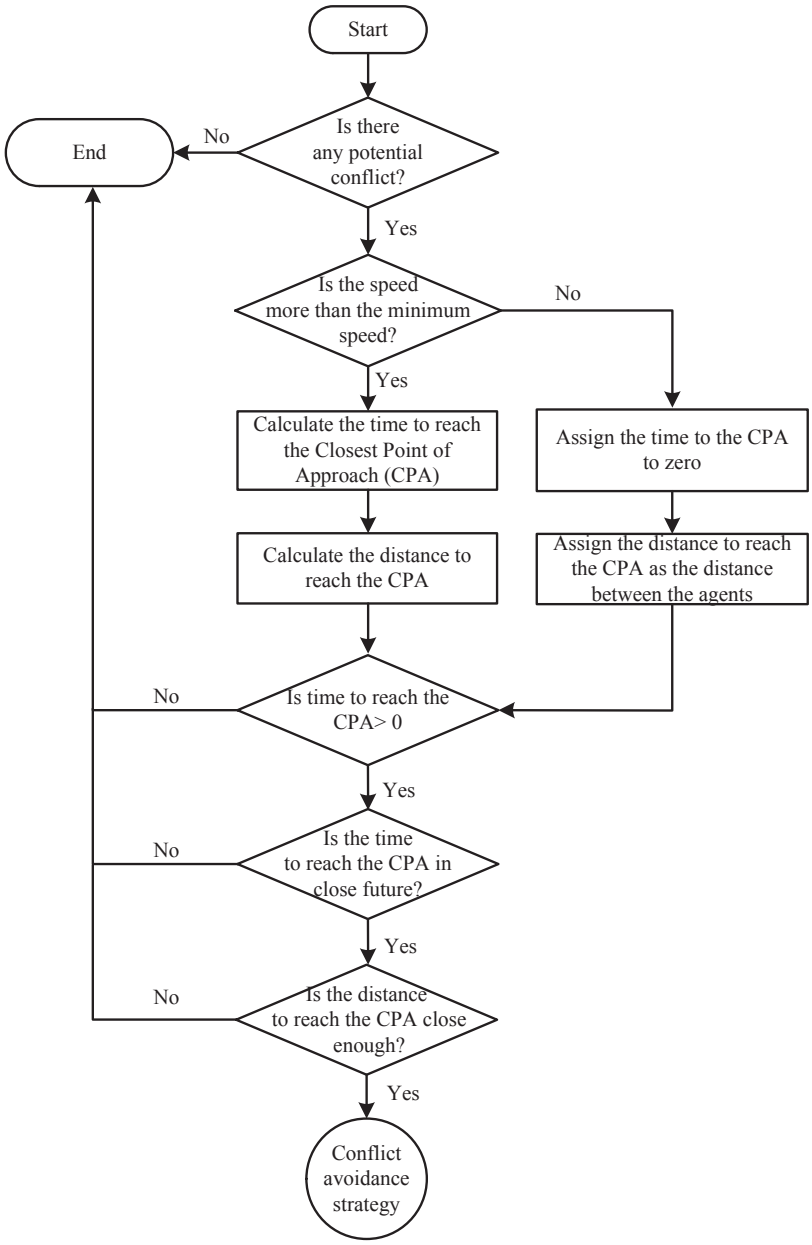

Figure 7.13: Flowchart for detecting a conflict between agents

7.3.4 Rule-based Model

In Section 6.3.1, the conflict detection strategy based on the instantaneous state of agents was explained for pedestrians and cars. It is implemented according to the flowchart in Figure 7.13. Assuming the distance between two agents is

given by a minimum distance, then no conflict occurs as long as the agents are outside the minimum distance during their motion in space. As discussed in Section 6.3.1, the minimum distance between two agents is the distance between the agent positions at their Closest Point of Approach (CPA). Once the time to reach the CPA t^{CPA} is known, the minimum distance can be calculated. A polyline approximation of a trajectory connects agents positions sampled at discrete time instances by line segments. After detecting a potential conflict and calculating the time to reach the CPA, an optimisation is applied to calculate the minimum velocity change $\Delta \boldsymbol{v}^{\min} = \boldsymbol{v}^{\mathrm{opt}}(t) - \boldsymbol{v}(t)$ to avoid the potential conflict (see Section 6.3.2). The algorithm for computing the optimised velocity over multi-segment trajectories is given in Figure 7.14. The conflict avoidance force is calculated using the optimised velocity and added to the sum of forces.

7.4 Qualitative Validation of the Implemented SFM based on Observed Crowd Phenomena

The SFM for pedestrian motions has been simulated for different observed phenomena such as lane formation, freezing by heating, oscillation and faster-is-slower patterns which can be described realistically by the SFM [221]. These self-organised spatio-temporal patterns occur without the interference of external influences (i.e. by traffic signs, laws, or conventions). These phenomena are reproduced by the simulation tool in the following sections. The reproduction of the phenomena prove the correct implementation of the SFM.

7.4.1 Lane Formation

The SFM reproduces the lane formation. The model explains lane formation without any a priori knowledge about the walking side preference of pedestrians. Bidirectional flow of pedestrians in a corridor leads to many interactions

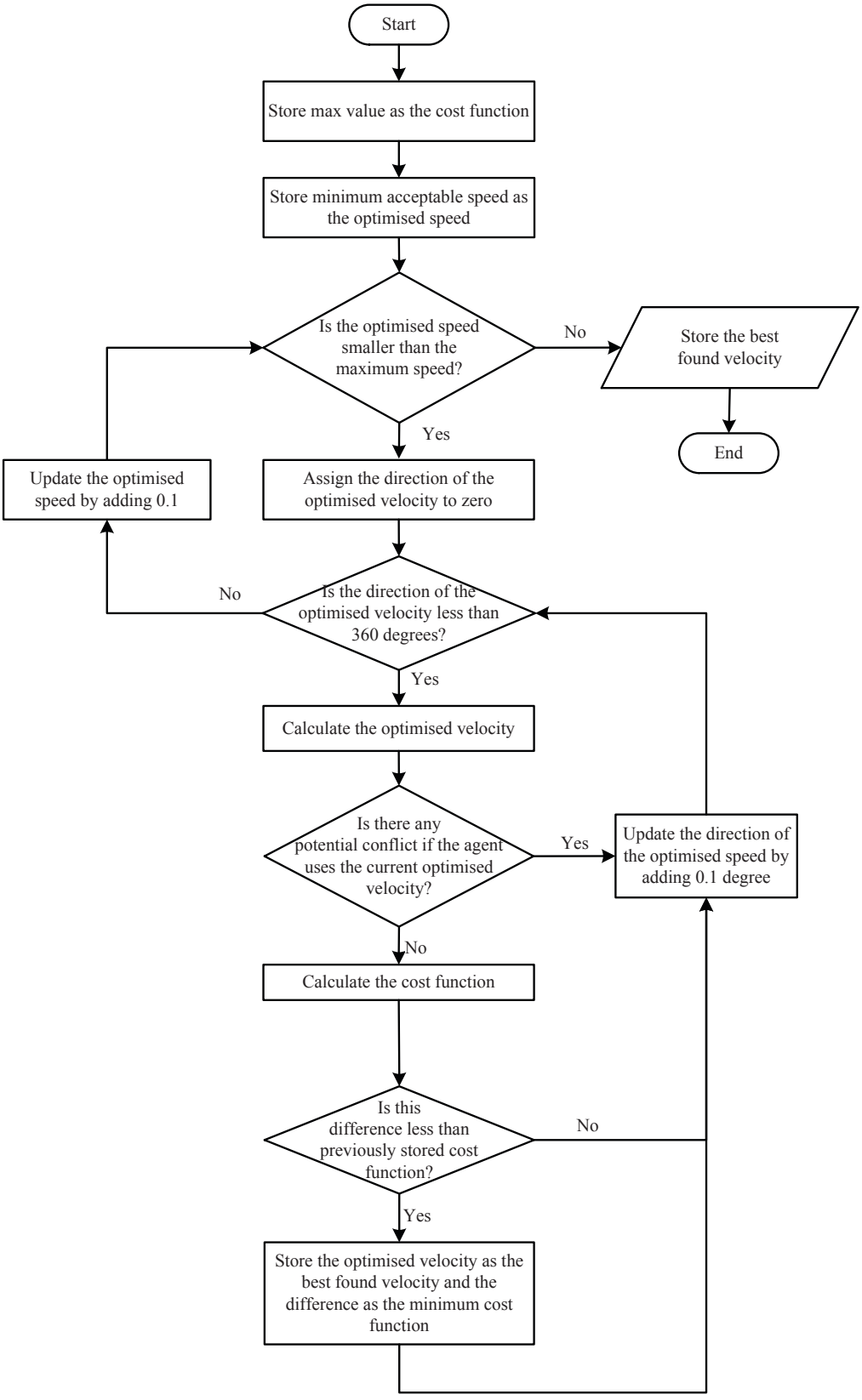

Figure 7.14: Flowchart for optimising the velocity change to avoid conflicts between agents

and results in sideways movements which finally leads to separation. The lane formation pattern minimises avoidance manoeuvres. An illustration of this phenomenon can be seen in Figure 7.15 by assigning the parameters in Table 7.2.

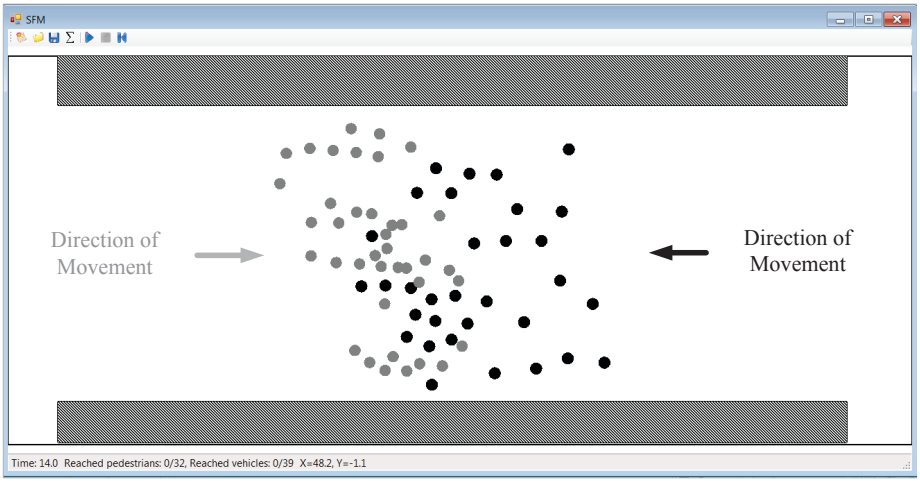

Figure 7.15: Simulated lane formation of bidirectional flow of pedestrians in a corridor

In the conventional interpretation of lane formation, it is assumed that pedestrians tend to walk on the side which is prescribed in vehicular traffic. However, the SFM can explain lane formation even without assuming a preference for any side.

7.4.2 Freezing by Heating

The freezing by heating phenomenon occurs when the lane formations break down due to extreme densities [221]. This results in clogging that brings the pedestrians to a deadlock. The illustration of this phenomenon as presented in [48] can be seen in Figure 7.16. Table 7.2 gives the summary of the parameters used to produce the lane formation and freezing by heating phenomena.

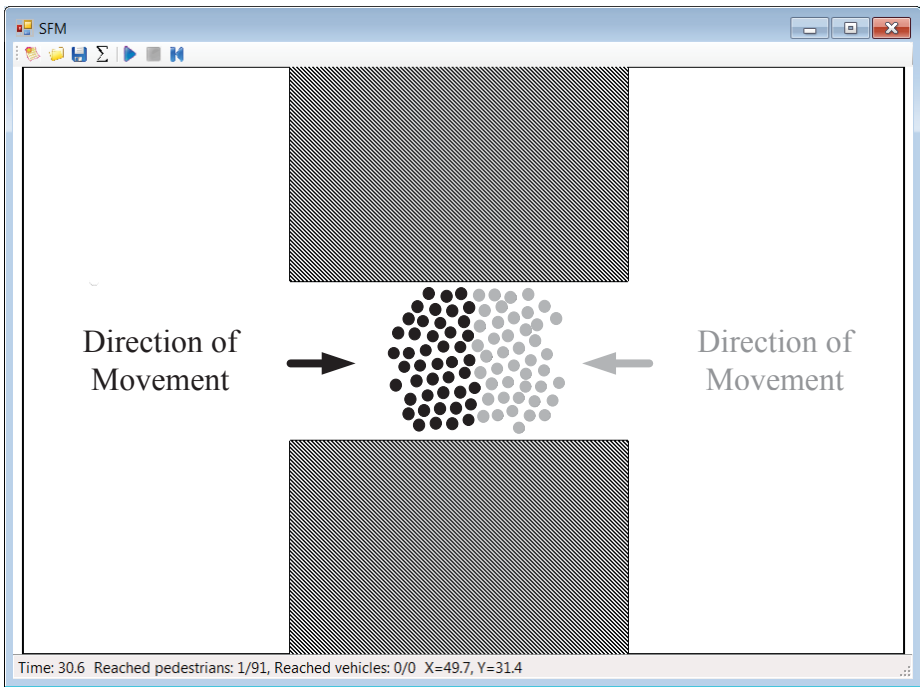

Figure 7.16: Simulation results for freezing by heating phenomenon

7.4.3 Oscillations

Oscillating flows follow when clogging occurs at a bottleneck and small groups of pedestrians from each direction alternate in getting through the bottleneck. The effect is described in [48]. In Figure 7.17, a simulated case of oscillation is used to demonstrate the effect. In a bidirectional flow from a narrow exit, only a few pedestrians reach the other side of the room. This flow continues until the pressure of the other side stops the flow. A short period of balance occurs until another few pedestrians reach the other side. This irregular out flow is due to clogging around the narrow exit as shown in Figure 7.17. Parameters used for the simulation are summarised in Table 7.2.

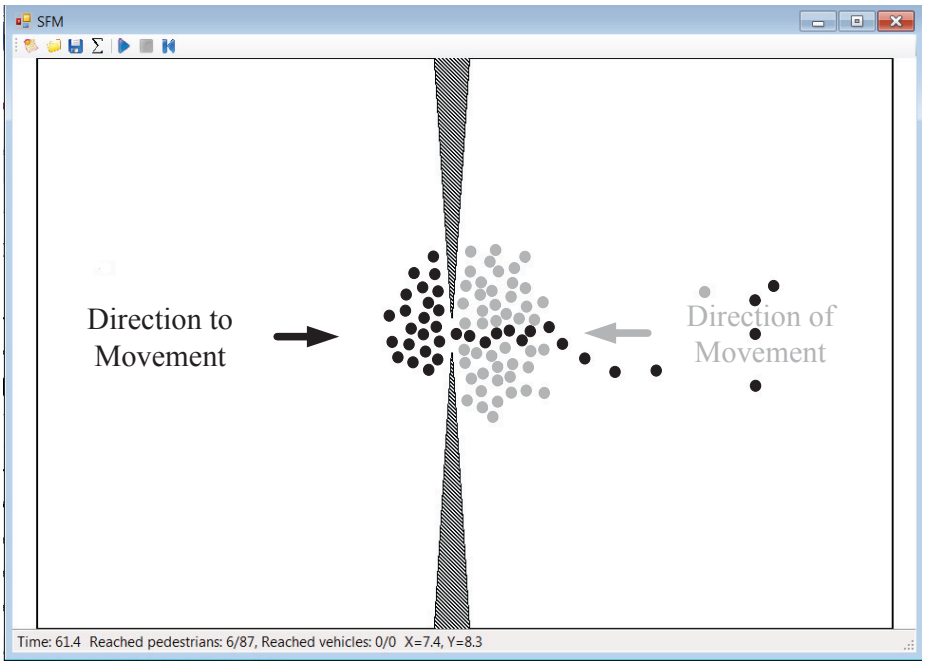

Figure 7.17: Simulation results for oscillation

7.4.4 Faster-Is-Slower

As discussed in Section 2.1, the Faster-Is-Slower (FIS) phenomenon is observed when pedestrians leave a room through a narrow exit. Faster desired movement speeds at the exit result in a longer time to empty the room. The result from simulation can be seen in Figure 7.18 and the parameters for this simulation are summarised in Table 7.2. Here, it is apparent that clogging occurs at the doorway leading to a longer time to clear the room for desired velocities above $3\,\frac{\mathrm{m}}{\mathrm{s}}$.

7.5 Graphical User Interface of the Simulation Tool

The proposed mathematical model for shared space users is developed in C#. This simulator has a Graphical User Interface (GUI) consisting of a main window and several user buttons. Figure 7.19 outlines the main components of the simulation tool. The main window allows the interactions and motion of the

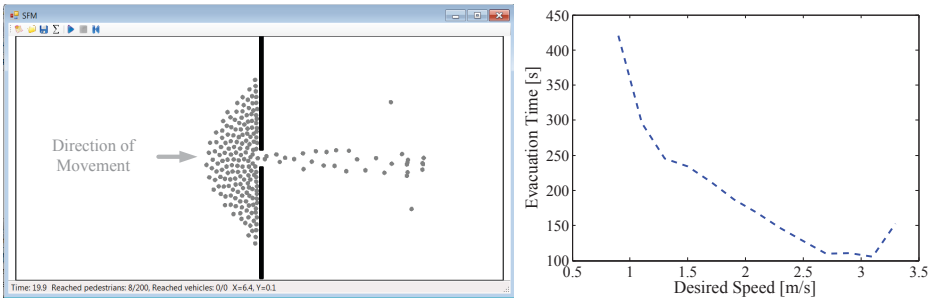

(a) (b)

Figure 7.18: Faster-Is-Slower simulation: (a) clogging at the exit and (b) evacuation time of 200 people versus desired velocity

Parameter Meaning	Parameter	Unit	Value
Desired Velocity	v_α^0	$\frac{\mathrm{m}}{\mathrm{s}}$	1.34
Relaxation Time	τ_α	s	0.5
Radius	r_α	m	0.5
Interaction Range with another Pedestrian	$B_{\alpha\beta}$	m	0.3
Interaction Strength with another Pedestrian	$A_{\alpha\beta}$	$\frac{\mathrm{m}}{\mathrm{s}^2}$	2.1
Anistropy Form Factor Constant with another Pedestrian	$\lambda_{\alpha\beta}$	-	1
Obstruction Effect with another Pedestrian	k	$\frac{\mathrm{kg}}{\mathrm{s}^2}$	2.1
Perpendicular Obstruction Effect with another Pedestrian	κ	$\frac{\mathrm{kg}}{\mathrm{ms}}$	0.1
Boundaries Interaction Range with an Obstacle/Boundary	$B_{\alpha b}$	m	0.2
Interaction Strength with an Obstacle/Boundary	$A_{\alpha b}$	$\frac{\mathrm{m}}{\mathrm{s}^2}$	10

Table 7.2: Parameters used in simulation of the phenomena described in Section 7.4 [72]

agents to be visualised for a defined shared space environment.

The menu list contains several buttons for defining and editing a scenario, opening a saved scenario, saving the current scenario, starting, stopping, rewinding, calibrating the simulation parameters for a defined scenario or producing momentory mean density and speed maps. The user can create a new scenario via the "Define and Edit Scenario" button. The time-space trajectories, velocities and accelerations of agents can be saved in a Comma Separated Value (CSV) file by the "Save History and Statistics" button. In the scenario definition window, the size of the environment can be defined, while in the pedestrians and vehicles group box, the "Add" button enables the user to enter the start location, target, intermediate destinations and start delay for new agents. It also allows reading a real world trajectory and velocity from a text file. The "Edit" icon allows the user to change related details of an existing agent in a scenario, the "Remove" icon to remove an existing agent and the "Save" icon to save the inserted details of the system. Obstacles can be defined in the environment by their vertices in the obstacles group box. Under the "Simulation parameters" icon, the user can define parameter values for the simulation tool in the parameter setting table. The "Define sections & areas" button allows section and area settings for measuring flow and density to be stipulated. The flow and density of the shared space traffic of the specified sections and areas are saved in a CSV file by activating the "Save History and Statistics" button at the end of a simulation. After defining and saving a scenario, but prior to running the simulation, the routing time report appears which estimates the calculation time to create the obstacle and routing map. As shown in Figure 7.20, an automatic calibration procedure is developed which calculates the relative distance between the real trajectory and the simulated one using different defined combinations of the parameters. The calibration strategy is explained in detail in Section 8.4. The mean density and speed of pedestrians or cars at different time steps can be developed by using

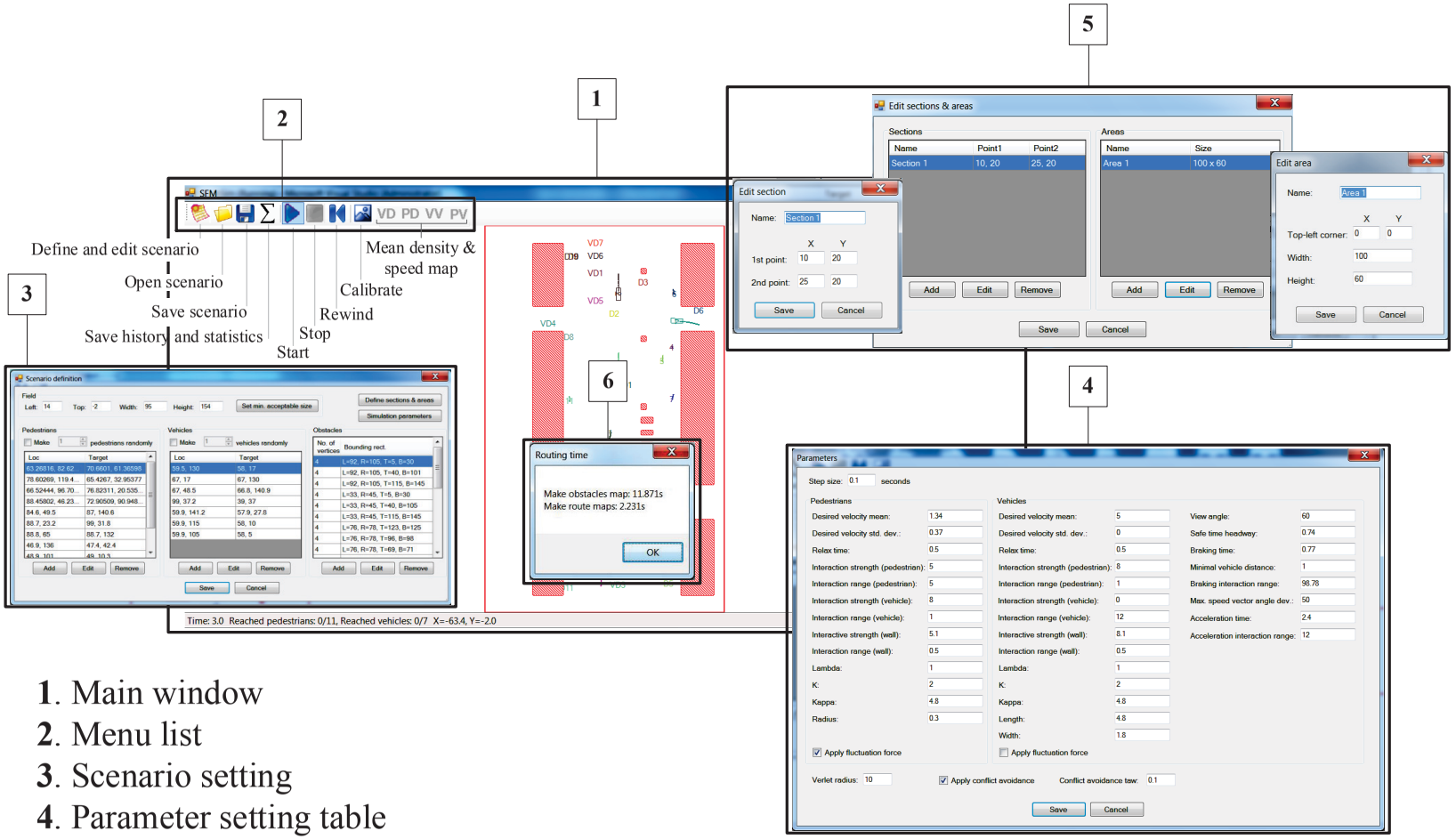

1. Main window
2. Menu list
3. Scenario setting
4. Parameter setting table
5. Section and area setting
6. Routing time report

Figure 7.19: Screenshot of the main window and the main components of the scenario setting

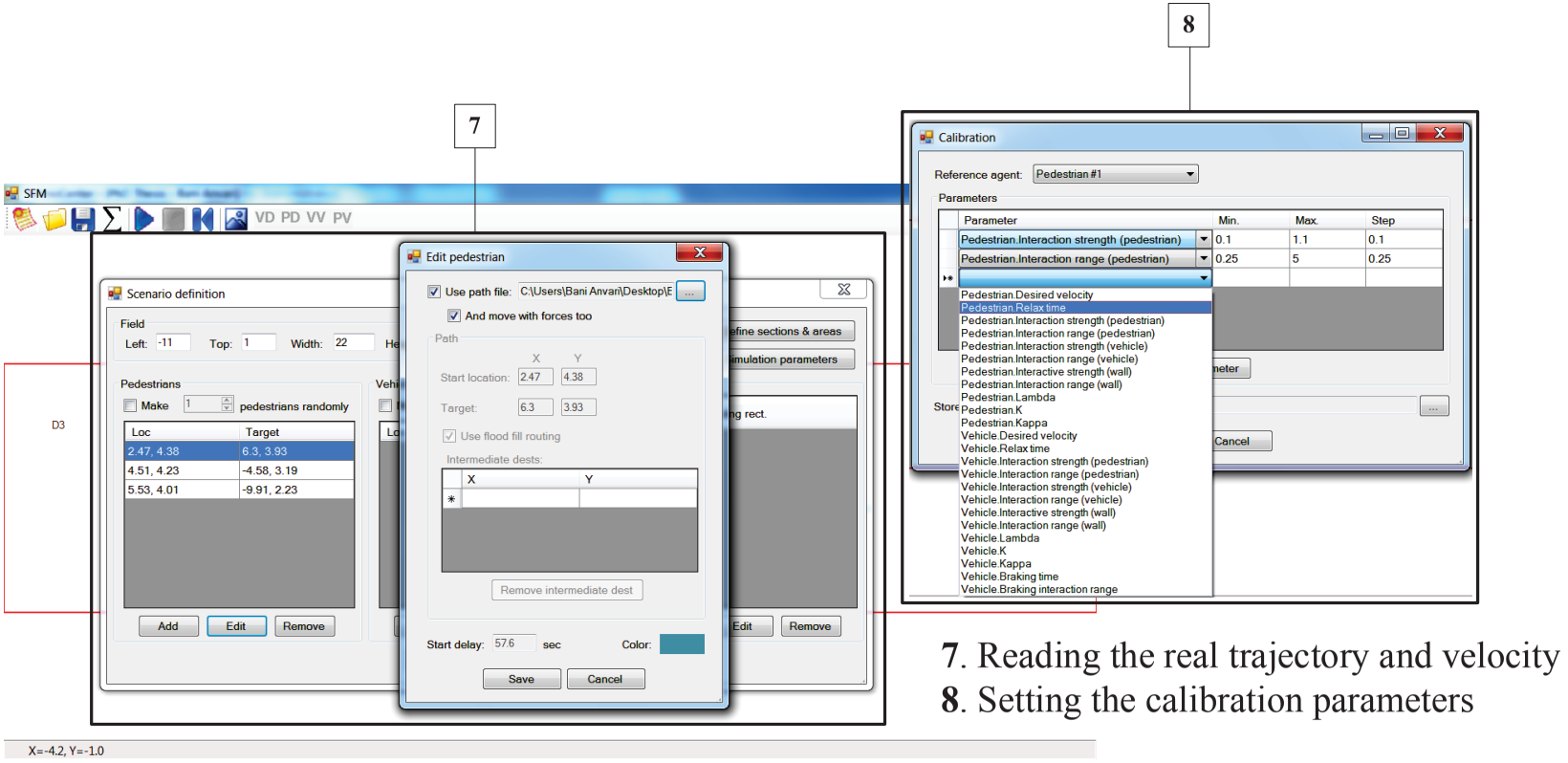

7. Reading the real trajectory and velocity
8. Setting the calibration parameters

Figure 7.20: Screenshot of the main components of the calibration setting

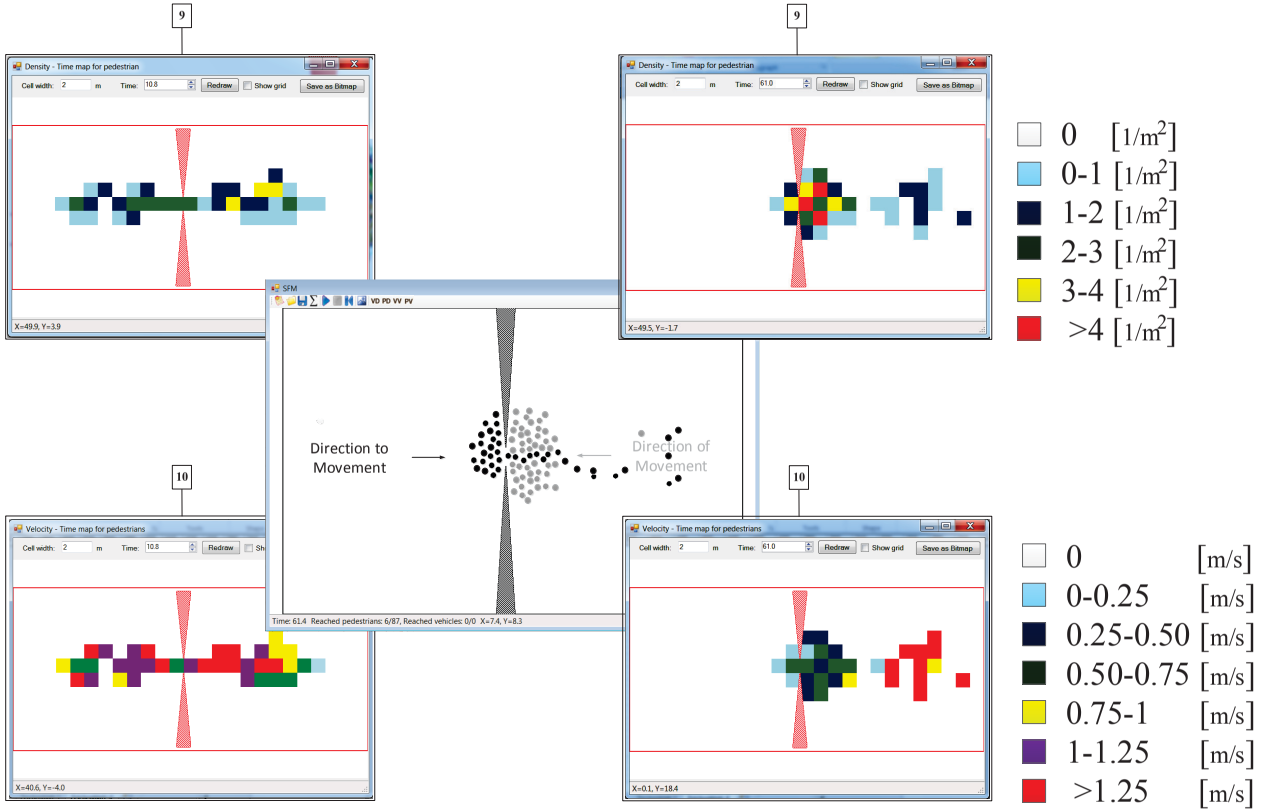

9. Density map at different time steps
10. Mean speed map at different time steps

Figure 7.21: Screenshot of the density and mean speed maps at different time steps for the oscillation simulation test

the "Mean density and speed map" buttons in the menu list: here, the field is divided into a grid, the mean density and speed for each cell is calculated at each time step and different colors are assigned accordingly. The mean density and speed maps of pedestrians for the oscillation simulation test (see Section 7.4.3) at $t = 10.8$ s and $t = 61.0$ s are shown in Figure 7.21.

7.6 Conclusions

This chapter presents the various algorithm flowcharts were presented which together describe how the mathematical model developed in this thesis was implemented in a C# environment. In the first layer, the flood fill algorithm is used to plan agents' trajectories around static obstacles along intermediate destinations to their final destination. The second layer uses a combination of the Verlet and link cell algorithms to identify neighbouring agents. The differential equations of the force directed model are solved based on the Gear's predictor-corrector algorithm so as to simulate the dynamic movement of pedestrians and cars. The conflict avoidance optimisation algorithm used to calculate the velocity change needed to avoid detected conflicts was also explained. Moreover, the GUI of the simulation tool was introduced. The micro-model set out in this and the preceding chapters is calibrated and validated in Chapter 8, using real data from the New Road in Brighton and Exhibition Road in London, two areas where shared space are operational.

Chapter 8

Data Collection, Model Calibration and Validation

This chapter presents the enhanced calibration and validation methodology of the new mathematical model for shared space schemes. Interactions of road users on New Road (Brighton) and Exhibition Road (London) are recorded and traffic characteristics are analysed. Performance indicators such as speed and acceleration distribution as well as agent trajectories are extracted by the Trajectory Extractor Software. A hybrid method is applied to calibrate the model based on the relative distance error between the simulation results and empirical data. Quantitative validation is made by comparing the performance indicators between real data and simulation results. The validation shows that the developed force directed mathematical model is suitable for simulating shared space environments and reproduces results obtained from observation within its limitations.

8.1 Introduction

The shared space schemes (link typology) of New Road (Brighton) and Exhibition Road (London) are used to calibrate and validate the new mathematical model. Site locations for the video analysis and the time of data collection are explained in Section 8.2. Speed and acceleration distributions and trajectories are extracted using the Trajectory Extractor software [222] and superimposed onto the real map in Section 8.3. This data is defined as the performance indicators to be reproduced by the new mathemathical model. The model parameters are categorised and calibrated based on a hybrid method by using the relative distance error between the empirical and simulated data in Section 8.4. Section 8.5 explains the quantitative validation of the model with respect to new sets of trajectories, speed and acceleration distributions from New Road and Exhibition Road. The validation results of the developed shared space simulation model are discussed in Section 8.6.

8.2 Case Studies

The behaviour of pedestrians and vehicles on New Road (Brighton) and Exhibition Road (London) were monitored by CCTV cameras and a camcorder from different angles. A bottom-up approach was followed for the data collection process in order to reduce operating costs with willing to repeat this procedure. New Road was video recorded with a CCTV camera (320×240 pixels) at $25\ \frac{\text{frames}}{\text{s}}$ and Exhibition Road with CCTV cameras (960×536 pixels) at $30\ \frac{\text{frames}}{\text{s}}$. A digital camera (Panasonic HDC-HS60, 1920×1080 pixels) was also used to record both New Road and Exhibition Road at $25\ \frac{\text{frames}}{\text{s}}$ and $30\ \frac{\text{frames}}{\text{s}}$ respectively. The frame rate of the digital camera is chosen to be analogous to the frame rate of the CCTV cameras. Figure 8.1 (a) and (b) show the densities of pedestrians

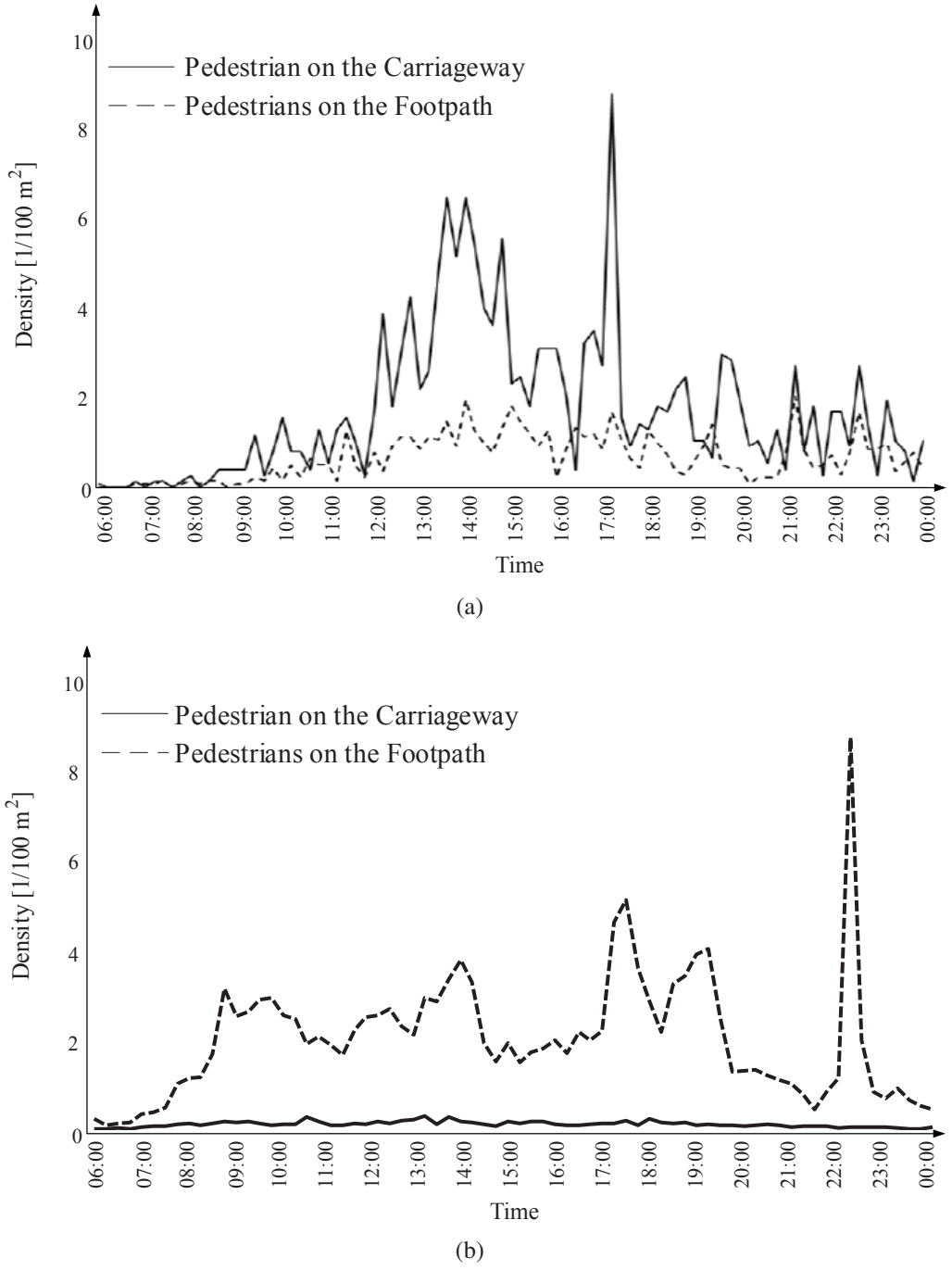

Figure 8.1: Pedestrian density (pedestrians per 100 m^2) from 06:00am to 00:00am on (a) New Road [33] and (b) Exhibition Road

on the carriageway and footway[1] from 06:00am to 00:00am for the two shared space schemes of New Road and Exhibition Road. On New Road, the pedestrian density on the carriageway is higher than on the footway for most of the day while the pedestrian density of Exhibition Road is the reverse. The traffic flow of New Road is up to 60 motorized vehicles and 2256 pedestrians during peak hours [33]. The traffic flow of Exhibition Road is up to 547 motorized vehicles and 3388 pedestrians during peak hours. A description of each of the two shared space schemes and camera angles is given in Section 8.2.1 and Section 8.2.2 respectively.

8.2.1 New Road in Brighton

New Road is in the middle of Brighton's cultural quarter, linking the Royal Pavilion gardens to the new library. The Lanes and North Laine shopping areas are nearby. The street is lined with theatres (Theatre Royal and the Brighton Pavilion Theatre), cafes and restaurants (see Figure 8.2). In 2007, the Gehl Architects (GAs), Martin Stockley Associates (MSAs) and the Brighton and Hove City Council (BHCC) redesigned the road to the city's first shared surface. New Road has become a popular area for visitors in the centre of Brighton's cultural quarter. Bidirectional behaviours of pedestrians and drivers were recorded using CCTV by Brighton and Hove Council between 06:00am and 00:00am on Saturday, 28 March 2009. The location and view angle of the camera are shown in Figure 8.3 (a) and (b). During the first camcorder recording on Saturday, 12 February 2011 , the digital camera was mounted in Position 1 (P1) and fixed at an elevation of about $5\,\mathrm{m}$ with a clear view of traffic (see Figure 8.3 (c) and (d)) between 01:00pm and 02:00 pm. During the second camcorder recording on Thursday, 12 September 2013, the digital camera was mounted in Position 2 (P2) and fixed at an elevation of about $12\,\mathrm{m}$ with a clear view of traffic (see

[1] The streets are shared surfaces but a clear distinction is created through a drainage channel between the traditional carriageway and footway areas.

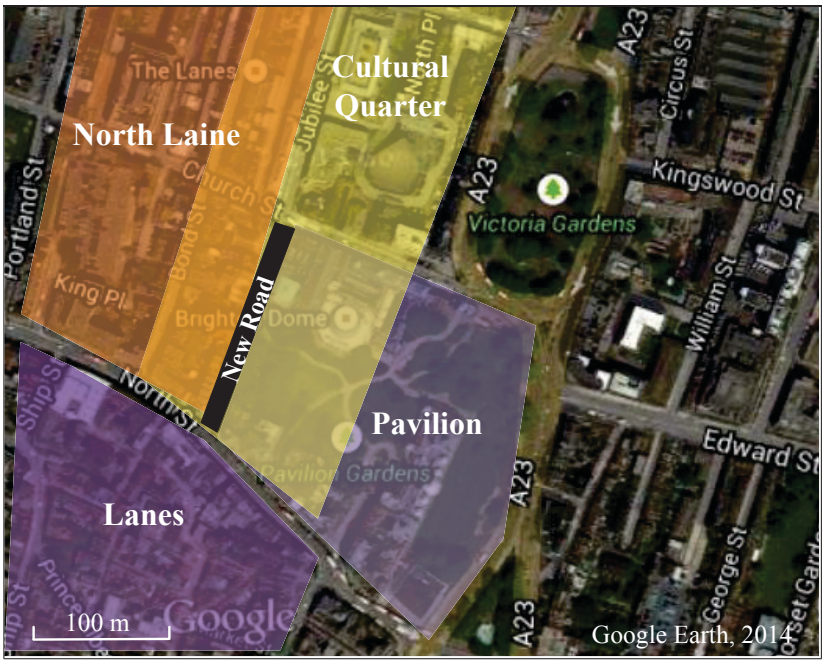

Figure 8.2: Attractions around New Road (Brighton, UK)

Figure 8.3 (e) and (f)) between 03:30pm and 05:30pm. These video recordings are used to calibrate and validate the model parameters. Pedestrian and driver trajectories, speeds, accelerations and decelerations are extracted with the Trajectory Extractor software by considering the correspondence frame rate (see Section 8.3).

8.2.2 Exhibition Road in London

Exhibition Road is located in South Kensington, one of the most cultural destinations in London. This road is located between many famous museums and institutions which attract over nine million visitors a year [223] (see Figure 8.4). The Exhibition Road streetscape is one of the busiest roads in South Kensington for both pedestrians and vehicles. In 2008, a steering group composed of the Royal Borough of Kensington and Chelsea (RBKC), Transport for London (TfL), City of Westminster Council (CWC), Guide Dogs for the Blind associ-

ation (GDB) and Imperial College London (ICL) started discussing the steps toward implementing a single surface shared space on Exhibition Road. The single surface with street de-cluttering, access restrictions, provision of parking locations, loading zones, and bus-stop facilities was completed in December 2011 (see Figure 8.5 (a) to (d)). The behaviour of pedestrians and cars between Imperial College Road and North of Cromwell Gardens was monitored with two CCTV cameras on Thursday, 15 December 2011. The peak hour from 01:00pm

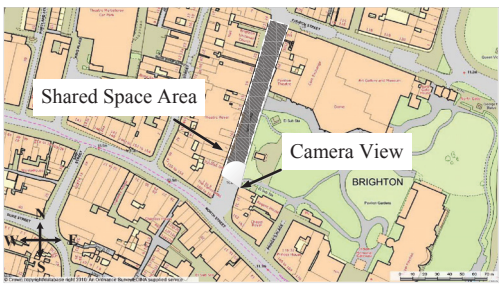

(a) Top view of area and camera angle

(b) Camera view of the CCTV camera

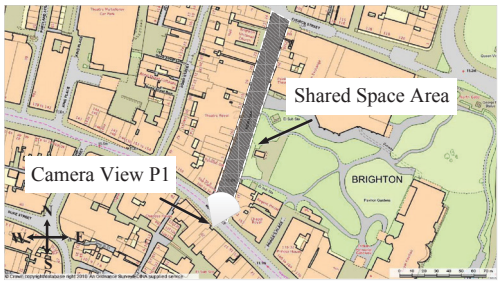

(c) Top view of area and camera angle P1

(d) Camera view of digital camera P1

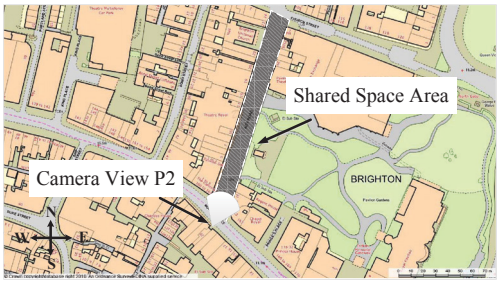

(e) Top view of area and camera angle P2

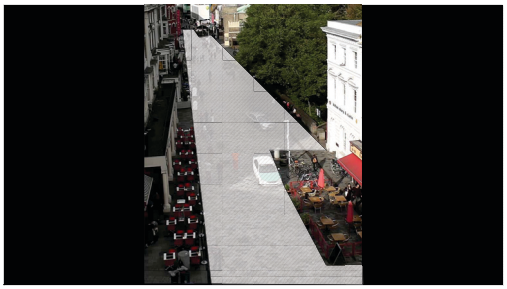

(f) Camera view of digital camera P2

Figure 8.3: Shared space of New Road (Brighton, UK)

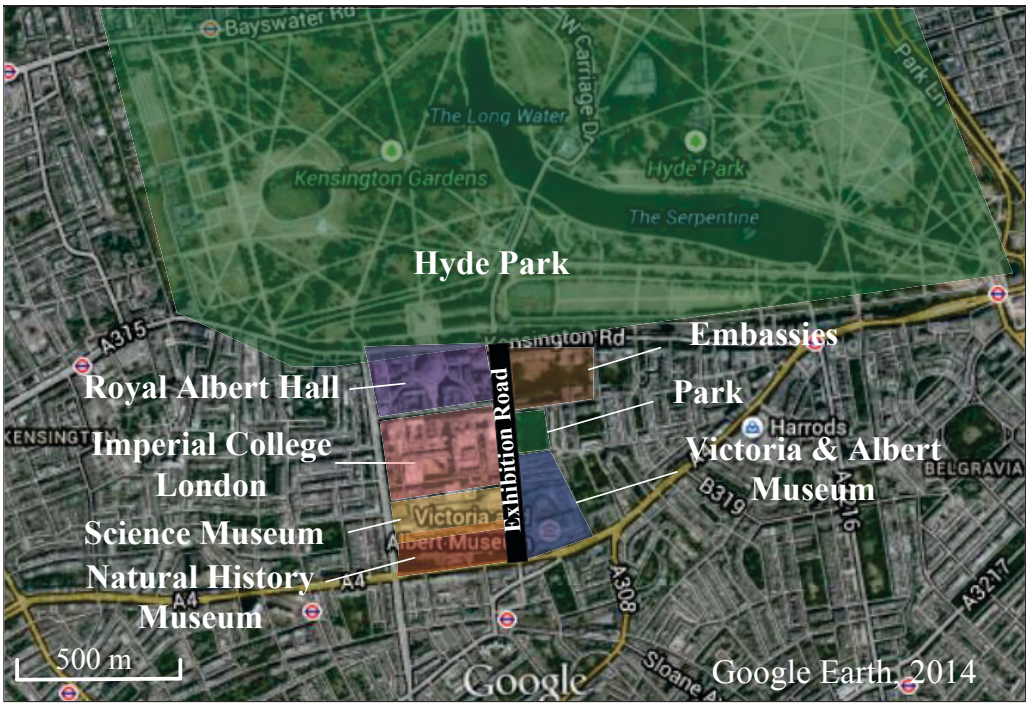

Figure 8.4: Attractions around Exhibition Road (London, UK)

to 02:00pm was chosen for extracting data. A digital camera was also mounted and fixed at an elevation of about 12 m for the same peak hour on Thursday, 16 February 2012 as shown in Figure 8.5 (e) and (f).

Section 8.3 explains extraction of instantaneous positions, speeds, directions, accelerations and decelerations of pedestrians and drivers from the video recordings of New Road and Exhibition Road.

8.3 Video Data Analysis

A software developed by Lee [222] called Trajectory Extractor was used to extract trajectories, speeds and accelerations of cars and pedestrians. Trajectory Extractor allows an adjustable frame-by-frame data extraction of pedestrians and vehicles by marking their position manually. One of the advantages of this software is having a zoom-in function for reducing the human error during data extraction

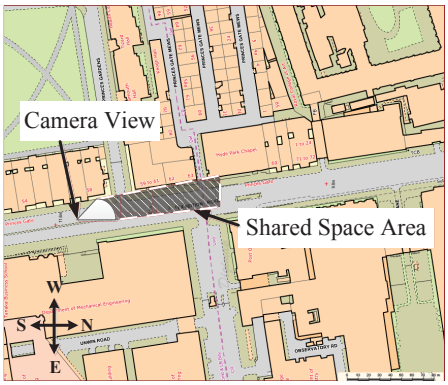

(a) Top view of area and camera angle

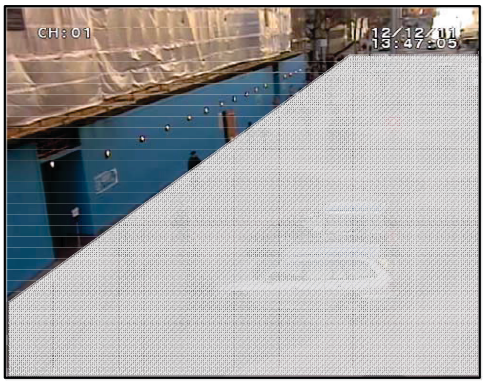

(b) Camera view of CCTV camera #1

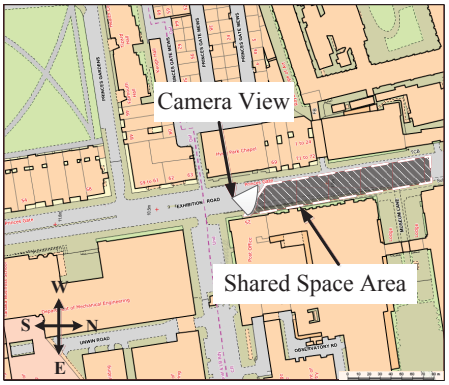

(c) Top view of area and camera angle

(d) Camera view of CCTV camera #2

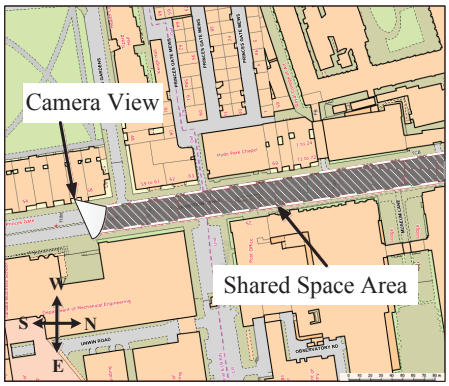

(e) Top view of area and camera angle

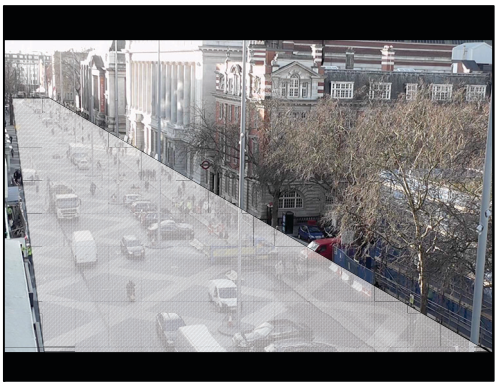

(f) Camera View of Digital camera

Figure 8.5: Shared space of Exhibition Road (London, UK)

process. In addition, the software provides two mechanisms for data verification: Trajectories can be overlaid onto the video images to allow the position of pedes-

trians and cars to be visually reviewed. Secondly, it has the ability to display the trajectories from a top-view angle to remove the perspective effect and allow accurate examination of movements. The output of the software provides instantaneous position, speed, steering angle, acceleration and deceleration, following distance and speed difference. In order to remove perspective effects and to display the trajectories from a top-view angle, a conversion process is carried out for all recordings as explained in Section 8.3.1. The accuracy of the extracted data depends on the number of real world reference points, pixel resolution of the videos, video frame processing intervals, the angle view and the elevation of the camera. Data that are closer to the camera have a higher pixel resolution than those further away which implies that the error of the data is proportional to the longitudinal distance from the camera. The literature shows that the extent of accuracy is around $0.3\,\mathrm{m}$ to $1.3\,\mathrm{m}$ [222]. Section 8.3.2 explains the accuracy of data in all video recordings and the cut-off point defined for the far side of each videos to retain acceptable accuracy for data analysis. Pedestrian and car manoeuvres, speed and acceleration distributions are reported in Section 8.3.3.

8.3.1 Conversion of a Perspective View to a Top View Angle

The video image coordinates are converted into real world coordinates by photogrammetry in order to remove the effect of perspective from the video recordings using Equation 8.1 [222].

$$\begin{aligned} x_{\mathrm{real}} &= \frac{\omega_1 x_{\mathrm{video}} + \omega_2 y_{\mathrm{video}} + \omega_3}{\omega_4 x_{\mathrm{video}} + \omega_5 y_{\mathrm{video}} + 1}, \\ y_{\mathrm{real}} &= \frac{\omega_6 x_{\mathrm{video}} + \omega_7 y_{\mathrm{video}} + \omega_8}{\omega_4 x_{\mathrm{video}} + \omega_5 y_{\mathrm{video}} + 1} \end{aligned} \tag{8.1}$$

Here, x_{real} and y_{real} are real world coordinates, x_{video} and y_{video} are video image coordinates, and ω_1 to ω_8 are coefficients. The coefficients are attained by measuring four clear distinctive real world reference points and matching them with their respective video image coordinates [222]. The coefficients for New

Road and Exhibition Road are reported in Table 8.1 and 8.2. Figure 8.6 (a), (b)

	CCTV Camera	Digital Camera P1	Digital Camera P2
ω_1	-0.0231	-0.0412	-0.0543
ω_2	0.0274	-0.0792	-0.0230
ω_3	2.6636	52.8226	15.8576
ω_4	-0.0015	-0.0006	-0.0025
ω_5	-0.0001	-0.0059	-0.0063
ω_6	-0.0280	-0.0079	-0.0132
ω_7	-0.0020	-0.2961	-0.0406
ω_8	15.2131	97.4666	9.8154

Table 8.1: List of coordinate conversion Coefficients for New Road

	CCTV Camera $\#1$	CCTV Camera $\#2$	Digital Camera
ω_1	-0.3890	1.4994	-0.7642
ω_2	0.3890	1.9517	-0.6244
ω_3	93.7571	-1217.0074	799.9181
ω_4	0.0019	-0.0165	0.0001
ω_5	-0.0504	0.2326	-0.0425
ω_6	0.0161	-1.6456	0.4791
ω_7	-2.1283	14.1792	-6.6769
ω_8	363.6454	-1243.0670	940.4374

Table 8.2: List of coordinate conversion coefficients for Exhibition Road

and (c) show the coordinate selection for three camera angles of New Road. Figure 8.7 (a), (b) and (c) show the reference points that were chosen on Exhibition Road. The size of the area within the reference points is maximised for accuracy and includes a majority of interactions.

8.3.2 Accuracy and Reliability

There are several stages during the extraction process where errors might occur: The accuracy depends partially on the quality of the coordinate conversion. In order to minimise the manual tracking error, a high resolution monitor (19 inch with a resolution of 1920×1080 pixels) is used as well as the zoom-in function of the software. Another systematic error is due to the view angle and elevation of the camera. This can be minimised by ensuring that the camera is placed as high

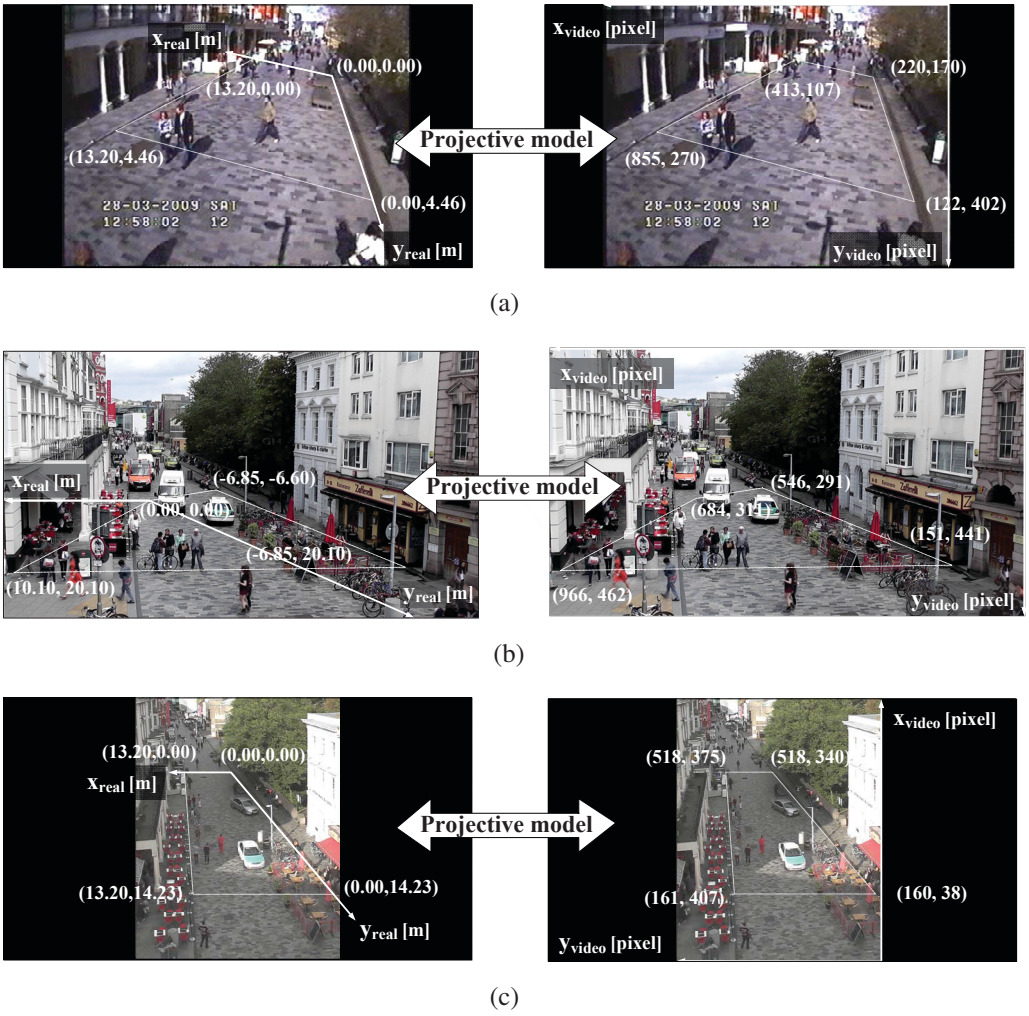

Figure 8.6: Conversion of coordinates between the real world (left) and video image (right) of New Road for the (a) CCTV camera, (b) Digital camera P1 and (c) Digital camera P2

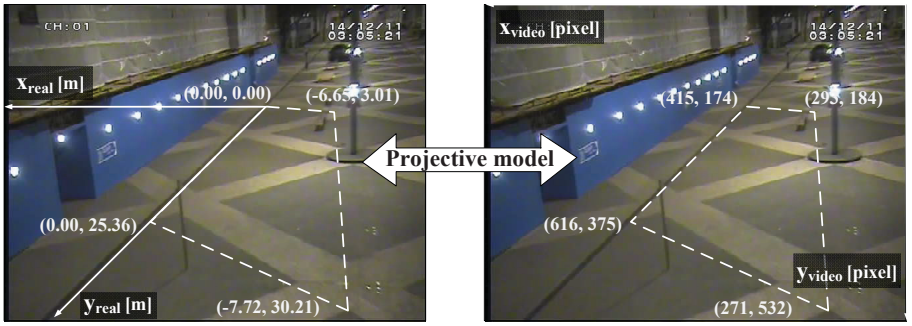

(a)

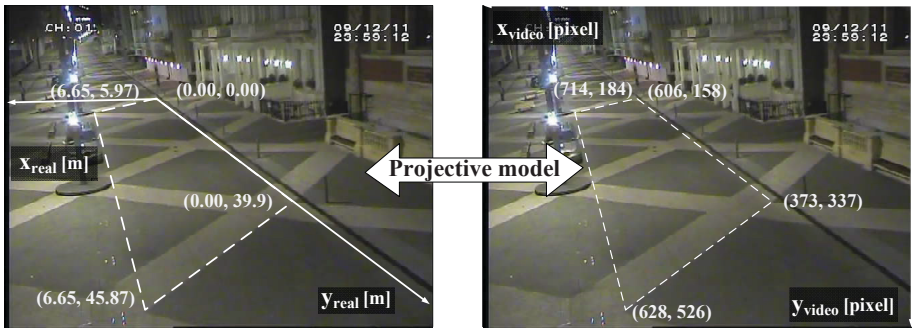

(b)

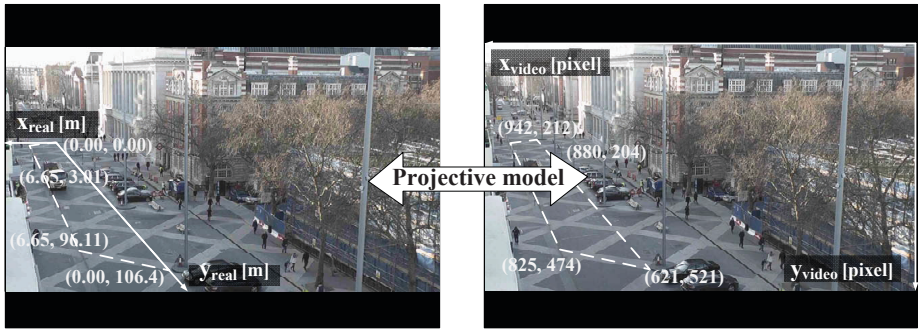

(c)

Figure 8.7: Conversion of coordinates between the real world (left) and video image (right) of Exhibition Road for the (a) CCTV camera #1, (b) CCTV camera #2 and (c) Digital camera

as possible. In addition, the data closer to the camera has higher pixel resolution than the one further away. This implies that the pixel resolution error of the data is proportional to the longitudinal distance from the camera [222]. The errors of the x_{video} and y_{video} variables are determined by the error propagation method. This is a calculus-derived statistical calculation with partial derivatives in Equation 8.2.

$$\begin{aligned}\sigma^2_{x_{\text{real}}} &= \sigma^2_x(\frac{\partial x_{\text{real}}}{\partial x})^2 + \sigma^2_y(\frac{\partial x_{\text{real}}}{\partial y})^2 \\ \sigma^2_{y_{\text{real}}} &= \sigma^2_x(\frac{\partial y_{\text{real}}}{\partial x})^2 + \sigma^2_y(\frac{\partial y_{\text{real}}}{\partial y})^2\end{aligned} \tag{8.2}$$

where σ^2_x and σ^2_y are the uncertainties of the real world position in x- and y-axis. These two errors are caused by manual tracking of agents and digitalisation. The quotient rule is used to partially derive the two function yielding Equation 8.3.

$$\begin{aligned}\frac{\partial x_{\text{real}}}{\partial x} &= \frac{(\omega_4 x_{\text{video}} + \omega_5 y_{\text{yvideo}} + 1)(\omega_1) - (\omega_1 x_{\text{video}} + \omega_2 y_{\text{video}} + \omega_3)(\omega_4)}{(\omega_4 x_{\text{video}} + \omega_5 y_{\text{video}} + 1)^2} \\ \frac{\partial x_{\text{real}}}{\partial y} &= \frac{(\omega_4 x_{\text{video}} + \omega_5 y_{\text{video}} + 1)(\omega_2) - (\omega_1 x_{\text{video}} + \omega_2 y_{\text{video}} + \omega_3)(\omega_5)}{(\omega_4 x_{\text{video}} + \omega_5 y_{\text{video}} + 1)^2} \\ \frac{\partial y_{\text{real}}}{\partial x} &= \frac{(\omega_4 x_{\text{video}} + \omega_5 y_{\text{video}} + 1)(\omega_6) - (\omega_1 x_{\text{video}} + \omega_2 y_{\text{video}} + \omega_3)(\omega_4)}{(\omega_4 x_{\text{video}} + \omega_5 y_{\text{video}} + 1)^2} \\ \frac{\partial y_{\text{real}}}{\partial y} &= \frac{(\omega_4 x_{\text{video}} + \omega_5 y_{\text{video}} + 1)(\omega_7) - (\omega_1 x_{\text{video}} + \omega_2 y_{\text{video}} + \omega_3)(\omega_5)}{(\omega_4 x_{\text{video}} + \omega_5 y_{\text{video}} + 1)^2}\end{aligned} \tag{8.3}$$

The accuracy of the data increases after a certain longitudinal distance from the camera. The errors in the x- and y-coordinate are calculated. A cut-off region for each data set of New Road and Exhibition Road is defined to retain accuracy. Each pixel represents a corresponding real-life distance as moving further away from the camera. The maximum average errors are calculated for x- and y-pixels in Table 8.3 and 8.4 for each camera of New Road and Exhibition Road.

	Y-Pixel Distance [pixel]	Average Error in X-Coordinate [m]	Average Error in Y-Coordinate [m]
CCTV Camera	200	1.06 (σ^2 =0.290)	1.9 (σ^2 =0.580)
	250	0.69 (σ^2 =0.086)	1.13 (σ^2 =0.192)
	300	0.49 (σ^2 =0.041)	0.69 (σ^2 =0.090)
	350	0.36 (σ^2 =0.026)	0.46 (σ^2 =0.053)
	400	0.11 (σ^2 =0.011)	0.43 (σ^2 =0.040)
Digital Camera P1	150	0.34 (σ^2 =0.046)	0.51 (σ^2 =0.064)
	200	0.24 (σ^2 =0.013)	0.37 (σ^2 =0.019)
	250	0.13 (σ^2 =0.016)	0.21 (σ^2 =0.025)
	300	0.08 (σ^2 =0.011)	0.13 (σ^2 =0.021)
	350	0.06 (σ^2 =0.005)	0.09 (σ^2 =0.008)
	X-Pixel Distance [pixel]	**Average Error in X-Coordinate [m]**	**Average Error in Y-Coordinate [m]**
Digital Camera P2	500	0.31 (σ =0.043)	0.08 (σ =0.008)
	450	0.20 (σ =0.033)	0.05 (σ =0.008)
	400	0.12 (σ =0.014)	0.03 (σ =0.005)
	350	0.08 (σ =0.009)	0.03 (σ =0.005)
	300	0.06 (σ =0.005)	0.02 (σ =0.001)

Table 8.3: List of average tracking errors for each camera of New Road

	Y-Pixel Distance [pixel]	Average Error in X-Coordinate [m]	Average Error in Y-Coordinate [m]
CCTV Camera #1	100	0.59 ($\sigma = 0.177$)	1.47 ($\sigma = 0.387$)
	150	0.22 ($\sigma = 0.047$)	0.64 ($\sigma = 0.104$)
	200	0.12 ($\sigma = 0.021$)	0.39 ($\sigma = 0.056$)
	250	0.09 ($\sigma = 0.007$)	0.26 ($\sigma = 0.024$)
	300	0.07 ($\sigma = 0.005$)	0.24 ($\sigma = 0.019$)
CCTV Camera #2	100	0.28 ($\sigma = 0.049$)	1.71 ($\sigma = 0.539$)
	150	0.17 ($\sigma = 0.014$)	0.63 ($\sigma = 0.122$)
	200	0.13 ($\sigma = 0.010$)	0.34 ($\sigma = 0.059$)
	250	0.10 ($\sigma = 0.006$)	0.20 ($\sigma = 0.022$)
	300	0.09 ($\sigma = 0.006$)	0.15 ($\sigma = 0.016$)
Digital Camera	250	0.16 ($\sigma = 0.043$)	0.83 ($\sigma = 0.404$)
	300	0.11 ($\sigma = 0.004$)	0.39 ($\sigma = 0.020$)
	350	0.10 ($\sigma = 0.003$)	0.35 ($\sigma = 0.021$)
	400	0.09 ($\sigma = 0.003$)	0.27 ($\sigma = 0.019$)
	450	0.08 ($\sigma = 0.003$)	0.22 ($\sigma = 0.016$)

Table 8.4: List of average tracking errors for each camera of Exhibition Road

As Table 8.3 and 8.4 show, the errors along the perspective view are higher compared to the those across the perspective view. In this thesis, a maximum error in any direction of camera $0.5\,\mathrm{m}$ is acceptable. Hence, the cut-off point for the CCTV camera of New Road is at $350\,\mathrm{pixels}$ in y-direction with maximum uncertainties of $0.46\,\mathrm{m}$ (longitudinal) by $0.36\,\mathrm{m}$ (lateral). This cut-off point results in excluding the majority of pedestrian and car data. Therefore, this data set is not useful for trajectory, speed and acceleration analysis in Section 8.3.3. The cut-off point for the digital camera P1 is defined at $150\,\mathrm{pixels}$ on the y-axis with maximum uncertainties of $0.51\,\mathrm{m}$ (longitudinal) by $0.34\,\mathrm{m}$ (lateral). For the digital camera P2, data above $500\,\mathrm{pixels}$ in x-direction are considered with maximum uncertainties of $0.31\,\mathrm{m}$ (longitudinal) by $0.01\,\mathrm{m}$ (lateral).

On Exhibition Road, the cut-off point for CCTV camera $\#1$ is at $200\,\mathrm{pixels}$ in y-direction with maximum uncertainties of $0.39\,\mathrm{m}$ (longitudinal) by $0.12\,\mathrm{m}$ (lateral). Acceptable data for CCTV camera $\#2$ are above $200\,\mathrm{pixels}$ with maximum uncertainties of $0.34\,\mathrm{m}$ (longitudinal) by $0.13\,\mathrm{m}$ (lateral). For the digital camera, agents above $300\,\mathrm{pixels}$ are analysed with maximum uncertainties of $0.39\,\mathrm{m}$ (longitudinal) by $0.11\,\mathrm{m}$ (lateral).

All position, speed and acceleration values outside the defined regions for New Road and Exhibition Road are excluded for data analysis and the calibration process.

8.3.3 Trajectory, Speed and Acceleration Data

The spatial distribution of pedestrians and cars on New Road and Exhibition Road is investigated in this section. Data of agents are extracted from the recorded videos at a time step of $1\,\mathrm{s}$. The new mathematical model calculates forces every $0.1\,\mathrm{s}$. Hence, the extracted trajectories are resampled to $0.1\,\mathrm{s}$ intervals which

correspond to a frame rate of $10\,\frac{\text{frames}}{\text{s}}$ using linear interpolation. Pedestrians and cars are tracked and their manoeuvres, speeds and accelerations discussed in Section 8.3.3.1 for New Road and in Section 8.3.3.2 for Exhibition Road.

8.3.3.1 Data from New Road in Brighton

Bidirectional behaviour of pedestrians and drivers is observed on New Road. The paths of pedestrians (white trajectories) and cars (red trajectories) are plotted on three camera screen shots in Figure 8.8. The data collection of New Road is shown Figure 8.9. The mean speed of pedestrians is $1.08\,\frac{\text{m}}{\text{s}}$ ($\sigma = 0.70\,\frac{\text{m}}{\text{s}}$) and $1.37\,\frac{\text{m}}{\text{s}}$ ($\sigma = 0.78\,\frac{\text{m}}{\text{s}}$) from the digital camera P1 and digital camera P2 respectively (see Figure 8.9 (a) and (c)). The graphs show an equal distribution of the speed for pedestrians. The mean speed of cars on New Road is about $2.14\,\frac{\text{m}}{\text{s}}$ ($\sigma = 1.79\,\frac{\text{m}}{\text{s}}$) and $2.44\,\frac{\text{m}}{\text{s}}$ ($\sigma = 2.82\,\frac{\text{m}}{\text{s}}$) from the two digital cameras (see Figure 8.9 (b) and (d)). Pedestrians accelerate and decelerate at the rate of $-0.005\,\frac{\text{m}}{\text{s}^2}$ ($\sigma = 0.59\,\frac{\text{m}}{\text{s}^2}$) and $0.00025\,\frac{\text{m}}{\text{s}^2}$ ($\sigma = 0.40\,\frac{\text{m}}{\text{s}^2}$) from the digital camera P1 and digital camera P2 (see Figure 8.10). This value is about $-0.04\,\frac{\text{m}}{\text{s}}$ ($\sigma = 1.22\,\frac{\text{m}}{\text{s}}$) and $0.07\,\frac{\text{m}}{\text{s}^2}$ ($\sigma = 2.47\,\frac{\text{m}}{\text{s}^2}$) for cars.

8.3.3.2 Data from Exhibition Road in London

The trajectories of pedestrians and cars on Exhibition Road are illustrated on three camera views in Figure 8.11. In Figure 8.12, the speed distributions of the three data sets for each traffic mode are shown which have a Gaussian distribution. The mean speed of pedestrians is about $1.42\,\frac{\text{m}}{\text{s}}$ ($\sigma = 0.68\,\frac{\text{m}}{\text{s}}$) according to the data from CCTV camera $\#1$ (see Figure 8.12 (a)). The mean speed of pedestrians is $1.22\,\frac{\text{m}}{\text{s}}$ ($\sigma = 0.63\,\frac{\text{m}}{\text{s}}$) from the data collected with the digital camera (see Figure 8.12 (c)). The mean speed of cars has a value of $6.67\,\frac{\text{m}}{\text{s}}$ ($\sigma = 2.76\,\frac{\text{m}}{\text{s}}$) from the data collected by CCTV camera $\#2$ (see Figure 8.12 (b)). The mean speed of cars is $8.21\,\frac{\text{m}}{\text{s}}$ ($\sigma = 3.15\,\frac{\text{m}}{\text{s}}$) from the data of the digital camera (see

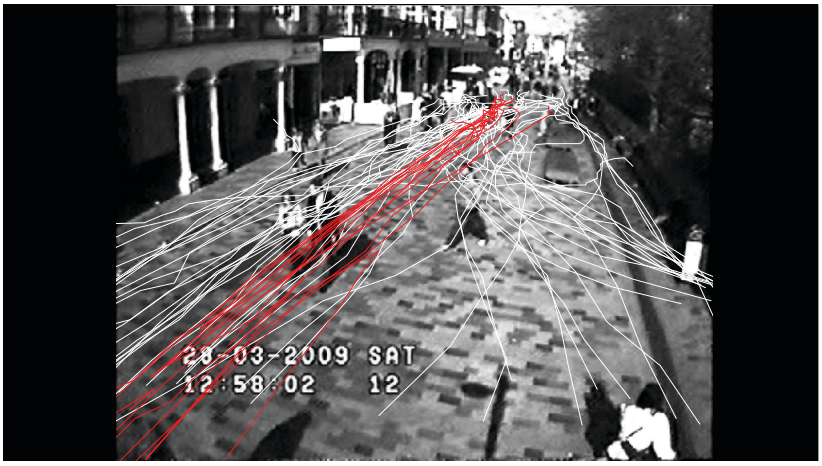

(a) Trackings of 53 pedestrians and 11 cars from CCTV camera

(b) Trackings of 150 pedestrians and 26 cars from digital camera P1

(c) Trackings of 23 pedestrians and 21 cars from digital camera P2

Figure 8.8: Shared space user trajectories from New Road (Brighton, UK)

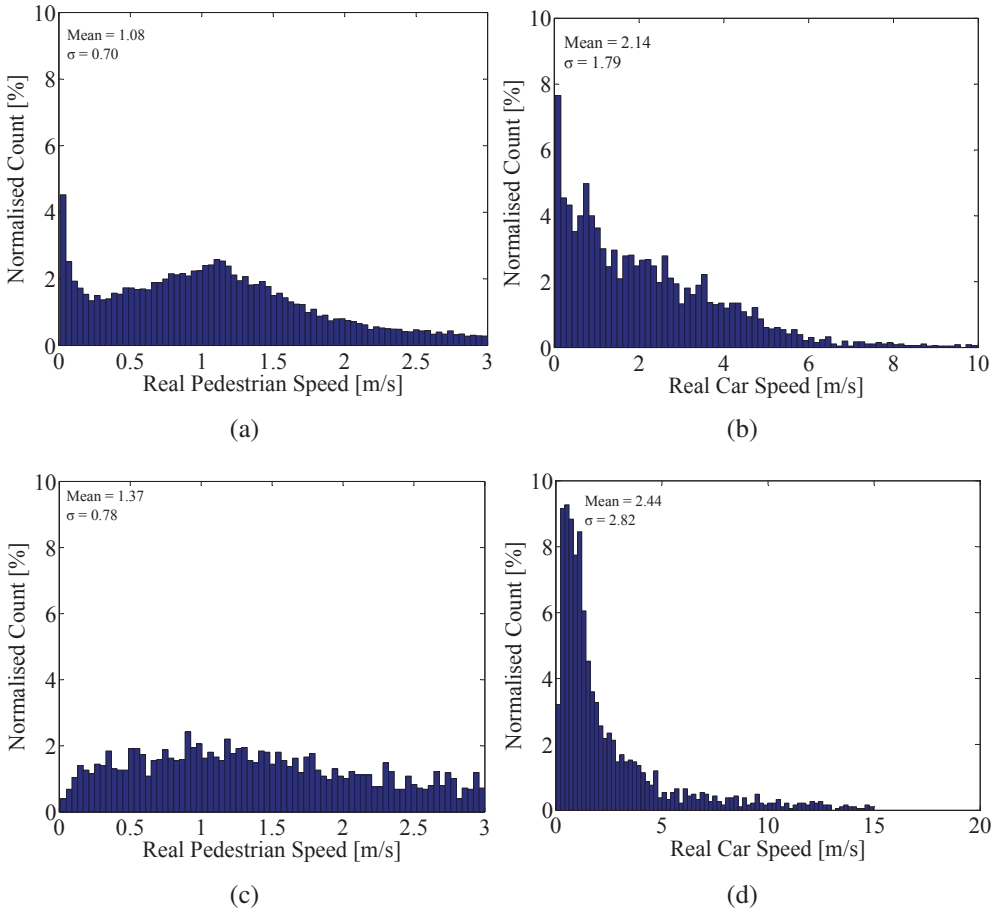

Figure 8.9: Speed histograms of pedestrians and cars on New Road from (a)-(b) Digital camera P1 and (c)-(d) Digital camera P2

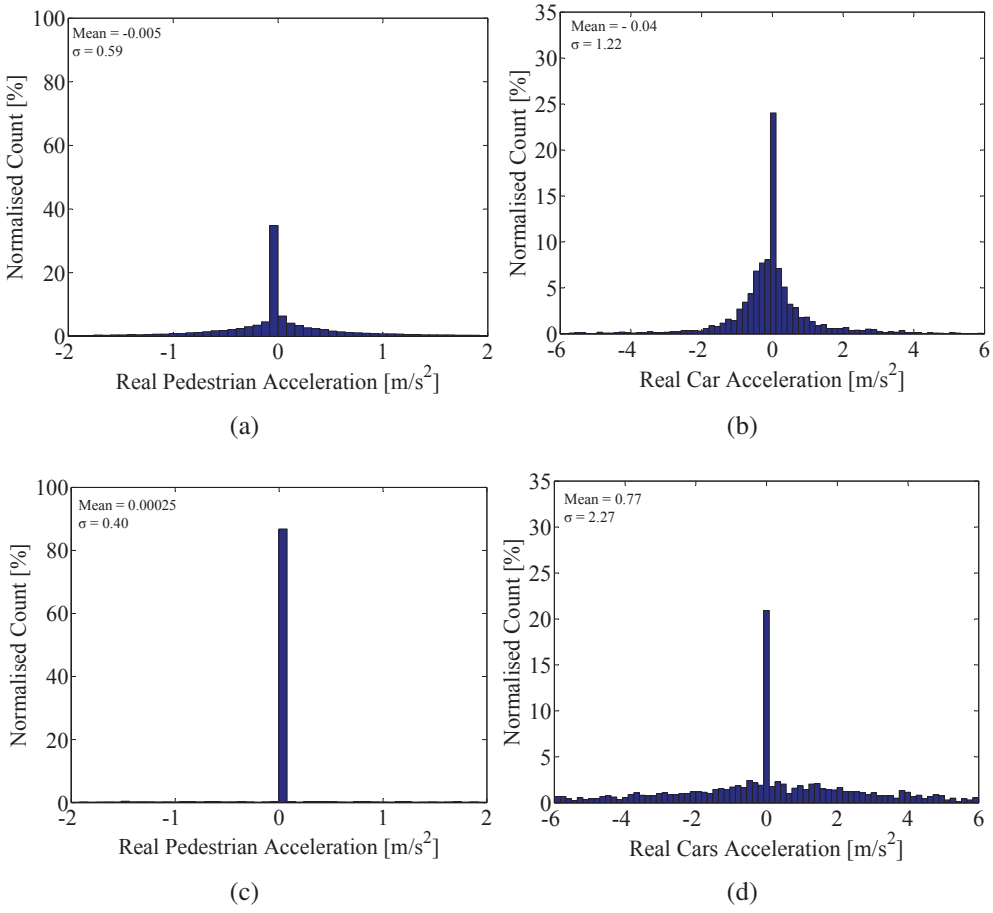

Figure 8.10: Acceleration histograms of pedestrians and cars on New Road from (a)-(b) Digital camera P1 and (c)-(d) Digital camera P2

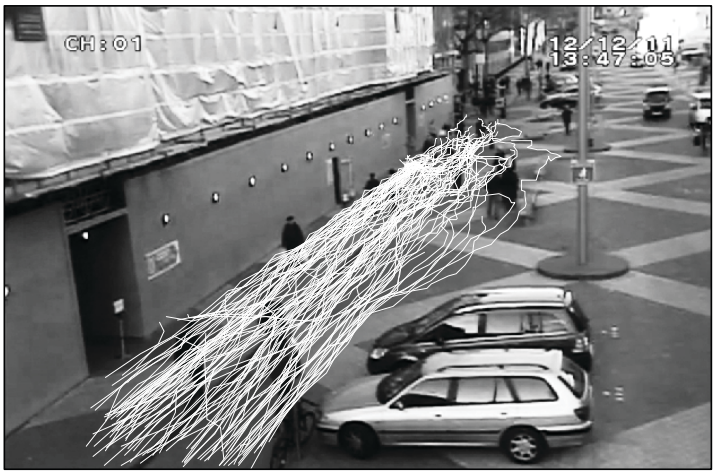

(a) Trackings of 152 pedestrians with CCTV camera #1

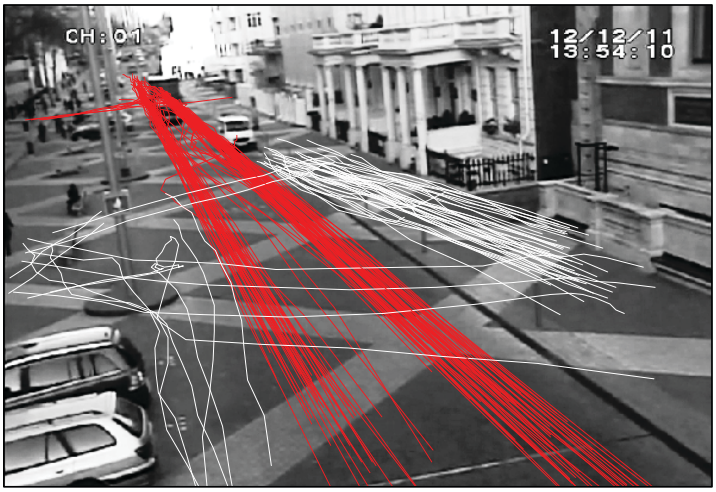

(b) Trackings of 108 cars with CCTV camera #2

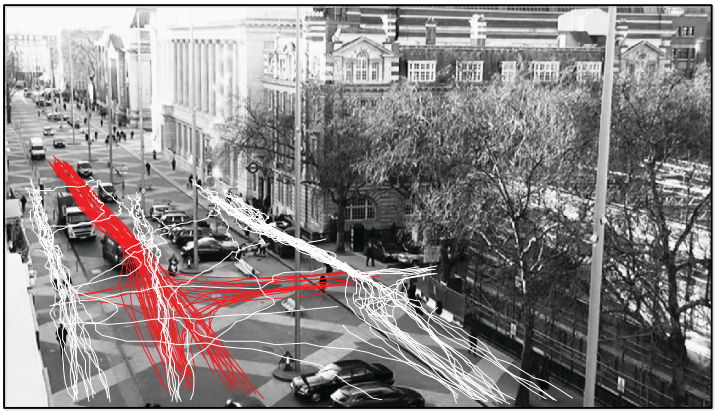

(c) Trackings of 70 pedestrians and 70 cars with the digital camera

Figure 8.11: Shared space user trajectories from Exhibition Road (London, UK)

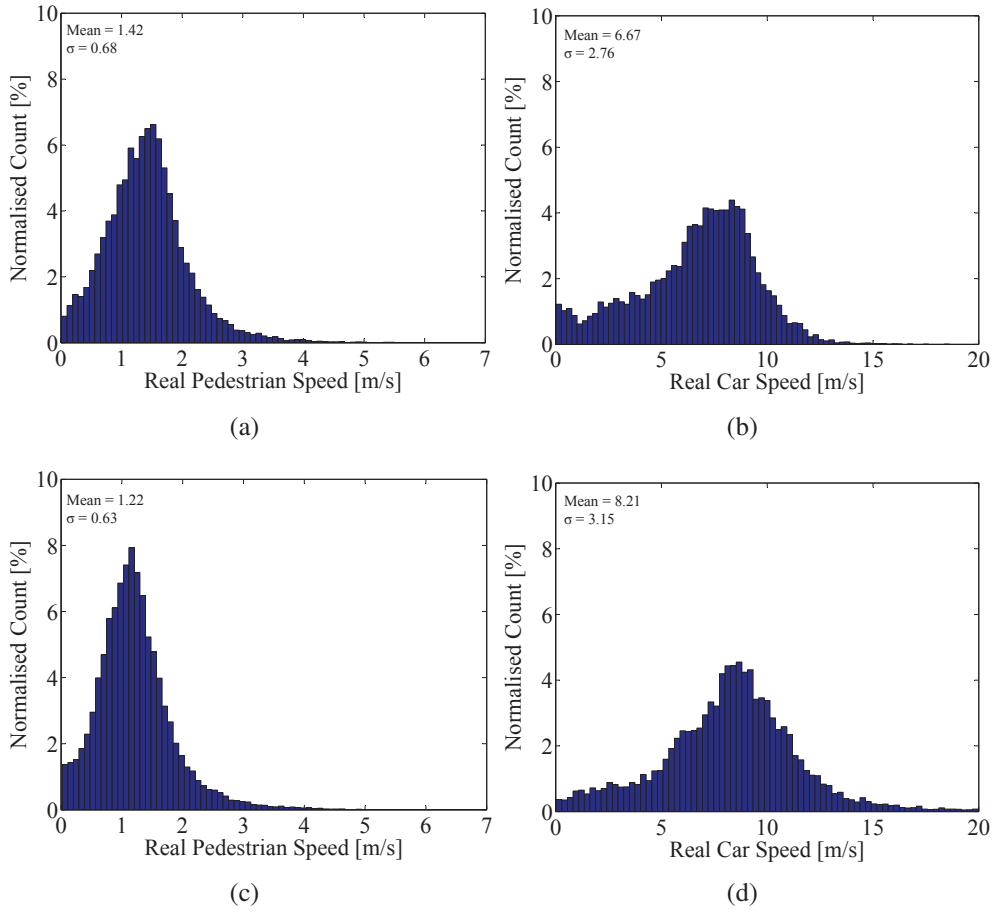

Figure 8.12: Speed histograms for pedestrians and cars on Exhibition Road from (a) CCTV camera #1, (b) CCTV camera #2 and (c)-(d) Digital camera

Figure 8.12 (d)). The data extracted from CCTV camera #1 shows a mean acceleration change of $-0.01\,\frac{\mathrm{m}}{\mathrm{s}^2}$ ($\sigma = 0.67\,\frac{\mathrm{m}}{\mathrm{s}^2}$) for pedestrians (see Figure 8.13 (a)). The mean acceleration change of pedestrians in Exhibition Road is $-0.00013\,\frac{\mathrm{m}}{\mathrm{s}^2}$ ($\sigma = 0.55\,\frac{\mathrm{m}}{\mathrm{s}^2}$) according to data extracted from the digital camera (see Figure 8.13 (c)). The mean acceleration of cars is about $-0.06\,\frac{\mathrm{m}}{\mathrm{s}^2}$ ($\sigma = 1.38\,\frac{\mathrm{m}}{\mathrm{s}^2}$) according to data collected by CCTV camera #2 (see Figure 8.13 (b)). The mean acceleration of cars is also $-0.07\,\frac{\mathrm{m}}{\mathrm{s}^2}$ ($\sigma = 1.85\,\frac{\mathrm{m}}{\mathrm{s}^2}$) according to data collected with the digital Camera (see Figure 8.13 (d)).

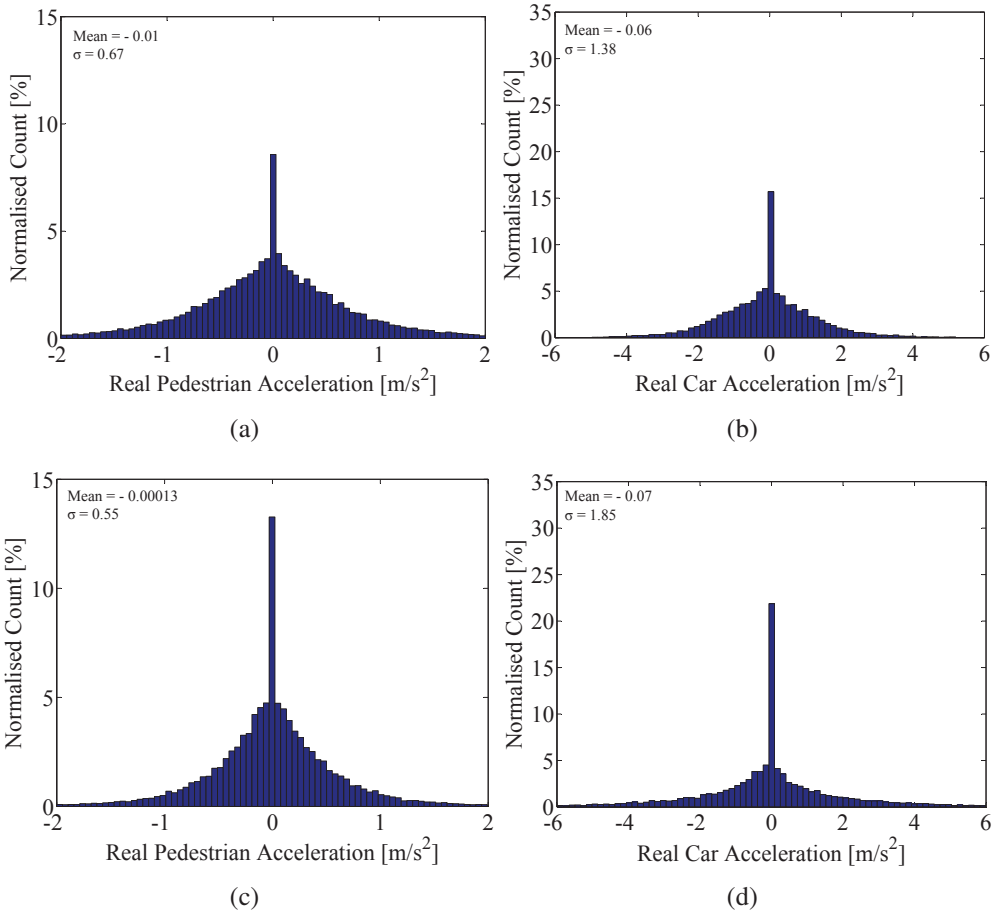

Figure 8.13: Acceleration histograms for pedestrians and cars on Exhibition Road from (a) CCTV camera #1, (b) CCTV camera #2 and (c)-(d) Digital camera

8.4 Calibration Process

Representation of reality is dependent on the choice of parameters. Time periods of the observed data with the highest density of pedestrians and cars are used in order to calibrate the model parameters. A summary of the parameters used in the new mathematical model is explained in Section 8.4.1. The calibration methodology of the interaction parameters with empirical data for pedestrians and cars is explained in Section 8.4.2. The interaction parameter values giving the best fitness value are reported for shared space schemes of New Road and Exhibition Road.

8.4.1 Specification of Model Parameters

The parameters of the new mathematical model for pedestrians and cars are listed in Table 8.5. The parameters for pedestrians such as the interaction strength, interaction range and relaxation time have been calibrated by many researchers [53, 73, 224] using video data during the past years. Since the SFM is extended to vehicles, new parameters have to be introduced. Car interactions are modelled with social forces and the related parameters need to be calibrated using empirical data. Some of the parameters result from empirical data such as the desired speed of pedestrians v_α^0 and cars v_γ^0, average shoulder width of pedestrians r_α, average length $2l$ and width $2w$ of cars, and maximum steering angle ψ.

On the other hand, parameters such as the relaxation time of pedestrians τ_α and cars τ_γ, anisotropy form factors λ, obstruction effect constants k and κ, effective view angle ϑ, interaction ranges B and interaction strengths A, safe time headway T_γ, braking time $\tau_\gamma^{'}$ and minimal vehicle distance $d_{\gamma\delta}^m$ depend on the perception, psychological motivations and social behaviours of road users which need to be calibrated.

	Parameter Meaning	Parameter	Unit	Calibration Needed?	Assigned Values
Parameters for a Pedestrian	Desired Velocity	v_α^0	$\frac{\mathrm{m}}{\mathrm{s}}$	No	1.30
	Relaxation Time	τ_α	s	Yes	0.5
	Radius	r_α	m	No	0.5
	Interaction Range with another Pedestrian	$B_{\alpha\beta}$	m	Yes	Calibration
	Interaction Strength with another Pedestrian	$A_{\alpha\beta}$	$\frac{\mathrm{m}}{\mathrm{s}^2}$	No	Calibration
	Anisotropy Form Factor Constant with another Pedestrian	$\lambda_{\alpha\beta}$	-	No	0.2
	Obstruction Effect with another Pedestrian	k	$\frac{\mathrm{kg}}{\mathrm{s}^2}$	Yes	1
	Perpendicular Obstruction Effect with another Pedestrian	κ	$\frac{\mathrm{kg}}{\mathrm{ms}}$	Yes	1.8
	Interaction Range with a Car	$B_{\alpha\gamma}$	m	Yes	Calibration
	Interaction Strength with a Car	$A_{\alpha\gamma}$	$\frac{\mathrm{m}}{\mathrm{s}^2}$	Yes	Calibration
	Anistropy Form Factor Constant with a Car	$\lambda_{\alpha\gamma}$	-	No	0.2
Parameters for a Vehicle	Desired Velocity	v_γ^0	$\frac{\mathrm{m}}{\mathrm{s}}$	No	8.9
	Relaxation Time	τ_γ	s	Yes	Calibration
	Length of Vehicle	$2l$	m	No	4.6
	Width of Vehicle	$2w$	m	No	1.8
	Effective View Angle	ϑ	$^\circ$	No	10
	Maximum Steering Angle	ψ	$^\circ$	No	30
	Safe Time Headway	T_γ	s	Yes	Calibration
	Braking Time	$\tau_\gamma^{'}$	s	Yes	Calibration
	Minimal Safety Distance	$d_{\gamma\delta}^m$	m	Yes	Calibration
	Acceleration Interaction Range with another Vehicle	$B_{\gamma\delta}^{'}$	m	Yes	Calibration
	Braking Interaction Range with another Vehicle	$B_{\gamma\delta}^{''}$	m	Yes	Calibration
	Interaction Strength with another Vehicle	$A_{\gamma\delta}$	$\frac{\mathrm{m}}{\mathrm{s}^2}$	Yes	Calibration
	Interaction Interaction with another Vehicle	$B_{\gamma\delta}$	m	Yes	Calibration
	Anisotropy Form Factor Constant with another Vehicle	$\lambda_{\gamma\delta}$	-	No	0.2
	Interaction Strength with a Pedestrian	$A_{\gamma\alpha}$	$\frac{\mathrm{m}}{\mathrm{s}^2}$	Yes	Calibration
	Interaction Range with a Pedestrian	$B_{\gamma\alpha}$	m	Yes	Calibration
	Anisotropy Form Factor Constant with a Pedestrian	$\lambda_{\gamma\alpha}$	-	No	0.2

Table 8.5: A summary of the parameters used in the shared space model

In reality, most parameters vary individually, however, identical values are assigned to a number of parameters. The desired speed of pedestrians is assigned to $1.30\,\frac{\mathrm{m}}{\mathrm{s}}$ based on the mean speed of pedestrians in the two shared space case studies in Section 8.3.3. The pedestrians' relaxation time is the elapsed time until $63\,\%$ of the desired speed is reached [162]. Assuming the desired speed of $1.30\,\frac{\mathrm{m}}{\mathrm{s}}$, the relaxation time τ_α is assigned to $0.5\,\mathrm{s}$. The physical interaction parameters k and κ are the pushing and friction coefficients which occur during panic situations. In shared spaces, pedestrians avoid physical contact. Therefore, k and κ are set to $1\,\frac{\mathrm{kg}}{\mathrm{s}^2}$ and $1.8\,\frac{\mathrm{kg}}{\mathrm{ms}}$. The pedestrian radius is assigned to $0.5\,\mathrm{m}$ [53]. The anisotropic form factor $\lambda_{\alpha\beta}$ and $\lambda_{\alpha\gamma}$ are set to 0.2 so that interactions outside the field of view have little effect on pedestrian movements.

The interaction range A describes the amplitude of a force in the centre mass and it affects how quickly the exerted force decreases with distance. The interaction strength parameter A represents the amount of influence that a force has and is not independent from B. The pedestrians and drivers interaction with boundaries were not observed and therefore, values are assigned that are in line with that in previous studies [162]. The parameters for the interactions with boundaries are set to $B_{\alpha b} = 0.5\,\mathrm{m}$, $A_{\alpha b} = 5.1\,\frac{\mathrm{m}}{\mathrm{s}^2}$, $B_{\gamma b} = 6\,\mathrm{m}$, $A_{\alpha b} = 0.5\,\frac{\mathrm{m}}{\mathrm{s}^2}$. The desired velocity of cars can be set to $8.9\,\frac{\mathrm{m}}{\mathrm{s}}$ according to the speed limit of shared space environments. The length and width of the cars are set to the averages of $4.8\,\mathrm{m}$ and $1.4\,\mathrm{m}$ respectively. The maximum steering angle is assigned 30^{o} as discussed in Chapter 6. The relaxation time τ_γ is a third of the time that a car needs to reach its desired speed [101]. The cars' anisotropic behaviour, the form factor $\lambda_{\gamma\delta}$ and $\lambda_{\gamma\alpha}$, are set to 0.2 so that interactions outside the field of view a driver have little effect on his decisions. The safety time headway T_γ is a characteristic parameter of the driving style and the braking time $\tau_\gamma^{'}$ is to explain the deceleration capability of a car [101]. Cars' safe time headway, braking time and minimal safety distance need to be calibrated. In order to calibrate the interaction range and

interaction strength between road users a hybrid method is used in Section 8.4.2. The interaction range and interaction strength between pedestrians, pedestrians and cars, cars and pedestrians and between cars are calibrated by minimising the relative distance between the real trajectory and simulated trajectory in Section 8.5.

8.4.2 Calibration Procedure and Results

Different calibration procedures exist for adjusting model parameters so that simulated trajectories and speed of pedestrians and cars reflect reality. Moussaid [171] proposed to extract the mathematical functions of a model by using real data. This process allows the interaction functions to explicitly represent the experimentally determined features of the data. However, most transportation models use predefined functions and fit the model parameters to the real data on the macroscopic and microscopic level [171, 225–229]. On the macroscopic level, micro-simulated traffic is compared to real cumulative traffic characteristics such as average speed, flow and density using continuity equations. Johansson [73] argued that fitting simulations to the fundamental diagrams does not necessarily produce realistic results. He mentions that fundamental diagrams are dependent on the characteristics of the considered sample and therefore, numerous calibrations are required in order to fit different scenarios. Charibi [74] also mentioned that density measurements without microscopic calibration can contribute to a fluctuation of density. On the microscopic level, three main approaches exist to assess how well model outputs match observed data: acceptable windows, minimising deviations and likelihood functions. The acceptable window approach compares simulated outcomes to observed ranges for each endpoint which does not capture the degree of closeness. The minimising deviation approach measures the relative distance of simulated results to real data according to different parameter sets and captures the magnitude of goodness of fit. The

likelihood function shows how matching the simulation results are with respect to observed data. In this approach, a distribution is produced by minimising the square distance between real and simulated data.

In this thesis, the minimising deviation method is applied which aims at minimising the deviations between real and simulated pedestrian and car trajectories. The relative distance is used for error analysis between the simulated and observed trajectories to capture the magnitude of deviations. The relative distance error is defined in Equation 8.4 [73].

$$E = \frac{\left\| r_U^{simulated}(t+T) - r_U^{tracked}(t+T) \right\|}{\left\| r_U^{tracked}(t+T) - r_U^{tracked}(t) \right\|} \tag{8.4}$$

where r_U is the position of an agent U, t is the starting time of the simulation and T is the duration of the simulation. The starting time t of the simulation is assumed identical while the duration of the simulation T is kept constant. For instance, if an agent takes $9\,\mathrm{s}$ to travel from its start point to its destination point in reality, it will take 6 simulation runs to calibrate its trajectory by assuming $T = 1.5\,\mathrm{s}$. The simulation time has to be small enough to accurately represent the movement of the corresponding road user. The relative distance errors are averaged for each road user with different starting times. Averaging the relative distance errors over all simulations allows calculating the fitness level of that particular parameter set.

A hybrid method using empirical and simulated trajectories is used for the calibration of parameters. Once the video tracking is completed, certain scenarios which include interactions between agents are chosen. For each pedestrian or car, a virtual pedestrian or car is assigned in the simulation domain. A simulation is initiated according to real data in which one agent (pedestrian or car) is moving with the new mathematical model while the others are moving according to the extracted trajectories. For instance, the green agents in Figure 8.14 follow

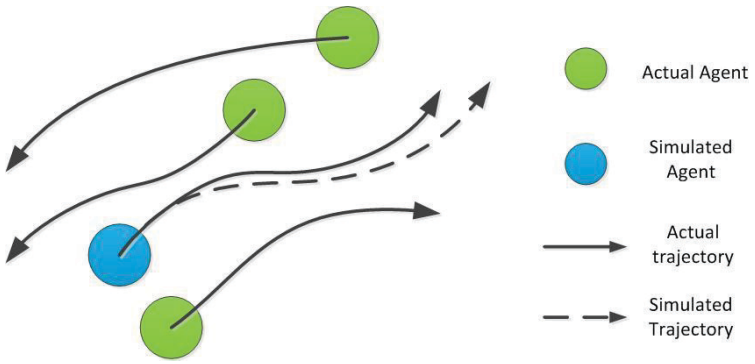

Figure 8.14: Illustration of the hybrid calibration method

the extracted trajectories. The blue agent moves according to the force directed model. The desired speed is specified equal to the maximum attained during the tracking time. Once these have been set, the simulated trajectory (dashed line) is compared to the empirical trajectory (solid line) for different combination values of parameters, for instance, interaction strength A and interaction range B in order to obtain the best fitness value. This procedure is repeated for every agent U at different starting times t^0 in a chosen scenario. After each run, the relative distance error is calculated based on Equation 8.4. Each simulation run can be summarised as follows:

1. Defining the infrastructural environment based on the video.
2. Assigning a desired speed, a starting point and an end point for one virtual agent according to the extracted trajectory.
3. Defining the trajectories and speeds of the surrounding agents based on the tracked trajectory.
4. Running the simulation where the virtual agent is moving and interacting with other agents based on the force directed model over T.
5. Determining the average relative distance error between the simulated and tracked trajectories.

After running the simulation over different starting times for different agents, the relative distance error in determined and the average E for all users over different starting times is taken as the "fitness" of the parameter set.

Interaction strength A and interaction range B are calibrated by empirical data using the shared space scheme of New Road and Exhibition Road. Figure 8.15 and 8.16 present the resulting fitness values as a function of different combinations of interaction strength A and the interaction range B. Different sets of scenarios are used for pedestrian-pedestrian, pedestrian-car, car-pedestrian and car-car interactions. The local minima show the best fitness for the corresponding choice of A and B. The travel time and total distance travelled by each agent is compared between the simulated and empirical data in order to find the best combination. Table 8.6 summarises the calibration results for New Road and Table 8.7 shows the resulting parameters for Exhibition Road. The combinations with the highest fitness values on New Road cover a narrow range compared to the results on Exhibition Road.

8.5 Validation Process

The validation procedure consist of two phases: a quantitative assessment and a qualitative assessment [230, 231]. Each assessment phase is further divided into different levels for detailed investigation of the relevant parameters. In Chapter 7, the qualitative assessment of the implemented SFM based on the crowd phenomena is presented. The qualitative assessments show how well the basis of the force directed model is implemented.

In this section, the quantitative assessment compares the performance indicators obtained by the empirical data of road user behaviours during mixed traffic conditions with the outcomes of the model. The common approach of quantitative validation is to show that the simulation model is able to reproduce real world

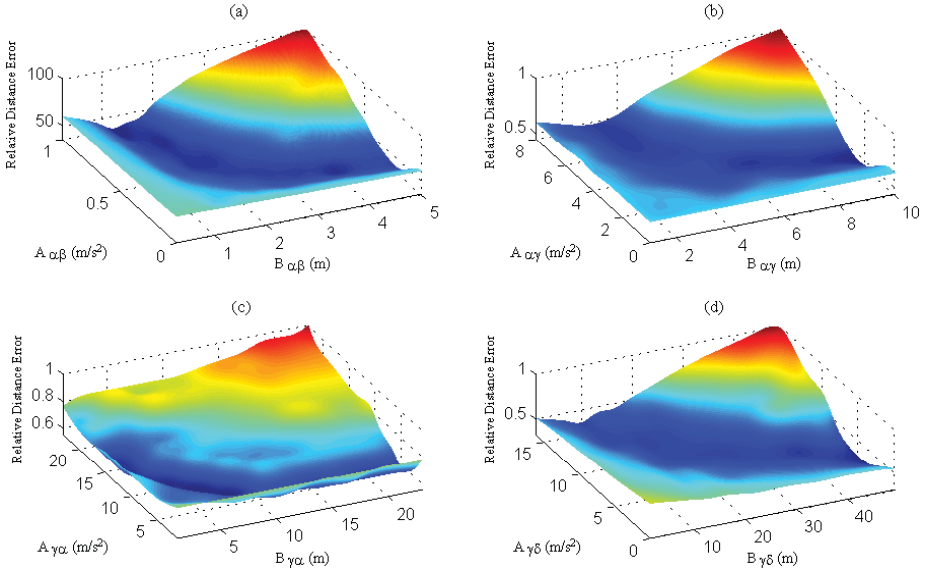

Figure 8.15: Fitness surface for parameter A and B for (a) Pedestrian-pedestrian-interactions, (b) Pedestrian-car-interactions (c) Car-pedestrian-interactions (d) Car-car-interactions of New Road

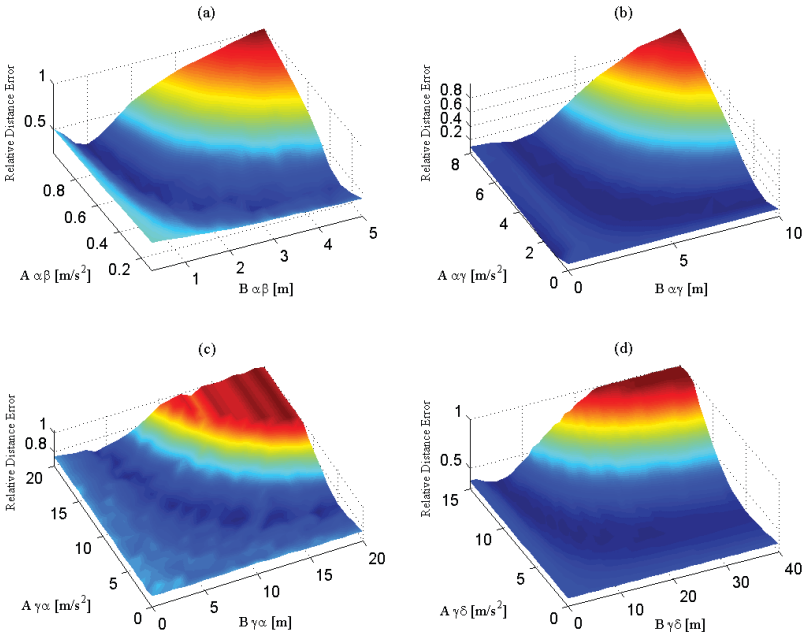

Figure 8.16: Fitness surface for parameter A and B for (a) Pedestrian-pedestrian-interactions, (b) Pedestrian-car-interactions (c) Car-pedestrian-interactions (d) Car-car-interactions of Exhibition Road

Parameter	Unit	Calibrated Value	Fitness
$A_{\alpha\beta}$	$\frac{\mathrm{m}}{\mathrm{s}^2}$	$[0.7 \pm 0.25]$	0.43
$B_{\alpha\beta}$	m	$[2.25 \pm 1]$	0.43
$A_{\alpha\gamma}$	$\frac{\mathrm{m}}{\mathrm{s}^2}$	$[3 \pm 1]$	0.49
$B_{\alpha\gamma}$	m	$[5 \pm 1]$	0.49
τ_γ	s	2	0.40
T_γ	s	0.74	0.40
$\tau_\gamma^{'}$	s	0.7	0.40
$d_{\gamma\delta}^{m}$	m	1	0.40
$B_{\gamma\delta}^{'}$	m	4	0.40
$B_{\gamma\delta}^{''}$	m	6	0.40
$A_{\gamma\alpha}$	$\frac{\mathrm{m}}{\mathrm{s}^2}$	$[6 \pm 1]$	0.57
$B_{\gamma\alpha}$	m	$[5 \pm 1]$	0.57
$A_{\gamma\delta}$	$\frac{\mathrm{m}}{\mathrm{s}^2}$	$[7 \pm 1]$	0.40
$B_{\gamma\delta}$	m	$[6 \pm 1]$	0.40

Table 8.6: A summary of the parameters from the calibration process of the New Road (Brighton, UK)

Parameter	Unit	Calibrated Value	Fitness
$A_{\alpha\beta}$	$\frac{\mathrm{m}}{\mathrm{s}^2}$	$[0.8 \pm 0.1]$	0.47
$B_{\alpha\beta}$	m	$[1 \pm 0.25]$	0.47
$A_{\alpha\gamma}$	$\frac{\mathrm{m}}{\mathrm{s}^2}$	$[3 \pm 1]$	0.49
$B_{\alpha\gamma}$	m	$[4 \pm 1]$	0.49
τ_γ	s	2.4	0.50
T_γ	s	0.7	0.50
$\tau_\gamma^{'}$	s	1.4	0.50
$d_{\gamma\delta}^{m}$	m	1	0.50
$B_{\gamma\delta}^{'}$	m	4	0.50
$B_{\gamma\delta}^{''}$	m	6	0.50
$A_{\gamma\alpha}$	$\frac{\mathrm{m}}{\mathrm{s}^2}$	$[7 \pm 1]$	0.59
$B_{\gamma\alpha}$	m	$[11 \pm 1]$	0.59
$A_{\gamma\delta}$	$\frac{\mathrm{m}}{\mathrm{s}^2}$	$[8 \pm 1]$	0.40
$B_{\gamma\delta}$	m	$[12 \pm 1]$	0.40

Table 8.7: A summary of the parameters from the calibration process of the Exhibition Road (London, UK)

data after calibration. The shared space model is validated by comparing distance, speed and acceleration distribution of real world data to the simulation

results on New Road and Exhibition Road in Section 8.5.1 and Section 8.5.2.

8.5.1 Validation Results for New Road

Figure 8.17 shows a system analysis of pedestrian and car flow on New Road. 16 pedestrians and 2 cars remained within this area during the observed period on average. These data were recorded during peak hours. Hence, the observed average number of 16 pedestrians and 2 cars per second was simulated. The simulation is defined according to the layout of New Road. Figure 8.18 illustrates the trajectories of pedestrians and cars during a time period for real data and simulation. The speed and acceleration distribution of cars and pedestrians according to empirical data and simulation results is shown in Figure 8.19 and 8.20.

8.5.2 Validation Results for Exhibition Road

A simulation environment is defined according to the recorded layout of Exhibition Road. Pedestrians and cars are free to move across this shared surface. Traffic demand from the observed data is shown in Figure 8.21. In Figure 8.22, the real and simulated trajectories of agents within a time period are plotted. A

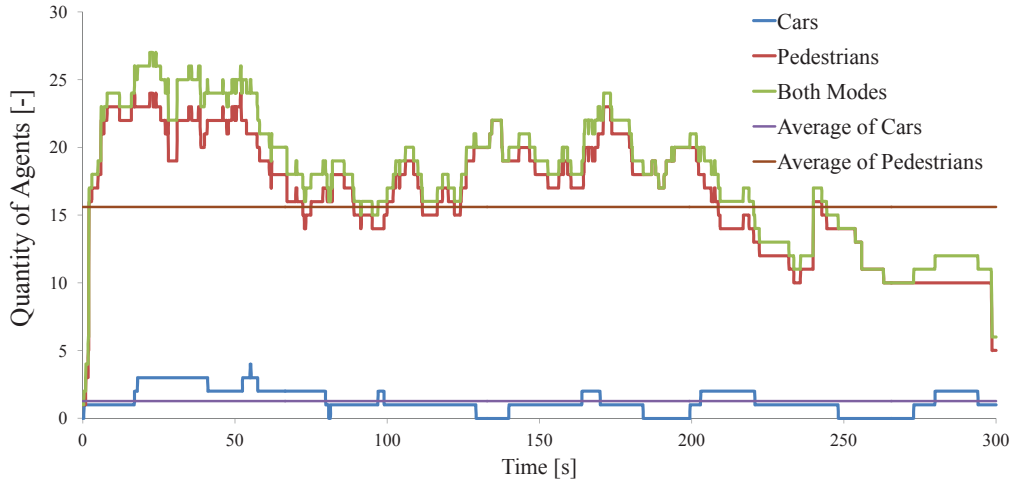

Figure 8.17: Traffic demand of tracked road users on New Road (Brighton, UK)

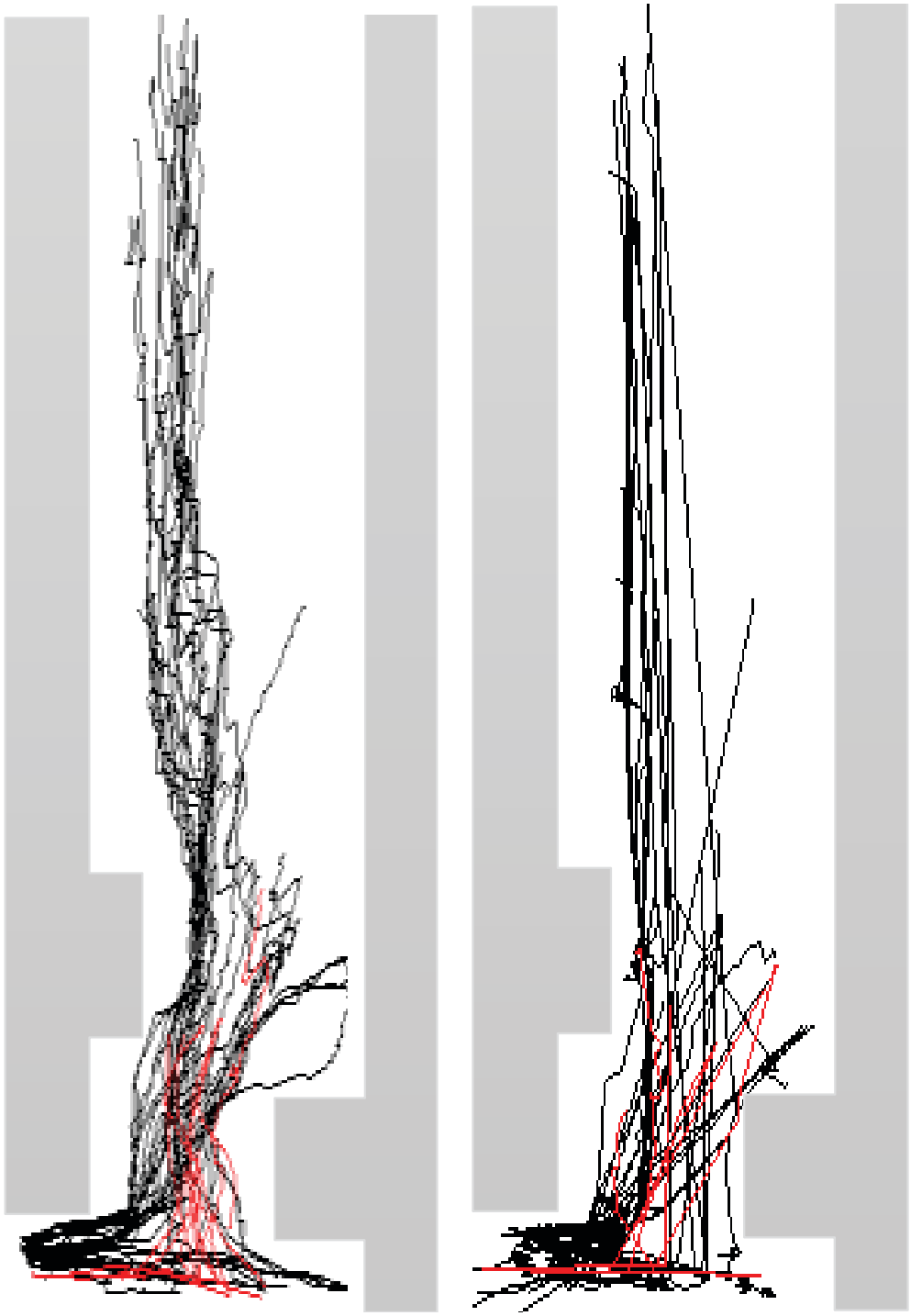

(a) (b)

Figure 8.18: Pedestrian (black) and car (red) trajectories on New Road (Brighton, UK) from (a) real data and (b) simulation

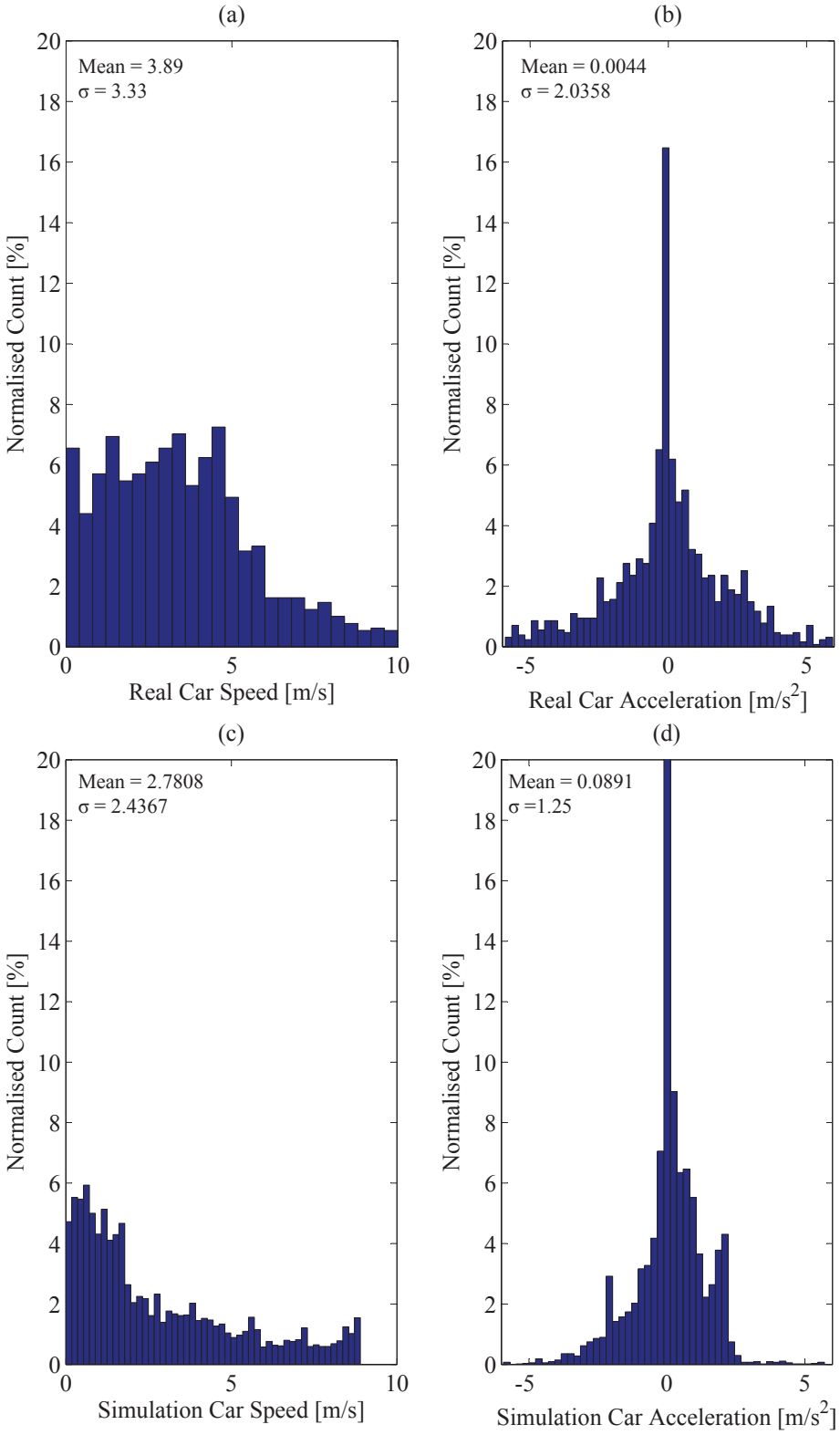

Figure 8.19: Speed and acceleration histograms of cars on New Road (Brighton, UK) According to (a)-(b) Empirical data and (c)-(d) Simulation results

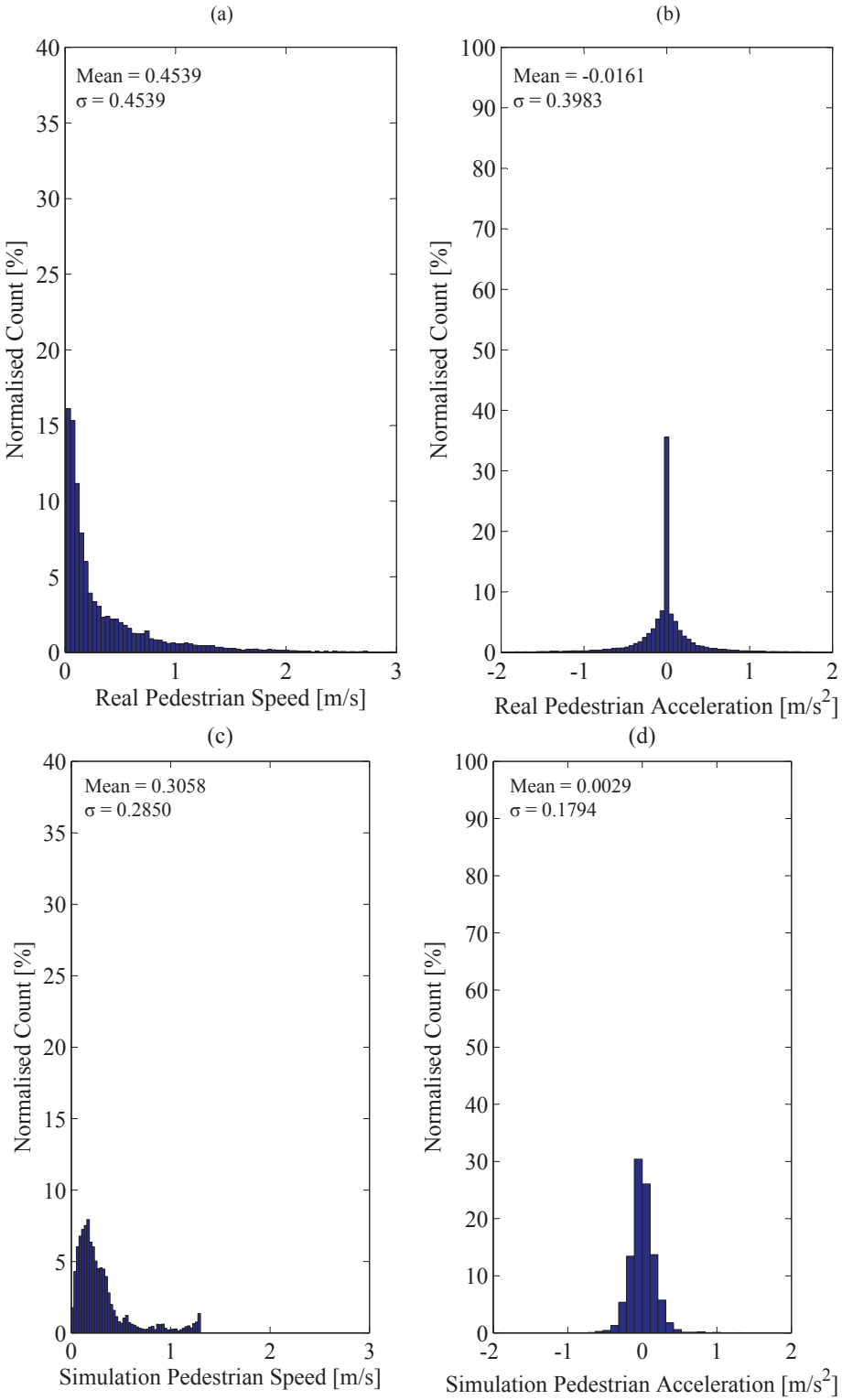

Figure 8.20: Speed and acceleration histograms of pedestrians on New Road (Brighton, UK) according to (a)-(b) Empirical data and (c)-(d) Simulation results

comparison of speed and acceleration analysis of the real data and simulation results for cars and pedestrians is shown in Figure 8.23 and 8.24.

8.6 Discussion and Conclusions

Two shared space schemes of link typology, New Road (Brighton, UK) and Exhibition Road (London, UK), have been analysed in Section 8.2. As shown in Figure 8.1, the density of pedestrians is much higher on the carriageway of New Road than on the footway in comparison to Exhibition Road. The high density of pedestrians on the carriageway of New Road can be explained by design characteristics. Since, restaurants, cafe and benches are placed on the footway of New Road, pedestrians use the carriageway area for walking through the environment. In addition, the flow of cars on New Road is about 10% of the car flow on Exhibition road while the pedestrian flows are high in both case studies.

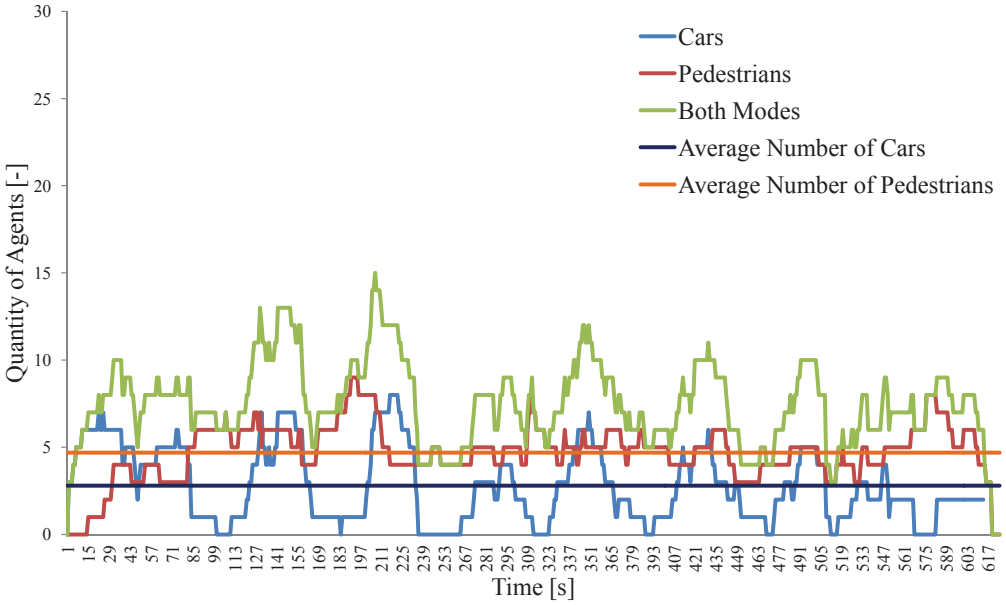

Figure 8.21: Traffic demand of tracked road users on Exhibition Road (London, UK)

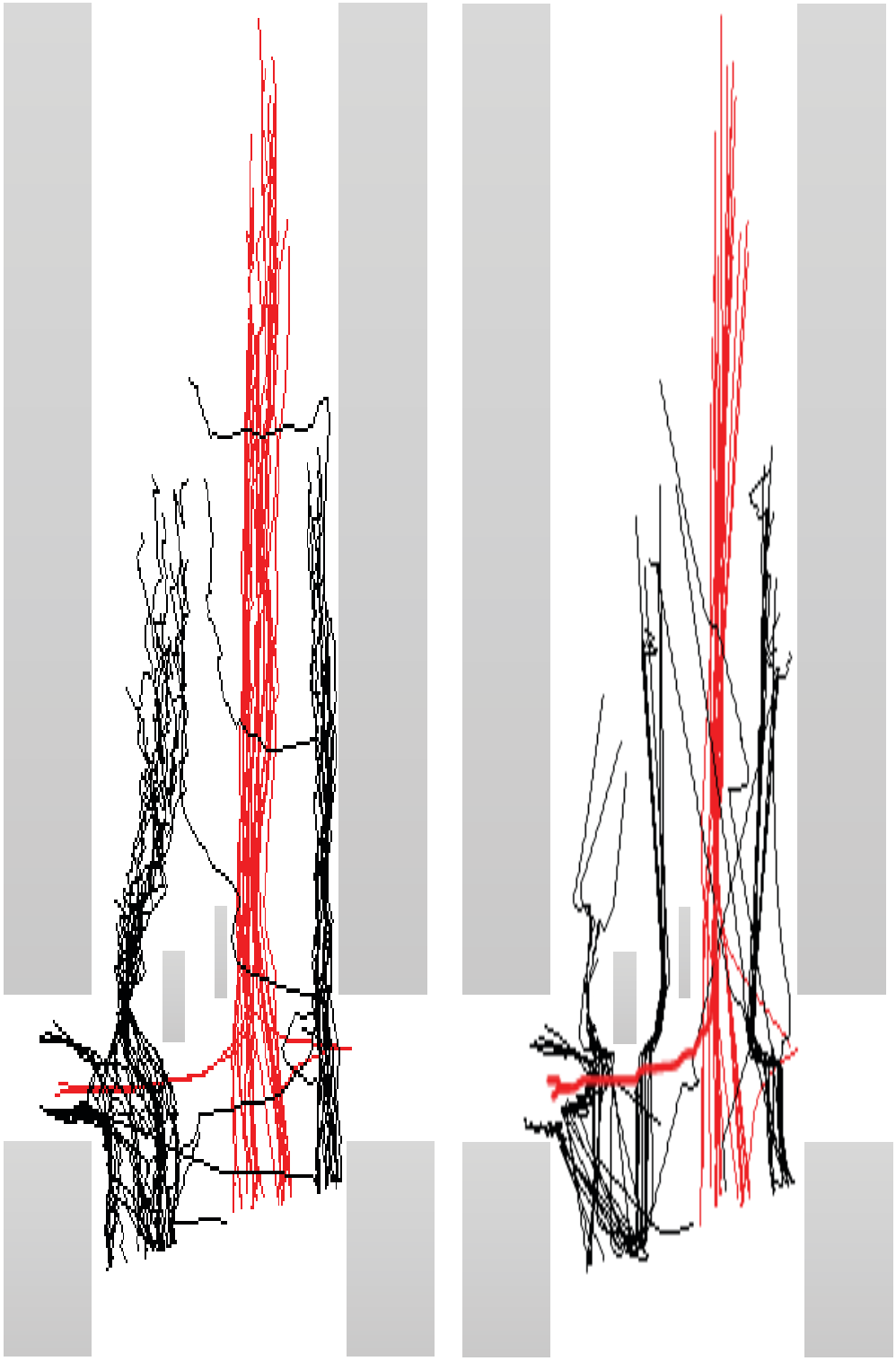

(a) (b)

Figure 8.22: Pedestrian (black) and car (red) trajectories on Exhibition Road (London, UK) from (a) real data and (b) simulation

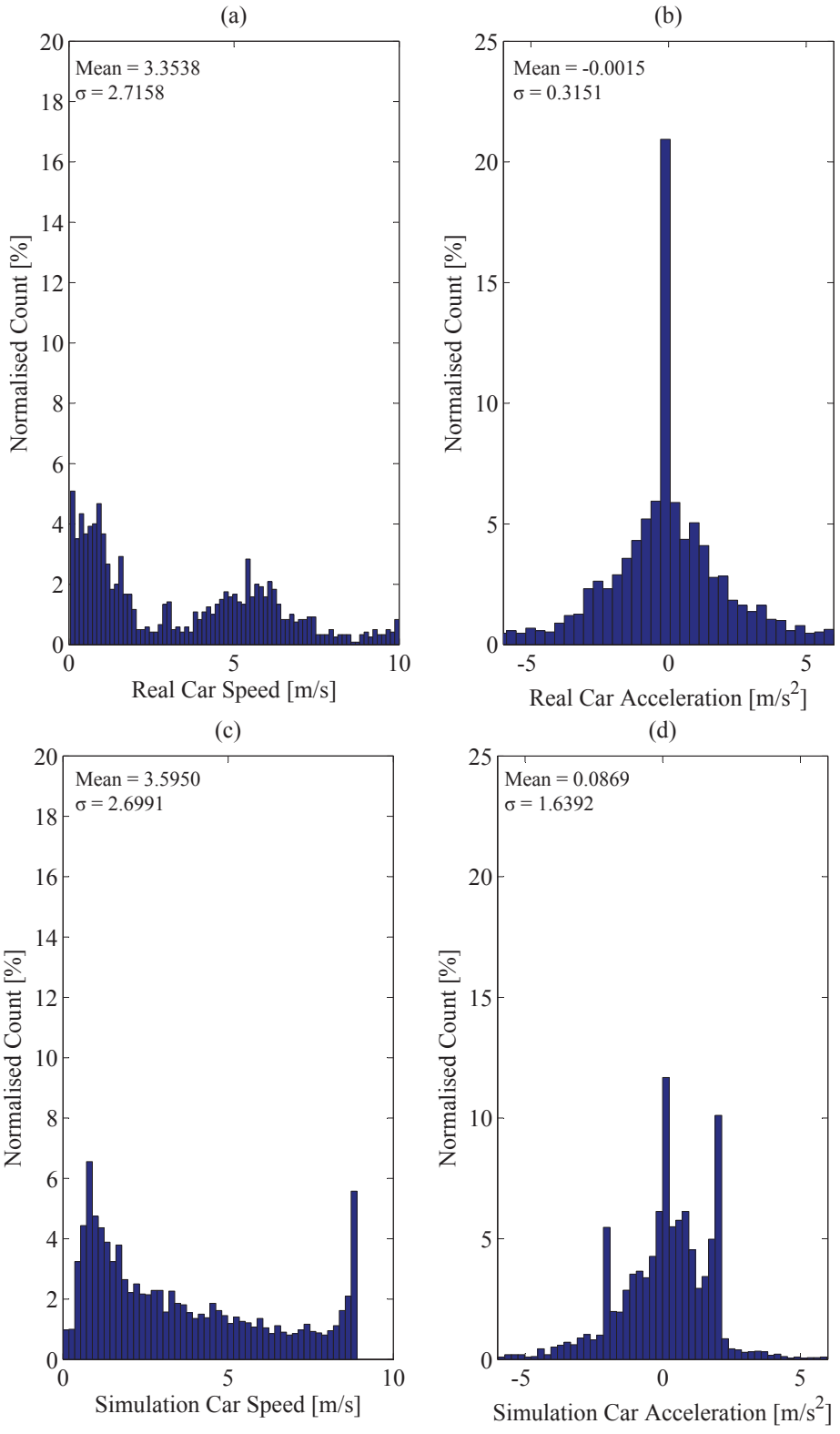

Figure 8.23: Speed and acceleration histograms of cars on Exhibition Road (London, UK) According to (a)-(b) Empirical data and (c)-(d) Simulation results

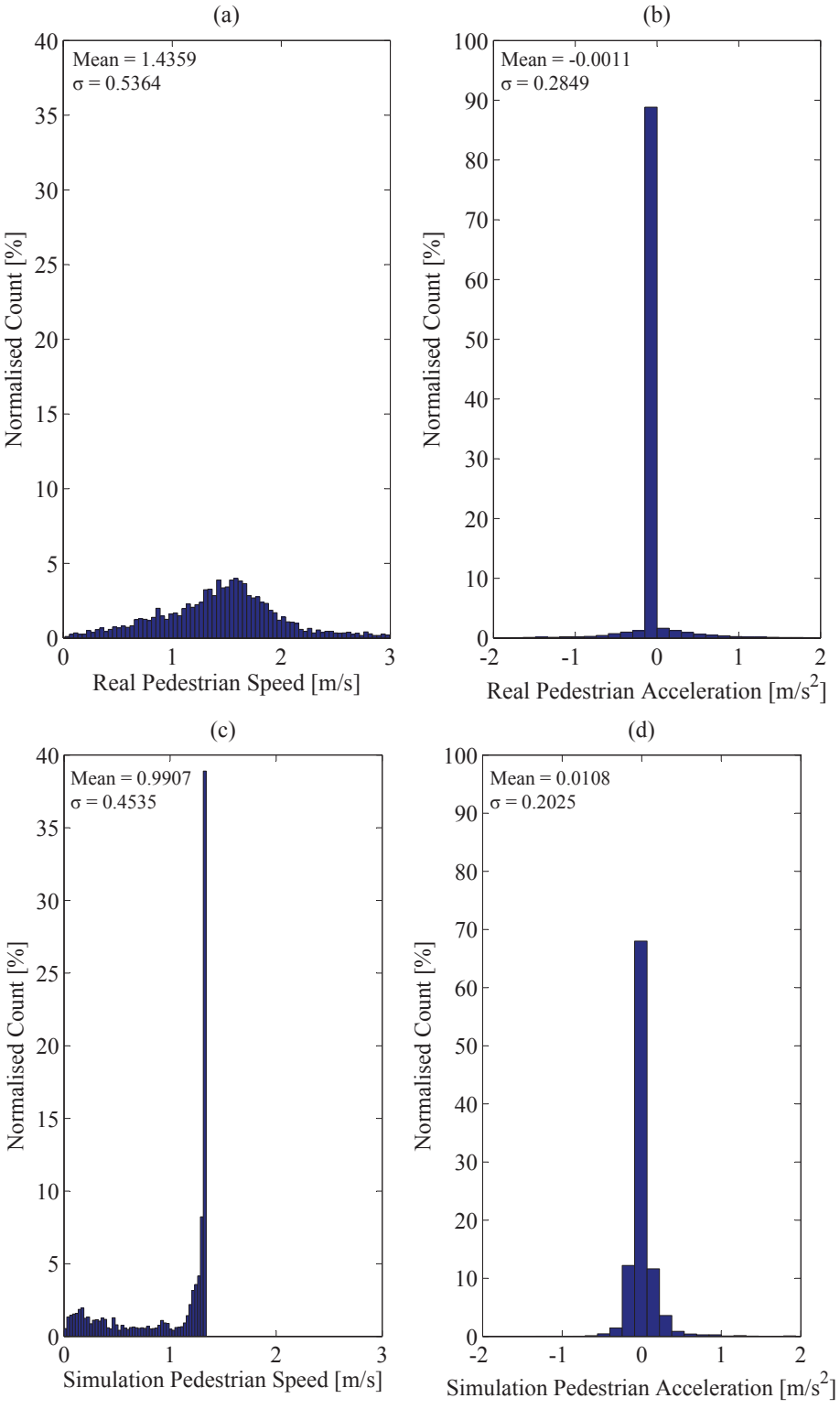

Figure 8.24: Speed and acceleration histograms of pedestrians on Exhibition Road (London, UK) According to (a)-(b) Empirical data and (c)-(d) Simulation results

Pedestrians and cars were tracked using the Trajectory Extractor software, the perspective view of the videos were converted to a top view angle and the trajectories, speeds and accelerations reported in Section 8.3. According to trajectories on New Road in Figure 8.8, pedestrian movements are distributed over the space and the occupancy of the given area is used within its limits. Cars negotiate their way through this pedestrian-dominated shared area of New Road. On Exhibition Road, pedestrians mainly remain on the sides of the road whereas cars follow the traditional traffic regulations and stay within assumed lanes as shown in Figure 8.11. The willingness to share space between pedestrians and cars is the main aim of the shared space concept [232]. Hence, one can conclude that Exhibition Road is a less shared design.

Another aim of shared space is calming traffic due to interactions rather than speed limitations. As shown in Figure 8.9 and Figure 8.12, the mean speed of pedestrians is about $1.25\ \frac{\mathrm{m}}{\mathrm{s}}$ on both sites while the speed of cars varies between New Road and Exhibition Road. The average speed, maximum acceleration and deceleration of the recorded car movements reflect the results reported in [233] for urban driving cycles of $30\ \frac{\mathrm{km}}{\mathrm{h}}$ zones. The mean speed of cars on New Road is about a third of that on Exhibition Road. This result corresponds to the high density of pedestrians in the carriageway on New Road which makes drivers to pay attention, negotiate their way and hence slow down. Comparing the speed distributions of pedestrians and cars on New Road and Exhibition Road in Figure 8.9 and 8.12, it can be seen that the speed of pedestrians is more equally distributed on New Road. The pedestrian and car interactions are not defined in shared space environments and cars slow down when many pedestrians move on the carriageway. At other times, they may increase their speed on New Road. The speed of drivers is considerably higher on Exhibition Road where the degree of separation is higher and therefore, the behaviour of road users is more independent and predictable.

Looking at the calibration results of New Road (Figure 8.15) and Exhibition Road (Figure 8.16) in Section 8.4, there are multiple combinations of interaction strength A and interaction range B with the best fitness value. The fitness values are distributed along a curve in both case studies. The trend of the heat map is compatible with the results attained for pedestrian interactions in [50]. However, the values of the best parameter combination for the shared space model are slightly higher. A reason for this can be that Johansson [50] calibrated his model for pedestrian interactions in the entrance/exit area of escalators, a shopping mall in Budapest and an experiment of students passing through a confined space. In these high density situations, pedestrians exhibit different behaviours and allow closer and even physical interactions. Shared space users' decision to change velocity to evade the road users depends on the velocity and density of traffic [50]. On Exhibition Road, combinations for A and B with the best fitness value cover a wider range compared to the results on New Road. This can be explained with the environmental design of New Road which contributes to more interactions at lower speeds compared to Exhibition Road. Hence, road user behaviours on New Road with higher density and lower speeds show higher level of common behaviour.
Comparing the values of the interaction range B between cars and pedestrians on Exhibition Road and New Road, the larger values for agents on Exhibition Road can be explained by the shared space design (which is more segregated than the one in New Road) and, therefore, the higher speed of cars. These results agree with the investigation of Kaparias et al. [234] exploring reaction distances of cars and pedestrians in case of potential collisions on Exhibition Road.

After calibrating the new mathematical model with respect to empirical data gained from digital cameras of New Road and Exhibition Road, the trajectories, speed and acceleration distributions of pedestrians and cars are compared to em-

pirical data in Section 8.5. The trajectory analysis (see Figure 8.18 and 8.22) reproduces the observed tendency of pedestrians to share the environment with vehicles on New Road and vice versa on Exhibition Road. Agents that are modelled by the new mathematical model strictly follow the shortest path via intermediate destinations. Comparing the observed and simulated trajectories, pedestrians show a descriptive[2] rather than a normative[3] behaviour according to empirical data. It can be concluded that shared space promotes this behaviour pattern as its philosophy is to attract pedestrians to spend time within the environment and move freely within the space. Regarding vehicles, the car-following feature and rule-based constraints have been simulated and agree with the observed data.
The speed distributions of the empirical data and simulation results match closely for the case study of New Road. The simulation results of Exhibition Road follow a Gaussian distribution as in reality. Since the desired speed of pedestrians and cars are set to $1.3\,\frac{\mathrm{m}}{\mathrm{s}}$ and $8.9\,\frac{\mathrm{m}}{\mathrm{s}}$ respectively, the speed distributions do not exceed the desired speeds. Comparing the acceleration distribution of real data and simulation, they are very similar but the standard deviation is higher in the simulation results in both case studies.

It can be concluded that shared space schemes are context-dependent and factors such as the infrastructural design of the environment and the flow and speed of pedestrians and vehicles affect the willingness to share space. The results of the assessments were presented in this chapter. The general conclusions of this thesis and the implications for the use of the presented microscopic model of shared space for future projects will be presented in Chapter 9.

[2]Descriptive behaviour is the displacement into different random directions or adaptive behavioural changes to other people or the environmental changes.
[3]Normative behaviour is structured by social rules and occurs in everyday life.

Chapter 9

Conclusions and Suggestions for Future Work

This chapter summarises and highlights the main achievements of each chapter. The limitations of the new microscopic model for the simulation of shared space schemes are identified leading to suggestions for future work.

9.1 Conclusions

This thesis has investigated mixed traffic modelling and developed a New Microscopic Model for the Simulation of Shared Space Schemes. The following conclusions are drawn:

Pedestrian and Vehicle Behaviour Modelling

1. A thorough and consolidated literature sought to classify microscopic models both phenomenologically and generically. The review determined that it is essential to reproduce a number of phenomenological behaviour patterns such as lane formation, stripe formation, freezing by heating, oscillation, herding, faster-is-slower, traffic hysteresis, capacity drop and stop-and-go wave when modelling crowd movements and vehicular traffic. The findings of this review add substantially to a growing body of literature on pedestrian, vehicular and mixed traffic and address the potential basis for shared space modelling.

2. Conventional vehicle and pedestrian modelling must account for the differences in concepts in which vehicle flow is along lanes (roads) and lateral movements are described as lane changes, while pedestrians interact in a two dimensional space either in a bounded domain or in the whole space. However, modelling of shared space users (pedestrians and vehicles) must consider space and time representations since shared space must be modelled in totality (no lane discipline) and agent movements allowed to be dynamically adaptive to the behavioural changes of others.

3. Force directed models (including the SFM) are the most appropriate models to reproduce crowd self-organising phenomena. While there is considerable experience with simulating pedestrians using in particular the SFM, it has not been applied to mixed traffic. The SFM offers the possibility

to model mathematically, not only pedestrians, but also vehicular traffic and their interactions with each other in a two dimensional space describing interactions by variables which have physical interpretations. Hence, this model forms the core of the new microscopic model developed in this thesis.

The Characteristic Behaviours and Conceptual Framework

4. In shared space environments, pedestrians and drivers exhibit specific manoeuvres: obstacles have a guiding effect, pedestrians and drivers follow the shortest path to the destination according to the infrastructure of the environment, and equal priority can be observed. Agents move and interact with each other keeping a certain distance from other users and obstacles along the way to their final destination. Road users seem to be more conscious about their surroundings and avoid collisions. These empirical findings of shared space user manoeuvres are captured in a pedestrian/vehicle modelling framework of three interrelated layers: a global trajectory planning layer, an operational force-based model layer and a diplomatic rule-based layer.

5. Equal priority and agent interactions with each other or obstacles are the strength of the SFM which supports the idea that this model is the most suitable base for modelling shared space users.

Trajectory Planning by Distance Map

6. The addition of intermediate destinations (way points) based on the flood-fill algorithm enhances the trajectory planning strategy of the SFM using a priori knowledge of the surrounding infrastructure. Agents follow the shortest path avoiding static obstacles from their origin to their final destination via these intermediate destinations.

Force-Based Modelling

7. The modified and extended SFM mathematically describes pedestrian and vehicular behaviour patterns based on their socio-psychological considerations. Agents move in a two dimensional space with no intrinsic lane system, have equal priority and negotiate the right of way. The new model is able to cover these main ideas of share space schemes and is therefore, the core of the new microscopic model developed in this thesis.

8. Empirical data show that vehicles tend to merge into assumed lanes when a number of cars move towards the same destination within a close distance between each other. The implementation of an additional car-following force allows car drivers to remain within assumed lanes defined by a leading car. This feature demonstrates the capability of the SFM to be reduced to a lane-based system.

Rule-Based Constraints for Shared Space Users

9. Building on the SFM for pedestrians (by Helbing [161], Molnar [72], Farkas and Vicsek [53]), the new model in this thesis incorporates cars. Contrary to pedestrians, vehicles are restricted to lateral movements. Hence, the steering angle of vehicular agents is related to the direction of movement and their speed. The correlation between these parameters depends on the maximum acceptable lateral acceleration for car drivers based on empirical data. A relationship is defined between car speed and steering angle considering the centrifugal acceleration to cover restriction of the lateral movement for cars.

10. Some road conflicts cannot be resolved by following the social force theory exclusively. Therefore, potential conflicts between cars and pedestrians are detected. A cost function minimises the direction of movement and speed

in order to avoid conflicts in shared spaces.

11. The UK is a left-hand traffic country. This rule avoids confusion between car drivers and decreases the possibility of accidents. When modelling shared space, this feature is essential as vehicles move in space with no physical lanes (i.e. with assumed lanes). Using the conflict avoidance strategy, the cost function is assigned subject to a defined steering constraint so that left-hand traffic is modelled for successive driving agents (this can be easily modified to right-hand traffic).

Software Implementation and Simulation

12. The new microscopic model is implemented into a simulation tool using the C#-Programming language which can be adapted to any shared space environment. The GUI allows building new scenarios, defining the number and type of agents, setting parameters for the agents, simulating the agent motions and retrieving resulting data.

Data Collection, Model Calibration and Validation

13. An enhanced calibration and validation methodology developed and executed to determine the SFM parameters and qualitatively and quantitatively assess the performance of the new mathematical model for shared space environments. Simulating pedestrian phenomena such as lane formation, freezing by heating, oscillations and faster-is-slower demonstrate the correct implementation of the SFM. Performance indicators (such as acceleration and speed distribution and trajectories of agents) validate the implemented model in comparison to real world data.

9.2 Suggestions for Future Work

This thesis contributes to mixed traffic modelling by mathematically describing and calibrating pedestrian and vehicle behaviours in shared space environments. Having implemented the three-layered microscopic model and highlighted its strengths, it is evident that there are also some limitations which serve to provide a basis for future work. These include:

1. Each of the two different modes (pedestrians and 4-wheeled motorised vehicles) has been assigned with identical parameter sets which have a physical meaning. However, in reality human behaviour is diverse particularly in shared space environments, which aim to increase the community texture of street surroundings and attract pedestrians to spend time within the area. The behaviour of elderly people and others who are physically impaired will, for example, differ from the able-bodied. Likewise, road users' age and cultural influences may affect their walking speed preference, their reaction time and interaction parameters. There is a similar need to categorise the behaviour of car drivers more in a nuanced way. For instance, one could specify typical parameter values for aggressive and conservative drivers or patient and reckless pedestrians. A cognitive model leading to fuller classification of different behavioural groups of pedestrians and car drivers could, therefore, be a focus of future research.

2. Shared space schemes aim to be more attractive for pedestrians than traditional segregated traffic areas and to encourage people to spend time in these particular environments. The findings in the validation of the new mathematical model show that the behaviour of pedestrians cannot exclusively be described by social forces. Since shared space promotes a variety of human activities in an open space, pedestrians have "descriptive" behaviour patterns which cannot be classified under social or physical inter-

actions. Further should explore this limitation and also investigate humans' adoptive behaviour to environmental changes by defining memory decay functions.

3. A priori knowledge of the static infrastructural environment is used in the global trajectory planner to move to the final destination by the shortest path incorporating intermediate destinations. In some cases, this study showed that the shortest paths are not always the most appropriate choice. An alternative approach, therefore, would be to implement dynamic trajectory planning so as to progressively determine the quickest path, considering not only static obstacles but also to avoid crowded areas.

4. The findings of this thesis are limited to two shared space roads in the UK. Hence, comparing the pedestrian and driver patterns in various shared space geometries is a topic for future research. In addition, the changes in pedestrian speed and the path change conditions obtained in this thesis cannot be generalised.

5. It could be of interest to extend the new mathematical model to include 2-wheeled motorised and non-motorised vehicles. These modes also make use of shared space areas and this additional diversity increases the challenge of simulating shared space schemes.

6. Safety indicators should defined for shared space areas. This innovative streetscape design, which seeks minimum separation between vehicle traffic and pedestrians, relies on users being attentive to other street participants. Furthermore, it could be useful to explore the extent to which people are able to satisfy the demand of attentiveness within only small geographical areas in big cities such as London. A future project could seek to answer the question of when safety is at risk and at what point shared space schemes reach their limitations. The latter case could investigate not

only limitations regarding safety but also regarding density considering different ratios of modes.

7. Of special interest would also be how different design approaches affect the behaviour patterns of shared space users. Case studies could examine areas before and after urban planners have converted the environment into a single surface. The next step could then be to select an area with a traditional street layout and propose a variety of new shared space designs. The new mathematical model developed in this thesis could help to determine the most beneficial layout.

List of the Publications Arisen from this Thesis

Journal Papers

B. Anvari, M.G.H. Bell, A. Sivakumar, and W.Y. Ochieng, Modelling Shared Space Users Via Rule-based SFM, **Transport Research Part C**, 2014. *(under review)*

Conference Papers

B. Anvari, "A Mathematical Model for Driver and Pedestrian Interaction in Shared Space Environments", *Universities' Transport Study Group*, Aberdeen, 2012.

B. Anvari, W. Daamen, V.L. Knoop, S.P. Hoogendoorn, and M.G.H. Bell, "Shared Space Modeling Based on Social Forces and Distance Potential Field", *International Conference on Pedestrian and Evacuation Dynamics*, Zurich, 2012.

B. Anvari, M.G.H. Bell, P. Angeloudis, and W.Y. Ochieng, "Prediction of Potential Conflicts and Velocity Optimisation of Long-range Collision Avoidance for Force-based Shared Space Simulation", *International Conference on Pedestrian and Evacuation Dynamics*, Delft, 2014. *(to be published)*

Bibliography

[1] C. Buchanan, "Traffic in Towns: A Study of the Long Term Problems of Traffic in Urban Areas," tech. rep., Reports of the Steering and Working Groups to the Minister of Transport. HMSO, London, 1963.

[2] B. Hamilton-Baillie, "Towards Shared Space," *Urban Design International*, vol. 13, no. 2, pp. 130–138, 2008.

[3] Department for Transport, "Manual for Streets," tech. rep., 2007.

[4] H. Tripp, *Road Traffic and Its Control*. London: Edward Arnold, 1950.

[5] L. Beth and T. Pharaoh, *Adapting Residential Roads for Safety and Amenity*. London: Department of Town Planning, South Bank Polytechnic, 1988.

[6] Department for Transport, "Shared Space," tech. rep., The Stationery Office (TSO), October 2011.

[7] P. Jones and N. Boujenko, "Street Planning and Design Using Link and Place," *JOURNEYS Sharing urban transport solutions*, vol. 6, pp. 7–14, May 2011.

[8] R. Schonauer, M. Stubenschrott, W. Huang, C. Rudloff, and M. Fellendorf, "Modeling Concepts for Mixed Traffic: Steps towards a Microscopic Sim-

ulation Tool for Shared Space Zones," *Research Record: Journal of the Transportation Research Board*, vol. 2316, no. 1, pp. 114–121, 2012.

[9] A. Quimby and J. Castle, "A Review of Simplified Streetscape Schemes," tech. rep., Transport for London, Street Management Division, 2006.

[10] K. Lynch, *The Image of the City*. Cambridge: MIT Press, 1960.

[11] J. Jacobs, *The Death and Life of Great American Cities*. New York: Vintage, 1961.

[12] A. Guttenberg, "The Woonerf: A Social Invention in Urban Structure," *Institute of Transportation Engineers*, pp. 17–22, 1981.

[13] D. Shearer, "Shared Spaces in New Zealand Urban Areas," Master's thesis, School of Surveying/Te Kura Kairuri, 2011.

[14] D. Appleyard, "Livable Streets: Protected Neighborhoods," *The ANNALS of the American Academy of Political and Social Science*, vol. 451, no. 1, pp. 106–117, 1980.

[15] N. Collarte, "The Woonerf Concept "Rethinking a Residential Street in Somerville"," Master's thesis, Tufts University, 2012.

[16] M. Southworth and E. Ben-Joseph, *Streets and the Shaping of Towns and Cities*. Washington, D.C: Island Press, 2003.

[17] T. Bendixson, "Space-Sharing and the Walk-in City," *Transportation*, vol. 6, pp. 215–216, Sept. 1977.

[18] C. Hass-Klau, *The Pedestrian and City Traffic*. London: Belhaven Press, 1990.

[19] D. Appleyard, "Styles and Methods of Structuring a City," *Environment and Behavior*, vol. 2, no. 1, pp. 100–117, 1970.

[20] J. Adams, *Risk*. UCL Press, 1995.

[21] D. Kopec, *Environmental Psychology for Design*. Fairchild Books, 2006.

[22] H. Monderman, "Designing Shared Space," Lecture, 13th November 2007. Reported by S. Tomlinson. Available at http://www.rudi.net/books/20021.

[23] B. Hamilton-Baillie and P. Jones, "Improving Traffic Behaviour and Safety Through Urban Design," *Civil Engineering*, vol. 158, no. 5, pp. 39–47, 2005.

[24] S. Lutz, "Shared Space - Final Evaluation and Results," tech. rep., Fryslan Province: Shared Space Institute, 2008.

[25] S. Reid and N. Kocak, and L. Hunt, "DfT Shared Space Project - Stage 1: Appraisal of Shared Space," tech. rep., Department of Transport, 2009.

[26] C. Buchanan, "Paved with Gold: The Real Value of Good Street Design," tech. rep., (Commission for Architecture and the Built Environment (CABE)), 2007.

[27] T. McNichol, "Roads Gone Wild," Tech. Rep. 12, Wired Magazine, 2004.

[28] R. Methorst, J. Gerlach, D. Boenk, and J. Leven, "Shared Space: Safe or Dangerous?," in *A contribution to the discussions on shared space at the WALK21 conference*, 2007.

[29] B. Hamilton-Baillie, "Shared Space: Reconciling People, Places and Traffic," *Built Environment*, vol. 34, no. 2, pp. 161–181, 2008.

[30] J. Edquist and B. Corben, "Potential Application of Shared Space Principles in Urban Road Design: Effects on Safety and Amenity," tech. rep., MONACH University, Accident Research Centre, 2012.

[31] B. Preston, "Cost Effective Ways to Make Walking Safer for Children and Adolescents," *Injury Prevention*, vol. 1, pp. 187–190, 1995.

[32] M. Biddulph, "Editorial," *Urban Design International*, vol. 13, no. 2, pp. 57–60, 2008.

[33] S. Andrews, "Understanding Shared Space: A Definition and Study of Its Operation," Master's thesis, Imperial College and the University College London, 2009.

[34] I. Kaparias, M. Bell, A. Miri, S. Cheng, J. Greensted, C. Taylor, and B. Mount, "Modelling the Willingness of Pedestrians to Share Space with Vehicles," 2010.

[35] D. Sutcliffe, "Shared Space and Naked Intersections-2008 Victorian Munucipal Overseas Study Tour," tech. rep., Central Goldfields Shire, 2009.

[36] T. Paterson, "Sharing The Road: A Sign of The Times?," September 2007. Available at: http://www.independent.co.uk/news/world/europe/sharing-theroadasignofthetimes402597.html.

[37] J. Gaventa, "Representation, Community Leadership and Participation: Citizen Envolvement in Neighbourhood Renewal and Local Governance Prepared for the Neighbourhood Renewal Unit Office of Deputy Prime Minister," Tech. Rep. July, Institute of Development Studies, 2004.

[38] E. Ben-Joseph, "Changing the Residential Street Scene: Adapting the Shared Street (Woonerf) Concept to the Suburban Environment," *Journal of the American Planning Association*, vol. 61, no. 4, pp. 504–515, 1995.

[39] B. Hamilton-Baillie and S. Melia, "Sharing or Separation: Which Way for Streets of the Future?," in *A debate with Ben Hamilton-Baillie and Steve Melia*, 2012.

[40] M. Jenks, "Residential Roads Researched," *Architects' Journal*, vol. 177, pp. 46–49, 1983.

[41] A. Clayden, K. Mckoy, and A. Wild, "Improving Residential Liveability in the UK: Home Zones and Alternative Approaches," *Journal of Urban Design*, vol. 11, no. 1, pp. 55–71, 2006.

[42] Guide Dogs and University College London, "Testing Proposed Delineators to Demarcate Pedestrian Paths in a Shared Space Environment: Report of Design Trials Conducted at University College London Pedestrian Accessibility and Movement Environment Laboratory (PAMELA)," tech. rep., The Guide Dogs for the Blind Association (Guide Dogs), London, 2007.

[43] O. Luca, F. Gaman, and O.-G. Singureanu, "Coping with Congestion: Shared Space," *Theoritical and Empirical Researches in Urban Management*, vol. 7, no. 4, pp. 53–62, 2012.

[44] J. Gerlach and R. Methorst, "Sense or Non-sense about Shared Space-For an Objective View of a Popular Planning Concept," *Transportation Research Board*, vol. 342, pp. 36–45, 2009.

[45] S. Alexandersson and E. Johansson, "Pedestrians in Microscopic Traffic Simulation," Master's thesis, Chalmers University of Technology, 2013.

[46] M. Lantin, "Computer Simulations of Developmental Processes," tech. rep., SFU CMPT, 1997.

[47] D. Helbing and A. Johansson, "Pedestrian, Crowd and Evacuation Dynamics," *Encyclopedia of complexity and System Science*, vol. 16, pp. 6476–6495, 2010.

[48] D. Helbing, I. J. Farkas, P. Molnar, and T. Viscek, "Simulation of Pedestrian Crowds in Normal and Evacuations Situations," *in Pedestrian and Evacuation Dynamics 2001*, pp. 21–58, 2002.

[49] D. Helbing, R. Jiang, and M. Treiber, "Analytical Investigation of Oscillations in Intersecting Flows of Pedestrian and Vehicle Traffic," *Physical Review E*, vol. 72, no. 4, pp. 0461301–04613010, 2005.

[50] A. Johansson, *Data-Driven Modeling of Pedestrian Crowd*. PhD thesis, Faculty of Transportation and Traffic Sciences, Dresden University of Technology, 2009.

[51] D. Helbing, A. Johansson, and H. Al-Abideen, "The Dynamics of Crowd Disasters: An Emperical Study," *Physical Review - Part E*, vol. 75, p. 046109, 2007.

[52] D. Helbing and A. Johansson, "Pedestrian, Crowd, and Evacuation Dynamics," *Encyclopedia of Complexity and Systems Science*, vol. 16, pp. 6476–6495, 2013.

[53] D. Helbing, I. Farkas, and T. Vicsek, "Simulating Dynamical Features of Escape Panic," *Nature*, vol. 407, pp. 487–490, 2000.

[54] B. Kerner, *The Physics of Traffic*. Berlin: Springer, 2004.

[55] B. Kerner, *Introduction to Modern Traffic Flow Theory and Control:The Long Road to Three-Phase Traffic Theory*. Berlin: Springer, 2009.

[56] M. Zamith, R. Leal-Toledo, M. Kischinhevsky, E. Clua, D. Brandao, A. Montenegro, and E. Lima, "A Parallelizable Probabilistic Cellular Automata Model for Highway Traffic Simulation: Periodic and Open Boundaries Conditions," in *International Meeting on High Performance Computing for Computational Science*, 2010.

[57] J. Treitere and J. Myers, "The Hysteresis Phenomenon in Traffic Flow," in *6th Int. Symp. on Transportation and Traffic Theory*, 1974.

[58] B. Kerner and H. Rehborn, "Experimental Features and Characteristics of Traffic Jams," *Phyical Review - Part E*, vol. 53, pp. R1296–R1300, 1996.

[59] W. Brilon, J. Geistefeldt, and M. Reglar, "Reliability of Freeway Traffic Flow: A Stochastic Concept of Capacity," in *16th International Symposium on Transportation and Traffic Theory*, pp. 125–144, 2005.

[60] M. Treiber, A. Kesting, and D. Helbing, "Delays, Inaccuracies and Anticipation in Microscopic Traffic Models," *Physica A*, vol. 360, pp. 71–88, 2006.

[61] D. Helbing, "Traffic and Related Self-driven Many-Particle Systems," *Review of Modern Physics*, vol. 73, pp. 1067 – 1141, 2001.

[62] M. Papageorgiou, "Some Remarks on Macroscopic Traffic Flow Modelling," *Transportation Research Part A: Policy and Practice*, vol. 32, no. 5, pp. 323–329, 1998.

[63] M. Brackstone and M. McDonald, "Car-following: A Historical Review," *Transportation Research Part F: Traffic Psychology and Behaviour*, vol. 2, no. 4, pp. 181–196, 1999.

[64] H. Zhang, "New Perspectives on Continuum Traffic Flow Models," *Networks and Spatial Economics*, vol. 1, pp. 9–33, 2001.

[65] S. Hoogendoorn and P. Bovy, "State-of-the-art of Vehicular Traffic Flow Modeling," *Journal of Systems and Control Engineering*, vol. 215, pp. 283–303, 2001.

[66] M. Treiber, A. Kesting, and D. Helbing, "Three-phase Traffic Theory and Two-phase Models with a Fundamental Diagram in the Light of Empirical

Stylised Facts," *Transportation Research Part B: Methodological*, vol. 44, pp. 983–1000, 2010.

[67] G. Orosz, R. Wilson, and G. Stepan, "Traffic Jams: Dynamics and Control," *Philosophical Transactions of the Royal Society A: Mathematical,Physical and Engineering Sciences*, vol. 368, pp. 4455–4479, 2010.

[68] R. Wilson and J. Ward, "Car-following Models: Fifty Years of Linear Stability Analysis: A Mathematical Perspective," *Transportation Planning and Technology*, vol. 34, no. 1, pp. 3–18, 2011.

[69] N. Bellomo and C. Dogbe, "On the Modeling of Traffic and Crowds: A Survey of Models, Speculations, and Perspectives," *SIAM Review*, vol. 53, pp. 409–463, 2011.

[70] F. Wageningen-Kessels, *Multi-class Continuum Traffic Flow Models: Analysis and Simulation Methods*. PhD thesis, Delft University of Technology, 2013.

[71] C. Reynolds, "Steering Behaviors for Autonomous Characters," in *Game Developers Conference*, pp. 763–782, 1999.

[72] D. Helbing and O. Molnar, "Social Force Model for Pedestrian Dynamics," *Physical Review - Part E*, vol. 51, pp. 4282–4286, 1995.

[75] L. F. Henderson, "On the Fluid Mechanic of Human Crowd Motions," *Transportation Research*, vol. 8, no. 6, pp. 509–515, 1974.

[76] N. Verlander and B. Heydecker, "Pedestrian Route Choice: An Empirical Study," in *PTRC European Transport Forum*, pp. 39–49, 1997.

[77] V. Blue and J. Adler, "Bi-directional Emergent Fundamental Pedestrian Flows from Cellular Automata Microsimulation," in *14th International Symposium on Transportation and Traffic Theory*, pp. 235–254, 1999.

[78] J. Funge, X. Tu, and D. Terzopoulos, "Cognitive Modeling: Knowledge, Reasoning and Planning for Intelligent Characters," in *26th Annual Conference on Computer Graphics and Interactive Techniques*, 1999.

[79] S. Hoogendoorn and P. H. L. Bovy, "Gas-kinetic Modeling and Simulation of Pedestrian Flows," *Transportaion Research Record*, vol. 1710, pp. 28–36, 2000.

[80] J. Kerridge, J. Hine, and M. Wigan, "Agent-based Modelling of Pedestrian Movements: The Questions that need to be Asked and Answered," *Environment and Planning B: Planning and Design*, vol. 28, no. 3, pp. 327–341, 2001.

[81] C. Burstedde, K. Klauck, and a. J. Z. A. Schadschneider, "Simulation of Pedestrian Dynamics using a To-dimensional Cellular Automaton," *Physica A: Statistical Mechanics and Its Applications*, vol. 295, pp. 507–525, 2001.

[82] M. Batty, *Agent-based Pedestrian Modelling*. Advanced spatial analysis: The CASA book of GIS, 2003.

[83] H. Klupfel, *A Cellular Automaton Model for Crowd Movement and Egress Simulation*. PhD thesis, University of Duisburg-Essen, 2003.

[84] C. Gloor, P. Stucki, and K. Nagel, "Hybrid Techniques for Pedestrian Simulations," *Cellular Automata*, vol. 3305, pp. 581–590, 2004.

[85] K. Nishinari, A. Kirchner, A. Namazi, and A. Schadschneider, "Extended Floor Field CA Model for Evacuation Dynamics," *IEICE Transactions on Information and System*, vol. E87D, pp. 726–732, 2004.

[86] T. Lakoba, D. J. Kaup, and N. Finkelstein, "Modifications of the Helbing-Molnar-Farkas-Vicsek Social Force Model for Pedestrian Evolution," *SIMULATION*, vol. 81, p. 339, 2005.

[87] G. Antonini and a. M. W. M. Bierlaire, "Discrete Choice Models of Pedestrian Walking Behavior," *Transportation Research Part B: Methodological*, vol. 40, no. 8, pp. 667–687, 2006.

[88] G. Rindsfuser and F. Klugl, "Agent-based Pedestrian Simulation: A Case Study of the Bern Railway Station," *disP-The Planning Review*, vol. 43, no. 170, pp. 9–18, 2007.

[89] "A Navigation Algorithm for Pedestrian Simulation in Dynamic Environments," 2007.

[90] A. Lerner, Y. Chrysanthou, and D. Lischinski, "Crowds by Example," *Computer Graphics Forum*, vol. 26, no. 3, pp. 655–664, 2007.

[73] A. Johansson, D. Helbing, and P. Shukla, "Specification of a Microscopic Pedestrian Model by Evolutionary Adjustment to Video Tracking Data," *Physics and Society*, vol. 9, no. 10, pp. 271–288, 2008.

[91] A. Sud, E. Andersen, S. Curtis, M. Lin, and D. Manocha, "Real-time Path Planning in Dynamic Virtual Environments using Multiagent Navigation Graphs," *IEEE Transactions on Visualisation and Computer Graphics*, vol. 14, pp. 526–538, 2008.

[92] T. Robin, G. Antonini, and a. J. C. M. Bierlaire, "Specification, Estimation and Validation of a Pedestrian Walking Behavior Model," *Transportation Research - Part B*, vol. 43, pp. 36 – 56, 2009.

[93] Y. Xia and a. C. S. S.C. Wong, "Dynamic Continuum Pedestrian Flow Model with Memory Effect," *Physical Review*, vol. 79, no. 6, p. 066113, 2009.

[94] E. Kirik, T. Yurgel'yan, and D. Krouglov, "The Shortest Time and/or the Shortest Path Strategies in a CAFF Pedestrian Dynamics Model," *Journal of Siberian Federal University*, vol. 2, no. 3, pp. 271–278, 2009.

[95] T. Kretz, "Pedestrian Traffic: On the Quickest Path," *Journal ofS tatistical Mechanics*, vol. 03, 2009.

[96] G. Koster, D. Hartmann, and W. Klein, "Microscopic Pedestrian Simulations: From Passenger Exchange Times to Regional Evacuation," in *Proceedings of the International Conference of Operations Research*, 2010.

[97] T. Kretz, S. Hengst, V. Roca, A. P. Arias, and a. U. H. S. Friedberger, "Calibrating Dynamic Pedestrian Route Choice with an Extended Range Telepresence System," in *IEEE International Conference*, pp. 166–172, 2011.

[98] A. Lachapelle and A. Wolfram, "On a Mean Field Game Approach Modeling Congestion and aversion in Pedestrian Crowds," *Transportation Research Part B: Methodological*, vol. 45, no. 10, pp. 1572–1589, 2011.

[74] M. Charibi, *Validated Force-based Modeling of Pedestrian Dynamics*. PhD thesis, University of Cologne, 2012.

[99] D. Ni, "Multiscale Modeling of Traffic Flow," *Mathematica Aeterna*, vol. 1, pp. 27–54, 2011.

[100] N. Bellomo, B. Piccoli, and A. Tosin, "Modeling Crowd Dynamics from a Complex System Viewpoint," *Mathematical Models and Methods in Applied Sciences*, vol. 2, pp. 12300041–123000429, 2012.

[101] D. Helbing and B. Tilch, "Generalized Force Model of Traffic Dynamics," *Physical Review E*, vol. 58, pp. 133–138, 1999.

[102] R. Chandler, R. Herman, and E. W.Montroll, "Traffic Dynamics: Studies in Car Following," *Operations Research*, vol. 6, no. 2, pp. 165–184, 1958.

[103] D. Gazis, R. Herman, and R. Potts, "Car-follwoing Theory of the Steady State Traffic Flow ," *Operations Research*, vol. 7, no. 4, pp. 499–595, 1959.

[104] K. Chang and K. Chon, "A Car-following Model Applied Reaction Times Distribution and Perceptual Threshold," *Journal of the Eastern Asia Society for Transportation Studies*, vol. 6, pp. 1888–1903, 2005.

[105] L. Edie, "Car Following ans Steady State of Theory for Non-congested Traffic," *Operations Research*, vol. 9, no. 1, pp. 66–76, 1961.

[106] Y. Weng and T. Wu, "Car-following Model for Vehicular Traffic," *Journal of Zhejiang University - Science A*, vol. 3, no. 4, pp. 412–417, 2002. (in Chinese).

[107] Y. Li and D. Sun, "Microscopic Car-following Model for the Traffic Flow: The State of the Art," *J Control Theory Appl*, vol. 10, no. 2, pp. 133–143, 2012.

[108] S. Darbha, K. R. Rajagopal, and V. Tyagi, "A Review of Mathematical Models for the Flow of Traffic and Some Recent Results," *Nonlinear Analysis*, vol. 69, no. 3, pp. 950–970, 2008.

[109] P. Gipps, "A Behavioural Car-following Model for Computer Simulation," *Transportation Research Part B: Methodological*, vol. 15, no. 2, pp. 105–111, 1981.

[110] B. Gunay, "Car Following Theory with Lateral Discomfort," *Transportation Research Part B: Methodological*, vol. 41, no. 7, pp. 722–735, 2007.

[111] M. Bando, K. Hasebe, A. Nakayama, A. Shibata, and Y. Sugiyarna, "Dynamical Model of Traffic Congestion and Numerical Simulation," *Physical Review E*, vol. 51, pp. 1035–1042, 1995.

[112] M. Bando and K. Hasebe, "Analysis of Optimal Velocity Model with Explicit Delay," *Physic Review E*, vol. 58, no. 5, pp. 5429–5435, 1998.

[113] M. Treiber and D. Helbing, "Explanation of Observed Features of Self-organization in Traffic Flow," 1999.

[114] H. Ge, S. Dai, L. Dong, and Y. Xue, "Stabilization Effect of Traffic Flow in an Extended Car-following Model based on an Intelligent Transportation System Application," *Physic Review E*, vol. 70, no. 6, pp. 66134–66140, 2004.

[115] H. Gong, H. Liu, and B. Wang, "An Asymmetric Full Velocity Difference Car-following Model," *Physica A*, vol. 387, no. 11, pp. 2595–2602, 2008.

[116] H. Ge, "Two Velocity Difference Model for a Car Following Theory," *Physica A*, vol. 387, no. 21, pp. 5239–5245, 2008.

[117] X. Zhao and Z. Gao, "A New Car-following Model: Full Velocity and Acceleration Difference Model," *The European Physical Journal B*, vol. 47, no. 1, pp. 145–150, 2005.

[118] X. Zhao and Z. Gao, "The Stability Analysis of the Full Velocity and Acceleration Difference Model," *Physica A*, vol. 375, no. 2, pp. 679–686, 2007.

[119] D. Xie, Z. Gao, and X. Zhao, "Stabilization of Traffic Flow based on the Multiple Information of Preceding Cars," *Communications Computational Physics*, vol. 3, no. 4, pp. 899–912, 2008.

[120] D. Sun, Y. Li, and C. Tian, "Car-following Model based on the Information of Multiple Ahead and Velocity Difference," *System Engenering Theory and Practice*, vol. 30, no. 7, pp. 1326–1332, 2010.

[121] R. Wiedmann and U. Reiter, "Microscopic Traffic Simulation: The Simulation System MISSION, Background and Actual State," Tech. Rep. 2, CEC project ICARUS (V1052) Final Report, Brussels, 1992. Appendix A.

[122] R. Michaels, "Perceptual Factors in Car Following," *International Symposium on the Theory of Road-Traffic Flow*, pp. 44–59, 1965.

[123] M. Brackstone, B. Sultan, and M. McDonald, "Motorway Driver Behaviour: Studies on Car Following," *Transportation Research Part F: Traffic Psychology and Behaviour*, vol. 5, no. 1, pp. 31–46, 2002.

[124] P. Hidas, "Modelling Lane Changing and Merging in Microscopic Traffic Simulation," *Transportation Research Part C: Emerging Technologies*, vol. 10, pp. 351–371, 2002.

[125] C. Kikuchi and P. Chakroborty, "Car following Model based on a Fuzzy Inference System," *Transportation Research Record*, vol. 1365, pp. 82–91, 1992.

[126] K. Nagel and M. Schreckenberg, "A Cellular Automaton Model for Freeway Traffic," *Journal de Physique*, vol. 2, no. 12, pp. 2221–2229, 1992.

[127] M. Fukui and Y. Ishibashi, "Traffic Flow in 1D Cellular Automaton Model including Cars Moving with High Speed," *Journal of the Physical Society of Japan*, vol. 65, no. 6, pp. 1868–1870, 1996.

[128] S. Krauss, P. Wagner, and C. Gawron, "Metastable States in a Microscopic Model of Traffic Flow," *Physic Review E*, vol. 55, no. 4, pp. 5597–5602, 1997.

[129] D. Helbing and M. Schreckenberg, "Cellular Automata Simulating Experimental Properties of Traffic Flow," *Physic Review E*, vol. 59, no. 3, pp. 2505–2508, 1999.

[130] N. Jia and S. Ma, "Comparison between the Optimal Velocity Model and the Nagel-Schreckenberg Model," *Acta Physica Sinica*, vol. 59, no. 2, pp. 832–842, 2010.

[131] P. Radhakrishnan and T. Mathew, "Hybrid Stochastic Cellular Automata-Driver-Vehicle-Object Simulation Model for Heterogeneous Traffic at Urban Signalized Intersections," *Journal of Copuing in Civil Engineering @ ASCE*, vol. 27, pp. 254–262, 2013.

[132] T. Toledo, "Driving Behaviour: Models and Challenges," *Transport Reviews*, vol. 27, no. 1, pp. 65–84, 2007.

[133] H. Fritzsche, "A Model for Traffic Simulation," *Traffic Engineering and Control*, vol. 35, no. 5, pp. 317–321, 1994.

[134] P. Gipps, "A Model for the Structure of Lane-changing Decisions," *Transportation Research Part B: Methodological*, vol. 20, no. 5, pp. 403–414, 1986.

[135] T. G. Oketch, "New Modeling Approach for Mixed-traffic Streams with Nonmotorized Vehicles," *Transportation Research Record*, vol. 1705, pp. 61–69, 2000.

[136] H. Wei, J. J. Lee, Q. Li, and C. Li, "Observation-based Lane-vehicle Assignment Hierarchy: Microscopic Simulation on Urban Street Network," *Transportation Research Record*, vol. 1710, pp. 96–103, 2000.

[137] T. Toledo, *Integrated Driving Behavior Modeling*. PhD thesis, Massachusetts Institute of Technology, USA, 2003.

[138] R. Herman and G.Weiss, "Comments on the Highway-Crossing Problem," *Operations Research*, vol. 9, no. 6, pp. 828–840, 1961.

[139] C. Daganzo, "Estimation of Gap Acceptance Parameters within and across the Population from Direct Roadside Observation," *Transportation Research Part B: Methodological*, vol. 15B, no. 1, pp. 1–15, 1981.

[140] H. Mahmassani and Y. Sheffi, "Using Gap Sequences to Estimate Gap Acceptance Functions," *Transportation Research Part B: Methodological*, vol. 15B, no. 3, pp. 143–148, 1981.

[141] S. M. Madanat, M. Cassidy, and M. Wang, "Probabilistic Delay Model at Stop-controlled Intersection," *ASCE Journal of Transportation Engineering*, vol. 120, no. 1, pp. 21–36, 1994.

[142] M. Cassidy, "Unsignalized Intersection Capacity and Level of Service: Revisiting a Critical Gap," *Transportation Research Record*, vol. 1484, pp. 16–23, 1995.

[143] K. Ahmed, *Modeling Drivers' Acceleration and Lane Changing Behavior*. PhD thesis, Massachusetts Institute of Technology, USA, 1999.

[144] M. Ben-Akiva, *Structure of Passanger Travel Demand Models*. PhD thesis, Massachysetts Institute of Technology, 1973.

[145] G. Gunnar, "Models of Wayfinding in Emergency Evacuations," *European Journal of Operational Research*, vol. 105, no. 3, pp. 371–389, 1998.

[146] H. Hamcher and S. Tjandra, "Mathematical Modelling of Evacuation Problems: A State of the Art," in *Pedestrian and Evacuation Dynamics*, pp. 227–266, 2002.

[147] H. Klupfel and T. Meyer-Konig, "Simulation of the Evacuation of a Football Stadium," in *Traffic and Granular Flow '03*, pp. 423–430, 2004.

[148] N. Shiwakoti and a. G. R. M. Sarvi, "Modelling Pedestrian Behaviour under Emergency Conditions - State-of-the-art and Future Directions," *Australasian Transport Research Forum*, vol. 31, pp. 457–473, 2008.

[149] N. Pelechano and A. Malkawi, "Evacuation Simulation Models: Challenges in Modeling High Rise Building Evacuation with Cellular Automata Approaches," *Automation in Construction*, vol. 17, no. 4, pp. 377–385, 2008.

[150] N. Shiwakoti, M. Sarvi, and a. M. B. G. Rose, "Enhancing the Safety of Pedestrians during Emergency Egress," in *Transportation Research Record-Series [P]*, pp. 31–37, 2009.

[151] G. Lammel, M. Rieser, and K. Nagel, "Large Scale Microscopic Evacuation Simulation," in *Pedestrian and Evacuation Dynamics '08*, pp. 547–553, 2010.

[152] S. Rodriguez and N. Amato, "Behavior-based evacuation planning," in *Proceedings of 2010 IEEE International Conference on Robotics and Automation*, 2010.

[153] N. Shiwakoti, M. Sarvi, and a. M. B. G. Rose, "Animal Dynamics based Approach for Modeling Pedestrian Crowd Egress under Panic Conditions," *Transportation Research B: Methodological*, vol. 45, no. 9, pp. 1433–1449, 2011.

[154] N. Shiwakoti, M. Sarvi, and a. M. B. G. Rose, "Consequence of Turning Movements in Pedestrian Crowds during Emergency Egress," *Transportation Research Record*, vol. 2234, pp. 97–104, 2011.

[155] A. Schadschneider, W. Klingsch, H. Klupfel, T. Kretz, C. Rogsch, and A. Seyfried, "Evacuation Dynamics: Empirical Results, Modeling and Applications," in *Extreme Environmental Events*, pp. 517–550, 2011.

[156] U. Wagoum and a. S. H. A. Seyfried, "Modelling Dynamic Route Choice of Pedestrians to Assess the Criticality of Building Evacuation," in *Advances in Complex Systems*, vol. 15, 2011.

[157] L. Hermant, M. Gersigny, R. Hermann, and R. Ahuja, "Applying Microscopic Pedestrian Simulation to The Design Assessment of Various Railway Stations in South Africa," in *26th Southern African Transport Conference*, pp. 334–344, 2010.

[158] M. Davidich, F. Geiss, H. Mayer, and a. C. R. A. Pfaffinger, "Waiting Zones for Realistic Modelling of Pedestrian Dynamics: A Case Study using two Major German Railway Stations as Examples," *Transportati on Research Part C: Emerging Technologies*, 2013.

[159] C. Loscos and a. A. M. D. Marchal, "Intuitive crowd behaviour in dense urban, environments using local laws," in *Theory and Practice of Computer Graphics*, no. 122-129, 2003.

[160] T. Robin, G. Antonini, M. Bierlaire, and J. Cruz, "Specification,Estimation and Validation of a Pedestrian Walking Behavior Model," *Transportation Research Part B: Methodological*, vol. 43, no. 1, pp. 36–56, 2010.

[161] D. Helbing, "A Mathematical Model for the Behaviour of Pedestrians," *Behavioral Science*, vol. 36, pp. 298–310, 1991.

[162] M. Apel, "Simulation of Pedestrian Flows Based on the Social Force Model Using the Verlet Link Cell Algorithm," Master's thesis, Poznan University of Technology, 2004.

[163] H. Xi, Y. Son, and S. Lee, "An Integrated Pedestrian Behaviour Model Based on Extended Decision Field Theory and Social Force Model," in

Proceedings of the 2010 Winter Simulation Conference (J. M.-T. J. H. B. Johansson, S. Jain and e. E. Yücesan, eds.), 2010.

[164] S. HeliÄovaara, "Computational Models for Human Behaviour in Fire Evacuations," Master's thesis, Helsinki University of Technology, Department of Engineering Physics and Mathematics, 2007.

[165] A. Schadschneider, "Cellular Automaton Approach to Pedestrian Dynamics Theory," *Pedestrian and Evacuation Dynamics*, vol. 75, 2001.

[166] S. Sarmady, "Simulating Crowd Movements using Fine Grid Cellular Automata," in *International Conference on Computer Modelling and Simulation*, 2010.

[167] W. Song, Y. Yu, W. Fan, and H. Zhang, "A Cellular Automata Evacuation Model Considering Friction and Repulsion," *Science in China - Series E: Technological Sciences*, vol. 48, pp. 403 – 413, 2005.

[168] S. Alghadi and H. Mahmassani, "Simulation of Crowd Behavior and Movement: Fundamental Relations and Applications," *Transportation Research Record*, vol. 1320, pp. 260 – 268, 1991.

[169] S. Hoogendoorn and P. Bovy, "Pedestrian Route-Choice and Activity Scheduling Theory and Models," *Transport Research Part B*, vol. 22, pp. 169–190, 2004.

[170] M. Campanella, S. Hoogendoorn, and W. Daamen, "Effects of Heterogeneity on Self-organized Pedestrian Flows," *Transportation Research Record*, vol. 2124, p. 21482156, 2009.

[172] S. Paris, J. Pettre, and S. Donikian, "Pedestrian Reactive Navigation for Crowd Simulation: A Predictive Approach," *Computer Graphics Forum*, vol. 26, pp. 665–674, 2007.

[171] M. Moussaid, D. Helbing, S. Garnier, A. Johansson, M. Combe, and G. Theraulaz, "Experimental Study of the Behavioural Mechanisms Underlying Self-Organization in Human Crowds," *Proceedings of the Royal Society B Biological Sciences*, vol. 276, pp. 2755–2762, 2009.

[173] I. Karamouzas and M. Overmars, "A Velocity-based Approach for Simulating Human Collision Avoidance," *Intelligent Virtual Agents*, pp. 180 – 186, 2010.

[174] P. Fiorini and Z. Shiller, "Motion Planning in Dynamic Environments using Velocity Obstacles," *The International Journal of Robotics Research*, vol. 17, no. 7, pp. 760 – 772, 1998.

[175] C. Reynolds, "Flocks, Herds, and Schools: A Distributed Behavior Model," 1987.

[176] J. Kennedy and R. Eberhart, "Particle Swarm Optimization," in *IEEE Intel Conference on Neural Networks*, (Perth, Australia), pp. 1942–1948, 1995.

[177] N. Wijermans, *Understanding Crowd Behaviour: Simulating Situated Individuals*. PhD thesis, University of Groningen, 2011.

[178] M. Shahin, "Pedestrian Behaviour with Mixed Traffic in Developing Countries," *Traffic Engineering and Control*, vol. 47, no. 8, pp. 303–309, 2006.

[179] G. Tiwari, S. Bangdiwala, A. Saraswat, and S. Gaurav, "Survival Analysis: Pedestrian Risk Exposure at Signalised Intersections," *Transport Research Part F*, vol. 10, no. 2, pp. 77–89, 2007.

[180] R. Rastogi, S. Chandra, J. Vamsheedhar, and V. Das, "Parametric Study of Pedestrian Speeds at Midblock Crossings," *Journal of Urban Planning and Development*, vol. 137, pp. 381–389, 2011.

[181] B. Kadali and P. Vedagiri, "Modelling Pedestrian Road Crossing Behaviour under Mixed Traffic Condition," *European Transport*, vol. 55, pp. 1–17, 2013.

[182] B. Li, "A Model of Pedestrians' Intended Waiting Times for Street Crossings at Signalized Intersections," *Transportation Research Part B: Methodological*, vol. 51, pp. 17–28, 2013.

[183] C. Pretto, H. Cybis, and A. Jacobsen, "A Multi-Layer Simulation Model for Vehicle and Pedestrian Interaction," in *TRB Annual Meeting*, 2011.

[184] D. Sun, S. Ukkusuri, R. Benekohal, and S. Waller, "Modeling of Motorist-Pedestrian Interaction at Uncontrolled Mid-block Crosswalks," *Urbana*, vol. 51, p. 61801, 2002.

[185] J. Sun, Y. Yang, and H. Wang, "Development and Application of a Simulation-Enhanced Platform for Pedestrian Crossing Behaviors Experiment," in *Transport Research Board*, 2011.

[186] T. Wang, J. Wu, P. Zhang, and M. Mc, "Study of Pedestrians' Gap Acceptance Behavior when They Jaywalk outside Crossing Facilities," in *International IEEE Annual Conference on Intelligent Transportation Systems*, 2010.

[187] X. Zhang and G. Chang, "A Pedestrian-Vehicle Mixed Flow Simulation Model for Urban Congested Intersections," in *Transportation Research Board*, 2012.

[188] M. Ottomanelli, G. Iannucci, and D. Sassanelli, "Simplified Model for Pedestrian-Vehicle Interactions at Road Crossings Based on Discrete Events System," *Transportation Research Record: Journal of the Transportation Research Board*, vol. 2316, no. 1, pp. 58–68, 2012.

[189] M. Ishaque and R. Noland, "Trade-offs between Vehicular and Pedestrian Traffic using Micro-Simulation Methods," *Transport Policy*, vol. 14, pp. 124–138, 2007.

[190] C. Boenisch and T. Kretz, "Simulation of Pedestrians Crossing a Street," in *Traffic and Granular Flow '09*, 2009.

[191] N. Bellomo, B. Piccoli, and A. Tosin, "Modeling Crowd Dynamics from a Complex System Viewpoint," *Mathematical Models and Methods in Applied Sciences*, vol. 22, pp. 1230004–1–29, 2012.

[192] K.J. Clifton and G. Davies and W.G. Allen, and N. Radford, "Pedestian Flow Modelling for Prototypical Maryland Cities," tech. rep., Maryland Department of Transportation Associates, Division of Highway Safety Programs (Hanover), 2004.

[193] S. Hoogendoorn and W. Daamen, *Traffic and Granular Flow '05*, ch. Microscopic Calibration and Validation of Pedestrian Models Cross-comparison of Models using Experimental Data, pp. 329–340. Springer Link, 2007.

[194] T. Kretz, S. Hengst, and P. Vortisch, "Pedestrian Flow at Bottlenecks - Validation and Calibration of Vissim's Social Force Model of Pedestrian Traffic and its Empirical Foundations," in *International Symposium of Transport Simulation*, 2008.

[195] D. R. Parisi, M. Gilmana, and H. Moldovana, "A Modification of the Social Force Model can Reproduce Experimental Data of Pedestrian Flows in Normal Conditions," *Physica A*, vol. 388, pp. 3600–3608, 2009.

[196] S. Bhatnagar, "Urbanism | sharing space in london." Available at http://shilpabhatnagar.com/2012/02/urbanism-sharing-space-in-london/#.UpLiryRFCdI, 2013.

[197] A. Karndacharuk, D. Wilson, and M. Tse, "Share Space Performance Evaluation: Quantitative Analysis of Pre-Implementation Data," tech. rep., IPENZ Transportation Group Conference Auckland, 2011.

[198] F. Shore and K. Uthayakumar, "Designing the Future - Shared Space: Operational Assessment," tech. rep., The UK Department for Transport, 2010.

[199] D. Bliek, "Impacts of Shared Space Design on Pedestrian and Motorist Behaviour," tech. rep., Institute of Transportation Engineers, 2010.

[200] B. Anvari, W. Daamen, V. Knoop, S. Hoogendoorn, and M. Bell, "Shared Space Simulation Based on Social Forces and Distance Potential Field," in *International Conference on Pedestrian and Evacuation Dynamics*, 2012.

[201] B. Anvari, "A Mathematical Model for Driver and Pedestrian Interaction in Shared Space Environments," in *Universities' Transport Study Group*, 2012.

[202] B. Anvari, M. Bell, P. Angeloudis, and W. Ochieng, "Prediction of Potential Conflicts and Velocity Optimisation of Long-range Collision Avoidance for Force-based Shared Space Simulation," in *International Conference on Pedestrian and Evacuation Dynamics*, 2014.

[203] S. Hoogendoorn, P. Bovy, and W. Daamen., "Microscopic Pedestrian Wayfinding and Dynamics Modeling," in *Pedestrian and Evacuation Dynamics*, pp. 123–154, 2001.

[204] A. Yufka and O. Parlaktuna, "Performance Comparison of Bug Algorithms for Mobile Robots," in *5th International Advanced Technologies Symposium*, 2009.

[205] P. Pecol, P. Argoul, S. D. Pont, and S. Erlicher, "The Non-smooth View for Contact Dynamics by Michel Fremond Extended to the Modelling of Crowd Movements," *Doscrete and Continuous Dynamical Systems Series S*, vol. 6, no. 2, pp. 547–565, 2013.

[206] E. Dijkstra, "A Note on Two Problems in Connexion with Graphs," *Numeric Mathematics*, vol. 1, pp. 269–271, 1959.

[207] A. Johansson and T. Kretz, *Agent-based Models of Geographical Systems*, ch. Applied Pedestrian Modeling, pp. 451–462. Springer Netherlands, 2012.

[208] T. Kretz, C. Bonisch, and P. Vortisch, "Comparison of Various Methods for the Calculation of the Distance Potential Field," *Pedestrian and Evacuation Dynamics*, no. 5, 2008.

[209] J. Bresenham, "Algorithm for Computer Control of a Digital Plotter," *IBM Systems Journal*, vol. 4, pp. 25–30, 1965.

[210] M. Schultz, T. Kretz, and H. Fricke, "Solving the Direction Field for Discrete Agent Motion," *Lecture Notes in Computer Science*, vol. 6350, pp. 489–495, 2010.

[211] K. Lewin, *Field Theory in Social Science: Selected Theoretical Papers*. New York: Harper & Row, 1951.

[212] J. Morgan and M. Blanco, "Synthesis Study of Light Vehicle Non-Planar Mirror Research," tech. rep., Centre for Truck and Bus Safety, Virginia Tech Transportation Reserach Plaza, 2010.

[213] K. Reif and K. Dietsche, *Kraftfahrtechnisches Taschenbuch*. 2010.

[214] G. Herrin and J. Neuhardt, "An Empirical Model for Automobile Driver Horizontal Curve Negotiation," *Human Factors: The Journal of the Human Factors and Ergonomics Society*, vol. 16, no. 2, pp. 129–133, 1974.

[215] S. Schmidl, "Untersuchung des Fahrverhaltens in unterschiedlichen Kurvenradien bei trockener Fahrbahn," Master's thesis, University of Agricultural Sciences Vienna, 2011.

[216] R. Isermann, *Fahrdynamik-Regelung: Modellbildung, Fahrerassistenzsysteme*. Mechatronik, 2006.

[217] L. Pallottino and E. M. Feron, "Conflict Resolution Problems for Air Traffic Management Systems Solved With Mixed Integer Programming," *Intelligent Transportation Systems, IEEE Transactions*, vol. 3, no. 1, pp. 3–11, 2002.

[218] J. Dormand and P. Prince, "A Family of Embedded Runge-Kutta Formulae," *Journal of Computational and Applied Mathematics*, vol. 6, no. 1, p. 19=26, 1980.

[219] D. Spangberg, "NGSSC course: Numerical Analysis - Project work," 2000.

[220] L. Hou and Z. Miskovic, "A Gear-like Predictor-Corrector Method for Brownian Dynamics Simulation," 2008.

[221] D. Helbing, P. Molnar, I. J. Farkas, and K. Bolay, "Self-organizing Pedestrian Movement," *Environment and Planning B: Planning and Design*, vol. 28, pp. 361–382, 2001.

[222] T. Lee, *An Agent-Based Model to Simulate Motorcycle Behaviour in Mixed Traffic Flow*. PhD thesis, Centre for Transport Studies, Department of Civil and Environmental Engineering, Imperial College London, 2007.

[223] The Royal Borough of Kensington and Chelsea, "Exhibition Road," January 2011. Available at http://www.rbkc.gov.uk/subsites/exhibitionroad.aspx.

[224] A. Steiner, M. Philipp, and A. Schmid, "Parameter Estimation for a Pedestrian Simulation Model," in *7th Swiss Transport Research Conference*, September 2007.

[225] J. Hongfei, Y. Lili, and T. Ming, "Pedestrian Flow Characteristics Analysis and Model Parameter Calibration in Comprehensive Transport Terminal," *Transportation Systems Engineering and Information Technology*, vol. 9, no. 5, pp. 117–123, 2009.

[226] C. Rudloff, T. Matyus, S. Seer, and D. Bauer, "Can Walking Behavior Be Predicted? Analysis of Calibration and Fit of Pedestrian Models," *Transportation Research Board of the National Academies*, vol. 2264, pp. 101–109., 2011.

[227] C. Rudloff, D. Bauer, T. Matyus, and S. Seer, "Mind the gap: Boarding and Alighting Processes using the Social Force Paradigm Calibrated on Experimental Data," in *14th International IEEE Conference on Intelligent Transportation Systems*, 2011.

[228] Pedestrian and E. Dynamics, eds., *Real-time Video Analysis of Pedestrians to Support Agent Simulation of People Behavior*, 2011.

[229] R. Deroo and J.-M. Auberlet, "A First Macroscopic-Microscopic Pedestrian Model - Results in the Case of a Unidirectional Flow," *Transportation Research Board 91st Annual Meeting*, vol. 12-1174, 2012.

[230] M. Campanella, S. Hoogendoorn, and W. Daamen, "Quantitative and Qualitative Validation for General Use of Pedestrian Models," in *Pedestrian and Evacuation Dynamics*, 2012.

[231] D. Parisi and C. Dorso, "Morphological and Dynamical aspects of the Room Evacuation Process," *Physica A: Statistical Mechanics and its Applications*, vol. 385, no. 1, pp. 343–355, 2007.

[232] C. Rudloff, R. Schoenauernauer, and M. Fellendorf, "Comparing a Calibrated Shared Space Simulation Model to Real Life Data," in *TRB 2013 Annual Meeting*, 2013.

[233] L. I. Panis, C. Beckx, and S. Broeckx, "Impact of 30 km/h Zone Introduction on Vehicle Exhaust Emissions in Urban Areas," *Association for European Transport and contributors*, 2006.

[234] I. Kaparias, M. Bell, A. Miri, C. Chan, and B. Mount, "Analysing the Perceptions of Pedestrians and Drivers to Shared Space," *Transportation Research Part F: Traffic Psychology and Behaviour*, vol. 15, no. 3, pp. 297–310, 2012.